MASTER'S OF SCIENCE THESIS: ANALYSIS OF ROANOKE REGION WEATHER PATTERNS UNDER GLOBAL TELECONNECTIONS

Eric LaRocque

Thesis submitted to the Faculty of the Virginia Polytechnic Institute and State University in partial fulfillment of the requirements for the degree of

Master of Science

in

Civil Engineering

Dr. G.V. Loganathan, Co-Chairman

Dr. V. Lohani, Co-Chairman

Dr. D.F. Kibler

February 7, 2006

Blacksburg, Virginia

Keywords: Global Circulations, Synoptic Scale Classification, Synoptic Scale Weather Patterns

Analysis of Roanoke Region Weather Patterns Under Global Teleconnections

Eric LaRocque

Abstract

This work attempts to relate global teleconnections, through physical phenomena such as the El Nino-Southern Oscillation (ENSO), Artic Oscillation (AO), North Atlantic Oscillation (NAO), and the Pacific North American (PNA) pattern to synoptic-scale weather patterns and precipitation in the Roanoke, Virginia region. The first chapter describes the behavior of the El Nino-Southern Oscillation (ENSO) by implementing non-homogeneous and homogeneous Markov Chain models on a monthly time series of the Troup Southern Oscillation Index (SOI), a sea level pressure based index. Meanwhile, in the second chapter the author has related or an attempt has been made to relate global teleconnections (through ENSO and AO) to a synoptic scale, station-centered set of weather types in order to assess trends in precipitation. The final portion of this work describes spatial variability of seasonal precipitation in southwestern Virginia in a context that incorporates global teleconnections (through AO, PNA, NAO, and ENSO) and frontogenesis. It was found that the Markov property can be used to describe and predict the monthly evolution of ENSO. Also evident is an increased probability of a wetter spring in the Roanoke region when El Nino combines with the negative phase of the AO during the previous winter. Meanwhile, Roanoke winters subsequent to a fall season described by this same El Nino-AO condition are predicted to receive more precipitation than average. This work additionally showed possible trends between frontal-precipitation events in the Roanoke region and global teleconnections.

Acknowledgment

This work was continuously supported by my co-chair committee advisors Dr. G.V. Loganathan of the Civil and Environmental Engineering department and Dr. Vinod Lohani of the Engineering Education department. Their expertise in hydrology, water resources systems, statistics, probability, and computer programming guided this research. Their work in the teleconnections field positions them in a small group of civil engineers who seek to develop hydrologic forecasting procedures that use measures of global circulation, such as El Nino Southern Oscillation (ENSO) as indicator parameters. I greatly enjoyed the brainstorming sessions the three of us had, during which ideas originated and concepts gained clarity. These meetings were the most enjoyable academic times of my graduate school experience. I thank Drs. Loganathan and Lohani for the opportunities they presented to me. In addition, the time Dr. Kibler dedicated to my research is greatly appreciated. It is also vital that the daily efforts made by Merry-Gayle Moeller and Lindy Cranwell be acknowledged.

Table of Contents

List of Tables

Chapter 1

Chapter 2

List of Figures

Chapter 1: Modeling the Southern Oscillation Index (SOI) with Markov Chain Models

Introduction

Characterizing the evolution of physical systems or phenomena is necessary for not only predicting their own future occurrence, strength, and persistence but also for their use in models that forecast related processes. This chapter describes the behavior of the El Nino-Southern Oscillation (ENSO) by implementing non-homogeneous and homogeneous Markov Chain models on a monthly time series of the Troup Southern Oscillation Index (SOI), a sea level pressure based index. See Appendix A for details on the computation of the SOI, Appendix E for pertinent physical and meteorological details of ENSO, and Appendix F for computational results of this chapter. Within this portion of the work, transitional expectations, long-term steady state tendencies, as well as mean residence and recurrence durations are gained for the three phases of ENSO: El Nino (warm), La Nina (cold), and Neutral. A conditional prediction scheme associated with the non-homogeneous model is also developed in this chapter to project the most probable future class the SOI will assume at a lead time of up to four months. For this analysis, original SOI data obtained from the Australian Bureau of Meteorology (BOM) was transformed into a 3-month moving mean series given the acknowledged high month to month variation typical of pressure indices (Lohani 1995). This 3-month moving mean series was then compartmentalized into severity classes, onto which the Markov models were applied.

Markov Chain Background

For the present analysis, the monthly SOI values from 1876 through 2004 are considered. Because 3-month moving averages are used in the Markov framwork, this period is reduced to 1877 through 2004. Seven severity classes shown in Table 1 were arbitrarily chosen to give resolution to the monthly series, while boundary values used to define each class followed guidance offered by (Sen et al. 2004), (Yue 2001), and (Simpson and Colodner 1999) for the Troup SOI.

Table 1. Troup Southern Oscillation Index (SOI) Severity Class Assignment

Severity Class	SOI Interval	ENSO Phase
1	-20 or less	Strong El Nino
2	-19.999 to -10	Moderate El Nino
3	-9.999 to -5	Weak El Nino
4	-4.999 to 4.999	Neutral
5	5 to 9.999	Weak La Nina
6	10 to 19.999	Moderate La Nina
7	20 or more	Strong La Nina

Within the Markov framework, class steady state probabilities, duration of uninterrupted class residence, and class recurrence times can be computed. The monthly chain must follow the Markov property for every month n and all classes i_1, i_2,… i_7, as shown here:

$$P[SOIclass_{n+1} = j \mid SOIclass_n = i, SOIclass_{n-1} = i_{n-1}, SOIclass_{n-2} = i_{n-2}, ..SOIclass_1 = i_1]$$
$$= P[SOIclass_{n+1} = j \mid SOIclass_n = i] \quad (1)$$

This property permits the index class occurrence probability at the following time step – month (n+1) – to be dependent only on the class observed at the current month (n). Equation (1) is the probability that the SOI class at month (n+1) is j given that SOI class i has been observed for the current month (n).

It is instructive to investigate the SOI's physical characteristics that provide the backdrop of its monthly computation. Interseasonal variation of conditions in the tropical Pacific Ocean is coupled to changes in global ocean-atmospheric circulations including the meridionally-oriented Hadley Cell and zonally-directed Walker Circulation. In fact, the Southern Oscillation – the atmospheric response to changes in sea surface temperatures (SST) – is an aberration of the typical Walker and Hadley circulations in the tropical Pacific basin (Philander 1990). The Hadley Cell is a tropical circulation driven by concentrated evaporation at the Intertropical Convergence Zone (ITCZ), which delineates the global band of maximum radiation and resulting convection and low pressure. While its low pressure branch follows the ITCZ, the circulation's high pressure branch defines the subtropical high near 30°N and drives the surface trade winds at the equator (Hasse and Dobson 1986). Describing the zonally-configured exchange of tropical Pacific air masses, the Walker Circulation results in part from disruption of the ITCZ path, which itself demonstrates a response to seasonal changes (Meehl 2003).

It is imperative that the cascading interaction of the physical characteristics that identify these two circulations, including thermocline depth, cold water upwelling, SSTs, and atmospheric convection and winds, is in accordance with the Markov property. The annual revolution of Earth around the sun causes ITCZ latitudinal fluctuation north and south of the equator (Philander 1990). Due to the elevated specific heat capacity of ocean

water relative to most other fluids, SST response to ITCZ position is generally lagged three months (Wang 2002). Thermal properties identifying the ocean's energy diffusive and storage qualities including molecular conduction, albedo, and radiation penetration, facilitate this lagged oceanic response and support assumption of the Markov property (Hasse and Dobson 1986). Referencing its massive heat capacity, Trenberth (2003) eludes to the ability of the tropical Pacific Ocean basin to control SST, thermocline depth, and atmospheric convection through memory of past conditions. The interseasonal variation typical of SSTs explicitly reflects the Markov property and is displayed by the oscillatory behavior of SOI time series, as seen in Figure 1 (BOM 2005).

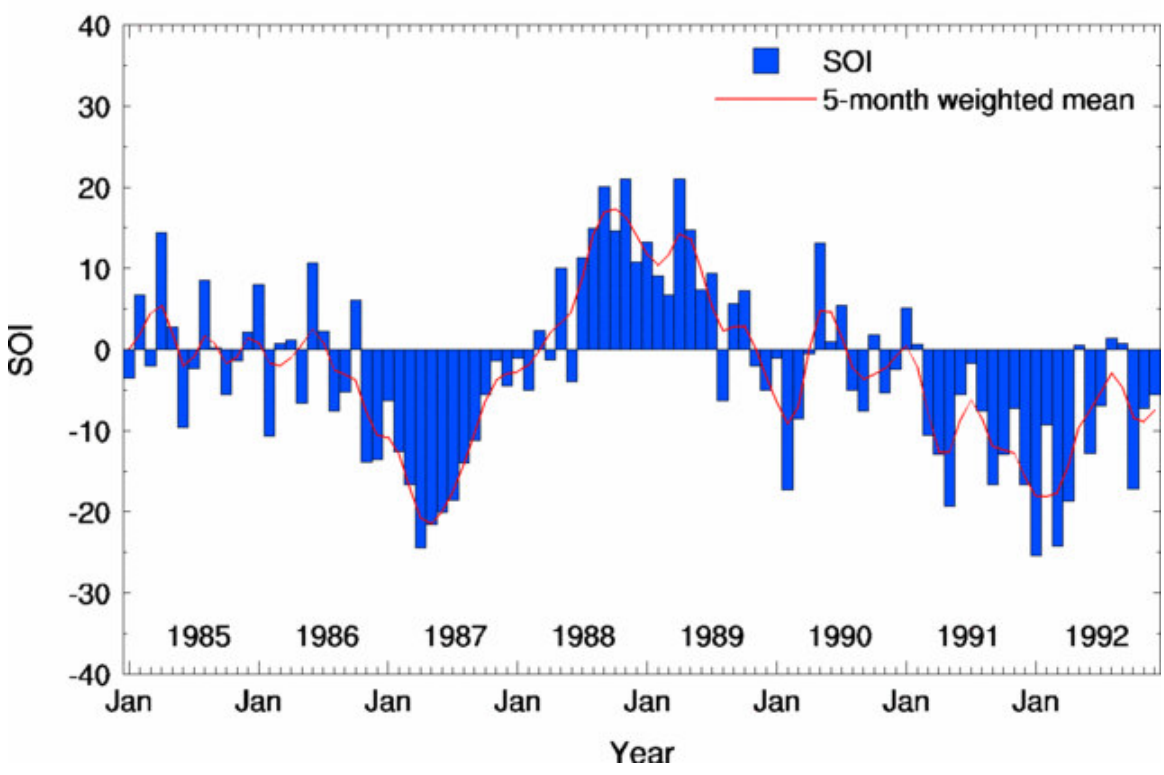

Figure 1. Southern Oscillation Index (SOI) 1985-1992 Time Series (Reproduced from Australian Bureau of Meteorology 2005)

Assumption of the Markov property is particularly justifiable for the SOI since evaporative and atmospheric convection processes – dictating sea surface pressure – are related significantly only to SST, as was shown by (Philander 1990). As a possible precursor to El Nino events, Kelvin waves function to alter thermocline depth in the equatorial Pacific and are able to convey anomalously warm water to the eastern portion of the basin over a two to three month propagation period (D'Aleo 2002). This finding further validates the assumption of the Markov property. Moreover, a monthly-based analysis of the relation between the Pacific North American (PNA) pattern and regional weather types performed by Sheridan (2003) helps to render the Markov property applicable for the SOI given ENSO's strong relation to the PNA (D'Aleo 2002).

A number of previous studies have implemented both non-homogeneous and stationary Markov chains into climatic and hydrologic problems. Woolhiser (1992) described the daily occurrence of wet and dry days by a first order Markov chain, where transition probabilities were a function of the SOI. Katz et al. (2003) also used a first order Markov model to predict precipitation occurrence by conditioning transitional probabilities on the current phases of teleconnective indices, including the SOI. Furthermore, a series of studies have employed a hidden state Markov (HSM) chain to connect hydrologic variables to large-scale atmospheric circulations through an unobserved, or hidden, weather state (Thyer and Kuczera 2000; Hughes and Guttorp 1999; Tebaldi 2000). The hidden weather state bridges the dissimilar time scales of the hydrologic and teleconnective variables (Hughes and Guttorp 1999) and often possess discernable precipitation distributions (Thyer and Kuczera 2000).

Non-Homogeneous and Homogeneous Markov Chain Models

When the monthly transition probabilities shown in equation (1) are dependent on the time (month) at which a transition is made, the Markov chain is non-homogeneous. Time-dependency of the SOI-class process is rationalized in part by the evolution of physical parameters responsible for relaxation of easterly trade winds in the tropical Pacific (giving way to El Nino events), which display monthly periodicity (Philander 1990). Transition probabilities corresponding to the non-homogeneous chain are computed as:

$$p_{i,j}^{(n,n+1)} = P[SOIclass_{n+1} = j | SOIclass_n = i] = N_{i,j}^{(n,n+1)} / N_i^{(n)} \quad (2)$$

where $N_{i,j}^{(n,n+1)}$ = number of occurrences where the climate index class moved from i in month n to j in month n+1; $N_i^{(n)}$ = number of occasions where class i was present during month n. (Lohani and Loganathan, 1997). Square 7x7 matrices for each month compile these transition probabilities for i,j = 1, 2, …7 and are reported in Table F1, within Appendix F. If a severity class is never observed to exist in a given month throughout the 1877-2003 period ($N_i^{(n)} = 0$), then $p_{i,j}^{(n,n+1)}$ is assigned a value of 1/7 for all j = 1, 2, …7. The straightforward conditions attached to these monthly transition matrices are as follows: (1) $p_{i,j} >= 0$ for i,j = 1, 2,…k and (2) $\sum_{j=1}^{k} p_{i,j} = 1$ for i = 1, 2, …k (Ross 1980).

From Table 2, transitional behavior of the non-homogeneous chain shows that if strong El Nino conditions have been observed in June, the tropical Pacific basin will move towards neutrality in July with a 25% likelihood. In addition, the SOI exhibits the

aptitude to discontinuously move from a moderate La Nina (class 6) condition to the neutrality (class 4) during this June to July transition with a probability of 0.273.

Table 2. June-July Transition Matrix of Troup SOI from Non-Homogeneous Markov Chain

SOI Class	1	2	3	4	5	6	7
1	0.750	0.250	0.000	0.000	0.000	0.000	0.000
2	0.000	0.733	0.267	0.000	0.000	0.000	0.000
3	0.000	0.111	0.333	0.556	0.000	0.000	0.000
4	0.000	0.000	0.052	0.759	0.172	0.017	0.000
5	0.000	0.000	0.000	0.333	0.429	0.238	0.000
6	0.000	0.000	0.000	0.273	0.000	0.727	0.000
7	0.000	0.000	0.000	0.000	0.000	0.000	1.000

Table F1 in Appendix F contains all monthly transition matrices for the non-homogeneous chain. Noteworthy from these results is the potential for class 2 to move into class 1 at the May-June transition (12.5%) and the tendency for a class 4 observed in May to propagate towards El Nino and La Nina classes. While all monthly transitions demonstrate a desire to persist in their neutral class, the October-November and November-December transition each possess substantially higher likelihoods that the neutral condition will propagate towards La Nina (class 5).

Homogeneity can be assumed for the SOI class series if its advancement is irrelevant to time (Isaacson and Madsen 1976). Transition probabilities belonging to the homogeneous chain are computed without regard of the months over which the step is made. The mean monthly probability of transition from class i to j is found via:

$$p_{i,j} = (N_{i,j}/N_T) / (N_i/N_T) = N_{i,j} / N_i \quad (3)$$

in which $N_{i,j}$ = number of occasions where the chain encounters a one-step change from class i to class j, N_T = total number of months in the record, and N_i = number of months in the record existing in class i (Lohani 1995). Evident in equation (3) is the removal of the (n,n+1) notation from equation (2). The mean monthly transition matrix is the collection of $p_{i,j}$ for i,j = 1,2,…7 and showcases the homogeneous, or stationary process. Table F2 in Appendix F presents the mean monthly matrix for the SOI. This outcome conveys a a general deficiency for El Nino (La Nina) classes to discontinuously move to La Nina (El Nino) classes, which is to say that neutrality is expected to bridge El Nino and La Nina . Also apparent is the increased potential for a strong La Nina to diminish to a moderate La Nina (0.4286) when compared against the tendency for a month of strong El Nino to weaken (0.2692) to a moderate El Nino.

Steady State Class Probabilities

Gained through fruition of the non-homogeneous transition matrices and mean monthly transition matrix is the ability to predict the SOI's [class] location when a given number of monthly transitions; however, it is intuitive that where the process is during a specific month in the future is directly affected by the class from which the chain begins. From (Isaacson and Madsen 1976), the class probability row vector, $f^{(k)}$, denotes the class probability distribution after k monthly transitions. When the non-homogeneous chain begins at month 1, $f^{(k)}$, can be obtained as:

$$f^{(k)} = [f^{(0)}]\,[P_1]\,[P_2]\,\ldots\,[P_k]. \quad (4)$$

From equation (4), $f^{(0)}$ is termed the initial class probability row vector, and $[P_t]$ represents the non-stationary transition matrix between months t and (t+1). It follows that $[P_1]$ would then denote the matrix for the January-February transition, $[P_{Jan,Feb}]$. Given that these monthly transitional matrices undergo no interannual change, the transition matrix, for example, corresponding to months 13 and 14 ($[P_{13}]$) equals $[P_1]$, or $[P_{Jan,Feb}]$. Similar to equation (4), the class probability row vector, $f^{(k)}$ is computed for the stationary process as:

$$[f^{(0)}]\,[P]^k \quad (5)$$

where [P] is the mean monthly transition matrix which is Table F2 for the current SOI analysis. Equations (4) and (5) become operable only when the initial class probability row vector ($f^{(0)}$), corresponding to the month designated to begin the chain for the non-stationary process, is known. A relation for $f^{(k)}$ as $k \rightarrow \infty$ that is independent of the initial class row vector is desired to assess the long-term, steady state behavior of the SOI (Lohani 1995).

According to Isaacson and Madsen (1976), $f^{(0)}$ is forced from equation (4) if $[P_1]\,[P_2]\,\ldots\,[P_k]$ equates to a constant stochastic matrix, defined as possessing identical rows. On the condition that $f^{(0)}$ remains a stochastic row vector – all entries >= 0 and all rows sum to 1 – then the chain's projected class probability distributions are only a function of

the number of monthly transitions performed, k, and the month the sequence commences, m. Thus equation (4) now becomes:

$$f_m^{(k)} = \text{row } \varphi^{(\text{month m, k})} = \text{row } [P_m]\,[P_{m+1}] \ldots [P_k] \quad (6)$$

where $\varphi^{(\text{month m, k})}$ is deemed the constant stochastic matrix for the non-homogeneous chain (Lohani and Loganathan 1997). For month m, $\varphi^{(\text{month m, k})}$ is taken to be the product of the set of 12 consecutive monthly transition matrices, with the matrix corresponding to month m included as the starting month (Lohani and Loganathan 1997). For instance, January's constant stochastic matrix for an infinite number of transitions is given as:

$$\varphi^{(1,\,\infty)} = [\text{Jan}] = \{[P_1]\,[P_2] \ldots [P_{12}]\} * \{[P_1]\,[P_2] \ldots [P_{12}]\} \ldots \quad (7)$$

from which the steady state class probability row vector for January, $f_1^{(\infty)}$ can be recognized as:

$$f_1^{(\infty)} = \text{row } [\text{Jan}]. \quad (8)$$

Given that $[\varphi] = [P][\varphi]$ for any constant row matrix $[\varphi]$ and stochastic matrix $[P]$, we also obtain:

$$f_2^{(\infty)} = \text{row } [\text{Feb}] = [\text{Jan}][P_1] \quad (9)$$

and $f_5^{(\infty)}$ = row [May] = [Apr] [P_4] = [Jan] [P_1] [P_2] [P_3] [P_4]. Thus equation (8) is consulted for all 12 months and is evaluated until a constant stochastic matrix is realized. Table 3 shows the monthly steady state probabilities for all the 12 months using the 3-month moving average SOI values.

Table 3. Monthly Steady State Occurrence Probabilities for the Non-Homogeneous Chain

Month	Class 1	Class 2	Class 3	Class 4	Class 5	Class 6	Class 7
Jan	0.00781	0.09581	0.15206	0.45520	0.13282	0.14066	0.01563
Feb	0.00781	0.07072	0.18623	0.44581	0.14092	0.14851	0.00000
Mar	0.01567	0.10156	0.11664	0.47674	0.13298	0.15641	0.00000
Apr	0.02348	0.10149	0.10913	0.46874	0.15639	0.14076	0.00000
May	0.01563	0.12495	0.10144	0.48430	0.18765	0.07820	0.00782
Jun	0.01566	0.12506	0.10149	0.48430	0.18754	0.07814	0.00781
Jul	0.01563	0.12493	0.10143	0.48430	0.18767	0.07821	0.00782
Aug	0.01563	0.12494	0.10144	0.48430	0.18767	0.07821	0.00782
Sep	0.01566	0.12504	0.10148	0.48429	0.18756	0.07815	0.00781
Oct	0.01567	0.12508	0.10149	0.48429	0.18752	0.07813	0.00781
Nov	0.01564	0.12499	0.10146	0.48430	0.18761	0.07818	0.00782
Dec	0.01562	0.12488	0.10142	0.48431	0.18772	0.07823	0.00782

An equivalent reduction can be applied to equation (5) for the stationary process, where the steady state probabilities are evaluated as follows:

$$\lambda_j = \sum_{i=1}^{7} \lambda_i p_{i,j} \tag{10}$$

which is subject to the constraint:

$$\sum_{j=1}^{7} \lambda_j = 1.0$$

where λ_j = steady state probability of occurrence for weather type j at any future month and $p_{i,j}$ = stationary probability for a monthly transition from SOI class i to j (Ross 1980). Table 4 offers the steady state SOI class distribution for the stationary process.

Table 4. Steady State SOI Class Occurrence Distribution from Stationary Markov Chain

Class 1	Class 2	Class 3	Class 4	Class 5	Class 6	Class 7
0.0169	0.1179	0.1342	0.4528	0.1498	0.1192	0.0091

Steady state probabilities belonging to the non-homogeneous chain represent the occurrence frequency distribution for each month over a long period. As Table 5 depicts the Markov steady state occurrence probabilities and empirical values for January, the non-homogeneous Markov chain predicts with a high measure of confidence that any January in the long-term future will attain class 4; however, there is a 15.2% likelihood class 3 will be realized. Empirical, or observed, values are obtained for a distinct class as the ratio of the total number of occurrences of that class during a given month over the 1877-2004 study period and the total number of occurrences of all classes over that same month and period. Results in Appendix F include monthly steady state probability distributions empirically obtained as well as those arrived at through the non-homogeneous Markov chain. Good correspondence between the empirical and Markov chain outcomes helps to validate the use of the non-homogeneous model for analyzing monthly SOI evolution.

Summations of non-homogeneous steady state results, from Table F3 in Appendix F, belonging to El Nino and La Nina classes, (1-3) and (5-7) respectively, across the three

winter months –December, January, and February – indicate that La Nina events have been favored over El Nino during the winter season over the study period. This parallels D'Aleo's (2002) study that proved La Nina shows a tendency for development in the winter season. Additional steady state inferences offered by the non-homogeneous chain include: (1) March's high affinity for class 6 (moderate La Nina) relative to all other months; (2) October's minimum neutral (class 4) likelihood; and (3) high proneness of strong El Nino conditions during April relative to all other months.

Table 5. January Steady State SOI Class Occurrence Distribution from Non-Homogeneous Markov Chain

	Class1	Class2	Class3	Class4	Class5	Class6	Class7
Markov	0.007811	0.095813	0.15206	0.455202	0.132823	0.140661	0.01563
Observed	0.007813	0.09375	0.15625	0.453125	0.132813	0.140625	0.015625

Uninterrupted Mean Residence

An ability to predict duration of persistence of SOI classes is imperative if a comprehensive analysis of ENSO is desired. Offered by the non-homogeneous chain is estimation of uninterrupted mean residence of m months for each SOI class, as shown for a two consecutive month stay of class i for a January observation (Lohani 1995):

$$P[m = 2 \mid X_{Jan} = i] = P[X_{Mar} \neq i, X_{Feb} = i \mid X_{Jan} = i] \quad (11)$$

$= P[X_{Feb} = i \mid X_{Jan} = i] * (1 - P[X_{Mar} = i \mid X_{Feb} = i])$ (12)

$= p_{i,i}^{1,2} * (1 - p_{i,i}^{2,3})$ (13)

Also, $P[m = 4 \mid X_{Mar} = i] = P[X_{July} \neq i, X_{Jun} = i, X_{May} = i, X_{Apr} = i \mid X_{Mar} = i] = p_{i,i}^{3,4} * p_{i,i}^{4,5} * p_{i,i}^{5,6} * (1 - p_{i,i}^{6,7})$. An identical procedure can be applied for m = 1, 2, 3… to some k_{max} with each m possessing a corresponding probability as shown in equation (13). It follows that the expected uninterrupted residence of class i can be obtained with:

$$E[R_i \mid startingmonth] = \sum_{k=1}^{k_{max}} k * P[R_i = k \mid startingmonth] \quad (14)$$

where R_i = uninterrupted residence of class i as a random variable conditioned on the month at which class i is first observed and k = the range in number of months over which R_i is defined, and m = uninterrupted residence in number of months (Lohani 1995). It follows from the time-dependency of the non-homogeneous chain that this expectation is a function of probabilities that are conditioned on the month on which a class is first observed as well as the number of terms considered, k_{max}.

An estimate of k_{max} can be obtained by the geometric series, which evolves from the significant reduction in the rate of increase of $E[R_i]$ for large values of m. The geometric mean for uninterrupted residence of class i is approximated by:

$$r = (p_{i,i}^{1,2} * p_{i,i}^{2,3} * p_{i,i}^{3,4} * p_{i,i}^{4,5} * p_{i,i}^{5,6} * p_{i,i}^{6,7} * p_{i,i}^{7,8} * p_{i,i}^{8,9} * p_{i,i}^{9.10} * p_{i,i}^{10,11} * p_{i,i}^{11,12} * p_{i,i}^{12,1})^{1/12} \quad (15)$$

The expected uninterrupted residence of class i is estimated from r by:

$$\sum_{k=1}^{k_{\max}} k * r^{k-1} * (1-r) = (1-r)\sum_{k=1}^{k_{\max}} \frac{d}{dr}(r^k) = (1-r)\frac{d}{dr}\sum_{k=1}^{k_{\max}} r^k = (1-r)\frac{d}{dr}(\frac{1-r^{k_{\max}+1}}{1-r}) =$$

$$\frac{[1+k_{\max} r^{(k_{\max}+1)} - (1+k_{\max}) r^{k_{\max}}]}{(1-r)} \qquad (16)$$

which reduces to:

$$E[R_i] = \frac{1}{1-r} \qquad \text{as } k_{max} \rightarrow \infty \qquad (17)$$

From iterations, it is found that $k_{max} = 48$ converges accurately for $r < 0.85$ between the exact formula in equation (16) and the limit in equation (17). This k_{max} value was retained for equation (14) for all classes and starting months; therefore, the maximum possible duration for all individual severity class is 4 years. This uninterrupted residence is more than 5 times the duration of class 1 during the so-called "super El Nino" in 1982-83 (Philander 1990).

Table 6 reports uninterrupted residence for all seven SOI classes, arranged by the month on which the duration of stay commences.

Table 6. SOI Class Expected Uninterrupted Residence Times According to Starting Month, $E[R_i \mid startingmonth]$ (# of months)

Class 1	5.548	4.548	3.548	2.548	4.644	3.644	3.526	3.788	4.183	4.774	7.548	6.548
Class 2	2.833	3.667	3.429	3.157	3.505	4.009	4.103	3.949	3.176	2.418	2.399	2.417
Class 3	2.115	1.858	1.872	1.869	2.029	1.672	2.015	1.884	2.100	1.870	1.837	1.987
Class 4	4.317	4.475	4.126	4.146	3.852	4.313	4.368	4.586	4.753	4.943	4.831	4.427
Class 5	1.796	1.692	1.781	1.896	1.629	1.886	2.066	2.026	2.436	2.035	1.881	2.057
Class 6	3.195	2.634	2.388	2.135	2.919	3.198	3.023	3.146	4.650	4.258	4.147	3.631
Class 7	1.000	1.179	1.252	1.762	5.333	4.333	3.333	2.333	2.000	1.500	1.000	1.143
Starting month	Jan	Feb	Mar	Apr	May	Jun	Jul	Aug	Sep	Oct	Nov	Dec

Apparent from Table 6 is the conspicuous duration of class 7, representative of strong La Nina condions, if a strong warm pool appears in May in the western tropical Pacific. With this mean residence being 5 1/3 months, lower than normal atmospheric pressures can be anticipated to persist in the western portion of the basin, thereby sustaining elevated easterly trade winds as well as cold ocean and atmospheric temperatures in the eastern Pacific throughout the summer and into fall. This coincides with the northern-most position of the ITCZ during August and September, which Philander (1990) reports is directly related to increased convection and precipitation in the northern Indian and western Pacific oceans – one effect of the La Nina event. Meanwhile, a cascading mean residence of the strong La Nina case appearing from May through October aids the notion of "smoothly" varying climatic conditions (and consequently climate indices) in the Pacific basin rendering an oscillatory variation above and below normal conditions (Trenberth 2003). This notion of a "smoothly" [time] varying atmospheric and oceanic state counters the irregular nature of precipitation time

series adopt and must be reconciled when modeling Virginia precipitation using ENSO and other synoptic-scale phenomena.

Also evident from the expected residence results is the pronounced escalation for class 1 residence if the strong El Nino state initiates in November, December, or January. These outcomes align with the southward displacement of the ITCZ near 8°S during the northern hemisphere winter, which, as Philander (1990) notes, is associated with the presence of El Nino. Significant similarities exist between this enhanced winter residence predicted by the Markov model and the deemed "mature" phase of El Nino defined for winter months by Wang (2002) of the year during which the peak of El Nino is attained. Also inferred from Table 6 is the sudden rise of mean expected residence for both the pronounced El Nino and La Nina class from April to May in a year for which their occurrence is predicted; this signals the tendency for both phases to increase severity during the latter month. Wang (2002) also found this time period customarily supports growth of El Nino, defining the duration of March through May during the year for which the event is forecasted as its "development" phase.

Comparisons of averaged El Nino and La Nina classes, 1 through 3 and 5 through 7 respectively, for each month serve notice to higher residences for the El Nino event throughout the entire year, excluding June. Physical reasoning that supplement the aforementioned findings evolve from less variation in SSTs in the western portion of the tropical Pacific during La Nina compared to those in the central and eastern equatorial Pacific during an El Nino episode (Philander 1990). Accompanying the belief that SST of 27.5°C functions as a threshold for significant atmospheric convection whereby moist air converges into regions delineated by this temperature with Philander's (1990) claim

that the La Nina event features relatively small regions in the western tropical Pacific with SST at or above this limit, and the reduced residence found through Markov analysis for La Nina gains validity (Gadgil et al. 1984).

Mean Class Recurrence Time

A measure of periodicity, the mean recurrence time, m_{jj} for an SOI class j, represents the expected number of monthly transitions required for the homogeneous Markov chain, starting in class j, to return to class j (Lohani 1995). This measure of the chain's affinity for a particular class is tied directly to its steady state behavior due to the per month occurrence frequency these probabilities (reported in Table 4) represent. For instance, we are able to predict that the homogeneous chain, from any starting class, will attain class 4 in its next transition roughly 45% of the time. Thus, the recurrence time for class 4 is substantially less than that of class 1 since a strong El Nino is forecasted to appear the following month with a likelihood of only 1.7%. A direct solution for mean recurrence is offered as (Hoel et al. 1972):

$$m_{jj} = 1 / \lambda_j \qquad (17)$$

This methodology allows estimation of long term SOI class distribution for the stationary chain since each λ corresponds to its class' steady state probability (Lohani, 1995).

Table 7. Mean Recurrence Times from Stationary Chain of SOI Class, m_{jj} (# of months)

SOI Class 1	59.053
SOI Class 2	8.481
SOI Class 3	7.451
SOI Class 4	2.209
SOI Class 5	6.674
SOI Class 6	8.388
SOI Class 7	109.642

A practical approach for analyzing results in Table 7 is to compute weighted averages for the El Nino (1-3) and La Nina (5-7) classes respectively, where each weight is the recurrence for the individual class divided by the sum of the El Nino or La Nina group of classes, with the neutral class excluded in both of these denominator sums. Weighted averages of 4 and 8 years for El Nino and La Nina respectively are generated from this procedure, which supports the higher positive ENSO occurrence observed in the historical record when evaluated against the negative phase (D'Aleo 2002). NOAA's (2005) claim that La Nina occurrence can be anticipated to follow a percentage of El Nino events is maintained by these weighted averages since these values (4 and 8 years) indicate that La Nino should follow every other El Nino event on average. D'Aleo (2002) cites El Nino frequency of 3 to 4 years on average and a mean La Nina frequency of 4 to 5 years, which helps to affirm the extended period attained for La Nina through the homogeneous Markov model. Other works that characterized ENSO have shown El Nino to exhibit an average period of 3 to 7 years (Trenberth 2003), 3 to 4 years (Philander 1990), and 4 years (Sen et al. 2004; The National Academies 1996).

While the low frequency component of ENSO variation has been revealed by this stationary chain recurrence procedure, Rasmusson et. al. (1990) and Barnett (1991) also exposed a quasi-biennial mode of ENSO variation with a period of 26 months. This implies an ENSO time series behavior that is inherently more complex than the one mode of recurrence arrived at through the stationary Markov chain.

Monthly Prediction of Future SOI Class

Critical to the characterization of ENSO is an ability to forecast its future condition. A procedure, developed by (Lohani 1995), employs the non-homogeneous Markov model to predict the expected future value of a discrete random variable, the SOI class in this study, given a current observation. For instance, equation (15) depicts the conditional, non-homogeneous expectation for the SOI class in February, given a class 1 observation in January (Lohani 1995).

$$E[X_{Feb} \mid X_{Jan} = i] = \sum_{j=1}^{7} j * P[X_{Feb} = j \mid X_{Jan} = i] = \sum_{j=1}^{7} j * p_{i,j}^{(1,2)} \qquad (18)$$

from which

$$X_{Feb} = \text{nearest integer}(E[X_{Feb} \mid X_{Jan} = i]) = w_1. \qquad (19)$$

"Nearest integer" is defined on the discrete state space of SOI classes 1, 2, …7. Equations (20) through (25) continue the sequence initiated by equations (18) and (19) that projects the May SOI class, w_4, from a January SOI class observation, i.

$$E[X_{Mar} \mid X_{Feb} = w_1] = \sum_{j=1}^{7} j * p_{w_1,j}^{(2,3)} \tag{20}$$

X_{Mar} = nearest integer($E[X_{Mar} \mid X_{Feb} = w_1]$) = w_2 (21)

$$E[X_{Apr} \mid X_{Mar} = w_2] = \sum_{j=1}^{7} j * p_{w_2,j}^{(3,4)} \tag{22}$$

X_{Apr} = nearest integer($E[X_{Apr} \mid X_{Mar} = w_2]$) = w_3 (23)

$$E[X_{May} \mid X_{Apr} = w_3] = \sum_{j=1}^{7} j * p_{w_3,j}^{(3,4)} \tag{24}$$

X_{May} = nearest integer($E[X_{Apr} \mid X_{Mar} = w_3]$) = w_4. (25)

This prediction scheme has been carried out for deemed El Nino calendar years 2002-'03 and 1982-'83, as well as 2001-'02, a reported La Nina year (NOAA 2005). A sample of arbitrarily chosen results is shown in Table 8, while Table F4 in Appendix F contains all monthly predictions pertaining to these years.

Table 8. Sample Results of 4-Month Lagged Prediction of SOI class from Non-Homogeneous Markov Chain

Year of Observation	Month of Observation	SOI Class Observed	Year of Predictio n	Month of Predictio n	SOI Class Predicted by Markov	Actual SOI Class
1982	Jan	6	1982	May	3	3
1982	Jun	2	1982	Oct	3	1
2001	Jan	6	2001	May	3	3
2001	Apr	4	2001	Aug	4	2
2001	Sep	4	2002	Jan	4	5
2001	Nov	5	2002	Mar	3	3
2002	Feb	6	2002	Jun	3	3
2002	May	2	2002	Sep	4	3
2002	Dec	2	2003	Apr	4	3

Applying this prediction scheme to chosen periods of the historical record renders a few notable conclusions. First, for months where a strong El Nino or La Nina class is observed, the series of expectations relied on by this prediction scheme imposes an unavoidable move towards neutrality (class 4). This was particularly evident for the late months of 1982, during the so called "super El Nino" (Philander 1990). Secondly, if the observed month corresponds to class 4, this prediction scheme has difficulty escaping this class even when lagging by more than four months. Moreover, results show this prediction scheme possesses the ability to track the SOI time series while ENSO fluctuates around neutral conditions; however an ability to augment non-homogeneous transition probabilities during ranges where the SOI is directed away from neutrality seems necessary. These performance deficiencies are a manifestation of the relatively high monthly transition probabilities involving class 4 as can be seen in Table F1 in Appendix F. Lastly, this current prediction methodology is not congruent with interseasonal change in the SOI from strong or moderate El Nino to strong or moderate La Nina, nor vise versa.

Summary

While this portion of the study focused on characterizing the ENSO phenomena with Markov chain models, physical parameters including SST, ITCZ position, thermocline depth, and atmosphere convection that help define the Southern Oscillation were found to possess monthly variation. This monthly rate of change behavior supports the application of the Markov property onto the Troup SOI. Secondly, good correspondence between steady state class probabilities attained empirically and with the analytical model (non-homogeneous chain), helps to validate the adoption of the Markov framework. Relative to all twelve months, the non-homogeneous chain generated a minimum neutral class steady state occurrence likelihood during October, and showed an affinity for the strong El Nino class to appear in April. Upon evaluation of expected class residence, relatively high residence of the strong La Nina class (class 7) was evident if it emerged in May (5.3 months). Furthermore, enhanced duration of stay resulted for the strong El Nino state (class 1) when initiated in November or December – 7.5 and 6.5 months respectively. This winter-El Nino relation is congruent with the southward displacement of the ITCZ, which is a signature of the ENSO-warm event, during northern hemisphere cold months. Periodicity of the Troup SOI, as assessed through mean recurrence times, rendered weighted average values of 4 and 8 years for El Nino and La Nina classes respectively. These computed outcomes correspond well with previous studies (Trenberth 2003; Philander 1990; Sen et al. 2004).

Gained through the non-homogeneous Markov chain, an SOI class prediction scheme with 4-month lead time is provided in this chapter. This scheme was tested for

an El Nino, La Nina, and antecedent El Nino calendar year and was found to be adequate where the SOI moved towards neutrality over a consecutive 4 month range; however, as a manifestation of the reliance on the expectation calculation, this procedure demonstrated a deficiency for predicting SOI class on 4 month ranges over which the index diverged away from neutrality.

References

Australian Bureau of Meteorology (BOM). 2005. Climate Glossary. http://www.bom.gov.au/climate/glossary/soi.shtml. Retrieved December 2005.

Barnett, T.P. 1991. The interaction of multiple time scales in the tropical climate system. J. Climate. Vol. 4, pp 269-285.

D'Aleo, J.S. 2002. El Nino and La Nina. Oryx Press: Westport, CT. pp. 1-71

Gadgil, S. Joseph, P.V., Joshi, N.V. 1984. Ocean-atmosphere coupling over monsoon regions. Nature. London. Vol. 312. pp. 141-143.

Hasse and Dobson 1986. Introductory Meteorology and Fluid Dynamics. D. Reidel Publishing. Boston: pp 1- 46.

Hoel, P.G., Port, S.C., and Stone, C.J. 1972. Introduction to Stochastic Processes. Houghton Mifflin. Boston.

Hughes, J. P., Guttorp, P. 1999. A non-homogeneous hidden Markov model for precipitation occurrence. Applied Statistics. Vol. 48. pp. 15-30.

Isaacson D.L. and Madsen, R. 1976. Markov Chains: Theory and Applications. John Wiley and Sons, New York, New York. pp. 6-50

Katz, R.W., Parlange, M.B., Tebaldi, C. 2003 Stochastic Modeling of the Effects of Large-Scale Circulation on Daily Weather in the Southeastern U.S. Cl. Change. pp. 189-216.

Lohani, V.K. et. Loganathan, G.V. 1997. An Early Warning System for Drought Management Using the Palmer Drought Index. J. of the American Water Resources Association. Vol. 33, No.6.

Lohani, V.K. 1995. Characterization of Palmer Drought Index as a Precursor for Drought Mitigation. Virginia Tech Dissertation. pp. 39-51, 100.

Meehl, Gerald. 2003. Handbook of Weather, Climate, and Water: The El Nino-Southern Oscillation (ENSO) System. John Wiley and Sons, Inc. pp. 57-68.

National Academies. 1996. Learning to Predict Climate Variations Associated with El Nino and the Southern Oscillation: Accomplishments and Legacies of the TOGA Program. www.nationacademies.org. Retrieved August 2005.

NOAA 2005. El Nino Theme Page. http://www.pmel.noaa.gov/tao/elnino/nino-home.html. Retrieved December 2005.

Philander, S.G. 1990. El Nino, La Nina, and Southern Oscillation. Academic Press. pp.1-56.

Rasmusson, E.M. Wang, X., Ropeelewski, C.F. 1990. The biennial component of ENSO variability. J. Maritime Systems. Vol.1, pp. 71-96.

Ross, S.M. 1980. Probability and Mathematical Statistics: Introduction to Probability Models. Academic Press. pp. 1-146.

Sen, Z et al. 2004. El Nino Southern Oscillation (ENSO) Templates and Streamflow Prediction. J. of Hydrologic Engineering. Vol. 9, No.5.

Sheridan, S.C. 2003. North American weather-type frequency and teleconnection indices. International J. of Climatology. Vol. 23, pp. 27-45.

Sheridan, S.C. 2002. The Redevelopment of a Weather-Type Classification Scheme for North America. Inter. J. of Climatology. pp. 51-68.

Simpson, H.J. and Colodner, D.C. 1999. Arizona precipitation response to the Southern Oscillation: A potential water management tool. Water Resources Research. Vol. 35, No. 12. pp. 3761-3769

Tebaldi, C. 2000. Influence of Large Scale Circulation Measures on Precipitation at Local Stations in the South East of the US. NRCSE Technical Report Series No. 055.

Thyer, M. and Kuczera, G. 2000. Modeling long-term persistence in hydroclimatic time series using a hidden state Markov model. Water Resources Research. Vol. 36, pp. 3301-3310.

Trenberth, K. 2003. Handbook of Weather, Climate, and Water: The El Nino-Southern Oscillation (ENSO) System. John Wiley and Sons, Inc. pp. 163-173.

Wang, C. 2002. Atmospheric Circulation Cells Associated with the El Niño–Southern Oscillation. J. of Climate. pp. 399-419.

Woolhiser, D.A. 1992. Modeling daily precipitation – progress and problems. Statistics in the Environmental and Earth Sciences. Edward Arnold: London. pp. 71-81.

Yue, S. 2001. A statistical measure of severity of El Nino events. Stochastic Environmental Research and Risk Assessment. pp.153-172.

Chapter 2: Synoptic Scale Classification (SSC2) and Application

Introduction

In this chapter, the author has related or an attempt has been made to relate global teleconnections (through ENSO and AO) to a synoptic scale, station-centered set of weather types in order to assess trends in precipitation. Synoptic scale weather types cover 100s to 1000s of square miles and persist for days to weeks, making them extremely well suited for seasonal precipitation trend analysis (Ahrens 2000). Such broad scale description of weather patterns is typically based on an air mass: an extremely large body of air with similar properties in horizontal planes. A given air mass is capable of occupying more than a half of the continental United States. Regions where air masses originate are called source regions. For a huge mass of air to develop uniform characteristics, ice covered Arctic plains in winter and subtropical oceans and desert regions during summer serve as ideal source regions (Ahrens 2000). As developed by (Bergeron 1930), air masses have been traditionally grouped into four categories as cP, mP, cT, mT, with c and m indicating the source region as either continental or maritime and while P and T referring to polar or tropical regions. Continental air masses are those formed above land and are generally dry, while moisture accompanies maritime air. Studies have been done to subdivide these air mass types by their meteorological character, in order to assign a daily weather type (Kalkstein et al. 1996; Sheridan 2002).

Synoptic Scale Classification (SSC2)

Sheridan's (2002) station based classification permits delineation of local response within a synoptic scheme, which can be further compartmentalized by global teleconnections. In this manner for designated ENSO-AO conditioning, it is anticipated that there will be a detectable response at the synoptic scale, which is then transferable to local precipitation through Sheridan's weather type classification.

Sheridan (http://sheridan.geog.kent.edu/ssc.html) provides a calendar of weather types for Roanoke, Virginia, along with 330 stations within the United States and Canada. For Roanoke each day from 1948 through 2004 is compartmentalized into one of seven weather types, or patterns, describing the daily air mass over Roanoke using his Synoptic Scale Classification (SSC2) methodology. Seven air masses are designated by the following local meteorological parameters: temperature, dew point, cloud cover, sea level pressure, and diurnal maximum 6 hour changes in dew point and temperature. The following station centered weather types are adopted in the SSC2 methodology: (1) Dry Polar (DP); (2) Dry Moderate (DM); (3) Dry Tropical (DT); (4) Moist Polar (MP); (5) Moist Moderate (MM); (6) Moist Tropical (MT); and (7) Transition (TR) (Sheridan 2002). Appendix A details each of these seven weather types. These weather patterns differ from Bergeron's (1930) classification of cP, cT, mP, and mT in DM, MM, and TR to facilitate use of the SSC2 to broader research problems, including precipitation intensity (Greene 1996), heat-stress mortality (Kalkstein and Greene 1997), and urban heat island (Sheridan 2000).

Weather Type Classification

Rendering a historical daily weather type calendar for Roanoke requires recognition and computation of the parameters that define to each of the seven designated air masses that construct the calendar. Throughout the climatology period (1948-1996), selected days that possess distinct meteorological characteristics for chosen parameters are identified within a specific 2-week period of each season.. A particular weather type is considered to belong to any day within a given seasonal 2-week period if the chosen meteorological parameter falls within theoretically-determined upper and lower limits; this day is then proposed as a candidate seed day for that specific weather type and seasonal window. Meteorological data belonging to these proposed days are verified against weather maps to validate that the selections do truly depict occurrence of the particular weather type. Upon confirmation, this captured data become nested within an algorithm that constructs a representative set of daily meteorological characteristics for each weather type. Characteristic sets of variables established for these defined seasonal periods are then linearly altered to "slide" parameter value sets across every day of the calendar.

Sliding Seed Day Procedure

"Seed day" selection initiates the development of Roanoke's daily weather type calendar. A "seed day" is an actual day in a weather station's historical record possessing meteorological characteristics that fall within pre-determined ranges. These pre-

determined ranges are reported specifically for a given weather type and seasonal window (Table 9). Seed days are determined within four 2 week periods, with each season accounted for, that represent the hottest and coldest durations as well as the temperature midpoints bisecting these bounds; subsequently for each season a set of 14 days per year serve as candidates for selection. The start dates for these periods shift by station and are as follows for Roanoke: (1) winter window – January 15th; (2) spring window – April 15th; (3) summer window – July 15th; and (4) fall window – October 14th (Sheridan 2005). To ensure reliable characterizations of the two boundary air masses, distinctively for winter and summer, the coldest DP and most humid MT days in the record are not considered for seed day selection (Sheridan 2002). The following parameters provide the selection process with objective criteria by which seed days emerge from candidate days:

- 16 h EST temperature
- 16 h EST dew point
- Mean daily cloud cover (of values at 04, 10, 16, 22 h EST)
- Diurnal dew point change (of values at 04, 10, 16, 22 h EST)
- 04 h EST temperature
- 16 h EST dew point depression

Table 9. Example of Seed-Day Selection Criteria, SSC2. MM Weather Type for Roanoke, VA During the Winter Window (Jan 15 thru Jan 28)

Parameter	Maximum	Minimum
16 h EST temperature (◦C) (maximum temp.)	12	7
16 h EST dew point (◦C)	9	None
Mean daily cloud cover (tenths)	10	4
Dew point range (◦C)	6	0
04 h EST temperature (◦C) (minimum temp.)	11	2
Diurnal maximum 6 hr dewpoint change	6	None

Manual analysis of historical synoptic weather maps for a given region identify days which ideally portray each weather type – i.e. conditions that are the driest, hottest, and sunniest relative to a particular season represent occurrence of a DP day. Upper and lower limit values of the six parameters listed above during these days are then registered as seed day selection criteria (Sheridan 2005). Table 9 shows threshold data on these seed day selection criteria for the Moist Moderate (MM) air mass during the winter window (Sheridan 2005). It is noted that afternoon meteorological parameters dominant this criteria since the SSC2 air masses are most dissimilar at this time (Greene 1996).

A candidate day is captured as a seed day only if all of its above meteorological variables satisfy the corresponding threshold criteria and it is successfully validated with weather maps of that particular day; if the day is not confirmed, threshold criteria for that weather type, during that seasonal window are adjusted (Sheridan 2002).

Transitional (TR) seed days are selected from slightly altered criteria, which focus on alteration of local meteorological conditions over the approximate interval of a day. For a candidate day to be registered as a TR seed day, it must possess parameter values that

are greater than the sum of the respective periodic means and 1.3 standard deviations on all three of the following [ranges]:

- diurnal dew point range (from values at 04, 10, 16, 22 h EST)
- diurnal sea level pressure range (from values at 04, 10, 16, 22 h EST), and
- diurnal wind shift (largest change between vectors at 04, 10, 16, 22 h EST).

Once the seed days are identified within their respective seasonal windows, a procedure is needed to define seed days during the remainder of the year. The sliding seed day framework conceived by (Sheridan 2002) relies on the data given below to arrange each day in the historical record into one of the seven SSC2 weather types:

- temperature at 04, 10, 16, 22 h EST
- dew point depression at 04, 10, 16, 22 h EST
- mean cloud cover (tenths) (average of 04, 10, 16, 22 h EST)
- mean sea level pressure (using values at 04, 10, 16, 22 h EST)
- diurnal temperature range (from values at 04, 10, 16, 22 h EST), and
- diurnal dew point range (from values at 04, 10, 16, 22 h EST)

The sliding seed day algorithm is exercised for all seven SSC2 weather types, on each of the 12 parameters listed above. To reflect meteorological change the seven designated air masses endure on a seasonal and daily time step at a given location, the algorithm quantifies sets of characterizing daily parameters that are prescribed

specifically to that day. Available upon its completion are daily values of the 12 parameters that offer a model description of each particular air mass. Steps involved in the calculation procedure are now detailed, and an example for 16 h EST for the MP air mass detailed in Figure 2 (as taken from Sheridan 2002). We will use Roanoke as the example.

Step 1. Select seasonal 2-week window periods. For Roanoke, the winter window is January 15 – January 28.

Step 2. For the parameter under evaluation, k, compute the long term (1948-1996) mean for season i, Xwindow(i,k), for all days within the 2-week window. In Figure 2, as computed for the winter window, this long term mean for the 16 h temperature is 2.4°C.

Step 3. Within each window for season i, identify seed days that satisfy the selection criteria for particular weather type, m (see Table 9 for MM weather type) for each year over long term (1948-1996) and calculate their mean Xseed(i,k,m). Note that over the 2-week window only a few days or none may qualify as seed days. In Figure 2, the mean 16 h EST temperature for MP seed days during the winter window, Xseed(winter,16h-temp,MP) is calculated as 1.5 degrees Celsius.

Step 3. Calculate the anomaly, A(i,k,m) = Xseed(i,k,m) – Xwindow(i,k).

Step 4. Fix each day of the year, j and obtain the long term mean, M(j,k) (normal for day j for variable k). Plot M(j,k) versus j as shown in Figure 2.

Step 5. Plot the season i, variable k, and weather type m, anomaly, A(i,k,m) from step 3 at the start day of season i window. For example, the winter anomaly will be plotted on January 15 for Roanoke. There are 4-such window start points January 15, April 15, July 15, and October 14 for Roanoke and the corresponding 4-anomalies for variable k and

weather type m are plotted. Connect these points by straight line segments as shown in Figure 2. The interpolated values between these points for day j are denoted by $\varepsilon(j,k,m)$.

Step 6. Corresponding to day j, variable k, and weather type m, the value $Z(j,k,m)$ is obtained as the sum of $X(j,k)$ and $\varepsilon(j,k,m)$; i.e. $Z(j,k,m) = X(j,k) + \varepsilon(j,k,m)$ in which $\varepsilon(j,k,m)$ is the linearly interpolated value from step 5. Plot $Z(j,k,m)$ versus j. Fit a tenth-order polynomial curve to the $Z(j,k,m)$ values against j (step 6). The polynomial is fitted to the curve comprised of the "central" and two surrounding half years so as to make reliable the values toward the marginal ends of the "central" year. It is noted that for k = 1,2,…, 12 and m = 1,2,…,7, there are 84-curves. Let $ZC(j,k,m)$ be the value taken from the curve for day j. Using $ZC(j,k,m)$, calculate the mean $\mu(k,m)$ and the standard deviation $\sigma(k,m)$ by

$$\mu(k,m) = \sum_{j=1}^{365} ZC(j,k,m) \qquad \text{for } k = 1,2,\ldots,12; \text{ and } m = 1,2,\ldots,7 \tag{1}$$

$$\text{and } \sigma(k,m) = \sqrt{\sum_{j=1}^{365} [ZC(j,k,m) - \mu(k,m)]^2 / (365-1)} \quad \text{for } k = 1,2,\ldots,12; \text{ and } m = 1,2,\ldots,7 \tag{2}$$

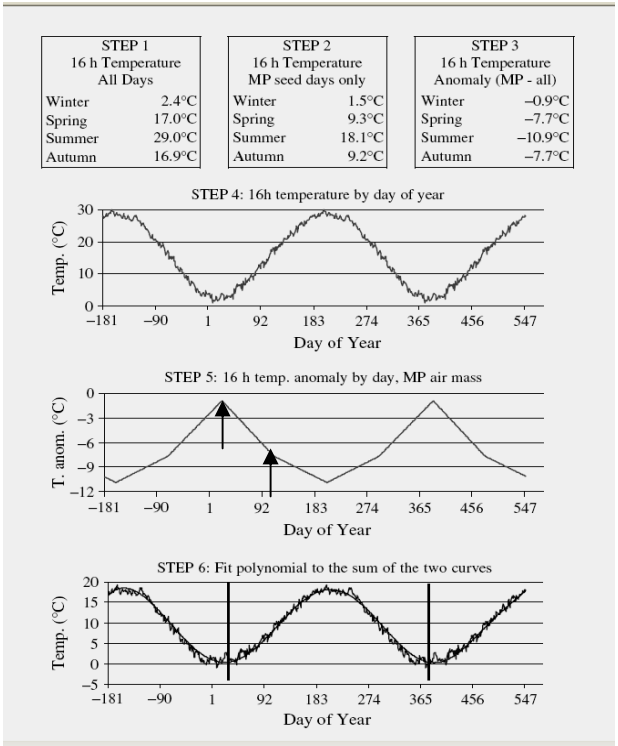

Figure 2. Adapted from (Sheridan 2002) of the sliding seed day calculation for 16 h EST temperature for the MP weather type at Wilmington, DE.

Roanoke's historical meteorological record can now be adapted into a daily weather type calendar by using the characteristic daily sets of the 12 air mass-distinguishing parameters provided by the sliding seed day calculation in the following computation:

$$h(i,m) = \sum_{k=1}^{12} \frac{[x(i,k) - \mu(k,m)]^2}{\sigma(k,m)} \qquad \text{for m = DP, DM, DT, MP, MM, MT} \qquad (3)$$

where, h(m) is the total "error score" for weather type m, x(i,k) the observed value of current day, i, variable k, and $\mu(k,m)$ and $\sigma(k,m)$ being the mean and standard deviation belonging to variable k for weather type m as found with the fit of the tenth-order polynomial from eqs (1) and (2). Equation (3) is also used for the TR weather type,

although only on its three associated variables – diurnal values of: dew point range, sea pressure range, and wind shift. The non-TR weather type which possesses the minimum error score is then evaluated against the error sum computed on TR. Each day, i, in the historical record takes on the weather type (including the possibility of TR) for which the corresponding computed error score is the least. Figure 3 portrays this procedure for a day, IDAY, at Wilmington, DE (Sheridan 2005). The IDAY under review is assigned as DM since its error sum is the least among all the weather types, including TR.

Weather	Actual	DP		DM		DT		MP		MM		MT	
Variable	Weather	Value	Error	Value	Error	Value	Error	Value	Error	Value	Error	Value	Error
4am T	7	-1	3	6	0	8	0	4	0	9	0	13	2
4am T-DP	5	5	0	6	0	5	0	2	1	2	1	2	1
10am T	10	4	1	11	0	19	3	4	1	10	0	17	2
10am T-DP	9	10	0	11	0	14	1	2	3	2	3	4	1
4pm T	13	8	1	15	0	25	5	5	2	11	0	20	2
4pm T-DP	12	14	0	15	0	21	2	2	3	2	3	7	1
10pm T	7	2	1	5	0	14	3	4	0	9	0	14	2
10pm T-DP	6	8	0	4	0	10	1	2	1	1	2	3	1
T Range	6	9	0	10	1	17	7	2	1	3	1	8	0
DP Range	1	4	1	5	1	4	1	3	0	3	0	4	1
Pressure	1005	1020	4	1017	2	1019	2	1015	1	1019	3	1015	1
Cloudiness	7	3	1	4	1	2	2	10	1	10	1	7	0
Error Sum			12		5		27		14		14		14

Weather	Actual	DM		TR	
Variable	Weather	Value	Error	Value	Error
DP Range	1	5	1	14	14
P Range	8	6	0	15	3
Wind Shift	22	8	28	10	21
Error Sum			29		38

Figure 3. Weather type assignment for March 29, 2000 at Wilmington, DE. (Reproduced from Sheridan 2005).

Application of SSC2 for Roanoke

Interannual and interseasonal fluctuation of global teleconnections, including the El Nino Southern Oscillation (ENSO), North Atlantic Oscillation (NAO), Artic

Oscillation (AO), and Pacific/North American pattern (PNA), is a dominant mode of their variability (Philander 1990; Davis et al 1996). Appendix A provides a description of these indices. It follows that regional meteorological and hydrological parameters possessing variability on a daily or weekly time scale render these teleconnections as possible predictors. Models which condition regional weather and hydrologic parameters on global circulations are referred to as "downscaling" or "weather state" models (Hughes et al. 1999). This study employs indices that define phases of the ENSO, NAO, and AO as conditional variables for spring and winter weather pattern distributions at Roanoke; daily winter weather pattern distributions are arrived at through a stationary Markov framework. A methodology is also developed for the prediction of total winter precipitation based on projections of winter weather pattern distribution.

Discerning Seasonal Teleconnective Predictors

Monthly SOI, NAO, AO, and PNA indices are used to calculate their fall and winter averages for each year from 1950 through 2003. The fall averages of SOI, NAO, AO, and PNA indices are individually regressed against that year's winter precipitation total. Similarly, the winter average index values are regressed against the subsequent spring precipitation totals. A step-wise regression is used to identify the indices that explain the most variability in the precipitation totals. The regression analysis is applied to seven stations in southwest Virginia: Bedford, Blacksburg, Roanoke, Lafayette, Buchanan, Pulaski, and Rocky Mount. Reported monthly index values from September, October, and November of the current year were averaged as the fall value, while the

index value belonging to December of the previous year and the following year's January and February values were averaged as the winter average index value. The fall index values are used as the independent variables against the winter precipitation. The dependent variable, winter precipitation, is defined as the sum of the Dec-Jan-Feb 90-day [daily] precipitation totals. Missing daily precipitation data for each station were replaced by the daily average obtained distinctively for the month during which the missing day arose.

Using MiniTab™, the step-wise regression is performed to reveal which [group of] indices from the previous season best explained the variability in the current season's aggregated station precipitation. Additional runs were performed using only November and February index values evaluated against winter and spring total precipitation respectively. The stepwise regression procedure is based on the contribution of adding a variable to the regression sum of squares. An F-statistic determines whether the contribution is significant at a chosen significance level. In this study a significance level of 0.15 is used.

Table 10. Stepwise Regression Results for Seasonally-Aggregated Precipitation and Seasonally-Averaged and Monthly Indices

	Predictor Variables in Final Model				
Response Variable	**SOI** in Final Model?	**NAO** in Final Model?	**PNA** in Final Model?	**AO** in Final Model?	R^2 (Final Model)
Bed_WP	FallAvgSOI			FallAvgAO	11.21
Bburg_WP	None				-
ROA_WP	FallAvgSOI			FallAvgAO	**15.84**
Laf_WP	FallAvgSOI				8.79
Buch_WP	FallAvgSOI		FallAvgPNA		10.77
Pul_WP	FallAvgSOI		FallAvgPNA		10.24
Rocky_WP	FallAvgSOI				10.2
Bed_WP	NovSOI			NovAO	12.41
Bburg_WP				NovAO	5.44
ROA_WP	NovSOI			NovAO	**17.0**
Laf_WP	NovSOI				7.41
Buch_WP				NovAO	6.75
Pul_WP	NovSOI	NovNAO			12.75
Rocky_WP	NovSOI			NovAO	14.88
MeanAreal_WP	NovSOI			NovAO	12.31
MeanAreal_WP	FallAvgSOI				7.95
Bed_SP	AvgWinterSOI			AvgWinterAO	**20.38**
Bburg_SP	AvgWinterSOI			AvgWinterAO	**23.05**
ROA_SP	AvgWinterSOI			AvgWinterAO	**30.22**
Laf_SP	AvgWinterSOI		AvgWinterPNA	AvgWinterAO	**27.62**
Buch_SP	AvgWinterSOI			AvgWinterAO	**20.04**
Pul_SP	AvgWinterSOI			AvgWinterAO	11.05
Rocky_SP	AvgWinterSOI			AvgWinterAO	**34.59**
MeanAreal_SP	AvgWinterSOI			AvgWinterAO	**29.31**
MeanAreal_SP	FebSOI				14.04
Bed_SP	FebSOI				8.6
Bburg_SP			FebPNA		10.7
ROA_SP	FebSOI				**18.59**
Laf_SP	FebSOI				8.96
Buch_SP	FebSOI				12.29
Pul_SP			FebPNA		8.8
Rocky_SP	FebSOI		FebPNA	FebAO	**24.83**

* WP, SP represent winter and spring total precipitation respectively at Bedford, Blacksburg, Roanoke, Lafayette, Buchanan, Pulaski, and Rocky Mount

It is evident from the coefficient of multiple determination, that the fall averages of the SOI and AO explain nearly 16% of the variability in ensuing winter accumulated precipitation at Roanoke, while nearly 35% and 30% of the spread in Rocky Mount and Roanoke spring precipitation, respectively, can be rationalized by the preceding winter means of the SOI and AO. In fact, the November SOI and AO unaided are able to describe 17% of the variability in Roanoke winter precipitation.

Roanoke precipitation was selected for entry into a weather type forecasting scheme given its nearly comprehensive data set, high stepwise regression R^2 values when assessed against the previous season's SOI and AO, and since the adopted SSC2 weather type calendar represents historical meteorological conditions observed at Roanoke. All raw data used in this analysis, including daily precipitation and monthly SOI and AO index values, are available from the author upon request.

Roanoke Seasonal Weather Type Distributions Conditioned on the SOI and AO of the Previous Season

As shown in Table 11, the SOI and AO indices are divided into 3 ranges each to yield 9 combinations. For each of these combinations, a 7x7 daily winter weather transition matrix is obtained by employing the SSC2 weather type classification scheme as follows. First, each year's winter is associated with one of the nine SOI-AO combinations. For example, Table 12 shows the fall season of years 1953, 1977, 1982, and 1994 fall under the El Nino-AO+ category. Secondly, the subsequent winter (e.g. 1953 December, 1954 January and February 1954 belongs to 1953 fall) daily weather

type sequence is assembled into an array. Table 12 shows the years identified by each of the nine ENSO-AO categories.

Table 11. Phases of SOI and AO to Condition Seasonal Weather Type Arrays at Roanoke

Value Assignment	Phase	Value Assignment	Phase
SOI <= 5	La Nina	AO <= 0.25	Postive
-5 < SOI < 5	ENSO Neutral	-0.25 < AO < 0.25	AO Neutral
SOI <= -5	El Nino	AO <= -0.25	Negative

Table 12. Years Identified as Corresponding Fall ENSO-AO Category

ENSO-AO Category	Identified Years of Fall ENSO-AO Category
El Nino, AO+	1953, 1977, 1982, 1994
El Nino, AO Neutral	1963, 1969, 1987, 1991, 1992, 1993
El Nino, AO-	1951, 1957, 1965, 1972, 1997, 2002
ENSO Neutral, AO+	1961, 1967, 1978, 1983, 1986, 1989, 1990, 2001
ENSO Neutral, AO Neutral	1954, 1958, 1985
ENSO Neutral, AO-	1952, 1960, 1966, 1968, 1976, 1979, 1980, 1981, 1984, 1995, 1996
La Nina, AO+	1956, 1971, 1975, 1988
La Nina, AO Neutral	1950, 1964, 1970, 1973, 1999
La Nina, AO-	1955, 1959, 1962, 1974, 1998, 2000

Third, subsequent to arrangement of winter and spring weather type arrays by the previous season's SOI-AO combination, a stationary Markov chain is applied to each weather type array. Stationarity implies that the likelihood the weather type chain encounters a daily transition from state i to j is independent of the time at which the step is executed. For instance, the probability the chain relocates to and from any of the seven discrete weather states remains unchanged for all December, January, and February days

when evaluating the winter weather type process. Within each of the nine distinct SOI-AO categories, all 7-individual daily weather type arrays (90 and 92 member arrays for winter and spring) are considered. The number of daily transitions from weather type i to weather type j for i,j = 1, 2, 3, 4, 5, 6, 7 is registered and the cumulative number of occurrences of each of the seven SSC2 weather types is compiled. Once these computations are completed for all arrays belonging to the current SOI-AO category, an overall 7x7 stationary transition matrix is computed, with each entry defined as:

$$entry_{i,j} = \sum_{k=1}^{N_A} \#timestransitioned_{i,j} \Big/ \sum_{k=1}^{N_A} \#occurrences_i \qquad (2)$$

for i,j = 1, 2, … 7 and N_A = number of arrays belonging to the current SOI-AO group.

For the El Nino-AO+ category, for the years 1953, 1977, 1982, and 1994, the number of transitions are as follows (read from row is day x to column in day x+1):

	DP	DM	DT	MP	MM	MT	TR	Row Sum
DP	41	12	8	19	8	0	2	90
DM	13	52	2	3	16	0	4	90
DT	3	0	1	3	1	2	4	14
MP	16	2	1	21	5	7	7	59
MM	5	12	1	12	24	0	3	57
MT	4	0	1	1	1	12	3	22
TR	7	12	0	0	3	0	2	24

from which the transition probability matrix is obtained as:

	DP	DM	DT	MP	MM	MT	TR
DP	0.4556	0.1333	0.0889	0.2111	0.0889	0.0000	0.0222
DM	0.1444	0.5778	0.0222	0.0333	0.1778	0.0000	0.0444
DT	0.2143	0.0000	0.0714	0.2143	0.0714	0.1429	0.2857
MP	0.2712	0.0339	0.0169	0.3559	0.0847	0.1186	0.1186
MM	0.0877	0.2105	0.0175	0.2105	0.4211	0.0000	0.0526
MT	0.1818	0.0000	0.0455	0.0455	0.0455	0.5455	0.1364
TR	0.2917	0.5000	0.0000	0.0000	0.1250	0.0000	0.0833

The corresponding steady state probabilities are evaluated using the stationary solution from (Ross 1980):

$$\lambda_j = \sum_{i=1}^{7} \lambda_i p_{i,j} \tag{3}$$

which is subject to the following constraint:

$$\sum_{j=1}^{7} \lambda_j = 1.0$$

where λ_j = the steady state probability of occurrence for weather type j and $p_{i,j}$ = stationary probability for a daily transition from weather type i to j, which is the i^{th} row, j^{th} column entry in the mean daily transition matrix for a particular SOI-AO arrangement. Steady state weather type probability distributions for both the winter and spring seasons for all nine of the SOI-AO conditions are given in Tables 13 and 14.

Table 13. Winter Stationary Steady State Weather Type Distributions as Conditioned by Fall Phases of the SOI and AO

El Nino and AO+						
DP	DM	DT	MP	MM	MT	TR
0.248358	**0.256764**	**0.038777337**	**0.16557093**	**0.165400941**	**0.055403983**	**0.06972486**
El Nino and AO Neutral						
DP	DM	DT	MP	MM	MT	TR
0.282407	**0.22929**	**0.031961479**	**0.12729487**	**0.199510162**	**0.039955884**	**0.089580656**
El Nino and AO-						
DP	DM	DT	MP	MM	MT	TR
0.280675	**0.191936**	**0.037678659**	**0.18740603**	**0.179720759**	**0.056748808**	**0.065834655**
La Nina and AO+						
DP	DM	DT	MP	MM	MT	TR
0.253883	**0.175741**	**0.070561005**	**0.18280592**	**0.126053275**	**0.094363595**	**0.096592485**
La Nina and AO Neutral						
DP	DM	DT	MP	MM	MT	TR
0.250659	**0.217577**	**0.07066642**	**0.11720001**	**0.169100338**	**0.08871296**	**0.08608397**
La Nina and AO-						
DP	DM	DT	MP	MM	MT	TR
0.288078	**0.228852**	**0.050808974**	**0.13940568**	**0.144215817**	**0.048942793**	**0.099696527**
ENSO Neutral and AO+						
DP	DM	DT	MP	MM	MT	TR
0.304005	**0.197915**	**0.048529884**	**0.12745488**	**0.172051177**	**0.068431673**	**0.081611934**
ENSO Neutral and AO Neutral						
DP	DM	DT	MP	MM	MT	TR
0.288232	**0.246708**	**0.015032492**	**0.12364627**	**0.176552278**	**0.060013173**	**0.08981588**
ENSO Neutral and AO-						
DP	DM	DT	MP	MM	MT	TR
0.248562	**0.266718**	**0.046876178**	**0.1211024**	**0.176714455**	**0.050996815**	**0.089030171**

Table 14. Spring Stationary Steady State Weather Type Distributions as Conditioned by Winter Phases of the SOI and AO

El Nino and AO+						
DP	DM	DT	MP	MM	MT	TR
0.279173	**0.162954**	**0.087048647**	**0.14928422**	**0.11623384**	**0.137384273**	**0.0679213**
El Nino and AO Neutral						
DP	DM	DT	MP	MM	MT	TR
0.243711	**0.186825**	**0.128748793**	**0.17689141**	**0.098018619**	**0.088661626**	**0.077143823**
El Nino and AO-						
DP	DM	DT	MP	MM	MT	TR
0.293902	**0.098077**	**0.11107711**	**0.12269824**	**0.142952186**	**0.144922286**	**0.08637113**
La Nina and AO+						
DP	DM	DT	MP	MM	MT	TR
0.346193	**0.119005**	**0.122030122**	**0.10601829**	**0.108363814**	**0.099645568**	**0.098744153**
La Nina and AO Neutral						
DP	DM	DT	MP	MM	MT	TR
0.245618	**0.172591**	**0.11579986**	**0.11618995**	**0.081480474**	**0.13329235**	**0.135028304**
La Nina and AO-						
DP	DM	DT	MP	MM	MT	TR
0.299196	**0.157702**	**0.11915345**	**0.10182656**	**0.099782521**	**0.103415374**	**0.118923919**
ENSO Neutral and AO+						
DP	DM	DT	MP	MM	MT	TR
0.26656	**0.160222**	**0.059437283**	**0.15864146**	**0.102896391**	**0.146472392**	**0.105769998**
ENSO Neutral and AO Neutral						
DP	DM	DT	MP	MM	MT	TR
0.282427	**0.171024**	**0.110019434**	**0.08420312**	**0.102702832**	**0.158011043**	**0.091613268**
ENSO Neutral and AO-						
DP	DM	DT	MP	MM	MT	TR
0.282694	**0.14548**	**0.132890806**	**0.1025666**	**0.0944889**	**0.138324209**	**0.103555692**

A Forecast of Total Winter Precipitation from SSC2 Weather Type Distribution

Serving as an initial attempt of optimizing the purchase of road maintenance materials, Roanoke winter precipitation was entered into a reduction procedure that predicts total winter precipitation based on phases of the SOI and AO observed the previous fall. Using the steady state weather type distributions for winter reported in Table 13, the number of winter days spent in each of the seven weather types can be computed considering the per winter day occurrence frequency these probabilities represent. From Table 13, using the steady state probability of 0.165557 for MP days conditioned on the El Nino-AO+ fall category, we estimate that there are 15 (0.165557*90) MP days during the subsequent winter. If the average winter precipitation for the MP weather type under El Nino-AO+ is known (in addition to all 6 remaining weather types, then the total expected precipitation can be ascertained.

The desired average precipitation estimate pertaining to the winter subsequent to a fall ENSO-AO category is obtained as follows, with El Nino-AO+ used here for explanation. Daily precipitation values are pooled together across the [four] years (1953, 1977, 1982, or 1994) belonging to each ENSO-AO category (El Nino-AO+), and are arranged by SSC daily weather type. Identified years are named for that year's fall season. Then, for each SSC weather type, wet days are separated from dry days and a probability density function (pdf) is fitted to each wet day array. There are seven of these wet day arrays, one for each SSC weather type based on pooled data for 1953, 1977, 1982, and 1994. The representative wet day precipitation value is taken as the 50^{th} percentile (median) wet-day daily precipitation value pertaining to a particular ENSO-AO

category and SSC weather type. Regarding wet MP days, for instance, in the winter following an El Nino-AO+ fall, this estimate comes from the pdf fitted to all MP wet days that were reported in 1953, 1977, 1982, and 1994. Table 15 provides all wet-day precipitation values for each of the seven SSC weather types for the El Nino-AO+ category that were pooled from 1953, 1977, 1982, and 1994.

Table 15. Winter Wet-Day Precipitation Values by SSC Weather Type for the Fall El Nino-AO+ Category, pooled from 1953, 1977, 1982, and 1994 (inches*100)

SSC Daily Weather Type								
DP	DM	DT	MP	MP cont'd	MM	MM cont'd	MT	TR
1	4	2	42	52	10	45	16	87
4	7	2	44	38	29	28	25	34
2	12		102	10	77	13	104	201
	2		71	36	13	8	21	5
	3		122	1	8	65	2	176
			13	140	6	9	13	10
			60	22	64	53	10	103
			5	3	4	83	202	1
			26	78	95	107	214	19
			69	83	60	25		22
			36	6	36	1		1
			54	7	186	35		89
			40	71	5	57		16
			1	7	1	37		
			8	13	4	30		
			2	28	1	76		
			54	16	22	2		
					18	34		

The total precipitation due to the i^{th} weather type during winter is calculated as follows. Total precipitation during the i^{th} weather type in winter, Tpw_i = (wet day precipitation during the i^{th} weather type in winter, Dpw_i)(# of i^{th} weather type wet days in winter, NDw_i). Further, we calculate NDw_i as = (λ_i)(# of winter days, Nw)(# of winter wet days for weather type i / # of winter days of weather type i). It is recognized that

while the product $(\lambda_i)(Nw)$ represents the number of days of weather type i in the winter under an ENSO-AO category, the final term is the fraction of the wet days in winter.

We calculate the wet day precipitation during winter for the i^{th} weather type, Dpw_i as follows. As an example, Table 16 shows the winter wet day precipitation values for the DM weather type under El Nino-AO+.

Table 16. Dry Moderate (DM) wet day precipitation Values Under the El Nino-AO+ Fall Condition (inches*100)

DM
4
7
12
2
3

By fitting suitable probability distributions to this data, we can estimate the 50^{th} percentile value, $X_{0.5}$. We take $X_{0.5}$ as the needed Dpw_i value.

Two probability density functions (pdf) are considered: shifted exponential; and 2-parameter gamma. The pdf of the shifted exponential density function (with a lower limit) is given by:

$$f(x) = \alpha e^{-\alpha(x-x_0)} \quad \text{for } x > x_0 \qquad (4)$$

$$= 0 \quad \text{elsewhere}$$

from which

$$x_{0.5} = x_o - \frac{1}{\alpha} \ln 0.5 \tag{5}$$

or

$$x_{0.5} = x_o + \frac{0.69315}{\alpha} \tag{6}$$

For each weather type, wet-day precipitation array, the gamma function is first appraised and if its shape parameter proves to be <= 1.0, a shifted exponential is applied using a threshold of 0.1. Figure 4 shows an example of a 2-p gamma fit to the MP wet-day precipitation array for the fall combination of La Nina and AO+ phase, while Figure 5 provides the DM wet-day fit to the shifted exponential distribution under the ENSO Neutral-AO negative fall scenario. For the gamma distribution, the median is evaluated from

$$0.5 = \int_0^{precip\_crit} \frac{y^{\alpha-1} e^{-y/\beta}}{\beta^{\alpha} \Gamma(\alpha)} dy \tag{7}$$

where: β = fitted scale parameter specific to each type of distribution, α = fitted shape parameter for the gamma function, y = wet day precipitation, and precip_crit = wet day precipitation positioned at 0.5 non-exceedence probability. However, since no closed-form solution is obtainable for the right hand side of equation (7), cumulative frequency distribution (CDF) ordinates are retrieved for each wet day series that fits the 2-p gamma function (Wackerly et al 2002). If no ordinate approaches 0.50, linear interpolation is

used to acquire the wet day precipitation value that complements this non-exceedence likelihood.

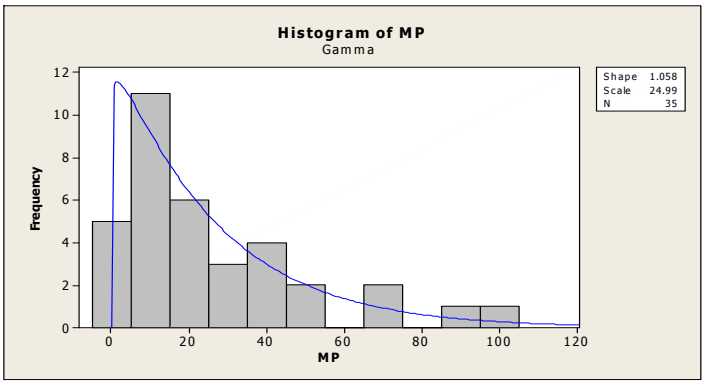

Figure 4. 2-p gamma fit with MiniTab™ for winter wet days of the Moist Polar weather type for the La Nina-AO+ fall condition.

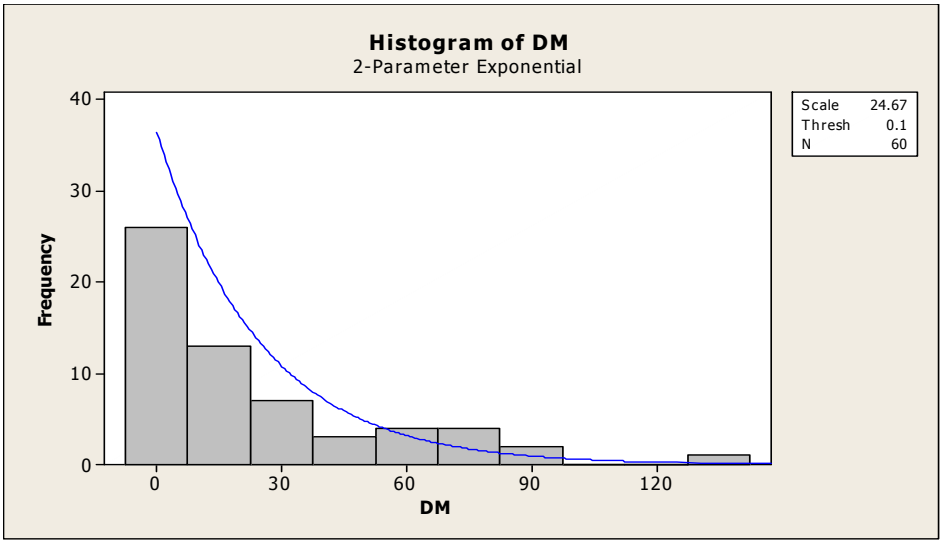

Figure 5. Shifted exponential fit with MiniTab™ for winter wet days of the Dry Moderate weather type for the ENSO Neutral-AO- fall condition.

Calculation of total precipitation contributed by the i^{th} SSC2 weather type during a winter that follows a given SOI-AO fall category is captured by:

$$precip_{SSC2_i} = precip\_crit_{SSC2_i} * P[x > 0]_{SSC2_i} * \lambda_{SSC2_i} * 90 winterdays \quad (8)$$

where: $precip\_crit_{SSC2i}$ = wet day precipitation value corresponding to 50% non-exceedence for the fit of either the 2-p gamma or shifted exponential distribution for weather type i, λ_{SSC2i} = the per winter day occurrence frequency of weather type i as computed from the stationary Markov chain, as reported in Table 13 above. The second term in equation (8) represents the fraction of the number of wet weather type i winter days from the total winter occurrence of weather type i for the given SOI-AO fall category, where x is daily winter precipitation. Summations of $precip_{SSC2i}$ for i = 1, 2, …7 offers a total winter precipitation forecast for Roanoke. Each is presented below along with $P[x>0]_{SSC2i}$ for the nine SOI-AO fall conditions:

Table 17. Results for Total Winter Precipitation, According to Fall SOI-AO Conditioning

Fall SOI-AO Condition	Total Winter Precipitation (inches)
El Nino, AO+	7.12
El Nino, AO Neutral	7.15
El Nino, AO-	8.01
ENSO Neutral, AO+	6.95
ENSO Neutral, AO Neutral	5.58
ENSO Neutral, AO-	5.30
La Nina, AO+	5.40
La Nina, AO Neutral	6.18
La Nina, AO-	5.56

Relative contributions of total winter precipitation by each SSC2 weather type as well as their respective P[x>0] and daily critical precipitation values are tabulated as shown:

Table 18. Results of Winter Precipitation Analysis with Respect to Fall SOI-AO

Fall SOI-AO Condition	Winter Results	SSC2 Weather Type						
		DP	DM	DT	MP	MM	MT	TR
El Nino, AO+	Contribution of Total Winter Precip. (%)	0.21	0.91	0.14	32.93	33.71	13.41	18.69
	P[x>0]	0.033	0.056	0.143	0.567	0.621	0.409	0.52
	precip_crit (daily inches*10^2)	2.00	5.00	2.00	27.76	25.97	46.78	40.77
El Nino, AO Neutral	Contribution of Total Winter Precip. (%)	0.59	1.11	0.19	26.97	43.75	11.02	16.38
	P[x>0]	0.046	0.048	0.235	0.623	0.596	0.571	0.542
	precip_crit (daily inches*10^2)	3.56	8.00	2.00	27.01	29.21	38.36	26.81
El Nino, AO-	Contribution of Total Winter Precip. (%)	0.88	0.86	1.37	34.39	41.28	7.21	14.00
	P[x>0]	0.053	0.037	0.300	0.616	0.667	0.400	0.694
	precip_crit (daily inches*10^2)	5.32	10.68	10.77	26.51	30.67	28.28	27.26
ENSO Neutral, AO+	Contribution of Total Winter Precip. (%)	9.54	13.13	4.49	22.84	25.79	6.62	17.59
	P[x>0]	0.194	0.257	0.229	0.440	0.385	0.367	0.517
	precip_crit (daily inches*10^2)	12.52	19.94	31.31	31.50	30.06	20.36	32.19
ENSO Neutral, AO Neutral	Contribution of Total Winter Precip. (%)	7.12	19.68	0.00	35.78	18.62	3.16	15.64
	P[x>0]	0.117	0.242	0.000	0.394	0.362	0.500	0.458
	precip_crit (daily inches*10^2)	13.09	20.39	0.00	45.52	18.07	6.53	23.54
ENSO Neutral, AO-	Contribution of Total Winter Precip. (%)	16.21	17.84	2.93	12.61	27.78	6.33	16.30
	P[x>0]	0.218	0.229	0.130	0.424	0.370	0.440	0.460
	precip_crit (daily inches*10^2)	17.61	17.20	28.22	14.46	25.02	16.60	23.44
La Nina, AO+	Contribution of Total Winter Precip. (%)	10.63	16.71	1.98	31.27	12.26	13.00	14.16
	P[x>0]	0.209	0.266	0.120	0.547	0.467	0.455	0.471
	precip_crit (daily inches*10^2)	12.04	21.48	14.00	18.77	12.51	18.19	18.69
La Nina, AO Neutral	Contribution of Total Winter Precip. (%)	13.09	25.18	7.84	20.50	12.56	7.89	12.94
	P[x>0]	0.198	0.255	0.290	0.500	0.355	0.359	0.500
	precip_crit (daily inches*10^2)	18.09	31.14	26.22	24.01	14.36	17.01	20.64
La Nina, AO-	Contribution of Total Winter Precip. (%)	19.29	11.88	0.61	16.56	27.24	4.65	19.76
	P[x>0]	0.292	0.211	0.111	0.432	0.416	0.308	0.566
	precip_crit (daily inches*10^2)	14.16	15.18	6.72	16.97	28.08	19.09	21.64

Testing for Significant Differences of Winter Wet Day Arrays

Winter wet day arrays for a fixed weather type are tested across SOI-AO fall conditions to detect differences in their distribution functions for the varying fall teleconnective treatments. Serving as a means for testing non-parametric data, as is

presumed for the wet day arrays, is the Mann-Whitney test. This procedure employs ranks of ordered arrays, opposed to precipitation data themselves, for admission into the following hypothesis structure. This rank-based test is guided by the null and alternative hypothesis where F(x) and G(x) are the distribution functions of the random variables X and Y respectively (Conover 1999):

$$H_o: F(x) = G(x) \qquad \text{for all } x$$

$$H_1: F(x) \neq G(x) \qquad \text{for some } x.$$

The test statistic, T remains defined as long as only a few precipitation values are equal between arrays:

$$T = \sum_{i=1}^{n} R(X_i) \tag{9}$$

where: X = a random variable denoting wet day precipitation within either of the SOI-AO groupings, for the current weather type, $R(X_i)$ = rank assigned to X_i, and n = the number of members belonging to the array of variable X (Conover 1999). Each combination – $({}_sC_w)$ with s = 7 SSC2 weather types and w = 2 current wet day arrays evaluated against one another – of weather types enter into the Mann-Whitney framework and are tested at a 95% confidence level. Listed below are those fall teleconnective combinations for which a significant difference in distribution functions (i.e. null hypothesis was rejected) between winter wet day arrays were seen, as arranged by SSC2 weather type.

Table 19. SOI-AO Fall Combinations Corresponding to Occurrence of a Significant Difference in Distribution Functions Between Their Winter Wet Day Arrays, for Each SSC2 Weather Type (α = 0.05).

DP	MP
EN,AO+ &amp LN, AONeut	EN,AO+ &amp ENSONeut,AO-
EN,AO+ &amp LN, AO-	EN,AO+ &amp LN,AO-
EN,AO+ &amp ENSONeut,AONeut	EN,AONeut &amp ENSONeut,AO-
EN,AO+ &amp ENSONeut,AO-	ENSONeut,AO+ &amp ENSONeut, AO-
EN,AONeut &amp LN,AONeut	**MM**
EN,AONeut &amp LN,AO-	EN,AONeut &amp LN,AO+
EN,AONeut &amp ENSONeut,AO+	EN,AONeut &amp LN,AONeut
EN,AONeut &amp ENSONeut,AONeut	EN,AO- &amp LN,AO+
EN,AONeut &amp ENSONeut,AO-	EN,AO- &amp LN,AONeut
EN,AO- &amp LN,AONeut	ENSONeut,AO+ &amp LN,AO+
EN,AO- &amp LN,AO-	ENSONeut,AO+ &amp LN,AONeut
EN,AO- &amp ENSONeut,AO-	LN,AO+ &amp LN,AO-
LN,AO+ &amp LN,AO-	LN,AONeut &amp LN,AO-
LN,AO+ &amp ENSONeut,AO-	**MT**
DM	EN,AO+ &amp ENSONeut,AO-
EN,AO+ &amp LN,AONeut	ENSONeut,AO+ &amp ENSONeut,AONeut
EN,AONeut &amp LN,AONeut	**TR**
ENSONeut,AO- &amp LN,AONeut	ENSONeut,AO+ &amp LN,AO-
LN,AONeut &amp LN,AO-	
DT	
NONE	

* Phase abbreviations: "EN" – El Nino, "LN" – La Nina, "ENSONeut" – ENSO Neutral, "AONeut" – AO Neutral.

Summary

As discussed in the Synoptic Scale Classification portion of this chapter, the most critical daily surface meteorological conditions – temperature, dew point, cloud cover, and sea level pressure - at Roanoke are captured by the SSC2. The historical series of SSC2 weather types reported for Roanoke has been employed in this study as a means to relate global teleconnections, which encompass vast regions of the Northern Hemisphere,

to local precipitation. As reported in Table 10, from the winter averages of four teleconnections considered (SOI, PNA, NAO, AO), the SOI and AO explained the most variability in subsequent spring total precipitation at Roanoke. When winter total precipitation was regressed against previous fall averages of these four teleconnections, the most reliable model also included the SOI and AO. From steady state analysis, this study also found that springs that follow winters possessing the El Nino-AO- condition, on average, display a higher incidence (0.41) of the three SSC2 moist weather types (MP, MM, MT) relative to the other eight SOI-AO categories (see Table 14). When this same El Nino-AO- condition is seen in the fall season, the subsequent winter at Roanoke can expect a higher frequency of the moist SSC2 weather types (0.42 from Table 13). Dry spring conditions, as represented by the total occurrence probability of the three dry weather types (DP, DM, DT) in Table 14, showed a maximum likelihood (0.59) when the preceding winter demonstrated the La Nina-AO+ condition. This resulted in large part to the high incidence (0.35) of Dry Polar (DP) spring days following this La Nina-AO+ winter condition. When a fall El Nino and the negative phase of the AO unite, the procedure used in this study shows (Table 17) that an increase in total winter precipitation, 8.01 inches, is evident. This maximum winter precipitation value is congruent with the high occurrence of the three SSC2 moist weather types when the fall season is described with El Nino-AO-.

References

Bergeron, T. 1930. Richtlinien einer dynamishen klimatologie. Met. Zeitung Vol. 47. pp. 246-262

Conover, W.J. 1999. Practical Non-Parametric Statistics. John Wiley and Sons Inc.

Davis, E.R., Hayden, B.P., Gay, D.A., Phillips, W.L., Jones, G.V. 1996. The North Atlantic Subtropical Anticyclone. J. Climate. pp 728-743.

Greene, J.S. 1996. A synoptic climatological analysis of summertime precipitation intensity in the eastern United States. Physical Geography. Vol. 17. pp. 401-418.

Hughes, J. P., Guttorp, P. 1999. A non-homogeneous hidden Markov model for precipitation occurrence. Applied Statistics. Vol. 48. pp. 15-30.

Kalkstein, L.S. and Greene, J.S. 1997. An evaluation of climate/mortality relationships in large U.S. cities and the possible impacts of a climate change. Environmental Health Perspectives. Vol. 105. pp. 84-93.

Kalkstein, L.S., Nichols, M.C., Barthel, C.D., Greene, J.S. 1996. A new spatial synoptic classification: application to air-mass analysis. International Journal of Climatology. Vol. 16. pp. 983-1004.

Philander, S.G. 1990. El Nino, La Nina, and Southern Oscillation. Academic Press. pp.1-56.

Ross, S.M. 1980. Probability and Mathematical Statistics: Introduction to Probability Models. Academic Press. pp. 1-146.

Sheridan, S.C. 2002. The Redevelopment of a Weather-Type Classification Scheme for North America. Inter. J. of Climatology. pp. 51-68.

Sheridan, S.C. 2005. Electronic personal communication: “Civil Engineering Research Using SSC2.”

Chapter 3: Global Teleconnections and Southwestern Virginia Precipitation

Introduction

This portion of the study describes spatial variability of seasonal precipitation in southwest Virginia in a context that incorporates global teleconnections (through AO, PNA, NAO, and ENSO) and frontogenesis. It is anticipated that the insight gained would aid identification will help identify groups of daily precipitation stations that demonstrate similar winter responses to changes in these teleconnections – so called homogeneous stations.

The Arctic Oscillation (AO) defines the exchange of mass in the atmosphere between polar regions and the midlatitudes, and also has been shown to encompass the North Atlantic Oscillation (NAO) (D'Aleo 2002). Outlining large-scale variation in geopotential heights in the upper atmosphere, predominately over the northern Pacific Ocean, northwestern Canada, and the southeastern United States, the Pacific North American pattern (PNA) dictates whether zonal or meridional flow prevails over North America. The El Nino-Southern Oscillation (ENSO) describes the zonal shift of anomalously warm sea-surface temperatures (SSTs) and the corresponding to atmospheric pressure variation in the tropical Pacific Ocean. Three phases of each teleconnection are used in this analysis. Details into these four teleconnections, including numerical bounds discriminating each teleconnection phase, are provided in Appendix A.

Winter storm tracks over North America are generally directed by the polar and subtropical branches of the jet stream since these high-speed currents of air in the upper

atmosphere are inherently linked to locations of broad high and low pressure regions throughout the northern hemisphere (D'Aleo 2002). This immense spatial distribution of surface pressure is initiated by uneven heating of the Earth (Thompson 1996). Large-scale atmospheric circulation associated with global teleconnections can energize or lessen the strength of the polar and/or subtropical jet streams, while also serving as their primary steering mechanism (NOAA 2005B). From their connection with the polar and subtropical jet streams, it follows that teleconnections such as the AO, PNA, NAO, and ENSO help dictate the character of storms that prevail in southwest Virginia for a given winter. The following factors are typically considered to discriminate between storm types passing through a given area: air mass source regions, air mass modification, upstream regeneration, displacement speed, precipitable water content, local atmospheric stability, and topography (UCAR 2005).

A substantial portion of Virginia's precipitation arrives from storms associated with warm and cold fronts frequently occurring during winter months when the temperature gradient poleward from the subtropics is most severe (Hayden 1979). A cold front is conceived when cold air originating in the polar latitudes, converges into the midlatitudes from the north, while warm air gliding over cold air induces an associated warm front – such translation of air according to (Nielson-Gammon 2002) occurs spontaneously in regions with a large-scale, latitudinal, temperature gradient. Zonal westerly flow, as forced by the Coriolis effect in the midlatitudes, prompts eddy formation when these large meridional temperature gradients arise. The induced disturbance is amplified when thermal energy converts to kinetic energy, forming troughs and ridges of low and high pressure throughout the northern hemisphere (Hasse and

Dobson 1986). In the region where the cold and warm fronts intersect (vertex), circulatory wind speed is enhanced with a reduction in pressure, manifesting the formation of a midlatitude, or extratropical, cyclone (Wiesner 1970).

Although the spatial precipitation distribution brought into a non-maritime area by a midlatitude cyclone is also dependent on baroclinic stability (which reflects the properties of the air masses associated with the cyclone), significant precipitation is typically observed north of the warm front as well as behind and in the vicinity of the low pressure (Nielson-Gammon 2002). Precipitation is likely to be more persistent and spatially extensive ahead of the warm front as warmer air ascends at a less severe slope (requiring more travel time) (Wiesner 1986).

Study Data

In this study, precipitation data from the following seven stations in southwestern Virginia are considered: Bedford, Blacksburg, Roanoke Airport, Lafayette, Buchanan, Pulaski, and Rocky Mount. Each station is highlighted in Figure 6.

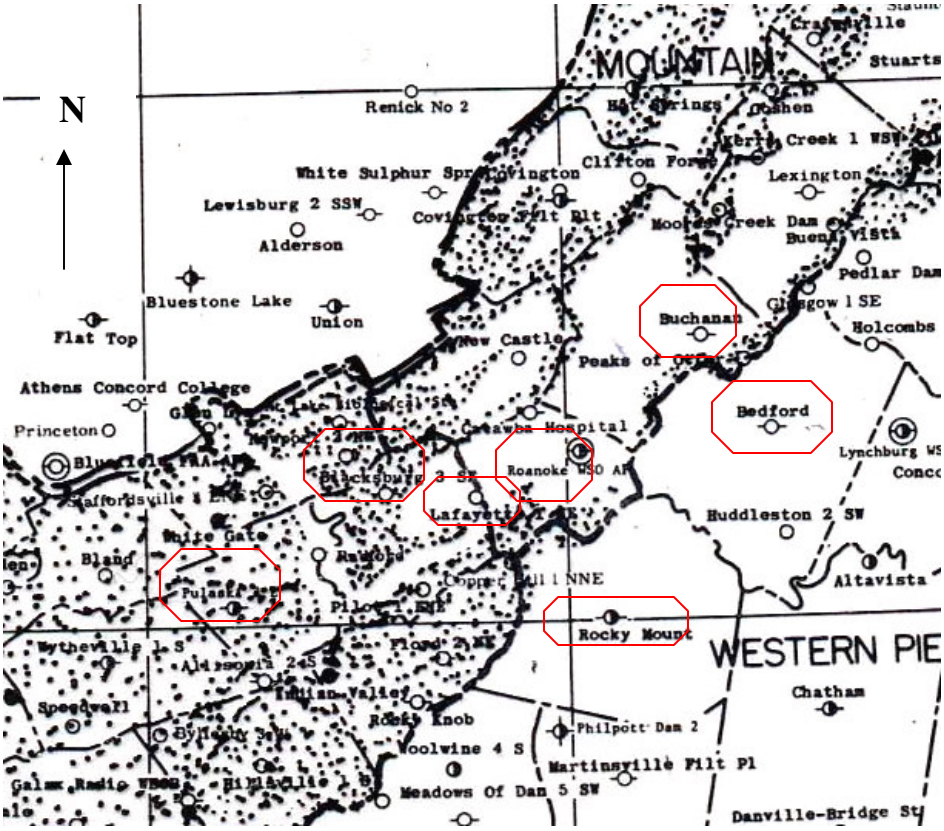

Figure 6. Seven precipitation stations in southwestern Virginia, with mountains over 1,450 feet high represented by points. (Reproduced from Hayden 1979)

Frontal-Precipitation Days

Days in which all the seven stations received precipitation are extracted for each winter from 1950-2003 and are referred to as "frontal-precipitation days". The winter season for year i is composed of December of year i-1, January of year i, and February of year i (DFJ) which is consistent with how (NOAA 2005A and Greenland 2001) defined winter. It is assumed that the "frontal-precipitation" constraint promotes the capture of a majority of the frontal events encountered in the region, while allowing days of purely convective, localized precipitation to be excluded. All station precipitation values

belonging to the array reported for each of these frontal-precipitation days are ranked from 1 through 7, where the station receiving the least (most) precipitation relative to that day's spatial distribution is assigned a rank of 1 (7). If two stations received equal precipitation for a given day, initially both receive the mean of the two boundary ranks, but then both are rounded down to the nearest integer rank. This encourages a station to achieve a lower than deserved rank. For example, precipitation ranks assigned to these 7 stations for the frontal-precipitation day of December 21, 1999 are shown in Table 20. Table 20 lists each station's recorded precipitation, bounding ranks, initial ranking, and final (rounded down) ranking. For this example, stations Rocky Mount and Bedford have a tie and the corresponding bounding ranks are 6 and 7.

Table 20. Precipitation Ranking Scheme used for all Frontal-Precipitation Days in Winter

	Precipitation (inches*100)	Bounding ranks	Initial Rank	Final Rank
Bedford	24	(6,7)	6.5(=[6+7]/2)	6 (rounded down from 6.5)
Blacksburg	16	NA	5	5
Roanoke	9	NA	4	4
Lafayette	8	NA	3	3
Buchanan	7	NA	2	2
Pulaski	3	NA	1	1
Rocky Mount	24	(6,7)	6.5	6

Upon ranking of each frontal-precipitation day, the number of occurrences of each rank for every station is summed over all frontal-precipitation days belonging to the current winter year. The acquired frequency histogram data permits a between-station spatial assessment for every winter in the record. Table 21 shows results obtained for the

1950-1951 winter, where out of the ten frontal-precipitation days belonging to this winter, the maximum precipitation relative to these seven stations (rank of 7) was reported for Bedford on two days.

Table 21. Precipitation spatial rank occurrence for each station, for frontal-precipitation days during winter 1950-1951 (# days)

Station	Station Precipitation Rank						
	1*	2*	3*	4	5**	6**	7**
Bedford	0	0	2	0	1	5	2
Blacksburg	1	0	2	3	1	1	2
Roanoke	3	1	2	2	1	1	0
Lafayette	4	6	0	0	0	0	0
Buchanan	0	2	0	1	2	0	5
Pulaski	2	0	1	3	3	1	0
Rocky Mount	0	1	3	2	1	2	1

* Dry Rank; ** Wet Rank

"Dry rank" is a relative term assigned to three stations that experienced less precipitation as compared to the other four stations during a specific frontal precipitation day in a winter season. For each winter and station, summations are computed for the number of dry rank (1-3) and wet rank (5-7) days and absolute differences are evaluated, separately for dry and wet rank summations, between every two station combination ($_7C_2$). The purpose of this summation is to investigate potential signals in spatial frontal-precipitation trends that may be linked to winter teleconnection conditions signals – i.e. if one or more stations tend to show wetter or drier responses during frontal events in El Nino-AO relative to the remaining stations. This absolute difference computation is shown in equations (1) and (2) for dry (X) and wet (Y) ranks between stations i and j respectively for winter t, where k demarks the current rank.

$$X_{i,j(t)} = \left| \sum_{k=1}^{3} dry\_days_{k(t),i} - \sum_{k=1}^{3} dry\_days_{k(t),j} \right| \qquad \text{for i} \neq \text{j} \tag{1}$$

For example, from Table 21, $X_{\text{Bedford, Blacksburg (winter 1950-'51)}} = | 2 - 3 | = 1$

$$Y_{i,j(t)} = \left| \sum_{k=5}^{7} wet\_days_{k(t),i} - \sum_{k=5}^{7} wet\_days_{k(t),j} \right| \quad \text{for i} \neq \text{j} \tag{2}$$

Likewise, from Table 21, $Y_{\text{Bedford, Blacksburg (winter 1950-'51)}} = | 8 - 4 | = 4$. These differences are then normalized by the number of frontal-precipitation days observed for winter t, and the maximum values ($NORM(X)_{max(t)}$, $NORM(Y)_{max(t)}$) are retained from the set of ${}_7C_2$ dry and wet possibilities; shown in equation (3) is normalization of the dry rank case for winter t between stations i and j.

$$NORM(X)_{(t)_{i,j}} = \frac{X_{i,j(t)}}{count(synoptic\_precip\_days)_{(t)}} * 100\% \quad \text{for i} \neq \text{j} \tag{3}$$

As an example for equation (3), $NORM(X)_{\text{Bedford,Blacksburg (winter 1950-'51)}} = 1/10 * 100 = 10\%$. Large values of NORM(X) (NORM(Y)) for a particular winter demonstrates that one of the included stations received more (less) precipitation during frontal events relative to its paired station during that winter. When more than one station-combination share the maximum value of $NORM(X)_{max(t)}$ for dry ranks and $NORM(Y)_{max(t)}$ for wet ranks for a given winter, all pairs of stations are retained. Table 22 provides these normalized between-station differences for winter 1952-'53, where the maximum dry ranks value is bolded, and highlighted are the 2 station combinations attaining the wet ranks maximum value.

Table 22. Winter 1952-1953 Results of Dry (X) and Wet (Y) Rank Differences (%).

Station i/j	NORM $(X)_{(t)\ i,j}$	NORM $(Y)_{(t)\ i,j}$	Station i/j	NORM $(X)_{(t)\ i,j}$	NORM $(Y)_{(t)\ i,j}$
Bed/Bburg	42	8	ROA/Laf	8	0
Bed/ROA	50	8	ROA/Buch	33	25
Bed/Laf	58	8	ROA/Pul	25	8
Bed/Buch	**83**	33	ROA/Rocky	17	8
Bed/Pul	25	0	Laf/Buch	25	25
Bed/Rocky	67	17	Laf/Pul	33	8
Bburg/ROA	8	0	Laf/Rocky	8	8
Bburg/Laf	17	0	Buch/Pul	58	33
Bburg/Buch	42	25	Buch/Rocky	17	17
Bburg/Pul	17	8	Pul/Rocky	42	17
Bburg/Rocky	25	8			

It can be seen from Table 22, the Bedford/Buchanan (Bed/Buch) and Buchanan/Pulaski (Buch/Pul) pairs would be seized as the station combinations which showed the highest difference in the number of wet rank (5-7) days relative to the total frontal-precipitation days observed during the winter of 1952-'53. Similarly, the Bedford/Buchanan combination was the station-pair that demonstrated the highest difference in the number of days belonging to dry ranks (1-3). It can thus be inferred that the Bed/Buch and Buch/Pul station pairs may display an association in winter frontal-precipitation for large-scale meteorological conditions possessed by the 1952-'53 winter. As analyzed in forthcoming sections, these between-station differences in winer frontal-precipitation may be related to teleconnection (AO, NAO, PNA, ENSO) and/or weather state forcing. Figures 7 and 8 display the frequency in number of winters over the investigated period where each station combination possessed $NORM(X)_{max}$ and $NORM(Y)_{max}$ respectively, with ties between station pairs included. Also depicted in these bar charts are the number of winters for each combination where $NORM(X)_{max}$ and

$NORM(Y)_{max}$ took on values >= 65%. This 65% threshold was arbitrarily chosen as a reasonable means of reducing large raw data sets.

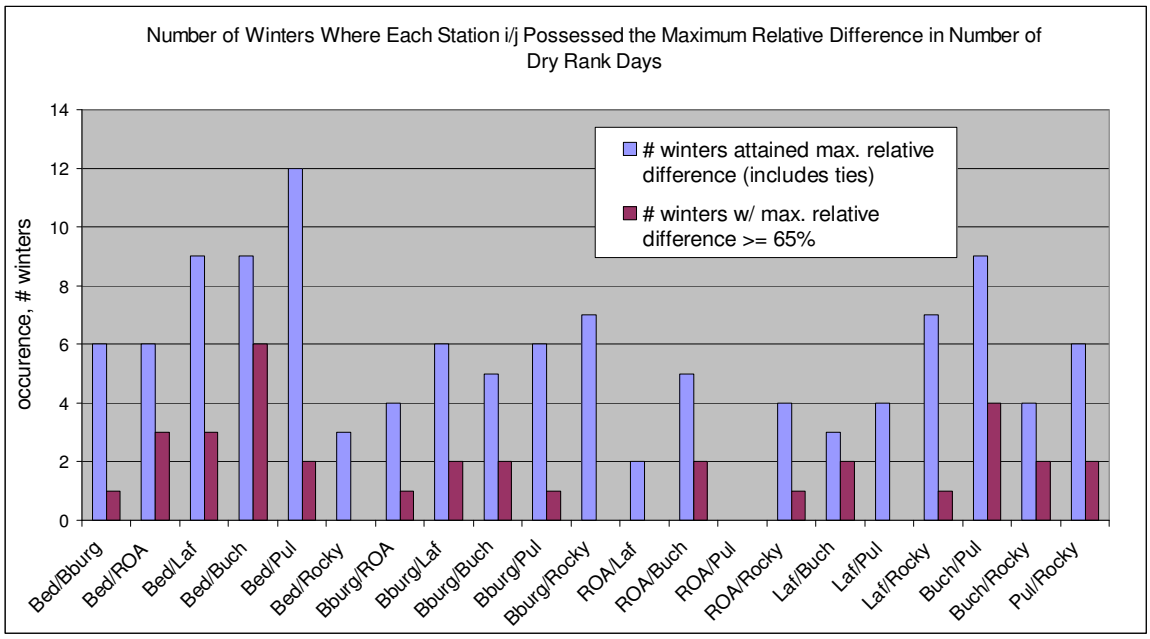

Figure 7. Occurrence of $NORM(X)_{max}$ for each station combination and those occurrences attaining values >= 65% (53 winters considered).

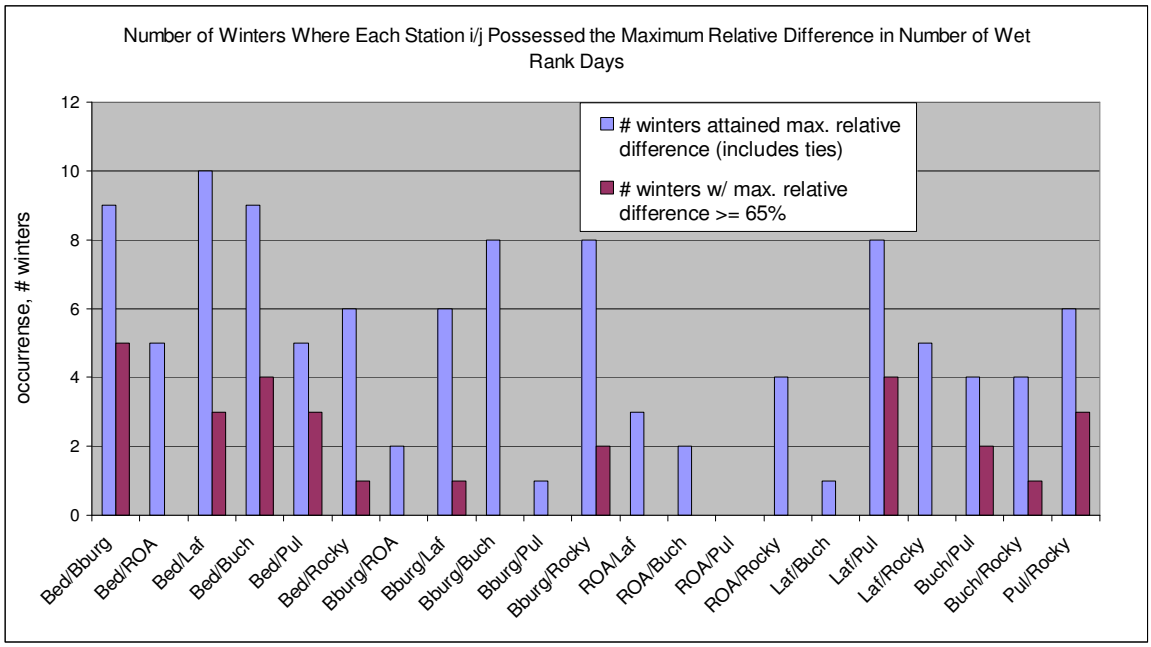

Figure 8. Occurrence of NORM(Y)$_{max}$ for each station combination and those occurrences attaining values >= 65% (53 winters considered).

It is evident from Figures 7 and 8 that detectable precipitation differences likely exist between the Bedford/Lafayette and Bedford/Buchanan station pairs during winter frontal events given the significant number of winters in which these two station pairs differed considerably in the number of dry and wet rank days out of the 53 winters considered for this analysis. These two figures also illustrate Roanoke/Pulaski and Roanoke/Lafayette as station combinations which are prone to associate, with respect to precipitation, during frontal passages. Additional station pairs that may demonstrate comparable precipitation responses include: Lafayette/Buchanan, Blacksburg/Roanoke, and Roanoke/Rocky Mount. With an exception of the Bedford/Rocky Mount combination, results in Figures 7 and 8 also warrant the prediction that Bedford behaves discriminately with respect to the other stations when depressions (cyclones) pass

through the region givn each of its station pairs attained at least five winters of $NORM(X)_{max}$ and $NORM(Y)_{max}$.

Between Station Frontal-Precipitation Variability Under Global Teleconnections

Winters that experienced 7-10, 11-14, and greater than 14 frontal-precipitation days, as arbitrarily adopted, within the study period (1950-2003) were segregated, with the occurrence of each phase of the four teleconnective indices (AO, PNA, NAO, SOI) totaled – each index was discriminately assessed. The winter phase for a given teleconnection is the phase of the average winter value (from December, January, and February monthly values). Bounds used to distinguish each of the three phases for all four indices are included in Appendix A. Table 23 displays the number of winters each index existed in its negative, positive, and neutral phase for these three categories (7-10, 11-14, > 14) of frontal-precipitation day occurrence. It can be seen by inspection of Table 23 that winters demonstrating more than 14 frontal-precipitation days occurred more frequently over the study period when the winter average of the AO, NAO, PNA, and ENSO (as individually analyzed) existed in their negative phase.

Table 23. Occurrence of Winter Phase of Four Teleconnections and Frontal-Precipitation in Southwest Virginia (# winters in period)

	AO			PNA		
	Negative	Positive	Neutral	Negative	Positive	Neutral
# Winters w/ 7-10 frontal-precip days	13	5	3	5	4	12
# Winters w/ 11-14 frontal-precip days	8	6	1	3	3	10
# Winters w/ >14 frontal-precip days	4	1	3	3	1	3
	NAO			ENSO		
	Negative	Positive	Neutral	Negative	Positive	Neutral
# Winters w/ 7-10 frontal-precip days	7	11	2	6	6	9
# Winters w/ 11-14 frontal-precip days	6	4	6	7	2	6
# Winters w/ >14 frontal-precip days	4	3	1	3	2	3

See Appendix A for bounds used for AO, PNA, NAO, ENSO phase designations.

Winters during which $NORM(X)_{max}$ or $NORM(Y)_{max}$, representing the dry and wet rank sum normalized differences respectively as provided by Equation (3), computed to be at least 65% are assessed for possible connections with phases of the AO, PNA, NAO, and SOI (a measure of ENSO phase and strength). Tables 24 and 25 highlight winters with at least seven frontal-precipitation days when $NORM(X)_{max}$ and $NORM(Y)_{max}$ achieved this threshold; also reported is the phase of each teleconnection for that winter.

Table 24. Winters during which at least one station combination i/j achieved $NORM(X)_{max}$ values >= 65%*.

Winter	NORM $(X)_{(t),max}$	Station Combinations w/ NORM $(X)_{(t),max}$	AO Phase	PNA Phase	NAO Phase	ENSO Phase
1950-'51	80%	Laf/Buch; Bed/Laf	AO-	Neutral	NAO+	La Nina
1952-'53	83%	Bed/Buch	AO-	Neutral	Neutral	El Nino
1957-'58	79%	Pul/Rocky	AO-	Neutral	NAO-	El Nino
1959-'60	90%	Pul/Rocky; Bburg/Pul	AO-	Neutral	NAO-	Neutral
1966-'67	71%	Bed/ROA	AO-	Neutral	NAO+	La Nina
1967-'68	71%	Buch/Pul; Buch/Rocky	AO-	Neutral	NAO-	Neutral
1969-'70	80%	Bburg/Buch	AO-	PNA+	Neutral	El Nino
1972-'73	82%	Bed/ROA	AO+	Neutral	NAO+	El Nino
1976-'77	71%	Bed/ROA; Bed/Laf; Bed/Pul	AO-	PNA+	NAO-	Neutral
1986-'87	71%	Bed/Buch; Buch/Pul	AO-	PNA+	NAO-	El Nino
1987-'88	86%	Bed/Buch; Buch/Rocky	AO-	Neutral	NAO+	Neutral
1988-'89	71%	Bed/Buch; Laf/Buch; ROA/Buch	AO+	PNA-	NAO+	La Nina
1989-'90	67%	Bed/Pul; Buch/Pul	AO+	Neutral	Neutral	El Nino
1990-'91	78%	Bburg/ROA	AO+	Neutral	NAO+	Neutral
1993-'94	71%	Bed/Bburg	AO-	Neutral	NAO+	Neutral
1994-'95	75%	Bburg/Buch	AO+	Neutral	NAO+	El Nino
1998-'99	73%	ROA/Rocky	AO+	Neutral	NAO+	La Nina

* Teleconnection phase for winter, k is the phase of average($Index\_Dec_k$, $Index\_Jan_k$, $Index\_Feb_k$). See Appendix A for the bounds used for phase designations.

Table 25. Winters during which at least one station combination i/j achieved $NORM(Y)_{max}$ values >= 65%*.

Winter	NORM $(Y)_{(t),max}$	Station Combinations w/ $NORM(Y)_{(t),max}$	AO Phase	PNA Phase	NAO Phase	ENSO Phase
1950-'51	80%	Bed/Laf	AO-	Neutral	NAO+	La Nina
1957-'58	71%	Pul/Rocky	AO-	Neutral	NAO-	El Nino
1959-'60	70%	Pul/Rocky; Bed/Pul	AO-	Neutral	NAO-	Neutral
1963-'64	67%	Bed/Bburg; Bburg/Rocky	AO-	Neutral	NAO-	El Nino
1966-'67	86%	Bed/Laf	AO-	Neutral	NAO+	La Nina
1967-'68	71%	Laf/Pul; Buch/Pul	AO-	Neutral	NAO-	Neutral
1969-'70	80%	Bed/Bburg	AO-	PNA+	Neutral	El Nino
1976-'77	100%	Bed/Pul	AO-	PNA+	NAO-	Neutral
1983-'84	70%	Laf/Pul	AO+	Neutral	NAO+	Neutral
1987-'88	71%	Buch/Rocky	AO-	Neutral	NAO+	Neutral
1989-'90	78%	Bed/Pul	AO+	Neutral	Neutral	El Nino
1990-'91	89%	Bed/Bburg	AO+	Neutral	NAO+	Neutral
1994-'95	75%	Bburg/Rocky	AO+	Neutral	NAO+	El Nino

* Teleconnection phase for winter, k is the phase of average($Index\_Dec_k$, $Index\_Jan_k$, $Index\_Feb_k$). See Appendix A for the bounds used for phase designations.

It is seen that during La Nina/AO- winters, the azmith between the two stations comprising each of the three station pairs (Bed/Laf, Laf/Buch, Bed/ROA) exhibits southwest-to-northeast orientation. As shown in Tables 24 and 25, this teleconnective condition occurred during the 1950-'51 and 1966-'67 winters. Secondly, in five of the six winters where Roanoke emerges as a member station in Table 24 (1966-'67, '72-'73, '76-'77, '88-'89, '90-'91, '98-'99), the NAO existed in its positive phase, with four of these five winters also showing the AO+ condition. Pulaski belongs to each of the two station combinations that show high rank variability (number of dry and wet rank days) for the only winter (1989-'90) characterized by AO+, PNA Neutral, NAO Neutral, and El Nino. Furthermore, the Bedford/Lafayette station pair shows high variability in the number of wet days only for winters 1950-'51 and 1966-'67, both of which the AO-, PNA Neutral, NAO+, La Nina condition applied. In four of the six occasions where

Rocky Mount was paired with either Pulaski or Blacksburg, an El Nino winter episode was seen, with the remaining two winters showing the ENSO-Neutral designation. Finally, Bedford exhibited contrasting behavior compared to Roanoke, Lafayette, and Pulaski in the 1976-'77 winter, which is the only case that a merger of AO-, PNA+, and NAO- was observed.

Inferences on Between Station Variability

Appropriate criteria for assessment of between-station variability include: (1) climatology; (2) climate division membership; (3) linear distance; and (4) direction or azmith. Each of these parameters is included in Table 26 for all seven stations used in this analysis, with climatology captured by 30-year winter precipitation normals, $x\_bar_{Station,s}$. See Appendix B for azmiths and linear distances between all station combinations.

Table 26. Precipitation Station Characteristics

Station	Winter Normal Precip: 1971-2000, x_bar (inches)*	Climate Division**	Northing (U.S. survey ft.)**	Easting (U.S. survey ft.)**
Bedford	9.77	Western Piedmont	3652582.268	11187405.22
Blacksburg	9.26	Southwestern Mountain	3602043.171	10924723.67
Roanoke	9.17	Central Mountain	3623815.777	11065841.27
Lafayette	8.72	Southwestern Mountain	3612968.951	10988035.03
Buchanan	9.36	Central Mountain	3719894.443	11139799.8
Pulaski	8.33	Southwestern Mountain	3549820.987	10816637.27
Rocky Mount	10.09	Western Piedmont	3520522.57	11074010.19

*from NOAA National Climate Data Center (NCDC); ** converted with Corpscon™ using Virginia State Coordinate System NAD83 from Latitude/Longitude (DMS) provided by National Weather Service (NWS)

It has been previously stated that Tables 24 and 25 document the contrasting behavior the Bedford/Roanoke, Bedford/Lafayette, and Bedford/Pulaski station combinations exhibited during the winter of 1976-'77. Large-scale atmospheric circulation during this winter included the positive phase of the PNA and a strong negative Arctic Oscillation (<= -1.0). Table 27 shows the percentage differences: (1) in total winter precipitation between the listed station pairs using frontal-precipitation days of the 1976-'77 winter; and (2) their 30-year winter normals (x_bar). In both sets of computations, the respective value for Bedford was employed as the denominator, making the percentage difference between Bedford and station s as: (Bedford precipitation – Station, s precipitation) / Bedford precipitation. This convention was adopted for1976-'77 winter frontal-precipitation as well as 30-year winter normal values.

Table 27. Percentage differences with respect to Bedford precipitation for total winter precipitation during frontal-precipitation days in 1976-'77 and 30-year winter normals*

	Percentage Difference	
Station Combination i/j	A. Total Precipitation from winter 1976-'77 Frontal-precipitation days	B. 30-year Winter Normals
Bed/ROA	54%	6%
Bed/Laf	32%	11%
Bed/Pul	47%	15%
Bed/Bburg	23%	5%

*% Difference Bed/Station, s = [(Bedford precipitation – Station, s precipitation)/Bedford precipitation]*100%.

Notable is the constraint placed on data used to compute column A in Table 27, which permitted use of only winter 1976-'77 days in which all seven stations received precipitation (i.e. frontal-precipitation days), while 30-year winter normals are reported

for each station and thus include all days in winter 1976-'77. All results computing to be positive demonstrate the overall wetter winter climate typical at Bedford, when compared against Roanoke, Lafayette, Pulaski, and Blacksburg. However the larger-than-climatology percentage differences shown in the column A – i.e. 54% and 6% for the Bed/ROA pair for 1976-'77 winter frontal-precipitation and 30-year normal values respectively – combined with low incidence of PNA+ in Tables 24 and 25 prompted inspection of between-station precipitation variability for all winters in which this flow pattern collaborated with a strong AO- (<< -0.25).

Winters within the study period (1950-2003) in addition to 1976-'77 which demonstrated a merger of PNA+ and a strong AO- are as follows: 1962-'63, 1969-'70, 1977-'78, 1985-'86. Percentage differences for these winters were evaluated in the same manner as was done for 1976-'77 winter, with results reported in Table 28.

Table 28. Percentage differences in total precipitation between stations during frontal-precipitation days of winters with PNA+ and strong AO-*.

Winter Year, k	Percentage difference in total precipitation between stations during frontal-precip. days in winter of year k			
	Bed/Bburg	Bed/ROA	Bed/Laf	Bed/Pul
1962-'63	21%	35%	29%	43%
1969-'70	49%	33%	22%	37%
1977-'78	33%	23%	24%	22%
1985-'86	27%	38%	38%	15%

*% Difference Bed/Station, s = [(Bedford precipitation – Station, s precipitation)/Bedford precipitation]*100%.

Relative differences displayed in Table 28 encourages the claim that variability in total winter precipitation during frontal-precipitation days between the listed Bedford

station combinations is intensified when winter large-scale atmospheric circulation features PNA+ and strong AO- characteristics.

Review of Tables 24 and 25, as formerly reported, also presented a potential connection between El Nino and winter precipitation variability between the Rocky Mount/Blacksburg station pair. An assessment of precipitation variability between these station combinations during all winters possessing an El Nino episode revealed a persistent wet response at Rocky Mount relative to Blacksburg. Out of the 14 El Nino winters with at least seven frontal-precipitation days and zero missing station precipitation values, 11 exhibited a wetter frontal-precipitation response at Rocky Mount compared to Blacksburg. Percentage differences (as normalized by Rocky Mount values) in total winter precipitation during frontal-precipitation days between Rocky Mount and Blacksburg for these 11 winters were then evaluated against the winter climatology relative difference, using $x\_bar_{RockyMount}$ = 10.09 inches and $x\_bar_{Blacksburg}$ = 9.26 inches, of 8.23%. Winters from this group of 11 for which its Rocky Mount-Blacksburg percentage difference exceeded the 8.23% climatology difference were retained. Uncovered from these retained winters (7 of the evaluated 11) was a trend of PNA+ and El Nino, which prompted a subsequent scan of all winters in the period possessing this teleconnection condition. The following summary table (29) displays all PNA+, El Nino winters in the study period and the corresponding percentage difference in total winter precipitation during frontal-precipitation days between Rocky Mount and Blacksburg.

Table 29. Percentage difference in total winter frontal-precipitation between Rocky Mount and Blacksburg for PNA+, El Nino winters within 1950-2003

Winter	A. Total Frontal-day Rocky Mount Precip. (inches)	B. Total Frontal-day Blacksburg Precip. (inches)	Percentage difference in total winter precipitation during frontal-precipitation days*
1969-'70	4.16	3.21	23%
1977-'78	7.91	4.74	40%
1982-'83	5.54	4.40	20%
1986-'87	7.56	4.70	38%
1991-'92	8.25	8.04	3%
1997-'98	13.20	9.33	29%

*% Difference in winter k = [(RockyMount precipitation$_k$ – Blacksburg precipitation$_k$) / RockyMount precipitation$_k$] *100%.

In all winter years listed in Table 29 excluding 1991-'92, the relative increase in total winter precipitation during frontal-precipitation days from Blacksburg to Rocky Mount is substantially greater than that shown by climatology (8.23%). Consequently, the winter PNA+, El Nino atmospheric flow condition may assume a role in dictating contrasting precipitation responses during frontal events between Rocky Mount and Blacksburg.

Common to all Bedford station pairs listed in Table 27 and the Rocky Mount/Blacksburg combination (as just discussed) is climate division (Western Piedmont) membership of the two stations – Bedford and Rocky Mount – showing wetter responses to frontal events during particular phases of winter teleconnections. In addition, the three teleconnection phases (PNA+, AO-, El Nino) observed on all winters during which this group of five station combinations showed potentially high-than-climatology differences in total winter frontal-precipitation are interrelated. While the negative phase of the Arctic Oscillation features a higher pressure center in the polar region and low pressure in the midlatitudes of the northern Atlantic Ocean, this

circulation incorporates aspects of PNA+ (Eichler and Bell 2001). In turn, PNA+ is congruent with weak to moderate El Nino conditions in the tropical Pacific, with a low pressure region in the Gulf of Alaska and an amplified ridge-trough pattern in upper atmospheric flow over North America (Philander 1990). Upper atmospheric flow patterns constituting the PNA have been decisively shown to affect winter surface meteorology (Sheridan 2003). These aforementioned connections impart reliability to the responses to PNA+ detected in this study.

It has been reported that years where winter circulation is dictated by the El Nino-AO- condition, regions east of the Appalachian Mountains encounter anomalously high total winter precipitation (Zhou et al. 2001; Katz et al. 2003). Abnormally dry winters experienced in the Ohio-Tennessee valley during El Nino-AO- winters serves as further evidence of an east-west precipitation gradient in Virginia during this teleconnective condition (Zhou el al. 2001). The wetter response in frontal precipitation apparent for Rocky Mount and Bedford relative to stations to their west, as seen in this analysis, supports this regional feedback to PNA+,AO- winter circulation. These results promote the claim that ENSO, through its association with midlatitude circulation, impacts winter southwest Virginia precipitation by inducing wetter responses to frontal systems during PNA+, AO- in the Western Piedmont region; however, the low incidence of the PNA+, AO- winter condition within the study period (6 out of 54 winters) and the length of the employed climatology record (30 years) raises the uncertainty accompanying this claim.

Frontal-Precipitation Days, ENSO, and SSC Weather Types

Between-station (i.e. spatial) variability in winter ranked precipitation during frontal-precipitation days is assessed for the concurrence of the three phases of ENSO and seven daily weather types. This portion of the study focuses on ENSO given that its winter circulation patterns are considered reliable and because seasonal forecasts reported by the Center for Climate Prediction (CPC) are typically based off ENSO (D'Aleo 2002; Zhou 2001).

All winter months in the 1950-2003 record are arranged by their SOI monthly value, where an SOI <= -5.0 and >= 5.0 designate El Nino and La Nina months, respectively, with ENSO-neutral months taken as intermediate SOI values (Simpson and Colodner 1999). Subsequently, these compartmentalized months are individually scanned for occurrence, at Roanoke, of each of the seven SSC daily weather types (see Chapter 2). Twenty-one daily data sets collaborating the three ENSO phases and seven daily weather types are then obtained. This staged conditioning is an example of a downscaling procedure that integrates monthly teleconnection data (SOI) and daily surface meteorological conditions (SSC weather types) at Roanoke, which is done to analyze winter daily frontal-precipitation events. The following station centered weather types are adopted in the SSC2 methodology: (1) Dry Polar (DP); (2) Dry Moderate (DM); (3) Dry Tropical (DT); (4) Moist Polar (MP); (5) Moist Moderate (MM); (6) Moist Tropical (MT); and (7) Transition (TR) (Sheridan 2002). A review of the first portion of Chapter 2 and Appendix A will brief the reader on the SSC scheme.

As a third stage of conditioning, days where all seven stations received precipitation (frontal-precipitation days) are extracted from each of these resulting twenty-one sets of daily data and ranked 1-7 as previously discussed. Tallied then for all stations is the number of occurrences of each of the seven ranks. Figures 9 and 10 report results found for days within winter (DJF) El Nino and La Nina months, respectively, where a Moist Polar (MP) day was observed on a frontal–precipitation day. Likewise, Figures 11 and 12 offer the same frequency data, but for Moist Moderate (MM) days.

This portion of the study concentrated purely on the MP and MM weather types because in general, MP and MM air masses are typically affiliated with mid-latitude/extratropical cyclones in the eastern U.S. While the three dry weather types (DP, DM, and DT) were excluded due to their low occurrence during winter frontal-precipitation days, the convective dominant characteristics shown by MT days eliminated it from the analysis. Moreover, the rapid changes in meteorological conditions experienced during TR days, on a time scale of hours, render it unsuitable for this seasonal study. (Greene 1996)

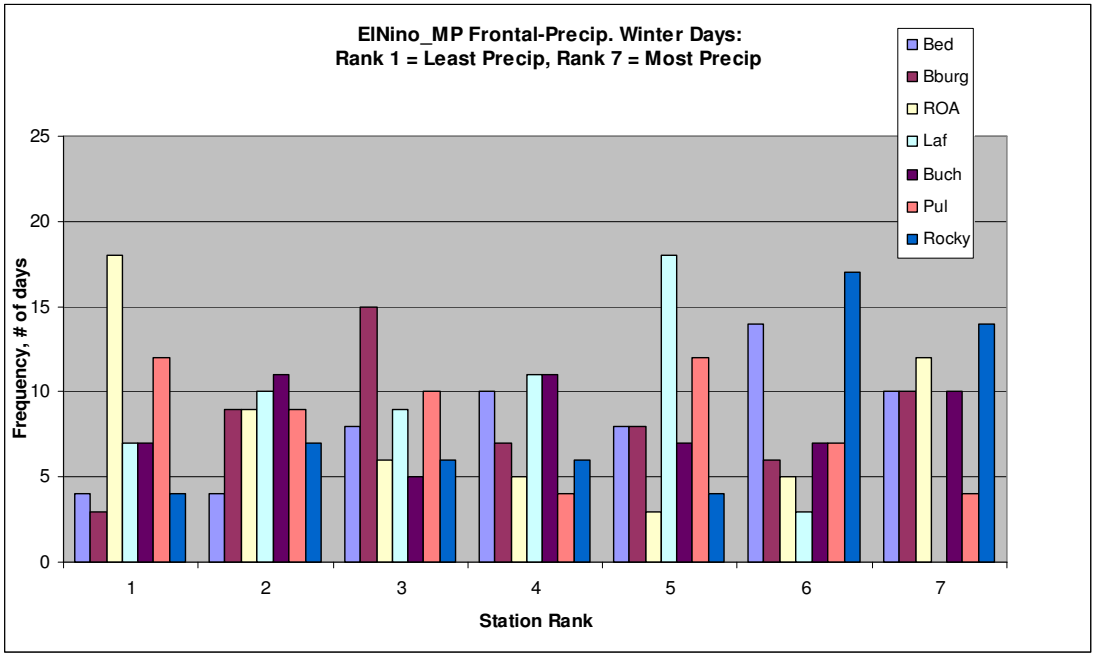

Figure 9. Frequency histogram of each precipitation rank for Moist Polar (MP), frontal-precipitation days within winter El Nino months (SOI <= -5.0).

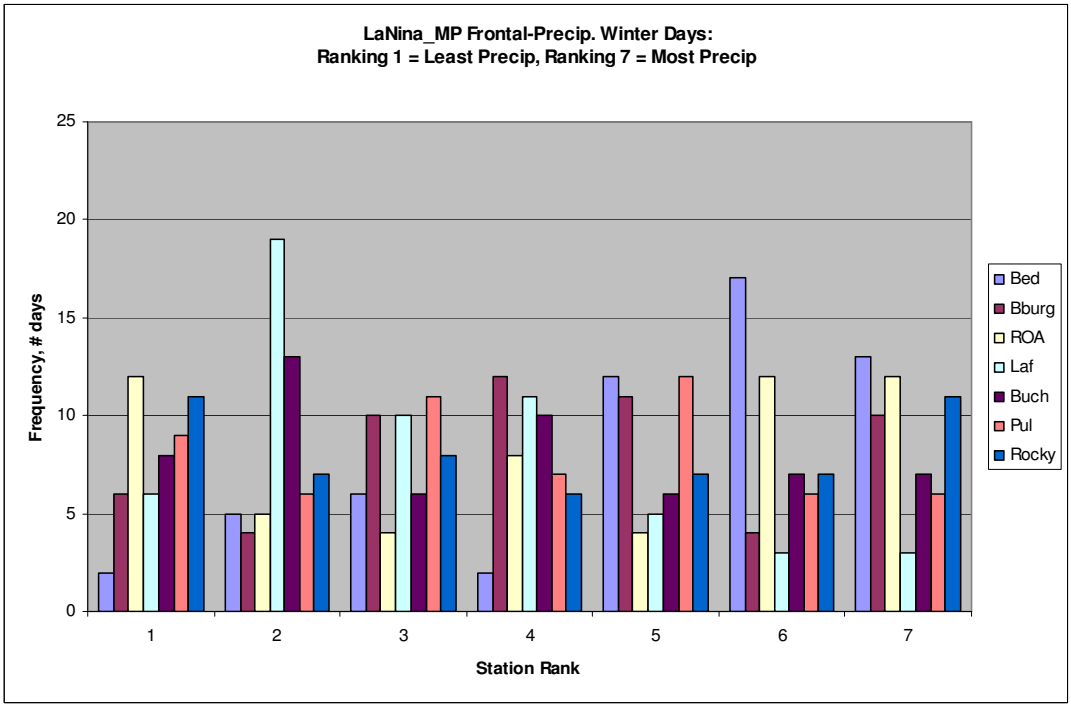

Figure 10. Frequency histogram of each precipitation rank for Moist Polar (MP), frontal-precipitation days within winter La Nina months (SOI >= 5.0).

It can be inferred from Figures 9, 10, and 11 that Rocky Mount is less likely to receive the least precipitation (rank 1) relative to the remaining 6 stations during MP days in El Nino months, compared to La Nina and ENSO-neutral months. In addition, Lafayette's modal frequency belongs to a wet rank (5) for the El Nino condition and a dry rank (2) during La Nina months. Lastly, Roanoke demonstrates higher rank variability over the seven ranks (s_x = 5.22 days) during synoptic precipitation, MP days for El Nino winter months compared to La Nina (s_x = 3.85 days) and ENSO-neutral (s_x = 3.77 days).

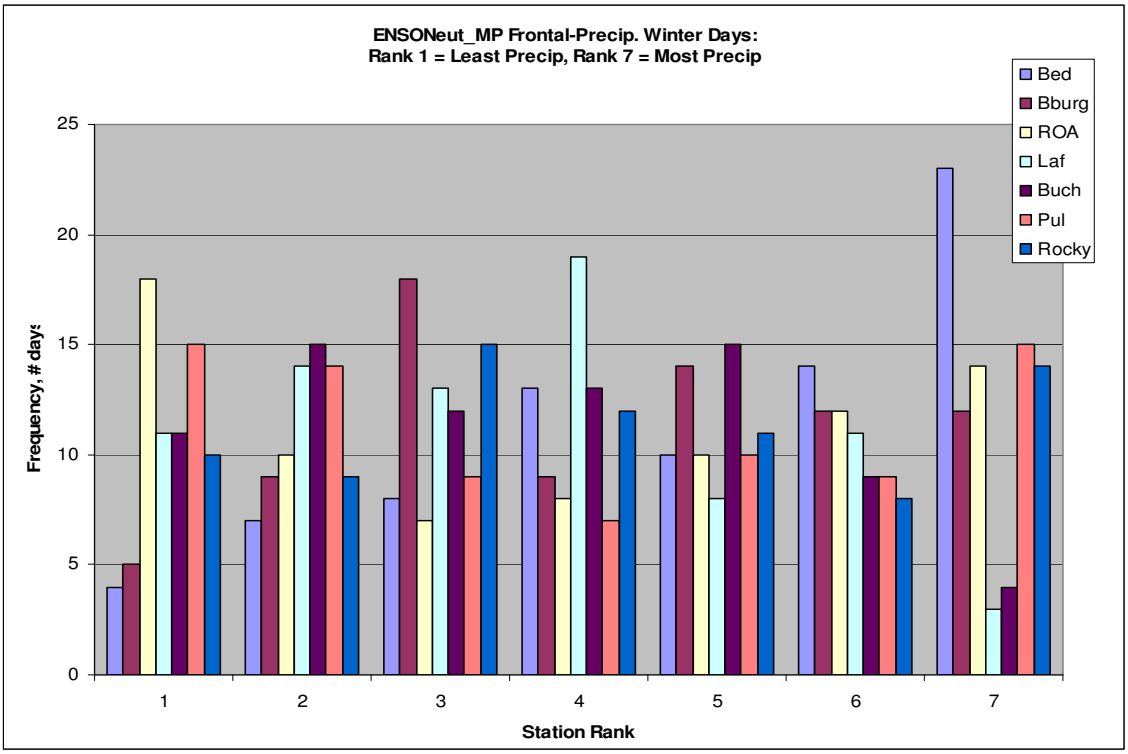

Figure 11. Frequency histogram of each precipitation rank for Moist Polar (MP), frontal-precipitation days within winter ENSO-neutral months.

Figures 12, 13, and 14 show a reduced prevalence of Moist Moderate (MM) frontal-precipitation days for La Nina winter months versus the El Nino and ENSO-neutral situations; in fact 34 days are registered during La Nina months, whereas 54 and 86 days are cataloged during El Nino and ENSO-neutral months respectively. It thus is suitable to claim that the winter storm track(s) associated with MM air in southwest Virginia may have less of an affinity for La Nina episodes. As is also evident from Figures 12 and 13, Roanoke explicitly received the most precipitation [out of the seven analyzed stations] on 17 days when MM, frontal-precipitation days fell within El Nino months, when contrasted against La Nina (i.e. 9 days). This winter wet rank response at Roanoke during El Nino months is significantly impacted by its high incidence in December, as depicted in Figure 15. It follows from Figures 9 and 12 that the MM condition during frontal-precipitation days within El Nino months supports wetter responses at Roanoke relative to the surrounding stations compared to El Nino_MP days. Additionally, Buchanan's frequency rank distribution exhibits a bi-model behavior for El Nino_MM frontal-precipitation days, minimizing at rank 4 and obtaining equal maxima at ranks 2 and 5. This effect is in conflict with this station's near normal La Nina and ENSO-neutral distributions.

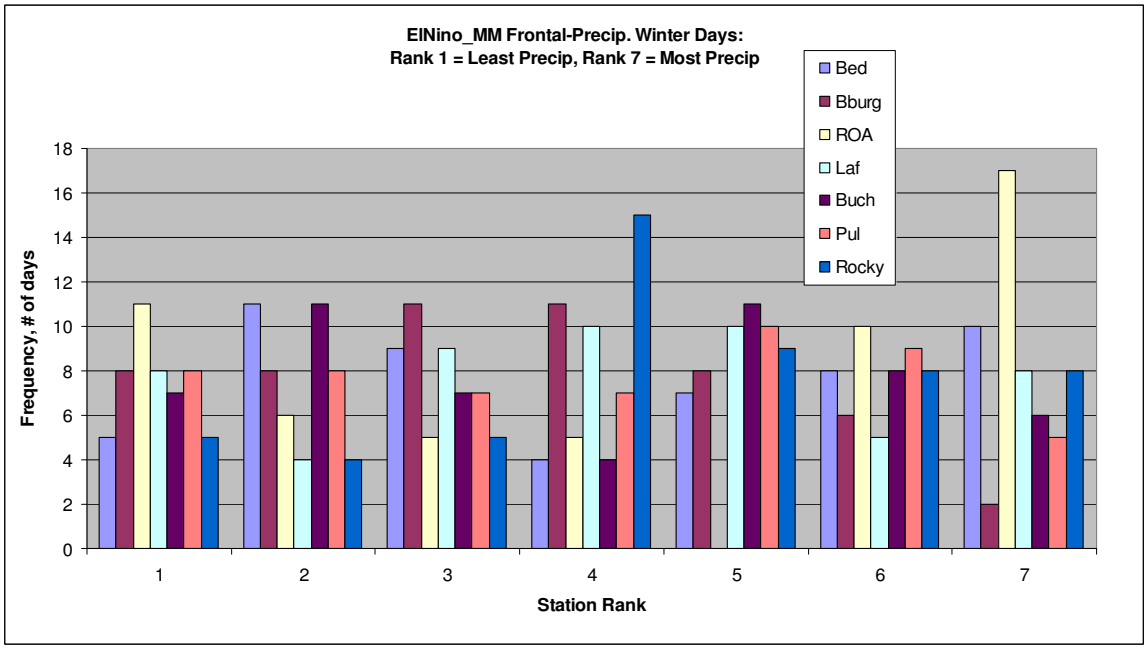

Figure 12. Frequency histogram of each precipitation rank for Moist Moderate (MM), frontal-precipitation days within winter El Nino months (SOI <= -5.0).

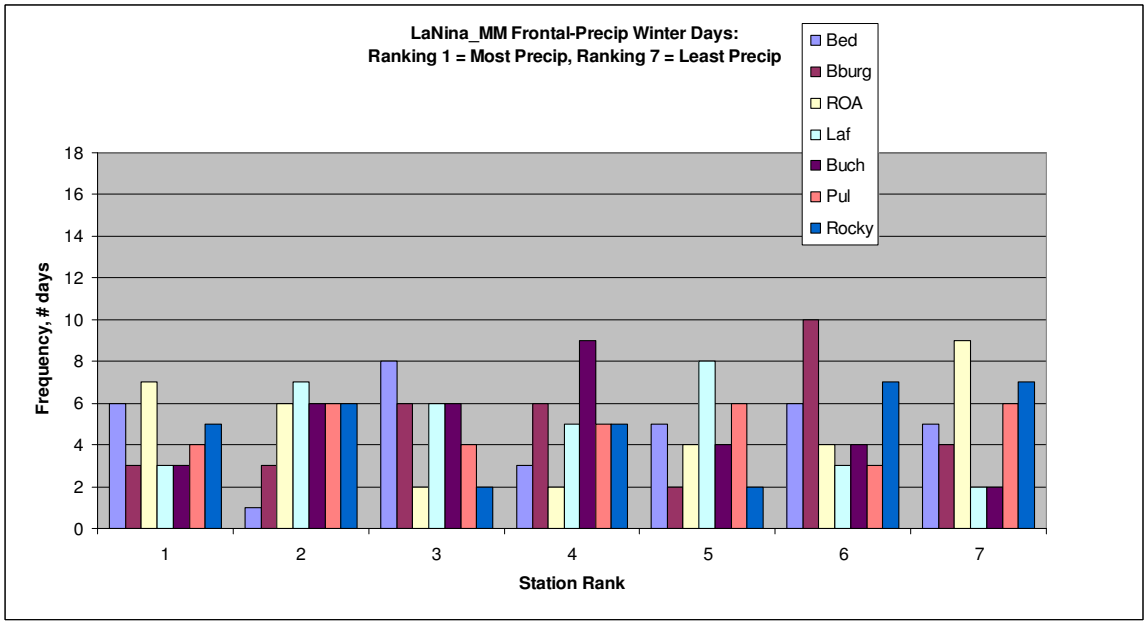

Figure 13. Frequency histogram of each precipitation rank for Moist Moderate (MM), frontal-precipitation days within winter La Nina months (SOI >= 5.0).

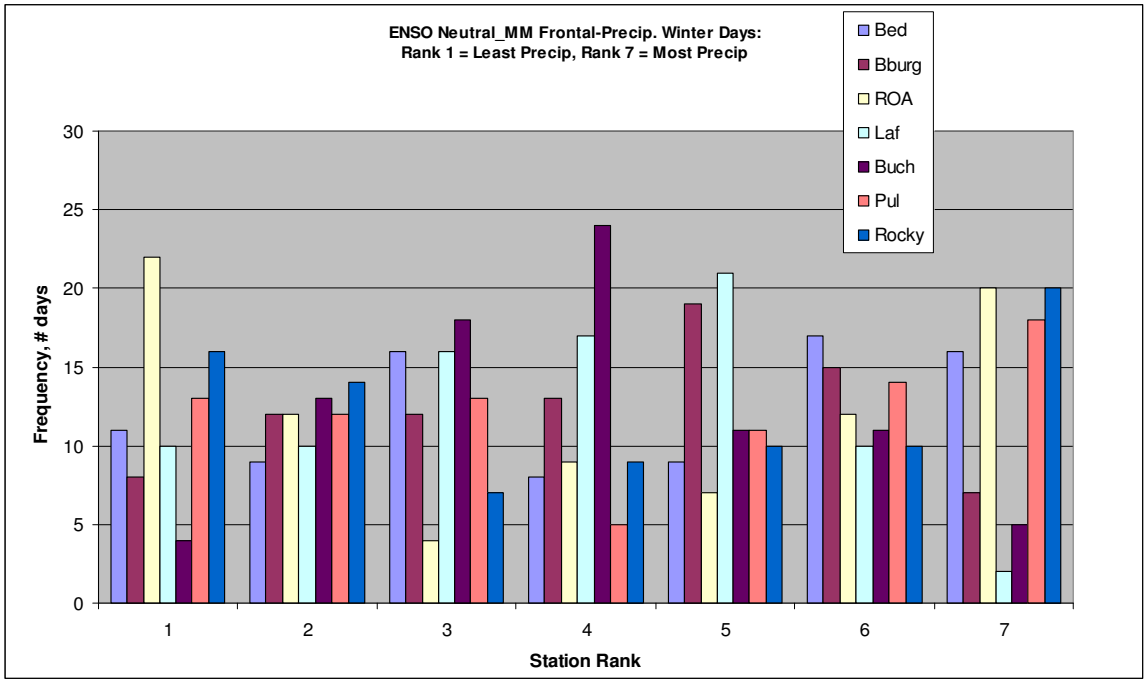

Figure 14. Frequency histogram of each precipitation rank for Moist Moderate (MM), frontal-precipitation days within winter ENSO-neutral months (SOI >= 5.0).

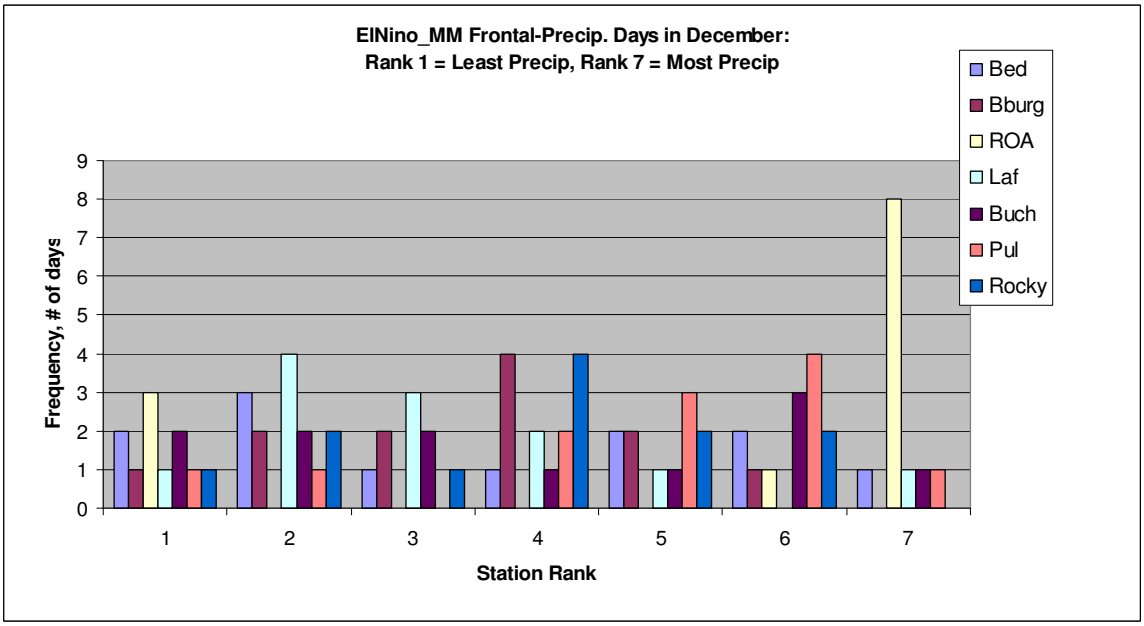

Figure 15. High incidence of the wettest areal rank (7) at Roanoke for synoptic precipitation, Moist Moderate (MM) days within El Nino Decembers.

Seasonal Precipitation, Teleconnections, and SSC Weather Types

Similar to the previous analysis in which daily precipitation is conditioned on the phase of monthly teleconnections and occurrence of each of the seven daily SSC weather types, this assessment aggregates resulting conditioned data by season for winter (DJF), spring (MAM), summer (JJA), and fall (SON). This portion of the study, however, does not apply the frontal-precipitation constraint, but includes all days that meet the applicable teleconnection-SSC weather type condition and uses historical data from 1950-2003. To exemplify, Table 30 shows daily precipitation on eight Dry Tropical (DT) days that transpired within El Nino months. As is shown here for El Nino, daily precipitation data was also segregated individually by months of La Nino, ENSO-neutral, PNA+, PNA-, NAO+, NAO-, and NAO-neutral. Moreover, El Nino, La Nina, and ENSO-neutral were each paired alongside AO+ and AO- to render two-tiered teleconnection constraints. It is noted that all missing daily precipitation values were assigned the historic daily average for the specific station and month and that Appendix A reports bounds used to discriminate phases of monthly teleconnection index values. In addition, see Appendix D for contemporaneous correlations between seasonally aggregated precipitation at Roanoke and these four teleconnective indices. Appendix D also reports lagged-correlations obtained between monthly total precipitation at Roanoke and the SOI and NAO during deemed El Nino calendar years; however, no clear inferences were evident from this analysis.

Table 30. Example of conditioned daily data for ElNino_DT precipitation

El Nino Months_Dry Tropical Days									
			Bedford	Blacksburg	Roanoke	Lafayette	Buchanan	Pulaski	RockyMount
Year	Month	Day	Station Precipitation (Inches *100)						
1953	5	1	3	0	0	47	60	32	75
1953	5	13	0	17	0	0	0	0	0
1953	9	1	0	0	0	0	0	0	0
1959	8	21	0	0	0	32	0	11.43	0
1961	3	29	7	16	0	11	15	0	5
1965	8	18	0	0	0	9	7	0	0
1965	10	16	3	0	0	0	0	0	0
1966	3	18	0	0	0	0	0	0	0

Figures 16 (a-c) illustrate the overall occurrence of each SSC weather type for months of El Nino, La Nina, and ENSO-neutral, with each day in the 54 year record (1950-2003) belonging to a single ENSO_SSC compartment. While these figures provide results from 54 springs, summers, and falls, only 53 winter data sets were available.

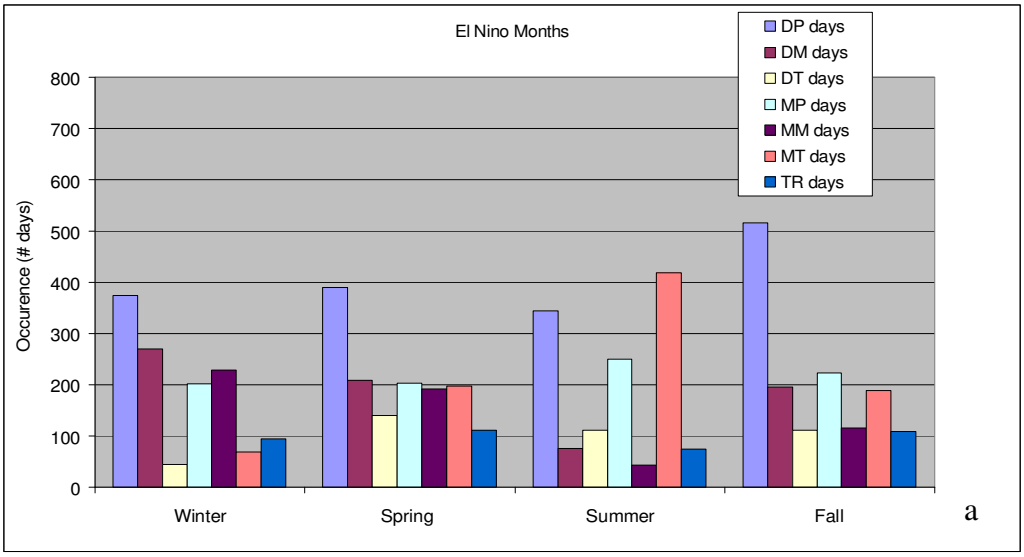

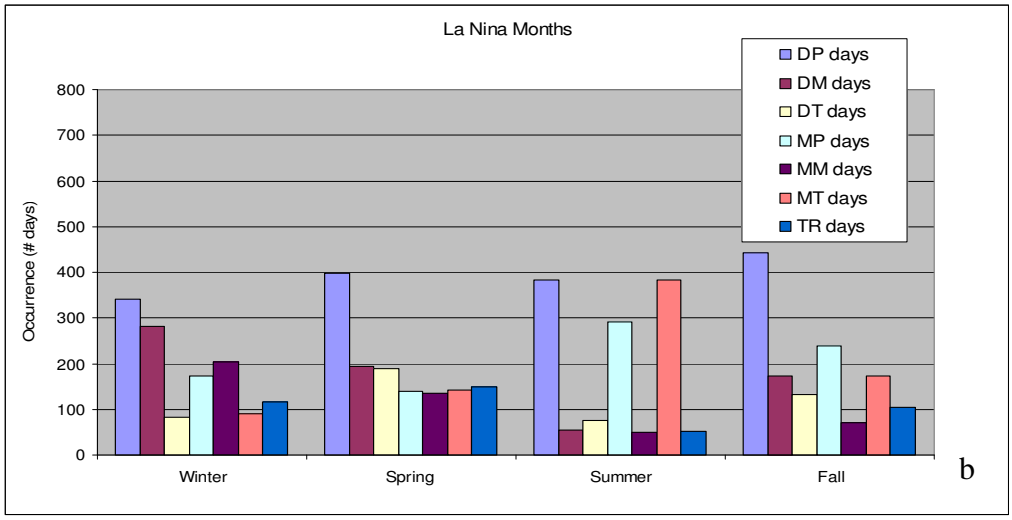

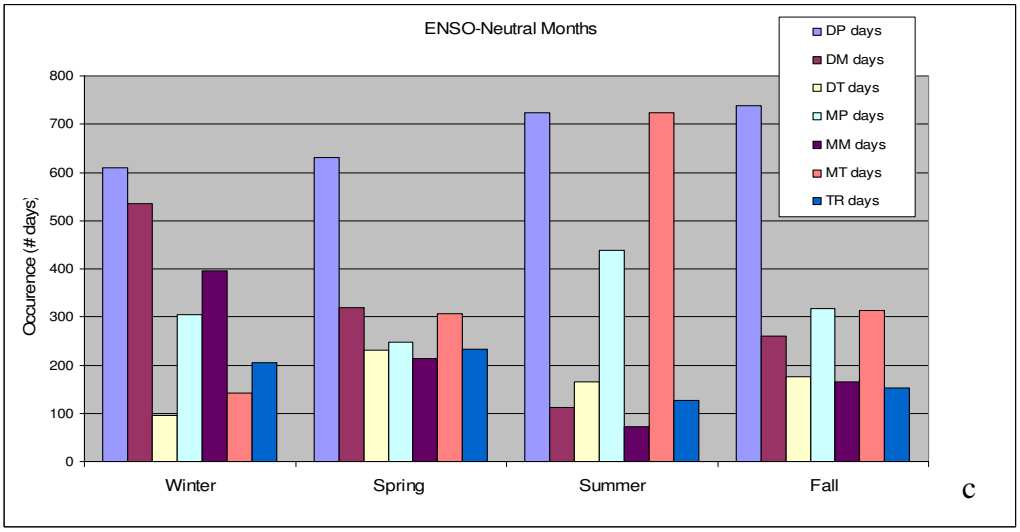

Figures 16 (a-c). Historical distributions of SSC weather types for (a) El Nino, (b) La Nina, and (c) ENSO-neutral months by season; 4770 total winter days, 4968 total spring days, 4968 total summer days, and 4914 total fall days comprise each seasonal population.

It is observed from Figures 16 (a-c) that the SSC weather type frequency distribution pattern remains fairly consistent over each of the four seasons for a given ENSO phase; however, the frequency outcomes do vary according to ENSO phase. It is

noteworthy that during winter, spring, and fall, DP days are the most prevalent and that Roanoke can expect few tropical meteorological conditions (DT and MT days) during winter.

Subsequent to monthly teleconnection and daily SSC weather type conditioning, all resulting days are pooled according to the season to which each belongs and their corresponding precipitation values totaled for each of the seven stations. This seasonal precipitation aggregation procedure is independent of the year in which the given monthly teleconnection(s) phase(s) were observed, rendering this work unsuitable for interdecadal analysis. Total seasonal precipitation for DT days during El Nino months, for each station is included in Table 31, while the number of DT days, for all four seasons, during El Nino months was shown in Figure 16(a). Also listed are the number of days this combined condition was observed, spatial precipitation average, and spatial standard deviation for each of the four seasons. Thus for winter from Table 31, a spatial average of 2.03 inches results from: average[Bedford(2.54), Blacksburg(2.70), Roanoke(0.89), Lafayette(1.64), Buchanan(2.16), Pulaski(2.01), Rocky Mount(2.25)].

Table 31. Total precipitation by station for Dry Tropical (DT) days within El Nino months arranged according to season; seasonal spatial averages and standard deviations also reported (inches*100)

Season	#days DT	Sum of Precipitation for all DT captured days during El Nino months (inches*100)							Spatially Averaged Seasonal Precip (inches*100)	Spatial St. Dev. (inches*100).
		Bedford	Blacksburg	Roanoke	Lafayette	Buchanan	Pulaski	Rocky Mount		
Winter	45	254	270	89	164	216	201	225	203	61
Spring	140	427	365	117	226	280	147	491	293	141
Summer	111	341	821	160	324	839	306	216	430	281
Fall	112	236	224	50	135	240	110	201	171	73

As completed for all four seasons and shown in equation (4), seasonal total precipitation at each station is standardized by that season's spatially average and spatial standard deviation.

$$TSsp_{i,s}^{k,j} = \frac{SeasonalTotal\,\mathrm{Pr}ecip_{i,s}^{k,j} - SpatiallyAvg\,\mathrm{Pr}ecip_{s}^{k,j}}{SpatialStDev_{s}^{k,j}} \quad (4)$$

where TSsp = total seasonal spatially standardized precipitation for station i, during season s for days of weather type j occurring within months of Index phase k. For clarity, $TSsp_{i,winter}^{ElNino,DT}$ for i = Bedford, Blacksburg, …Rocky Mount is displayed in Table 32, while Figures 17 (a-c) provide $TSsp_{i,s}^{k,DT}$ over all seasons and stations for k = El Nino, La Nina, and ENSO-neutral. It is evident from Figures 17 (a-c) that large variation in fall TSsp is displayed. Appendix C offers TSsp results for ENSO, NAO, PNA, and AO.

Table 32. Total winter spatially standardized precipitation for the El Nino_Dry Tropical condition, $TSsp_{i,winter}^{ElNino,DT}$

Bedford	Blacksburg	Roanoke	Lafayette	Buchanan	Pulaski	Rocky Mount
0.8425	1.1013	-1.8683	-0.6362	0.2180	-0.0232	0.3660

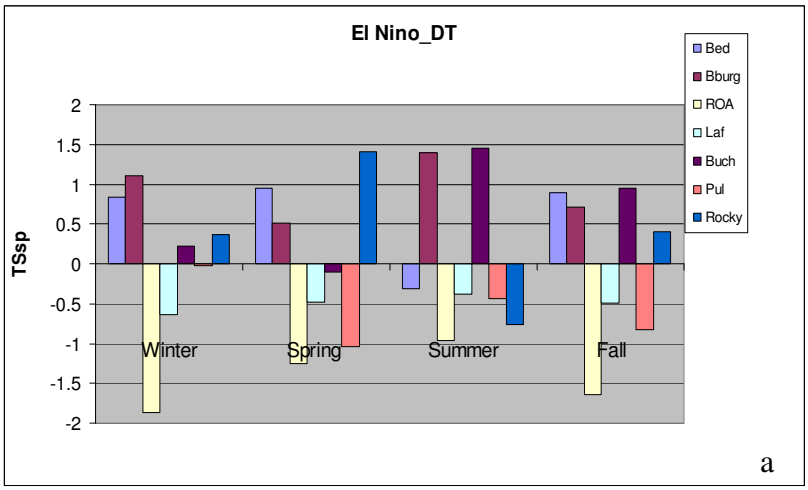

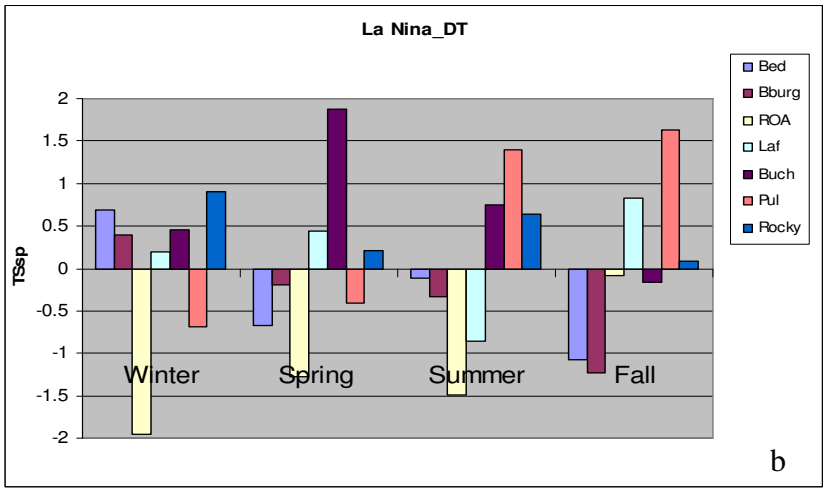

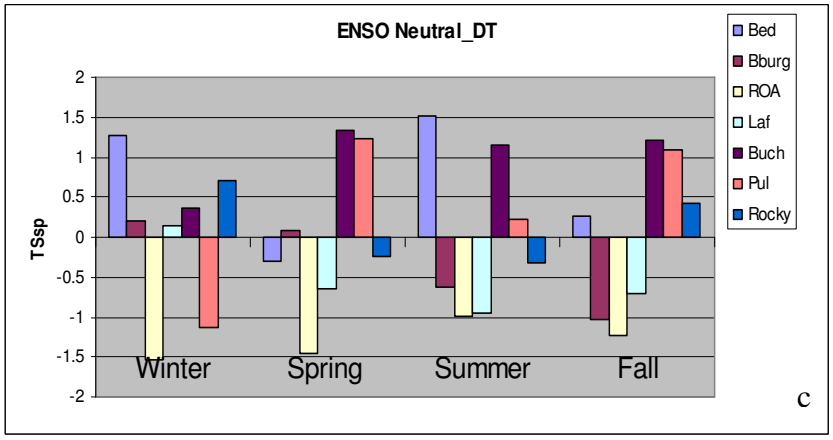

Figures 17 (a-c). Total seasonal spatially standardized precipitation (TSsp) over all seasons and stations, for (a) El Nino, (b) La Nina, and (c) ENSO-neutral months throughout the 1950-2003 period.

Notable results from Appendix C include substantial variation in winter and spring TSsp between the El Nino and AO+_Dry Polar (i.e DP days in winter and spring months were El Nino and AO+ occurred concurrently) and La Nina and AO+_Dry Polar condition for all seven stations and in spring and winter TSsp amid the NAO+_MT and NAO-_MT conditions was seen for Roanoke, Bedford, Blacksburg, and Buchanan. In addition, anomalous station distribution of TSsp is evident with the PNA-_DT condition during winter and fall, while Bedford frequently displays variation between phases of the indices considered over all seasons.

Summary

While this chapter investigated spatial variability in conditioned seasonal precipitation, focusing on winter-frontal events, a few of the notable inferences are now re-highlighted. Foremost, the Bedford/Buchanan station pair showed high variation in winter frontal-precipitation over the 1950-2003 study period (see Figures 7 and 8). Moreover, both the Roanoke/Pulaski and Roanoke/Lafayette combinations demonstrated similar precipitation behavior during winter frontal winter events as seen in Figures 7 and 8. Also, it should be remarked that Roanoke possessed anomalous frontal-precipitation during NAO+ winters (see Table 24) and Bedford exhibited dissimilar trends, relative to the remaining six stations, during frontal-precipitation days when a strong winter AO- merged with the PNA+ circulation (see Table 28). Furthermore, the Rocky Mount/Blacksburg station pair demonstrated contradictory behavior in total winter

frontal-precipitation when PNA+ winters united with the El Nino phase of ENSO (see Table 29). When Moist Polar air existed within winter El Nino months, Rocky Mount showed a propensity for receiving higher frontal-precipitation, upon spatial evaluations, when compared with La Nina and ENSO-Neutral winter months (see Figures 9, 10, and 11). Lastly, winter daily frontal-storm events that were congruent with Moist Moderate (MM) air showed a reduced occurrence during La Nina months verses El Nino and ENSO-Neutral months (see Figures 12, 13, and 14).

References

D'Aleo, J.S. 2002. El Nino and La Nina. Oryx Press: Westport, CT. pp. 1-71.

Eichler, T. and Bell, G. 2003. Special Climate Survey: October 2002 – June 2003 Cool and Wet in Eastern Untied States. Climate Prediction Center (CPC).

Greene, J.S. 1996. A synoptic climatological analysis of summertime precipitation intensity in the eastern United States. Physical Geography. Vol. 17. pp. 401-418.

Greenland, David. 2001. Multiyear variation of temperature and precipitation in the coastal states of the southeastern United States. Southeastern Geographer. Vol 41. No. 1. pp. 36-52.

Hasse and Dobson 1986. Introductory Meteorology and Fluid Dynamics. D. Reidel Publishing. Boston: pp 1- 46.

Hayden, Bruce P. 1979. Atlas of Virginia Precipitation. University of Virginia Press.

Katz, R.W., Parlange, M.B., Tebaldi, C. 2003 Stochastic Modeling of the Effects of Large-Scale Circulation on Daily Weather in the Southeastern U.S. Cl. Change. pp. 189-216.

Nielson-Gammon 2003. Handbook of Weather, Climate, and Water.. John Wiley and Sons, Inc. pp. 59-70.

NOAA. 2005A http://www.noaanews.noaa.gov/stories2005/s2534.htm). Retrieved 2006.

NOAA 2005B http://www.srh.noaa.gov/srh/jetstream/global/jet.htm. Retrieved 2006.

Oklahoma Climatology Survey. 1997. http://okfirst.ocs.ou.edu/train/meteorology/. Retrieved 2006.

Philander, S.G. 1990. El Nino, La Nina, and Southern Oscillation. Academic Press. pp.1-56.

Sheridan, S.C. 2002. The Redevelopment of a Weather-Type Classification Scheme for North America. Inter. J. of Climatology. pp. 51-68.

Simpson, H.J. and Colodner, D.C. 1999. Arizona precipitation response to the Southern Oscillation: A potential water management tool. Water Resources Research. Vol. 35, No. 12. pp. 3761-3769

Thompson 1996. Weather Fundamentals. http://www.atmos.umd.edu/~owen/POSTIX/index.html. Retrieved 2006.

UCAR. 2005 www.meted.ucar.edu. Retrieved 2006.

Zhou, Y.P.,Higgins, R.W. and H.-K. Kim 2001. Relationships between El Nino-Southern Oscillation and Arctic Oscillation: A Climate Weather Link. Climate Prediction Center (CPC).

Appendix A: Teleconnective Indices

Southern Oscillation Index (SOI)

The El Nino/Southern Oscillation (ENSO) phenomena can be captured by the Southern Oscillation Index (SOI) by computation of the sea surface pressure differences between Tahiti in the eastern tropical Pacific basin and at Darwin, Australia in the western Pacific. While negative values of the SOI is generally indicative of El Nino, positive values demonstrate La Nina conditions in the tropical Pacific Ocean. This study uses the monthly SOI reported by the Australian Bureau of Meteorology, known as the Troup SOI (BOM 2005) and is calculated as follows:

$$SOI = \frac{[Pdiff - Pdiffav]}{SD(Pdiff)} * 10$$

where:

Pdiff = (average Tahiti Mean Sea Level Pressure for the month) - (average Darwin Mean Sea Level Pressure for the month),

Pdiffav = long term average of Pdiff for the month in question, and

SD(Pdiff) = long term standard deviation of Pdiff for the month in question.

A comprehensive discussion of ENSO can be found in Appendix E.

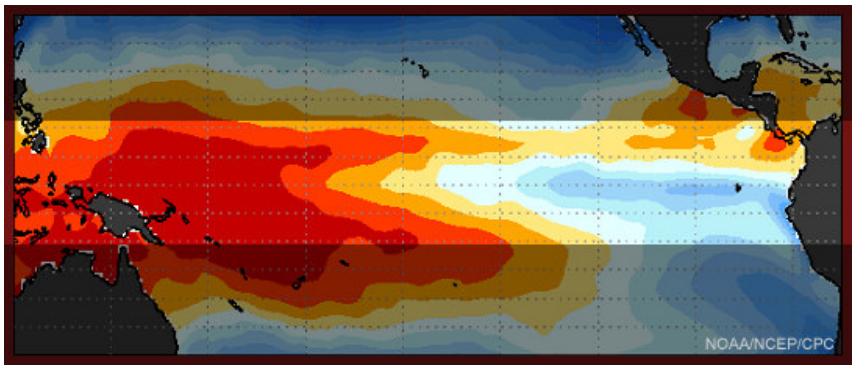

Figure 18. Development of the warm (El Nino) phase of the El Nino-Southern Oscillation (ENSO). (Reproduced from CPC 2005)

Pacific North American pattern (PNA)

The Pacific North American (PNA) index is a derived measure of the zonal/meridional flow of air across North America in the mid-troposphere, as computed in the following manner (Greenland 2001):

PNA = 0.25 * [Z(20N,160W) - Z(45N,165W) + Z(55N,115W) - Z(30N,85W)]

where Z = standardized 500 hPa geopotential height values (Mitchell 2004). Positive values are associated with meridional flow over the continent, with high pressure blocking in northwest Canada and a low pressure trough in east/southeastern U.S (Eichler and Bell 2003). This amplified ridge/trough pattern is dampened during PNA- periods, allowing a zonal flow to persist over the continent (Sheridan 2003). Wintertime precipitation events in the southeastern U.S. are typically less frequent during the PNA- event, while the amplified North American jet stream during PNA+ periods is consistent

with higher frequency of cold air masses and storm events in the eastern U.S. (D'Aleo 2002).

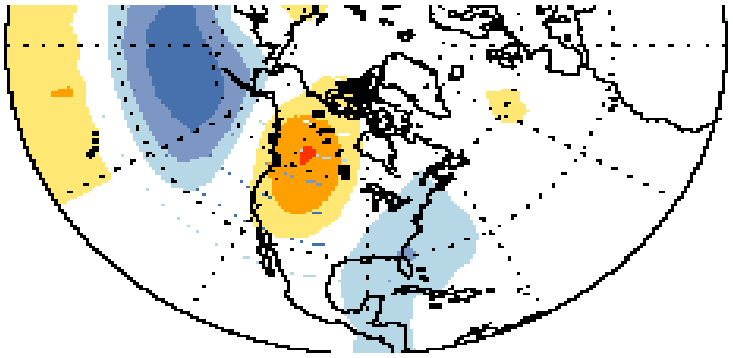

Figure 19. The positive phase of Pacific North American pattern (PNA). (Reproduced from Eichler and Bell 2003)

North Atlantic Oscillation (NAO)

The NAO constitutes a north-south dipole of sea-level pressure anomalies, with its northern center positioned over Greenland and southern center fluctuating in the central Atlantic ocean between 35°N and 40°N (CPC 2005). A monthly value of the NAO index is obtained by applying Rotated Principal Components Analysis (RPCA) on monthly mean standardized 500mb geopotential height anomalies in the region of 20°N-90°N (CPC 2005). The region encompassing its northern branch is referred to as the Icelandic Low pressure zone, while its subtropical southern branch is termed the Azores, or Bermuda, High pressure zone (Greenland 2001). Positive values of the NAO indicate that a stronger than normal low pressure region near Iceland is coupled with a well-defined high pressure zone in the subtropics (Sheridan 2003). When the NAO is negative, a relatively weak low pressure center in the North Atlantic Ocean is positioned

south of Greenland, while the Azores High is significantly weakened. It has been proposed that the NAO is related to a vast meridional circulation in the ocean, called the thermohaline, that possesses decadal periodicity (Eichler and Bell 2003).

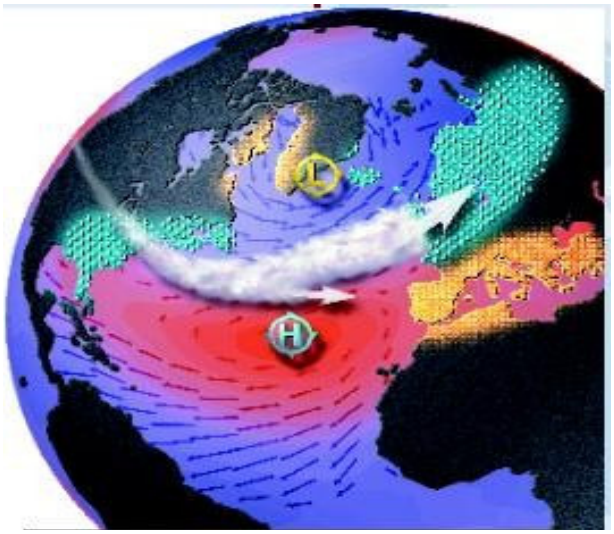

Figure 20. Positive phase of the North American Oscillation (NAO). (Reproduced from CPC 2005).

Arctic Oscillation (AO)

Transfer of atmospheric mass between the higher midlatitudes and polar latitudes greater than 20°N defines the Arctic Oscillation (AO) (CPC 2005). Daily AO index values are produced by projecting daily 1000mb height anomalies, north of 20°N onto a statistical loading pattern resulting from empirical orthogonal function (EOF) analysis (CPC 2005). These daily values can be averaged to construct a monthly series, with negative AO values portraying a general persistence of high pressure at the polar latitudes and relatively low pressures over the eastern North Atlantic Ocean and off the Alaskan Aleutian islands (Eichler and Bell 2003). Since the negative phase of the AO is related to the positive phase of the PNA, it is also related to weak to moderate El Nino episodes

(Eichler and Bell 2003). Moreover, the Arctic Oscillation has been proven to encompass the North Atlantic Oscillation (Higgins et al. 2000).

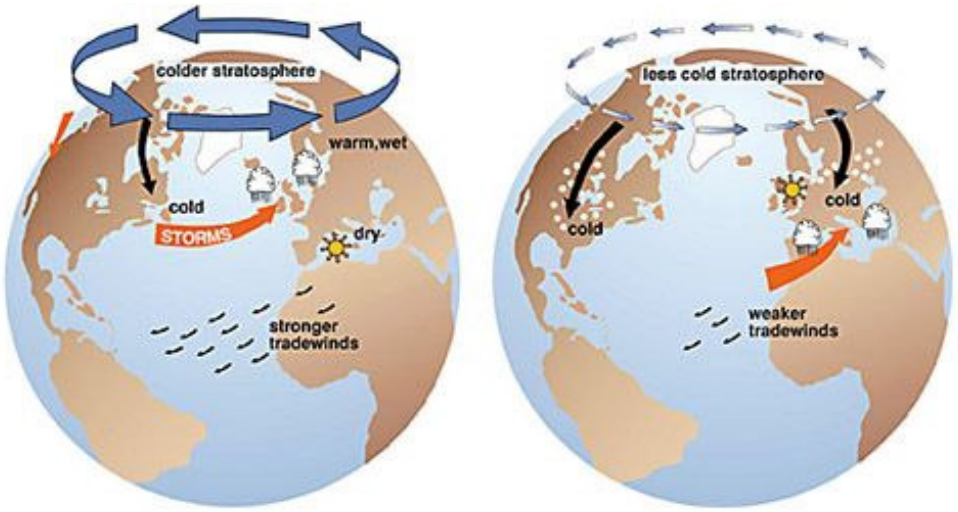

Figure 21. The negative phase of the Arctic Oscillation (AO). (Reproduced from CPC 2005)

Table 33: Bounds Used for Index Phase Designation

Value Assignment	Phase	Value Assignment	Phase
SOI ≥ 5	La Nina	AO ≥ 0.25	AO+
-5 < SOI < 5	Neutral	-0.25 < AO < 0.25	AO Neutral
SOI ≤ -5	El Nino	AO ≤ -0.25	AO-
PNA ≥ 0.5	PNA+	NAO ≥ 0.25	NAO+
-0.5 < PNA < 0.5	PNA Neutral	-0.25 < NAO < 0.25	NAO Neutral
PNA ≤ -0.5	PNA-	NAO ≤ -0.25	NAO-

Synoptic Scale Classification (SSC2) Daily Weather Types

Dry Polar (DP)

This weather type is used to signal cool or cold dry air which is introduced into a region in the midlatitudes via a cold-core anticyclone. A region exposed to the DP air mass likely experiences a northerly/northwesterly/northeasterly wind and zero to little cloud cover. Its low moisture content is an effect of its typical source regions: Northern Canada and/or Alaska. During fall through winter, the DP air mass is more prevalent in eastern North America when a PNA+ circulation appears during this period. The DP air mass is on occasions analogous to Bergeron's (1930) cP (continental polar) or cA (continental arctic). (Sheridan 2002)

Dry Moderate (DM)

While this air mass designation is dry and demonstrates little to no cloud cover, it is mild in temperature, particularly when compared against DP. It can be expected to arrive in the eastern U.S. when a zonal flow pattern dominates the upper atmosphere due to the adiabatic drying that takes place east of the Rocky Mountains. Although zonal flow is typically associated with DM, it has no reliable source region(s). Through its link with upper atmospheric circulation, the DM air mass characteristically replaces DT and MT during PNA+. (Sheridan 2002)

Dry Tropical (DT)

Days in the historical record possessing the hottest, sunniest, and driest conditions (relative to seasonal climatology) are adopted as DT days. Continental source regions usually are responsible for this air mass, with the deserts in southwest U.S. offering ideal conditions for DT conception. In addition, this designation can result from compressional heating of an air mass subsequent to rapid descent. DT is often affiliated with Bergeron's (1930) cT (continental tropical) air mass category. (Sheridan 2002)

Moist Polar (MP)

Light precipitation, cool, and cloudy are traits of the MP air mass. These cool and humid conditions can enter into the U.S. through advection with flow off either the North Pacific or North Atlantic oceans; however, when DP air gains moisture as it passes over inland water bodies (e.g. the Great Lakes or Hudson Bay), MP air can emerge. This weather type is often related to the occurrence of warmer air aloft and cool surface temperatures (frontal inversion or overrunning), which can often provide the signature for cold air damming in western and southwestern Virginia (Ok. Clim. 1997; Myatt 2005). Furthermore, the MP air mass is often referred to as mP (maritime polar) or cP (continental polar). (Sheridan 2002)

Moist Moderate (MM)

MM air is similar to MP, although it carries with it higher temperatures, humidity, and cloudiness. This link allows MP air to augment into MM depending on surface conditions encountered by the former air mass once exiting its source region. Moreover,

an MM air mass can often be found south of MP air, closer to a passing warm front. When humidity conditions linked to MT air collaborate during summer months with elevated cloud cover, which serves to reduce temperature, an MM air mass can transpire. (Sheridan 2002)

Moist Tropical (MT)

Three source regions are responsible for introduction of MT air into the U.S.: Gulf of Mexico, tropical Atlantic Ocean, and tropical Pacific Ocean. Significant humidity, warm temperatures, and varying cloud cover (partially in summer and high in winter) accompany this air mass. Summer convective-dominating precipitation events are typical manifested by MT air. Additionally, it lies in the warm portion of an extratropical (mid-latitude) cyclone, where conditions are conducive for intense convection, as well as on the western region of a surface high pressure center. (Sheridan 2002)

Transitional (TR)

Days which separate two dissimilar weather types (of the above 6) accept the TR designation. Criteria used to capture TR days focus on variation of regional meteorological conditions over the approximate interval of a day. These criteria are diurnal ranges of dew point, sea level pressure, and wind direction. Days on which tropical depressions (e.g. hurricanes, tropical storms) propagate through a given region are most likely to be categorized as TR given the fast-moving nature of these systems (Greene 1996). (Sheridan 2002)

References

Australian Bureau of Meteorology (BOM). 2005. Climate Glossary. http://www.bom.gov.au/climate/glossary/soi.shtml. Retrieved December 2005.

Bergeron, T. 1930. Richtlinien einer dynamishen klimatologie. Met. Zeitung Vol. 47. pp. 246-262.

Climate Prediction Center (CPC). 2005. Teleconnections. CPC Internet Team. http://www.cpc.ncep.noaa.gov/products/precip/CWlink/daily_ao_index/teleconnections.shtml. Retrieved December 2005.

D'Aleo, J.S. 2002. El Nino and La Nina. Oryx Press: Westport, CT. pp. 1-71.

Eichler, T. and Bell, G. 2003. Special Climate Survey: October 2002 – June 2003 Cool and Wet in Eastern Untied States. Climate Prediction Center (CPC).

Greene, J.S. 1996. A synoptic climatological analysis of summertime precipitation intensity in the eastern United States. Physical Geography. Vol. 17. pp. 401-418.

Greenland, David. 2001. Multiyear variation of temperature and precipitation in the coastal states of the southeastern United States. Southeastern Geographer. Vol 41. No. 1. pp. 36-52.

Higgins, R.W., Leetmaa, A., Xue, Y. Barnston, A. 2000. Dominant factors influencing the seasonal predictability of US precipitation and surface air temperature. J. of Climate. Vol. 13. pp. 3994-4017.

Mitchelle, T. 2004. Pacific/North American (PNA) index. Joint Institute for the Study of the Atmosphere and Ocean. University of Washington and NOAA. http://tao.atmos.washington.edu/data_sets/pna/. Retrieved December 2005.

Myatt, K. 2005. Weather Journal. The Roanoke Times. http://www.roanoke.com/weather/. Retrieved 2005.

Oklahoma Climatological Survey. 2004. Overview of Meteorology. http://okfirst.ocs.ou.edu/train/meteorology/. Retrieved December 2005.

Sheridan, S.C. 2003. North American weather-type frequency and teleconnection indices. International J. of Climatology. Vol. 23, pp. 27-45.

Sheridan, S.C. 2002. The Redevelopment of a Weather-Type Classification Scheme for North America. Inter. J. of Climatology. pp. 51-68.

Appendix B: Virginia Precipitation Station Data

Table 34: Station Positioning

Station	Latitude (DM)*	Longitude (DM)*	Elevation (feet above sea level)*
Bedford	37 21	-79 31	297.2
Blacksburg	37 12	-80 25	640.1
Roanoke	37 16	-79 56	278
Lafayette	37 14	-80 12	402.3
Buchanan	37 32	-79 41	268.2
Pulaski	37 03	-80 47	563.9
Rocky Mount	36 59	-79 54	400.8

*From National Weather Service (NWS)

Table 35: Planimetric Station Data

Stations i/j	Distance btwn. stations i/j (miles)*	Azmith btwn. stations i/j (degrees)*
Bed/Bburg	51.4	259.11
Bed/ROA	25.7	256.69
Bed/Laf	40.0	258.76
Bed/Buch	15.2	324.73
Bed/Pul	74.3	254.51
Bed/Rocky	32.4	220.65
Bburg/ROA	25.7	81.23
Bburg/Laf	11.4	99.79
Bburg/Buch	45.7	61.28
Bburg/Pul	24.8	244.21
Bburg/Rocky	33.3	118.64
ROA/Laf	15.2	262.06
ROA/Buch	21.9	37.59
ROA/Pul	50.5	253.46
ROA/Rocky	14.3	175.48
Laf/Buch	36.2	54.83
Laf/Pul	35.2	249.77
Laf/Rocky	23.8	137.08
Buch/Pul	71.4	242.24
Buch/Rocky	39.0	198.26
Pul/Rocky	49.5	96.49

*From (Hayden 1979)

Appendix C: Teleconnection through ENSO, NAO, PNA, and AO and SSC weather type conditioning on historical seasonally-standardized precipitation, TSsp

EN – El Nino month; LN – La Nina month; N – ENSO Neutral month

SSC1 – Dry Polar (DP) days; SSC2 – Dry Moderate (DM) days; SSC3 – Dry Tropical (DT) days; SSC4 – Moist Polar (MP) days; SSC5 – Moist Moderate (MM) days; SSC6 – Moist Tropical (MT) days; SSC7 – Transitional (TR) days

Figures 22-139: Teleconnections and SSC Conditions on Seasonally-Standardized Precipitation

ENSO_SSC Conditioning

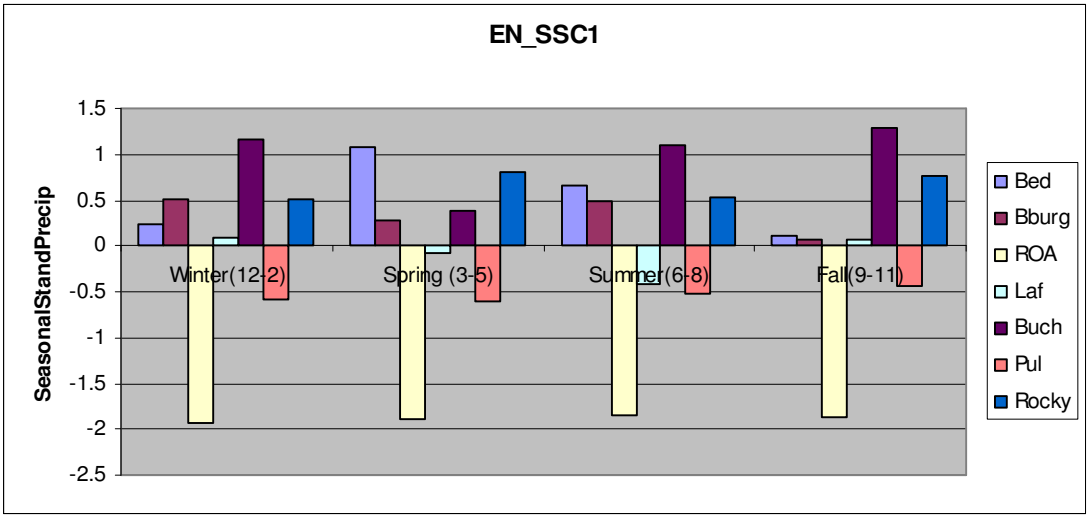

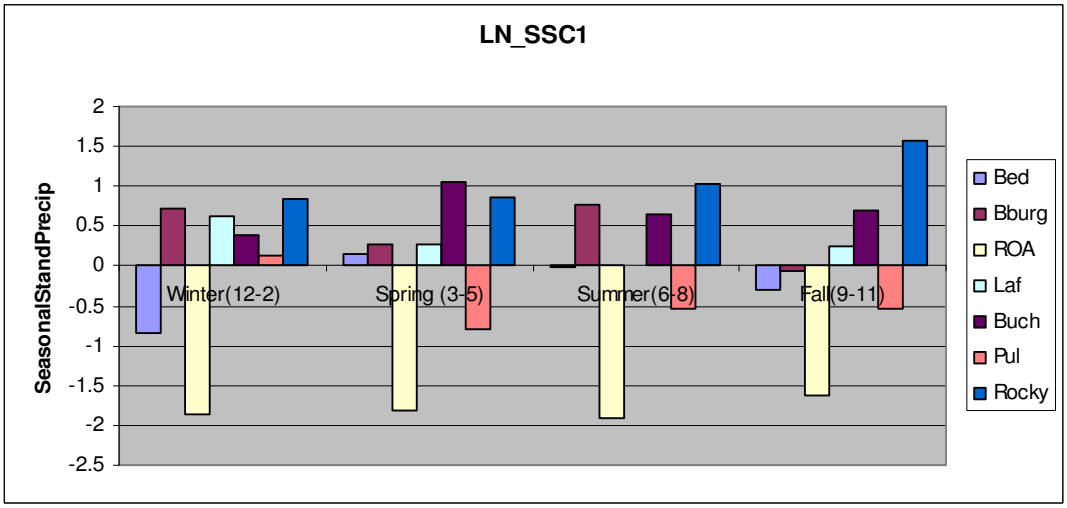

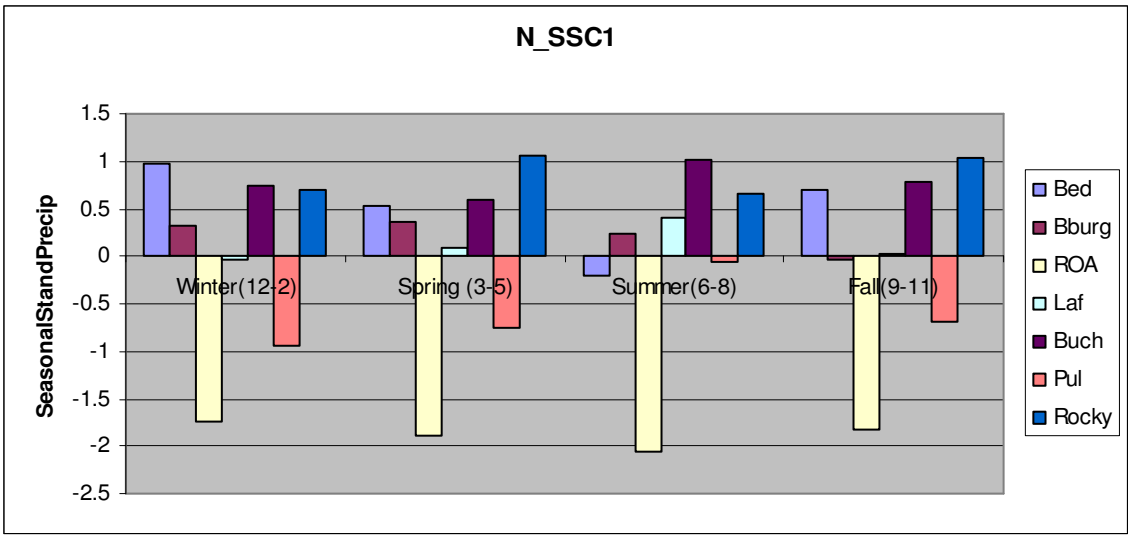
N_SSC1
SeasonalStandPrecip
1.5
1
0.5
0
-0.5
-1
-1.5
-2
-2.5
Winter(12-2)
Spring (3-5)
Summer(6-8)
Fall(9-11)
Bed
Bburg
ROA
Laf
Buch
Pul
Rocky

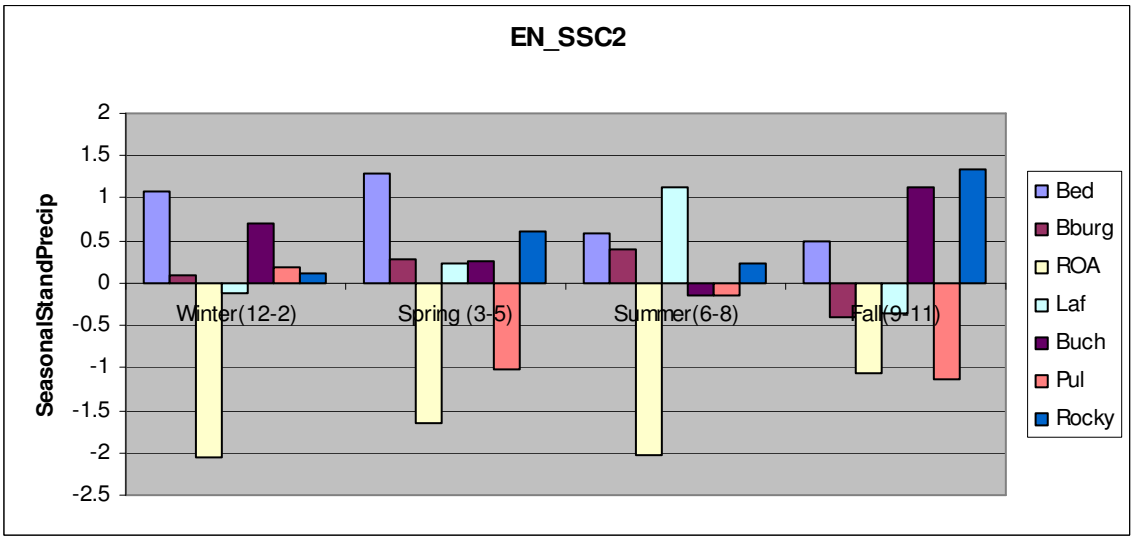
EN_SSC2
SeasonalStandPrecip
2
1.5
1
0.5
0
-0.5
-1
-1.5
-2
-2.5
Winter(12-2)
Spring (3-5)
Summer(6-8)
Fall(9-11)
Bed
Bburg
ROA
Laf
Buch
Pul
Rocky

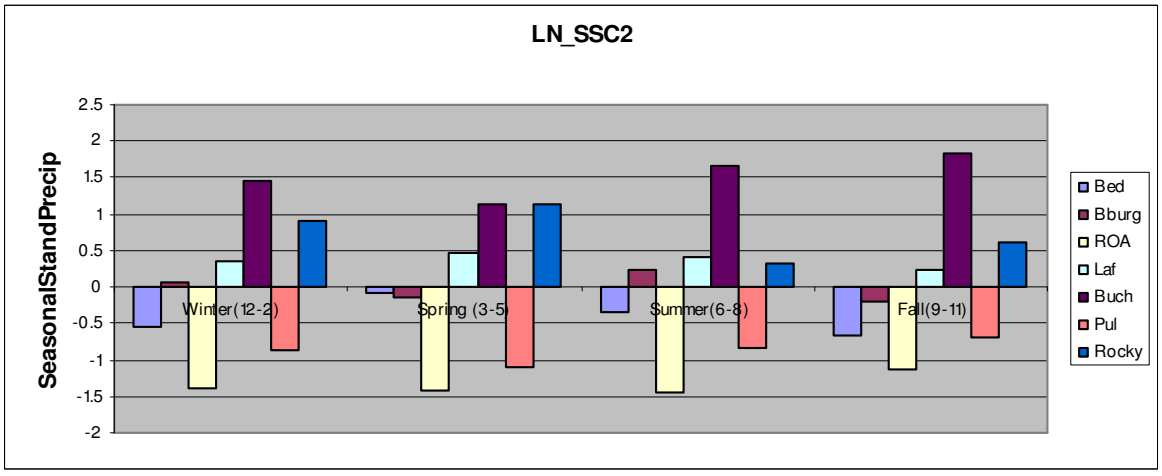
LN_SSC2
SeasonalStandPrecip
2.5
2
1.5
1
0.5
0
-0.5
-1
-1.5
-2
Winter(12-2)
Spring (3-5)
Summer(6-8)
Fall(9-11)
Bed
Bburg
ROA
Laf
Buch
Pul
Rocky

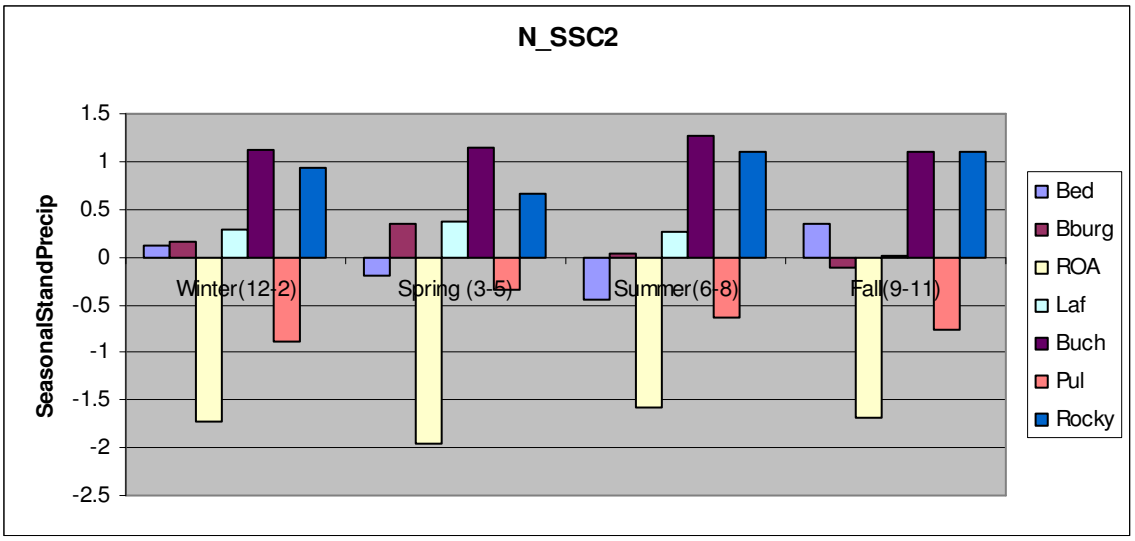
N_SSC2
SeasonalStandPrecip
1.5
1
0.5
0
-0.5
-1
-1.5
-2
-2.5
Winter(12-2)
Spring (3-5)
Summer(6-8)
Fall(9-11)
Bed
Bburg
ROA
Laf
Buch
Pul
Rocky

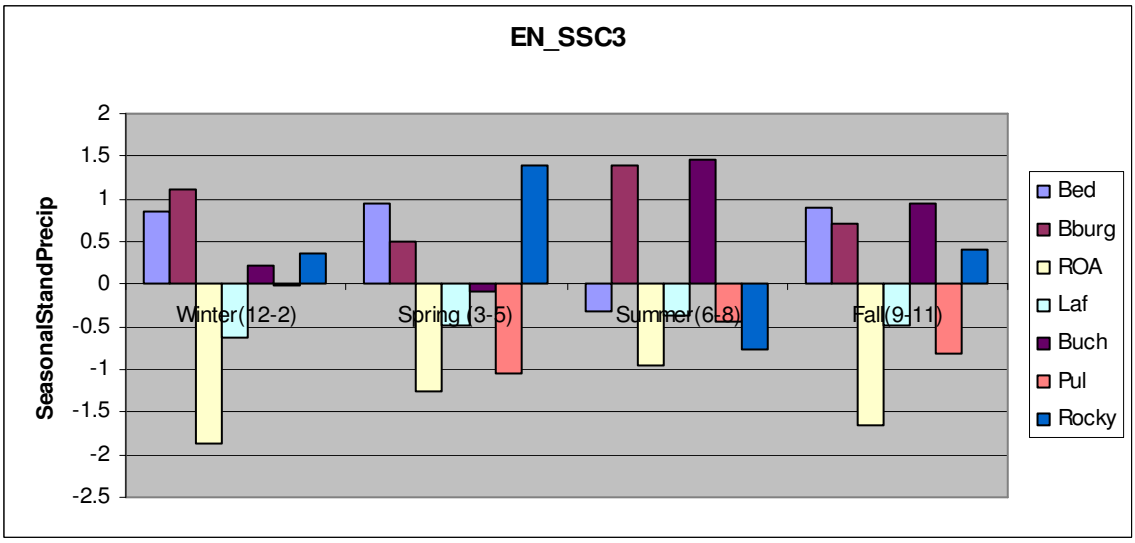
EN_SSC3
SeasonalStandPrecip
2
1.5
1
0.5
0
-0.5
-1
-1.5
-2
-2.5
Winter(12-2)
Spring (3-5)
Summer(6-8)
Fall(9-11)
Bed
Bburg
ROA
Laf
Buch
Pul
Rocky

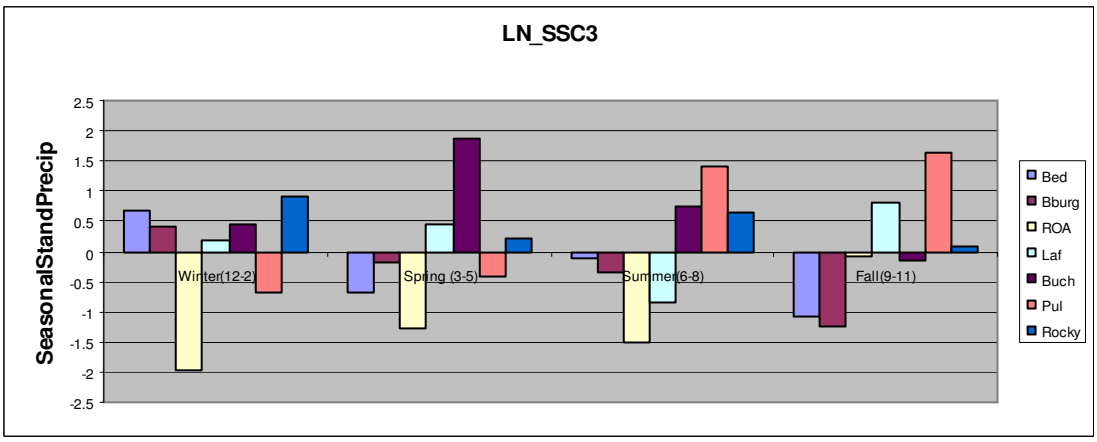
LN_SSC3
SeasonalStandPrecip
2.5
2
1.5
1
0.5
0
-0.5
-1
-1.5
-2
-2.5
Winter(12-2)
Spring (3-5)
Summer(6-8)
Fall(9-11)
Bed
Bburg
ROA
Laf
Buch
Pul
Rocky

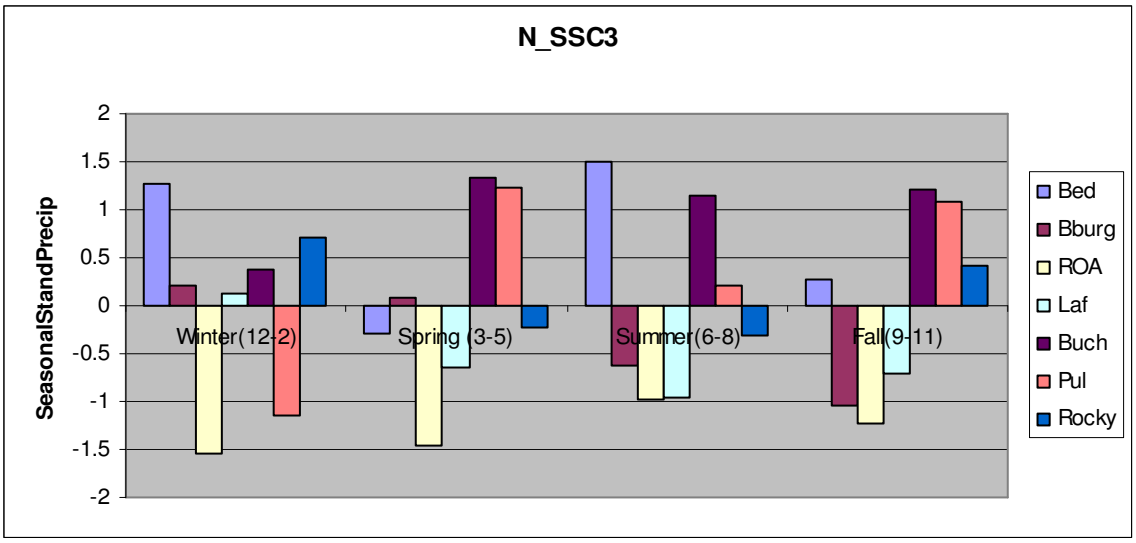
N_SSC3
SeasonalStandPrecip
2
1.5
1
0.5
0
-0.5
-1
-1.5
-2
Winter(12-2)
Spring (3-5)
Summer(6-8)
Fall(9-11)
Bed
Bburg
ROA
Laf
Buch
Pul
Rocky

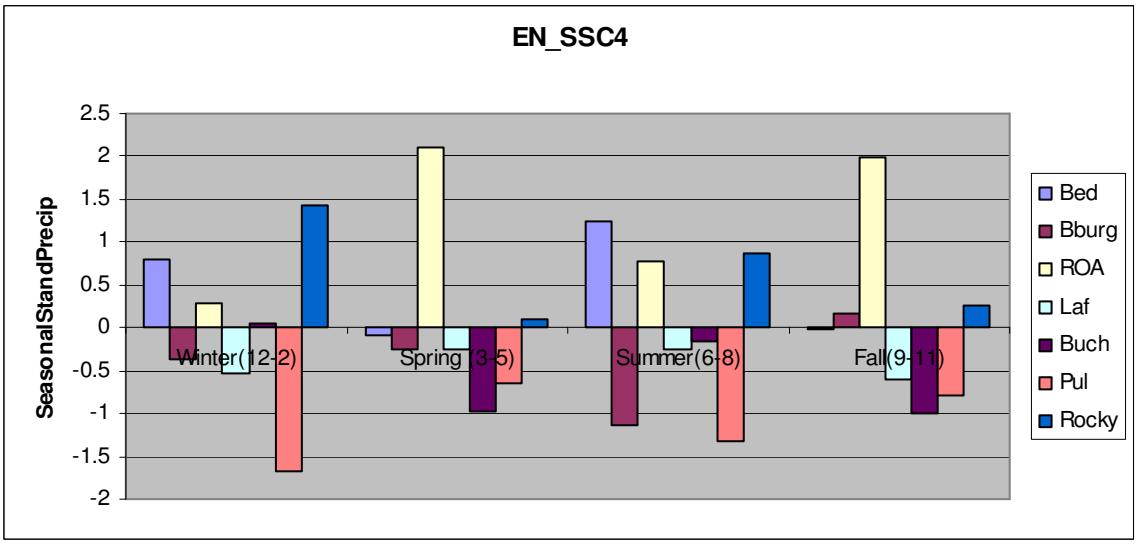
EN_SSC4
SeasonalStandPrecip
2.5
2
1.5
1
0.5
0
-0.5
-1
-1.5
-2
Winter(12-2)
Spring (3-5)
Summer(6-8)
Fall(9-11)
Bed
Bburg
ROA
Laf
Buch
Pul
Rocky

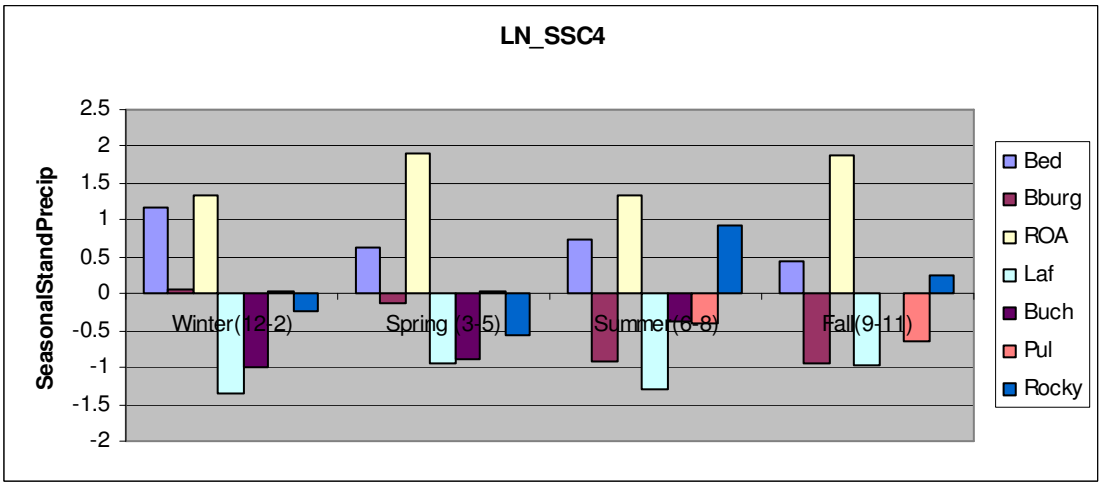
LN_SSC4
SeasonalStandPrecip
2.5
2
1.5
1
0.5
0
-0.5
-1
-1.5
-2
Winter(12-2)
Spring (3-5)
Summer(6-8)
Fall(9-11)
Bed
Bburg
ROA
Laf
Buch
Pul
Rocky

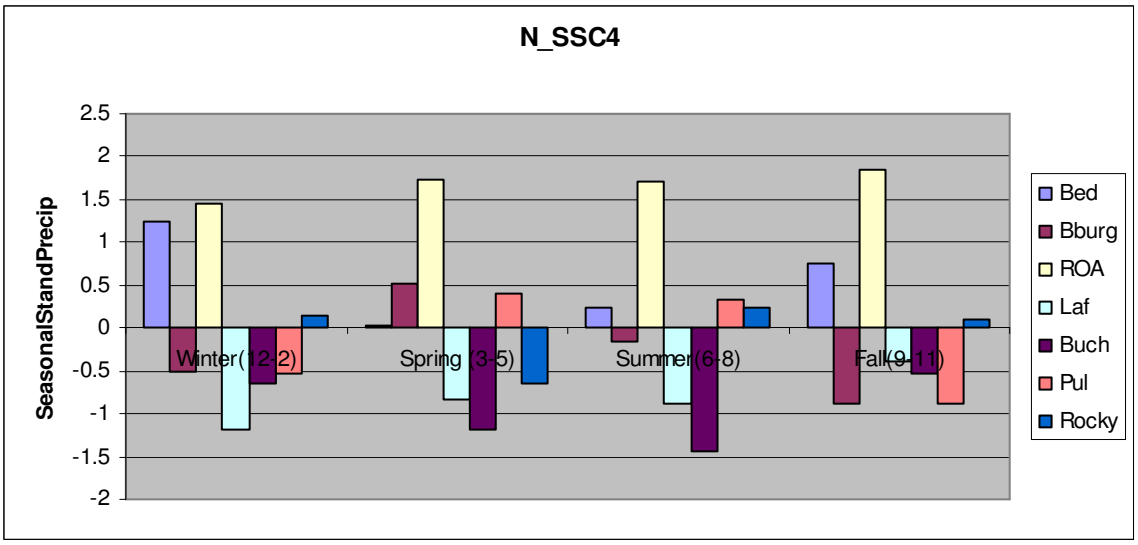
N_SSC4
SeasonalStandPrecip
2.5
2
1.5
1
0.5
0
-0.5
-1
-1.5
-2
Winter(12-2)
Spring (3-5)
Summer(6-8)
Fall(9-11)
Bed
Bburg
ROA
Laf
Buch
Pul
Rocky

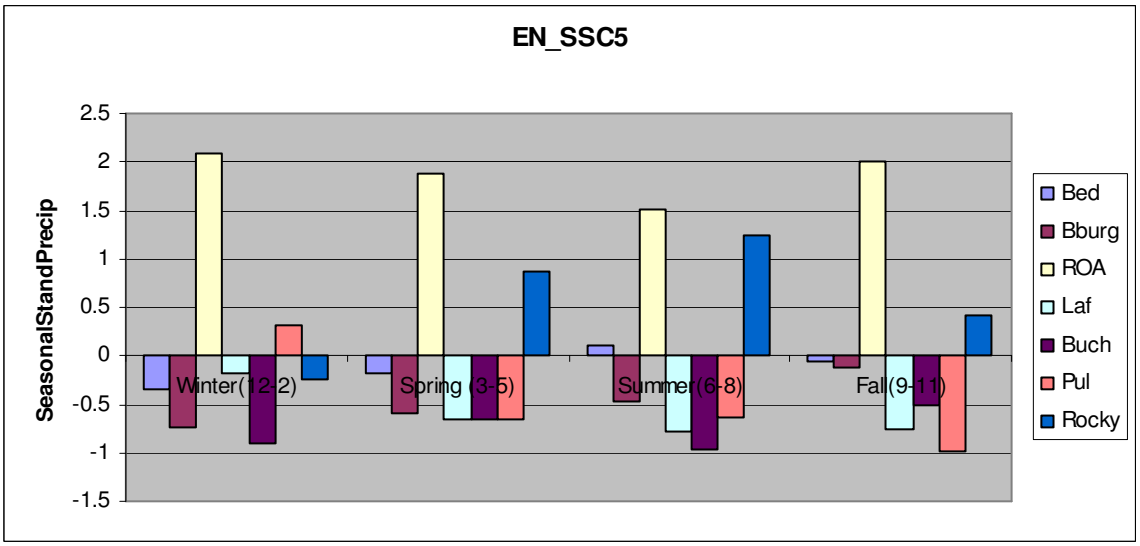
EN_SSC5
SeasonalStandPrecip
2.5
2
1.5
1
0.5
0
-0.5
-1
-1.5
Winter(12-2)
Spring (3-5)
Summer(6-8)
Fall(9-11)
Bed
Bburg
ROA
Laf
Buch
Pul
Rocky

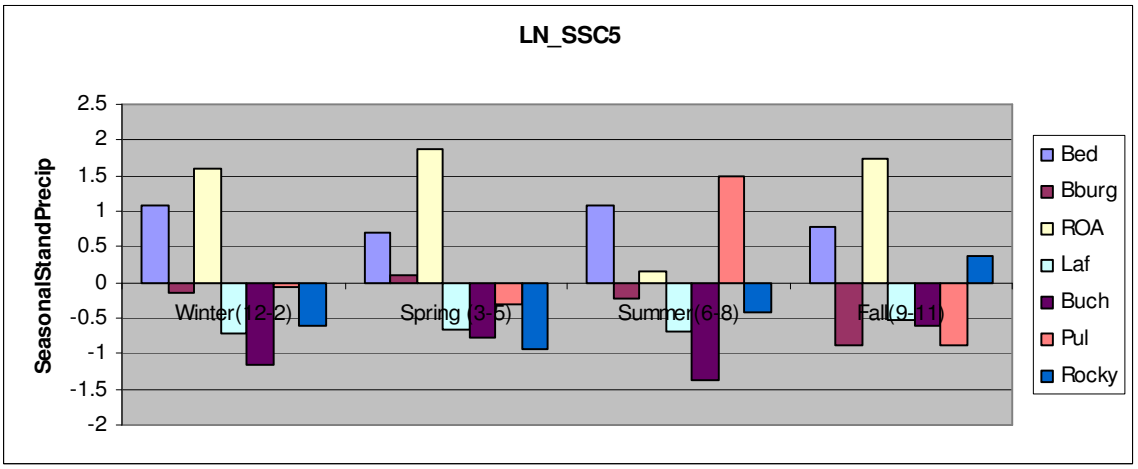
LN_SSC5
SeasonalStandPrecip
2.5
2
1.5
1
0.5
0
-0.5
-1
-1.5
-2
Winter(12-2)
Spring (3-5)
Summer(6-8)
Fall(9-11)
Bed
Bburg
ROA
Laf
Buch
Pul
Rocky

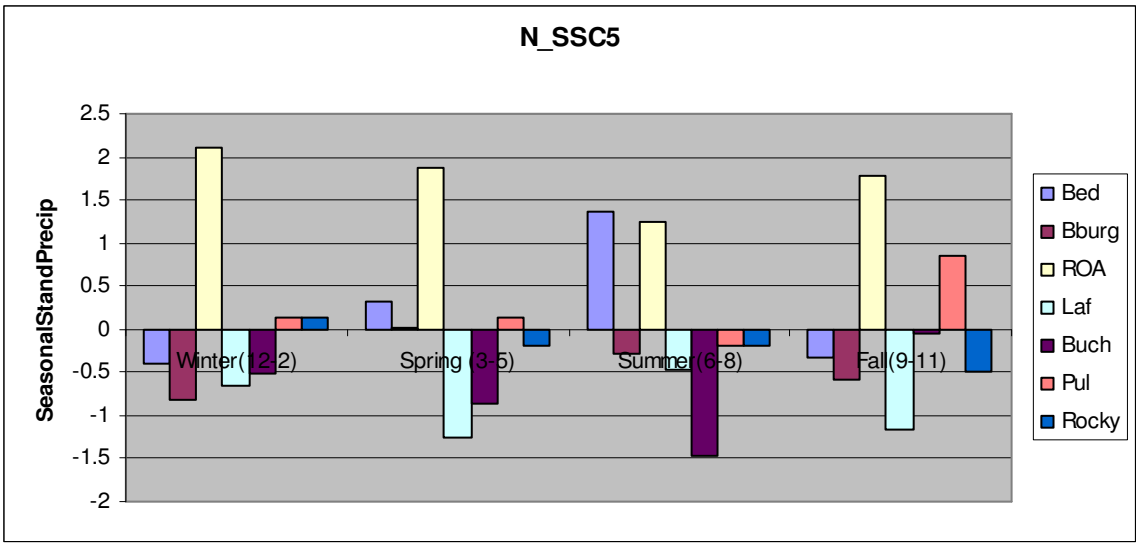
N_SSC5
SeasonalStandPrecip
2.5
2
1.5
1
0.5
0
-0.5
-1
-1.5
-2
Winter(12-2)
Spring (3-5)
Summer(6-8)
Fall(9-11)
Bed
Bburg
ROA
Laf
Buch
Pul
Rocky

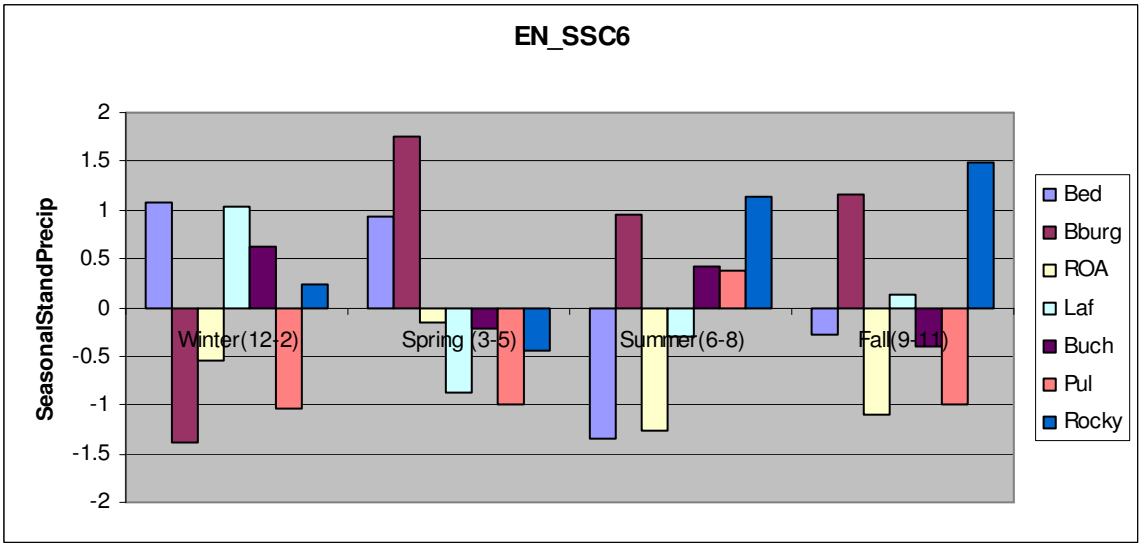
EN_SSC6
SeasonalStandPrecip
2
1.5
1
0.5
0
-0.5
-1
-1.5
-2
Winter(12-2)
Spring (3-5)
Summer(6-8)
Fall(9-11)
Bed
Bburg
ROA
Laf
Buch
Pul
Rocky

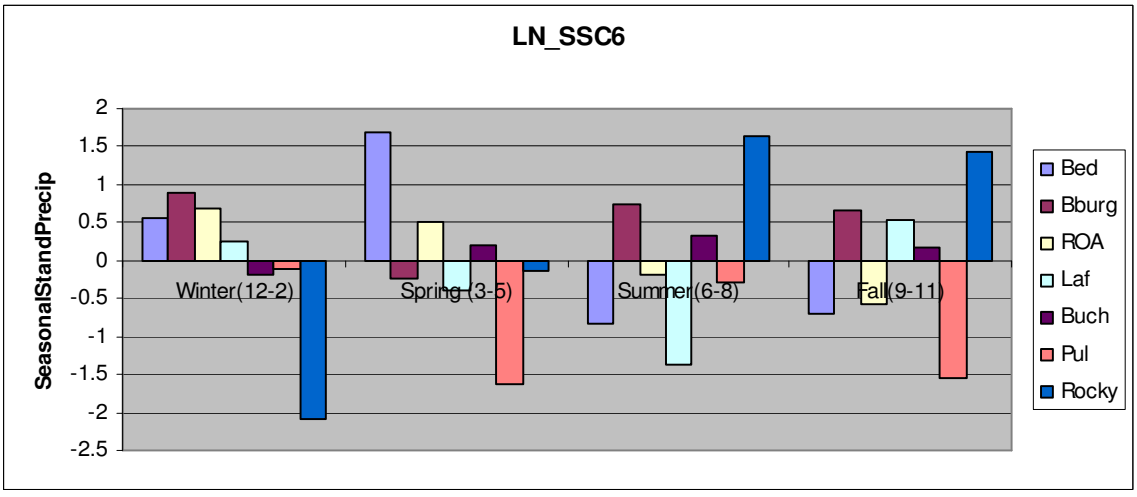
LN_SSC6
SeasonalStandPrecip
2
1.5
1
0.5
0
-0.5
-1
-1.5
-2
-2.5
Winter(12-2)
Spring (3-5)
Summer(6-8)
Fall(9-11)
Bed
Bburg
ROA
Laf
Buch
Pul
Rocky

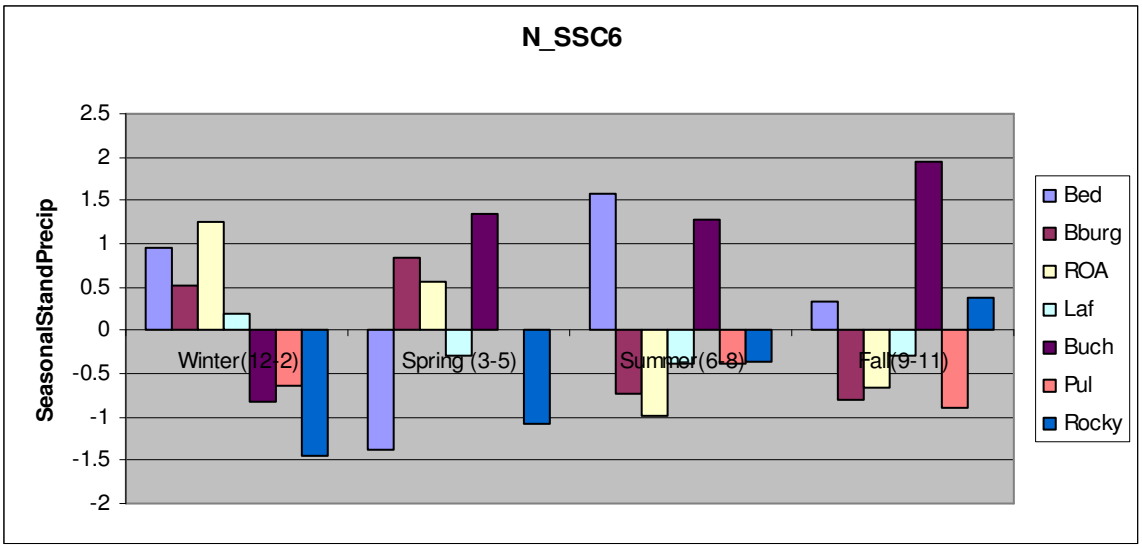
N_SSC6
SeasonalStandPrecip
2.5
2
1.5
1
0.5
0
-0.5
-1
-1.5
-2
Winter(12-2)
Spring (3-5)
Summer(6-8)
Fall(9-11)
Bed
Bburg
ROA
Laf
Buch
Pul
Rocky

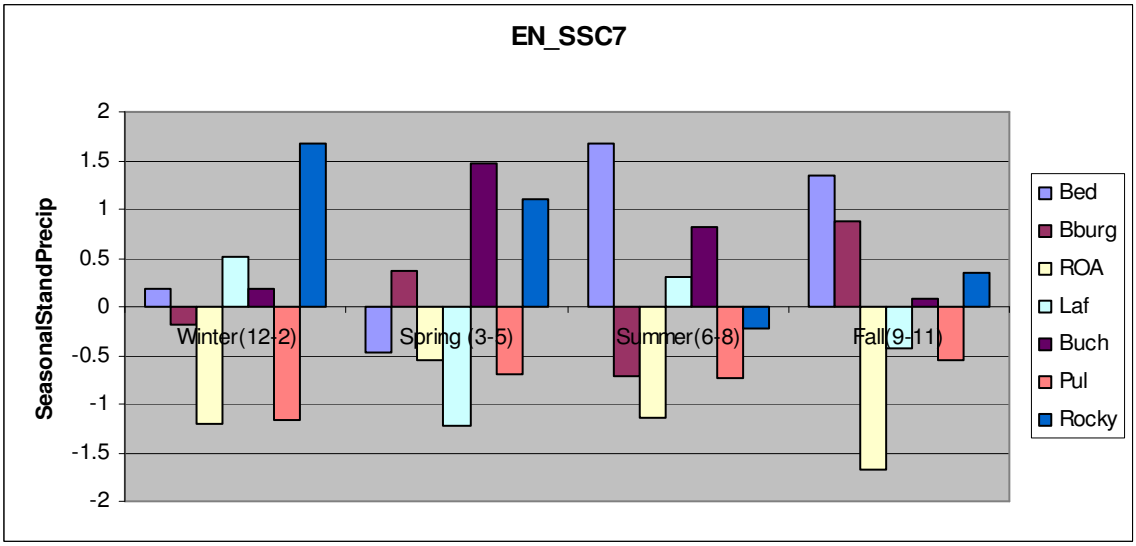
EN_SSC7
SeasonalStandPrecip
2
1.5
1
0.5
0
-0.5
-1
-1.5
-2
Winter(12-2)
Spring (3-5)
Summer(6-8)
Fall(9-11)
Bed
Bburg
ROA
Laf
Buch
Pul
Rocky

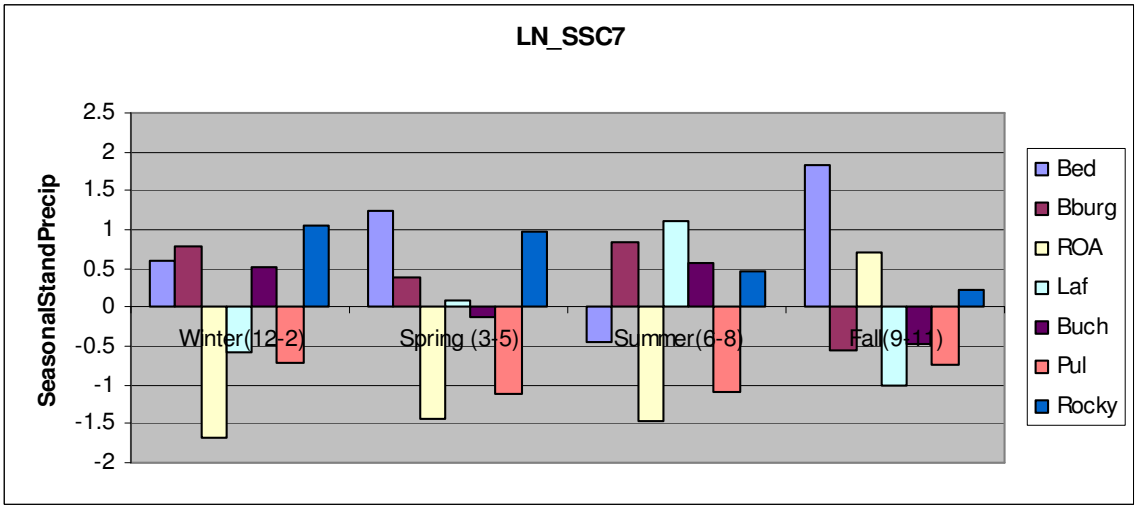
LN_SSC7
SeasonalStandPrecip
2.5
2
1.5
1
0.5
0
-0.5
-1
-1.5
-2
Winter(12-2)
Spring (3-5)
Summer(6-8)
Fall(9-11)
Bed
Bburg
ROA
Laf
Buch
Pul
Rocky

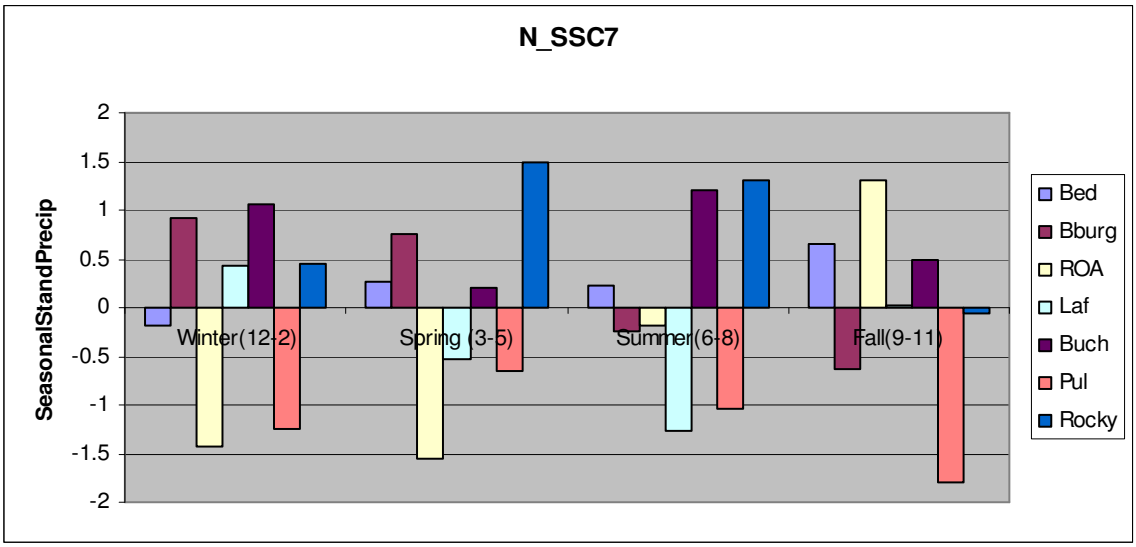

NAO_SSC Conditioning

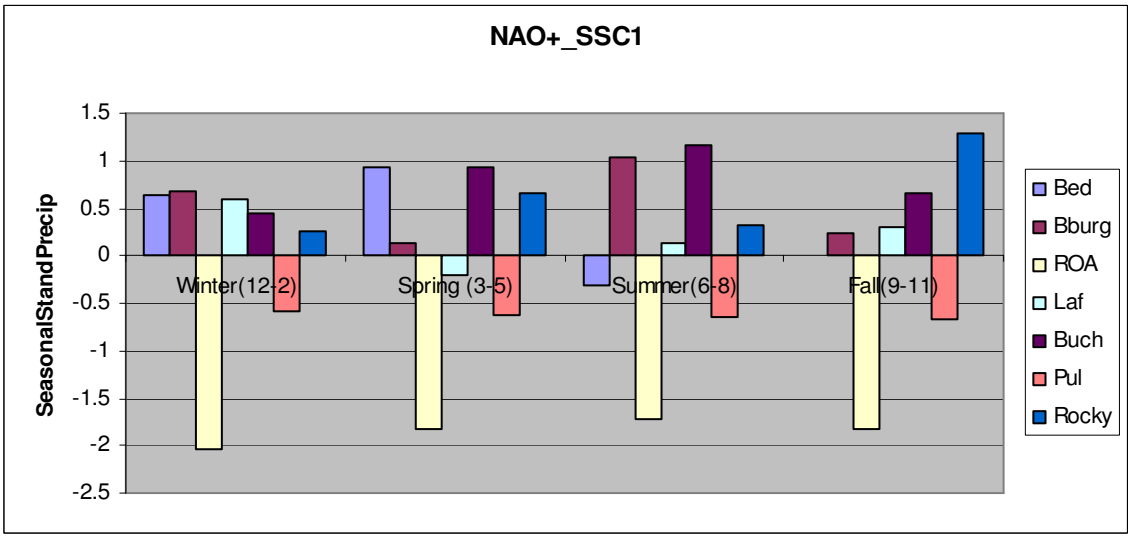

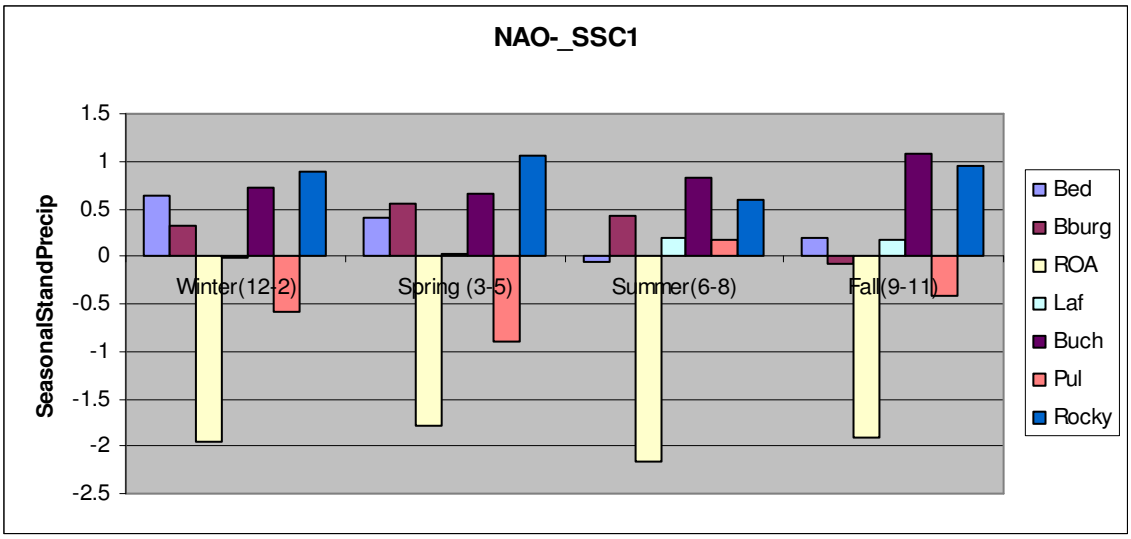
NAO-_SSC1
SeasonalStandPrecip
1.5
1
0.5
0
-0.5
-1
-1.5
-2
-2.5
Winter(12-2)
Spring (3-5)
Summer(6-8)
Fall(9-11)
Bed
Bburg
ROA
Laf
Buch
Pul
Rocky

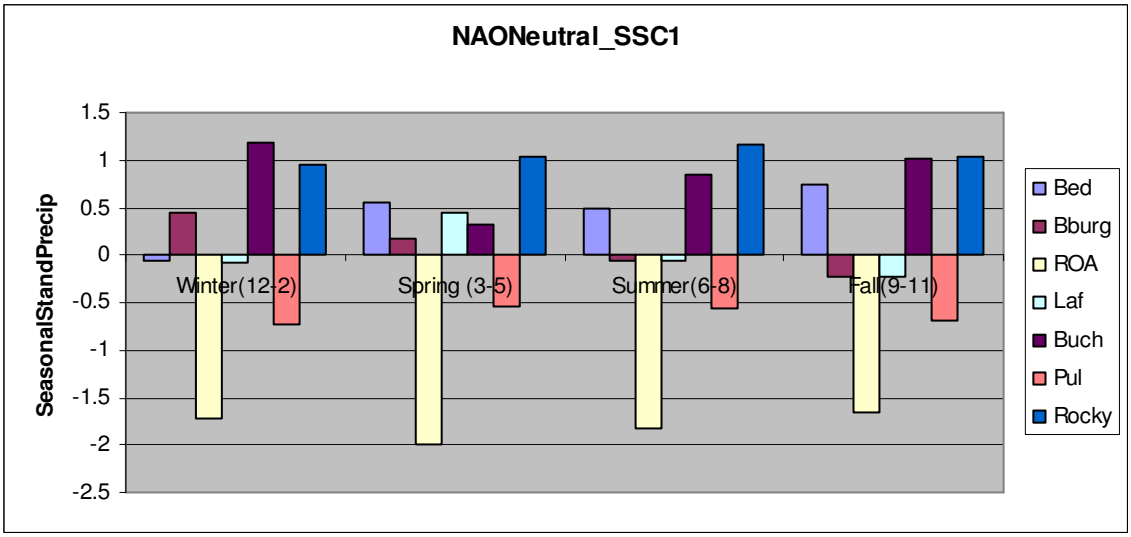
NAONeutral_SSC1
SeasonalStandPrecip
1.5
1
0.5
0
-0.5
-1
-1.5
-2
-2.5
Winter(12-2)
Spring (3-5)
Summer(6-8)
Fall(9-11)
Bed
Bburg
ROA
Laf
Buch
Pul
Rocky

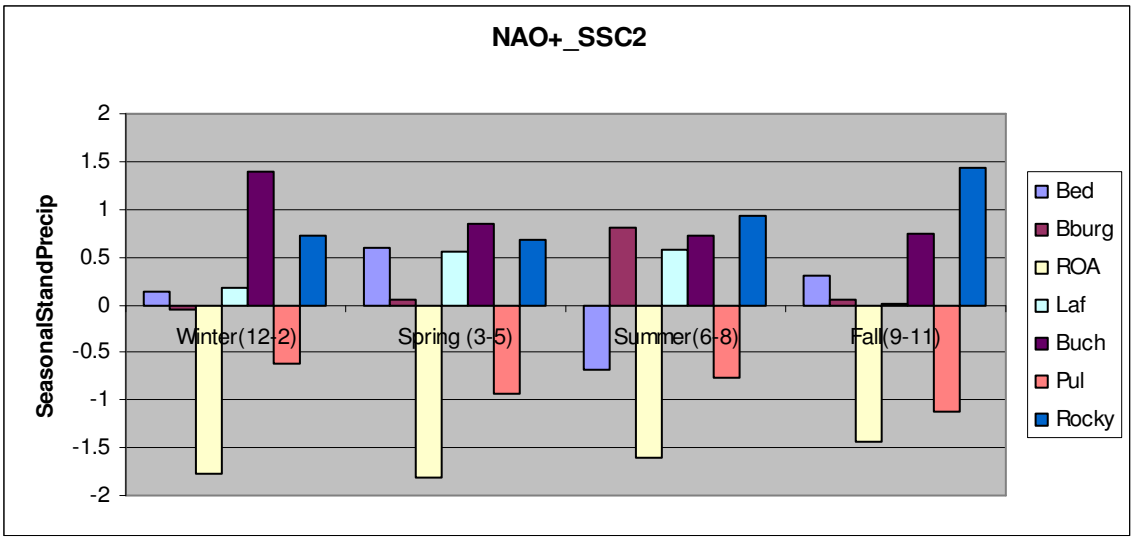
NAO+_SSC2
SeasonalStandPrecip
2
1.5
1
0.5
0
-0.5
-1
-1.5
-2
Winter(12-2)
Spring (3-5)
Summer(6-8)
Fall(9-11)
Bed
Bburg
ROA
Laf
Buch
Pul
Rocky

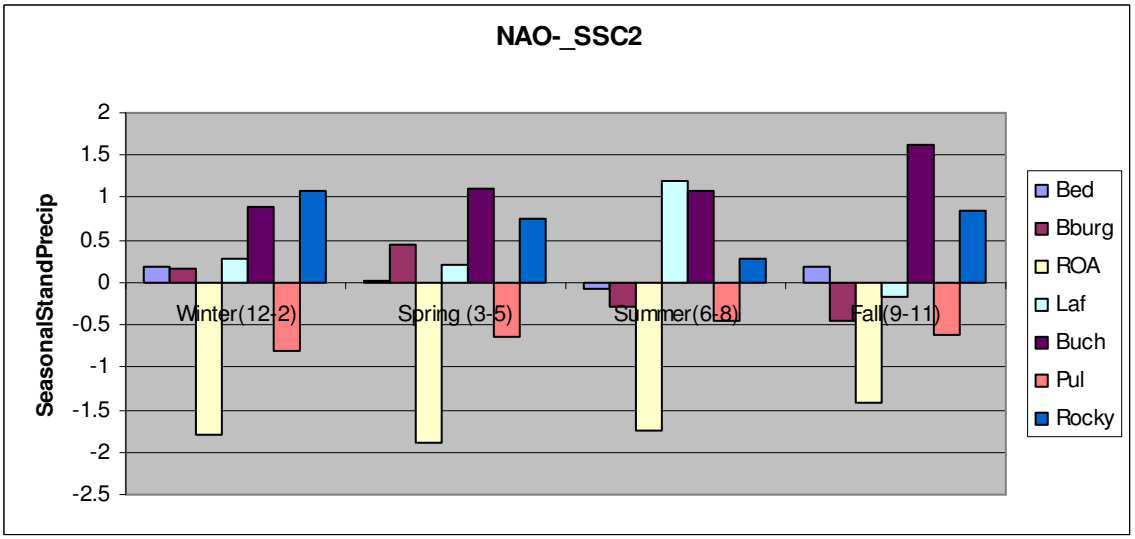
NAO-_SSC2
SeasonalStandPrecip
2
1.5
1
0.5
0
-0.5
-1
-1.5
-2
-2.5
Winter(12-2)
Spring (3-5)
Summer(6-8)
Fall(9-11)
Bed
Bburg
ROA
Laf
Buch
Pul
Rocky

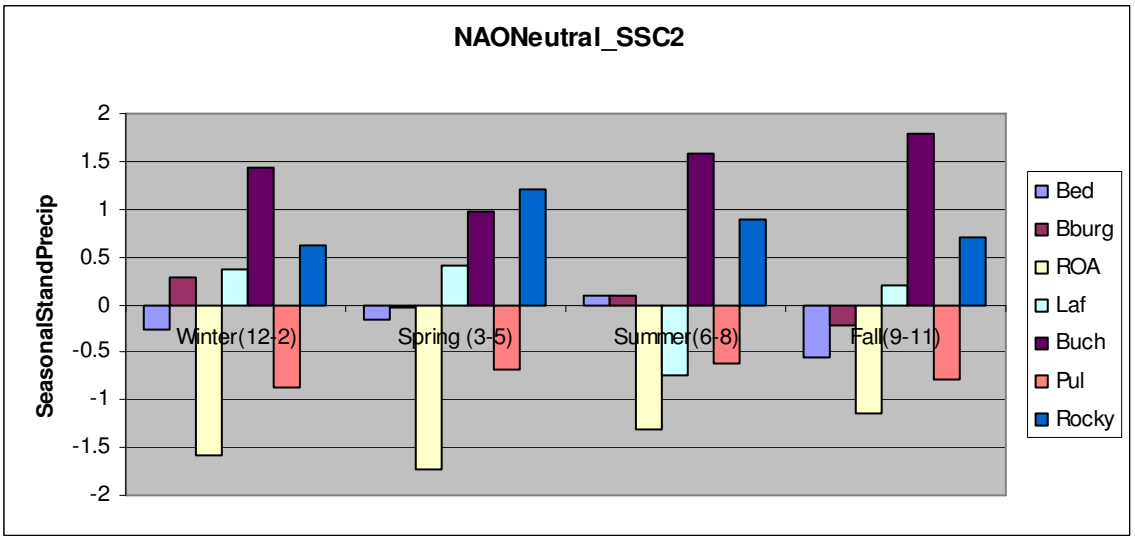
NAONeutral_SSC2
SeasonalStandPrecip
2
1.5
1
0.5
0
-0.5
-1
-1.5
-2
Winter(12-2)
Spring (3-5)
Summer(6-8)
Fall(9-11)
Bed
Bburg
ROA
Laf
Buch
Pul
Rocky

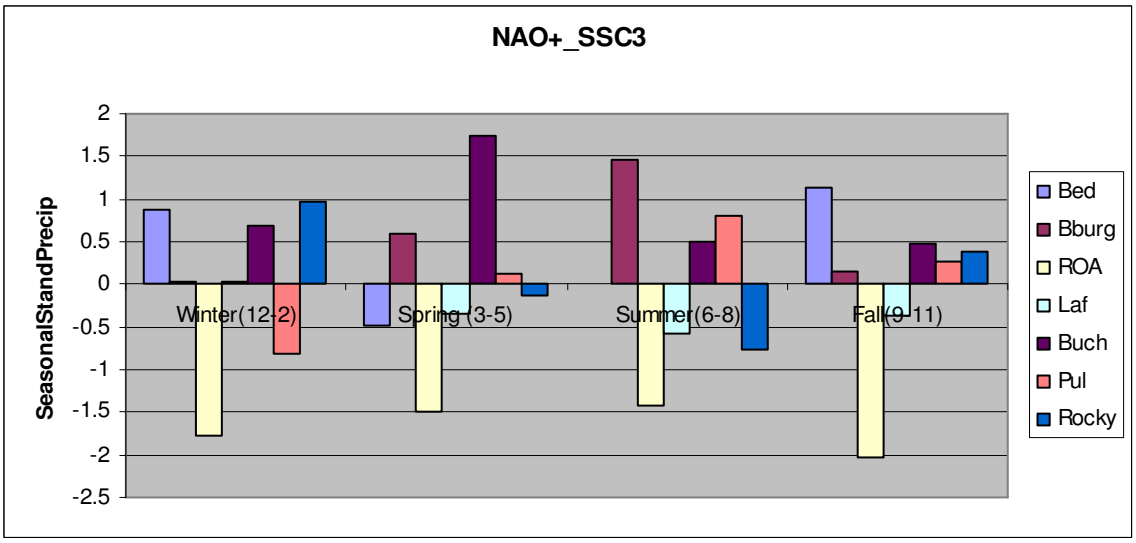
NAO+_SSC3
SeasonalStandPrecip
2
1.5
1
0.5
0
-0.5
-1
-1.5
-2
-2.5
Winter(12-2)
Spring (3-5)
Summer(6-8)
Fall(9-11)
Bed
Bburg
ROA
Laf
Buch
Pul
Rocky

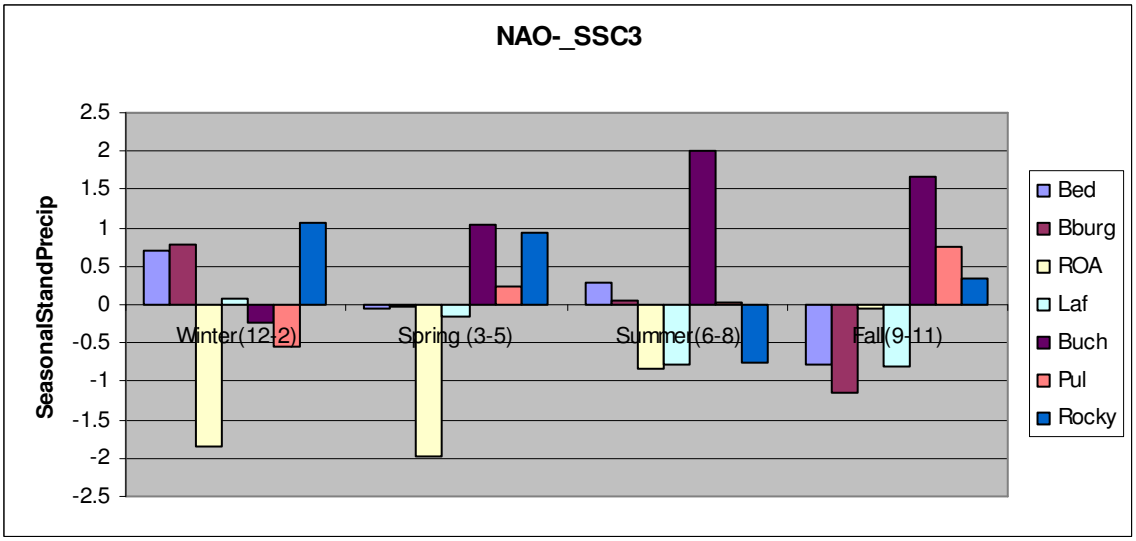
NAO-_SSC3
SeasonalStandPrecip
2.5
2
1.5
1
0.5
0
-0.5
-1
-1.5
-2
-2.5
Winter(12-2)
Spring (3-5)
Summer(6-8)
Fall(9-11)
Bed
Bburg
ROA
Laf
Buch
Pul
Rocky

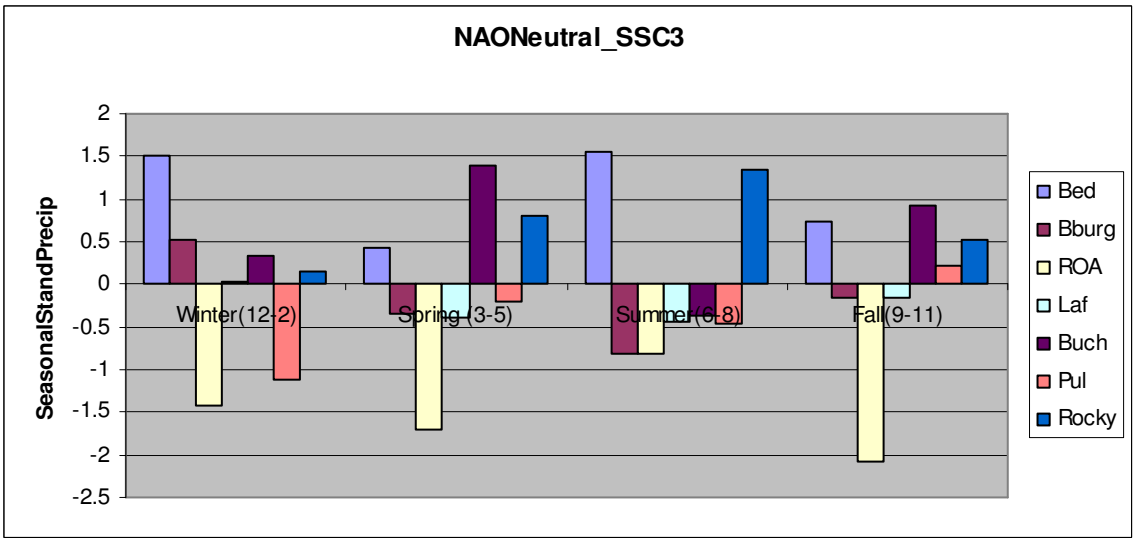
NAONeutral_SSC3
SeasonalStandPrecip
2
1.5
1
0.5
0
-0.5
-1
-1.5
-2
-2.5
Winter(12-2)
Spring (3-5)
Summer(6-8)
Fall(9-11)
Bed
Bburg
ROA
Laf
Buch
Pul
Rocky

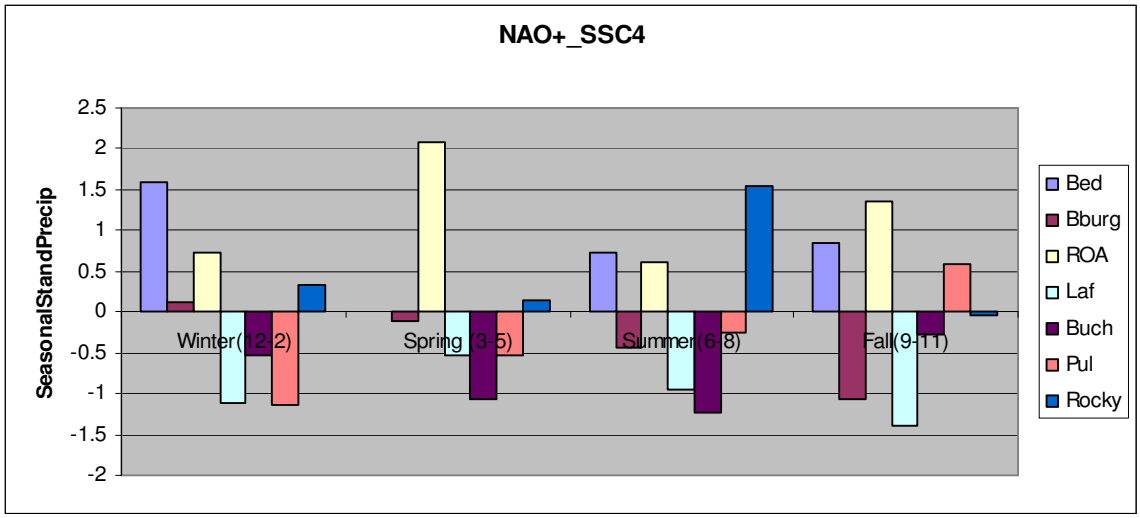
NAO+_SSC4
SeasonalStandPrecip
2.5
2
1.5
1
0.5
0
-0.5
-1
-1.5
-2
Winter(12-2)
Spring (3-5)
Summer(6-8)
Fall(9-11)
Bed
Bburg
ROA
Laf
Buch
Pul
Rocky

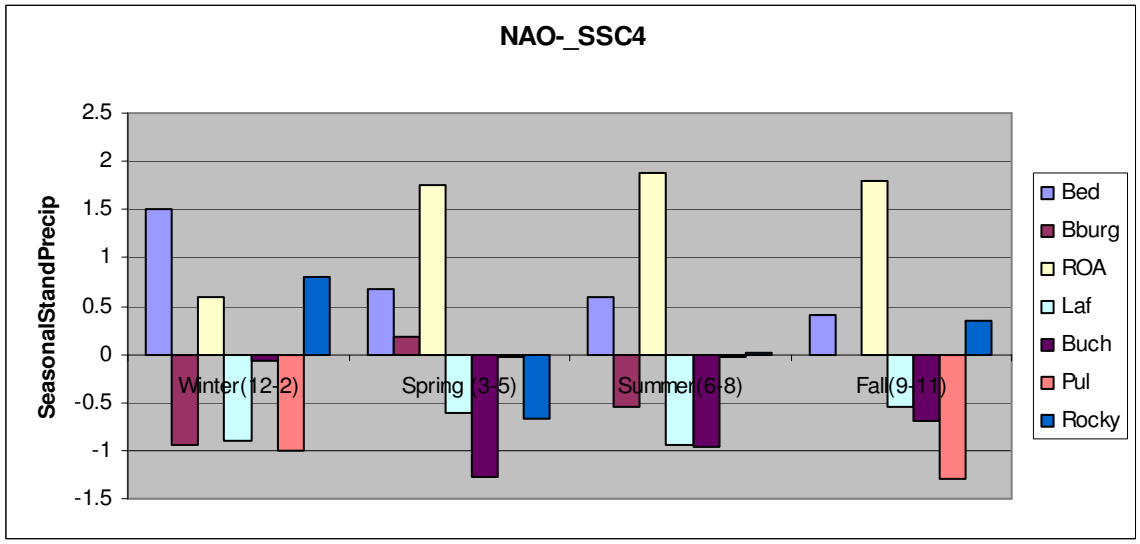
NAO-_SSC4
SeasonalStandPrecip
2.5
2
1.5
1
0.5
0
-0.5
-1
-1.5
Winter(12-2)
Spring (3-5)
Summer(6-8)
Fall(9-11)
Bed
Bburg
ROA
Laf
Buch
Pul
Rocky

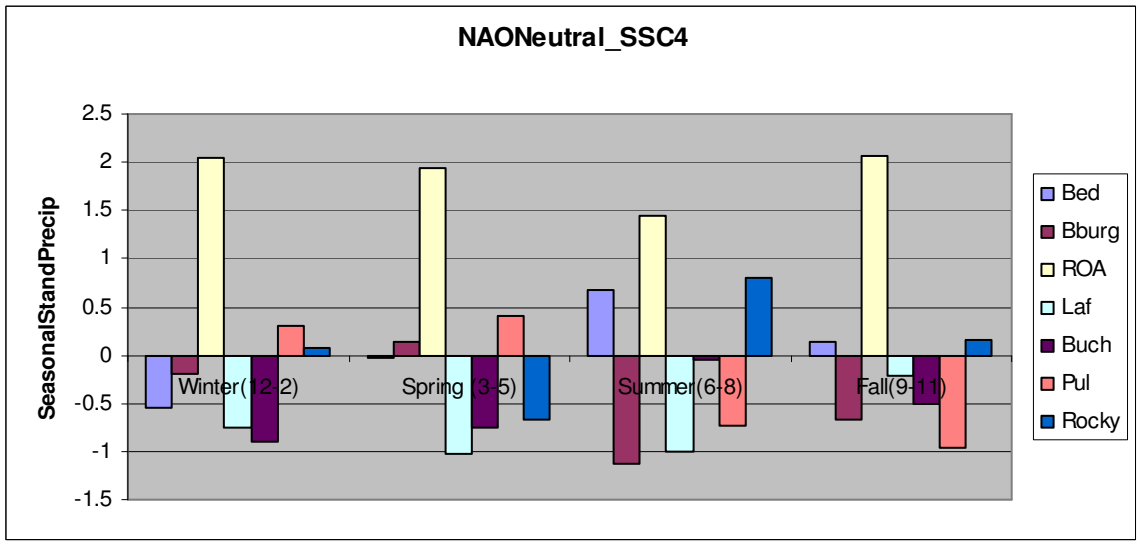
NAONeutral_SSC4
SeasonalStandPrecip
2.5
2
1.5
1
0.5
0
-0.5
-1
-1.5
Winter(12-2)
Spring (3-5)
Summer(6-8)
Fall(9-11)
Bed
Bburg
ROA
Laf
Buch
Pul
Rocky

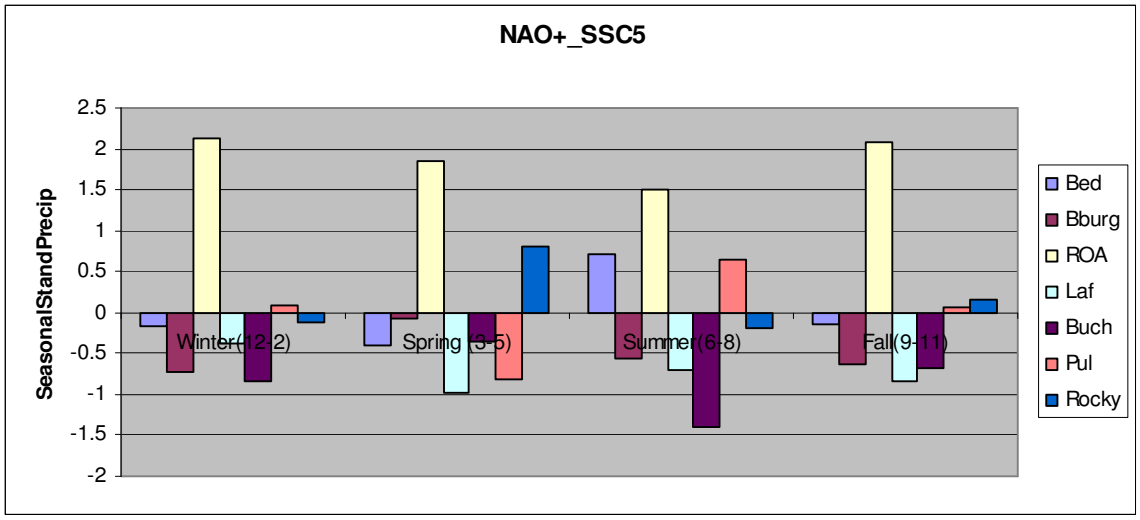
NAO+_SSC5
SeasonalStandPrecip
2.5
2
1.5
1
0.5
0
-0.5
-1
-1.5
-2
Winter(12-2)
Spring (3-5)
Summer(6-8)
Fall(9-11)
Bed
Bburg
ROA
Laf
Buch
Pul
Rocky

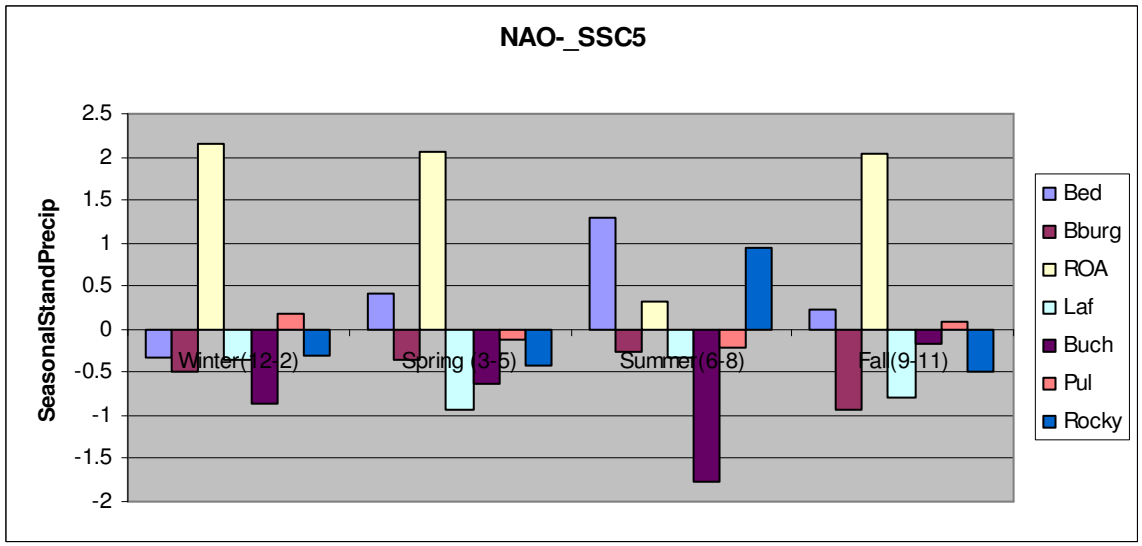
NAO-_SSC5
SeasonalStandPrecip
2.5
2
1.5
1
0.5
0
-0.5
-1
-1.5
-2
Winter(12-2)
Spring (3-5)
Summer(6-8)
Fall(9-11)
Bed
Bburg
ROA
Laf
Buch
Pul
Rocky

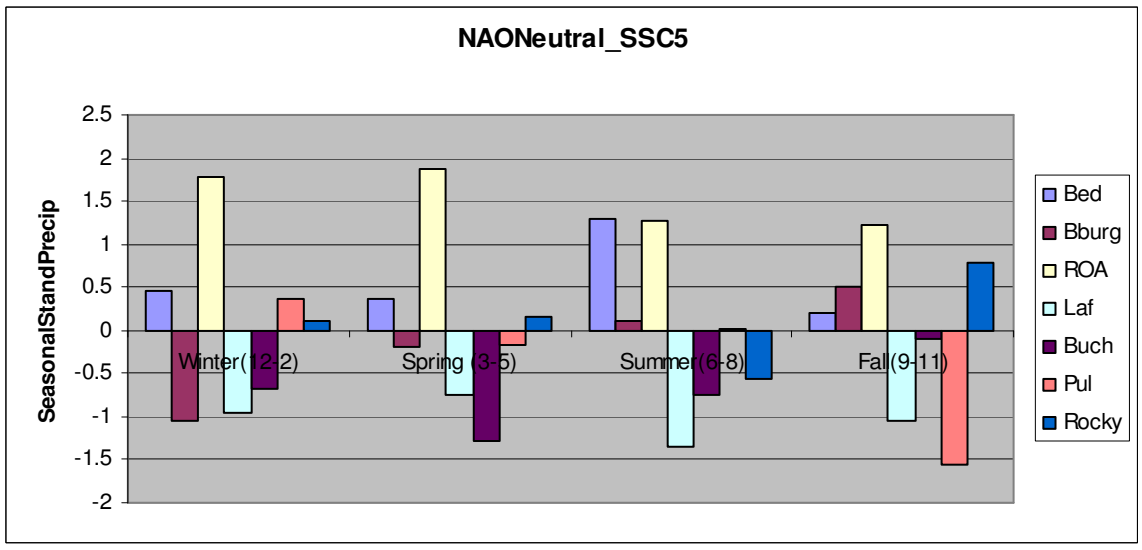
NAONeutral_SSC5
SeasonalStandPrecip
2.5
2
1.5
1
0.5
0
-0.5
-1
-1.5
-2
Winter(12-2)
Spring (3-5)
Summer(6-8)
Fall(9-11)
Bed
Bburg
ROA
Laf
Buch
Pul
Rocky

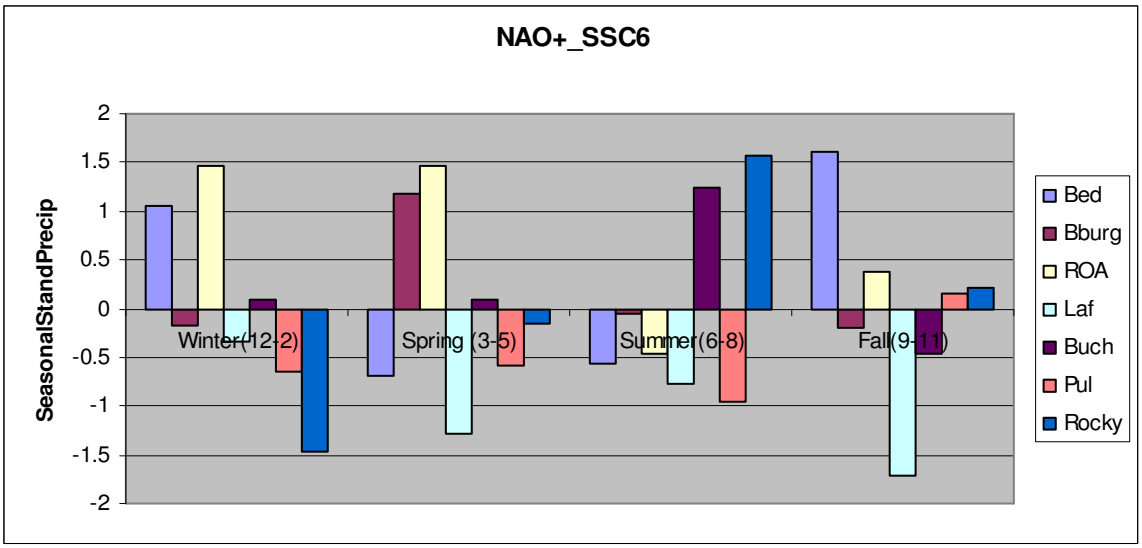
NAO+_SSC6
SeasonalStandPrecip
2
1.5
1
0.5
0
-0.5
-1
-1.5
-2
Winter(12-2)
Spring (3-5)
Summer(6-8)
Fall(9-11)
Bed
Bburg
ROA
Laf
Buch
Pul
Rocky

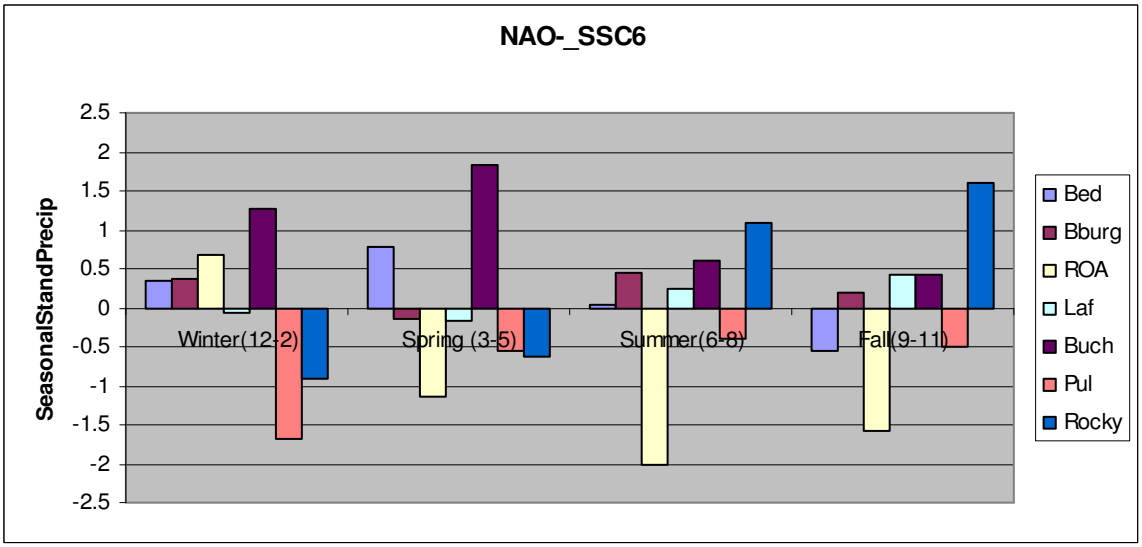
NAO-_SSC6
SeasonalStandPrecip
2.5
2
1.5
1
0.5
0
-0.5
-1
-1.5
-2
-2.5
Winter(12-2)
Spring (3-5)
Summer(6-8)
Fall(9-11)
Bed
Bburg
ROA
Laf
Buch
Pul
Rocky

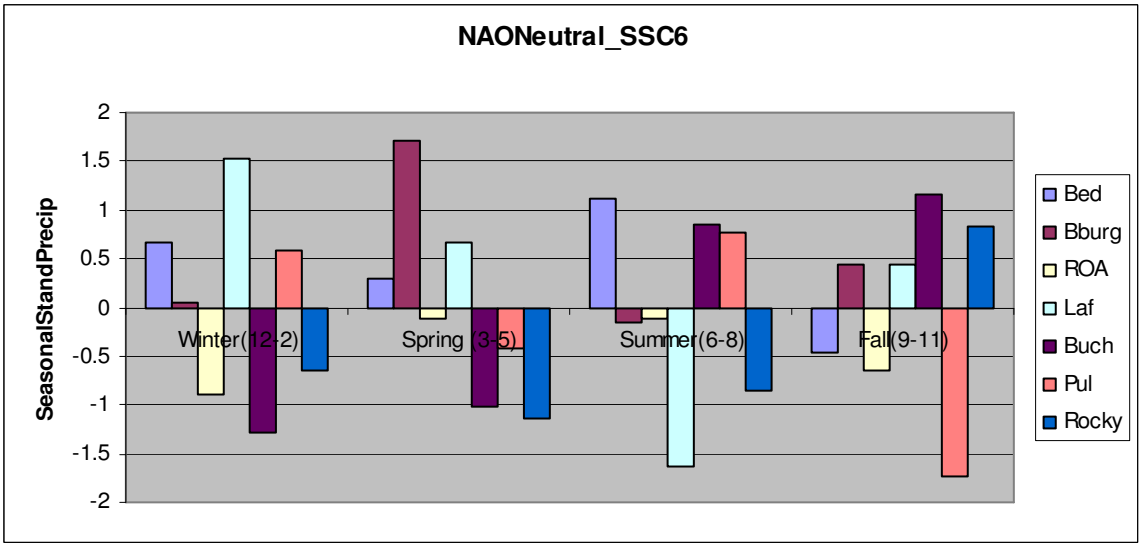
NAONeutral_SSC6
SeasonalStandPrecip
2
1.5
1
0.5
0
-0.5
-1
-1.5
-2
Winter(12-2)
Spring (3-5)
Summer(6-8)
Fall(9-11)
Bed
Bburg
ROA
Laf
Buch
Pul
Rocky

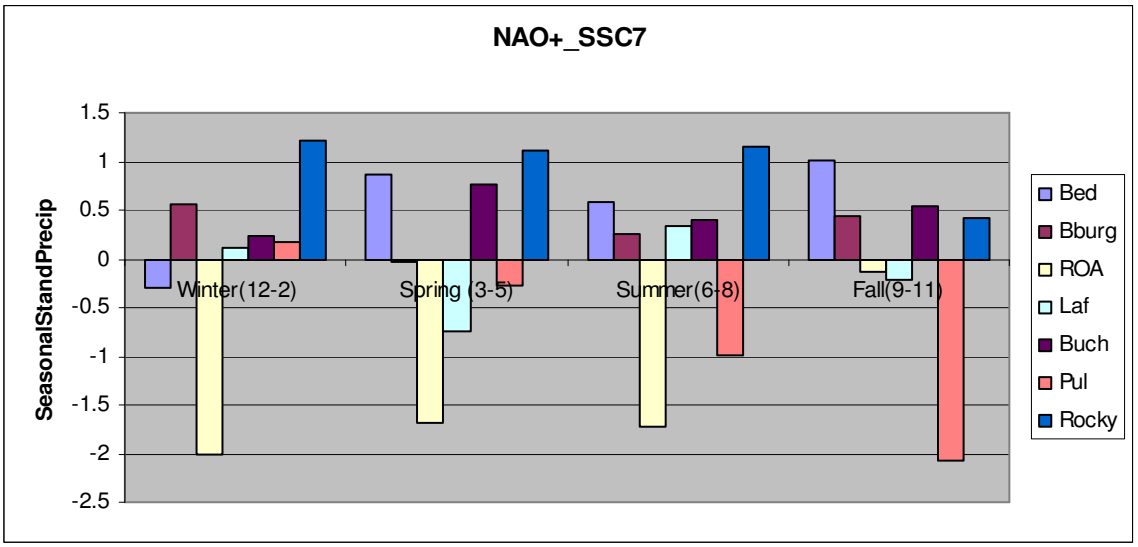
NAO+_SSC7
SeasonalStandPrecip
1.5
1
0.5
0
-0.5
-1
-1.5
-2
-2.5
Winter(12-2)
Spring (3-5)
Summer(6-8)
Fall(9-11)
Bed
Bburg
ROA
Laf
Buch
Pul
Rocky

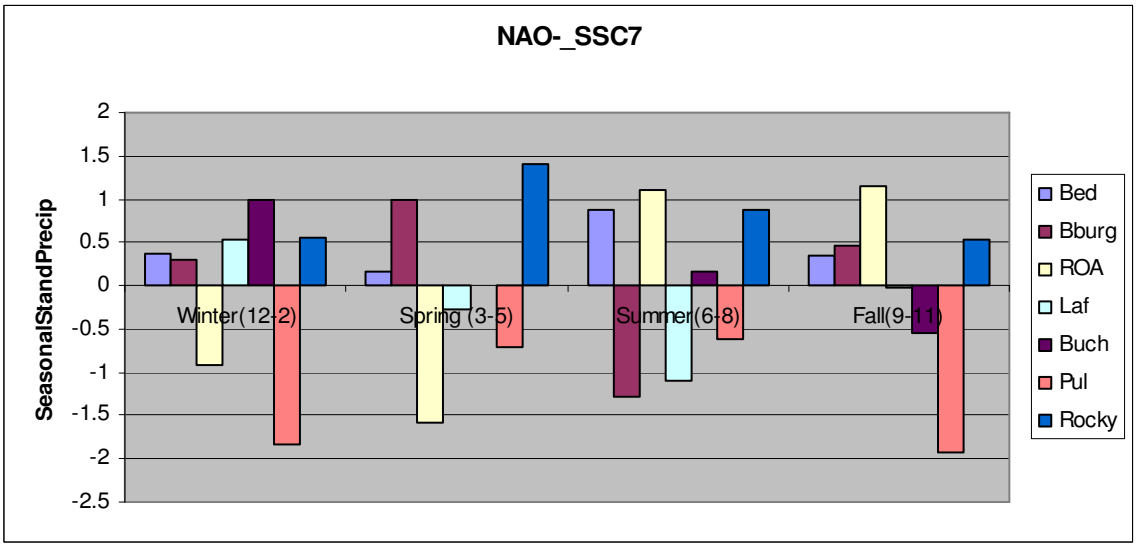
NAO-_SSC7
SeasonalStandPrecip
2
1.5
1
0.5
0
-0.5
-1
-1.5
-2
-2.5
Winter(12-2)
Spring (3-5)
Summer(6-8)
Fall(9-11)
Bed
Bburg
ROA
Laf
Buch
Pul
Rocky

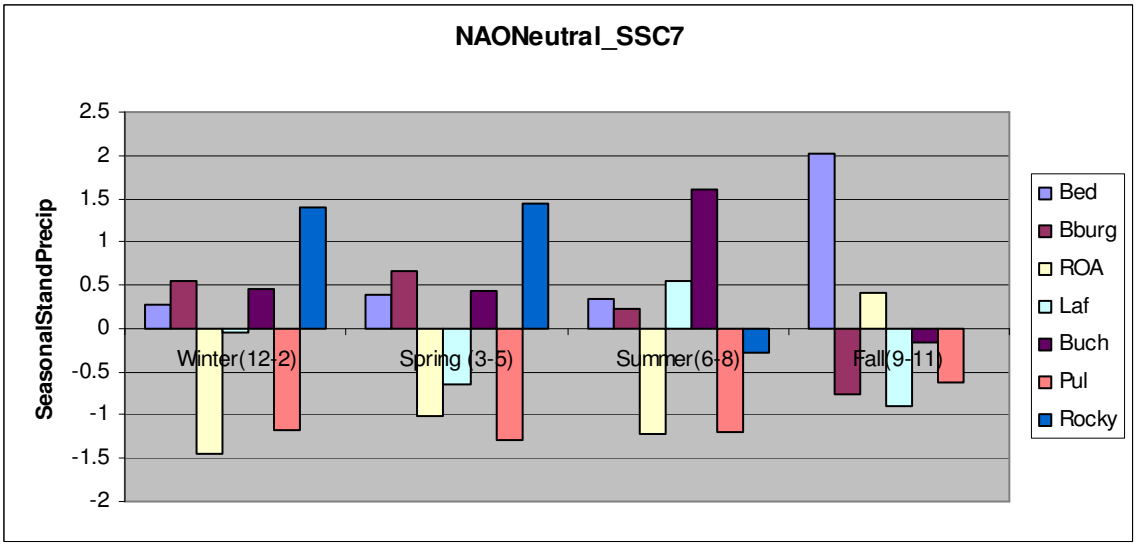
NAONeutral_SSC7
SeasonalStandPrecip
2.5
2
1.5
1
0.5
0
-0.5
-1
-1.5
-2
Winter(12-2)
Spring (3-5)
Summer(6-8)
Fall(9-11)
Bed
Bburg
ROA
Laf
Buch
Pul
Rocky

PNA_SSC Conditioning

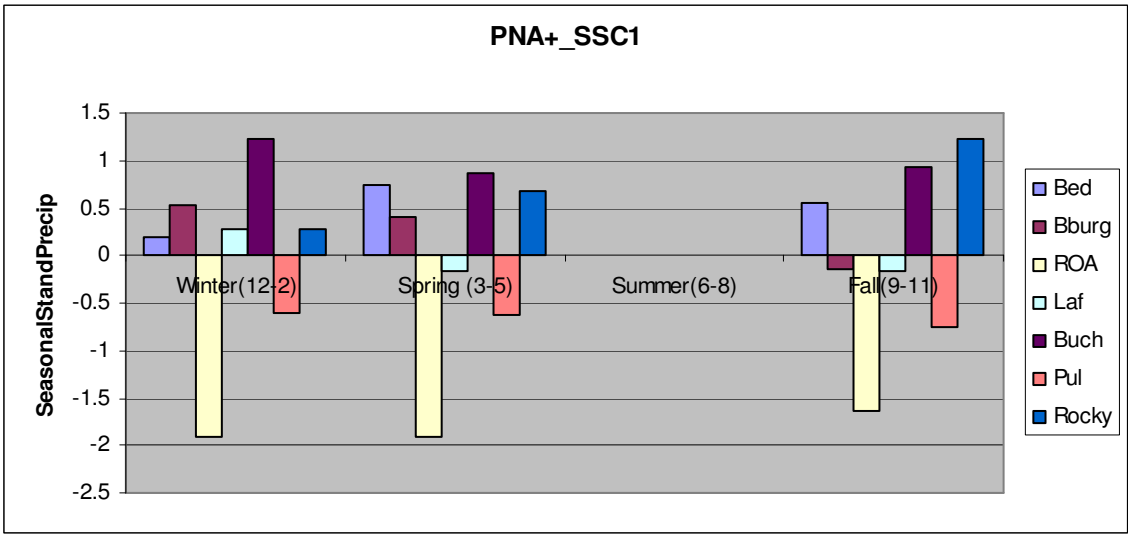

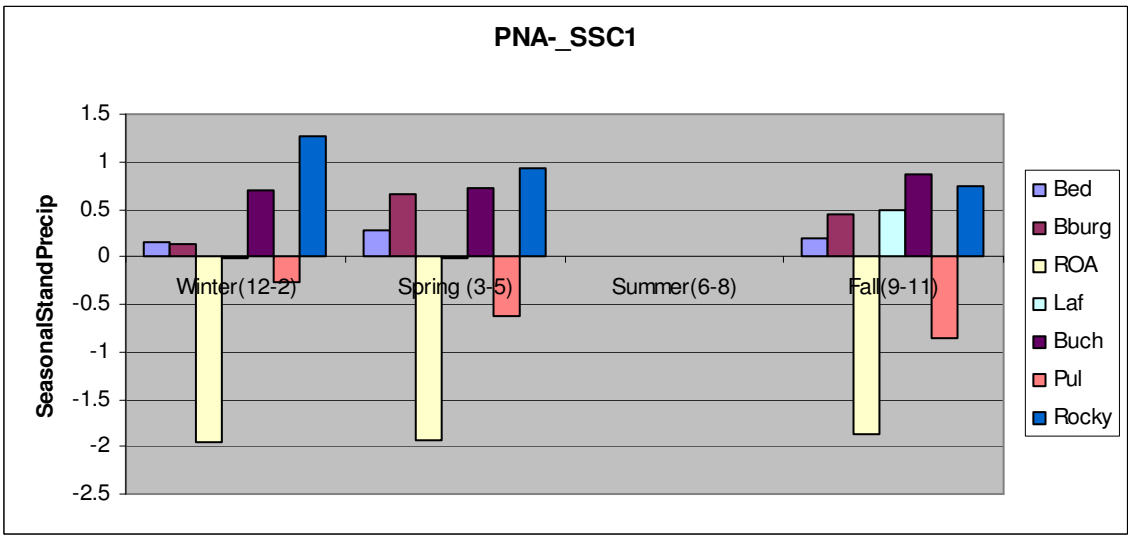

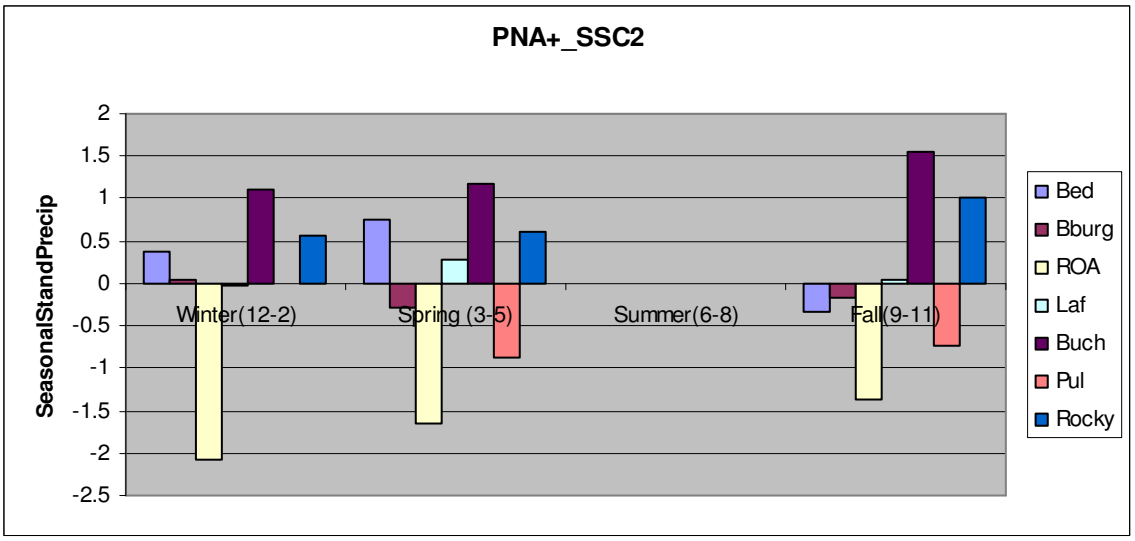
PNA+_SSC2
SeasonalStandPrecip
2
1.5
1
0.5
0
-0.5
-1
-1.5
-2
-2.5
Winter(12-2)
Spring (3-5)
Summer(6-8)
Fall(9-11)
Bed
Bburg
ROA
Laf
Buch
Pul
Rocky

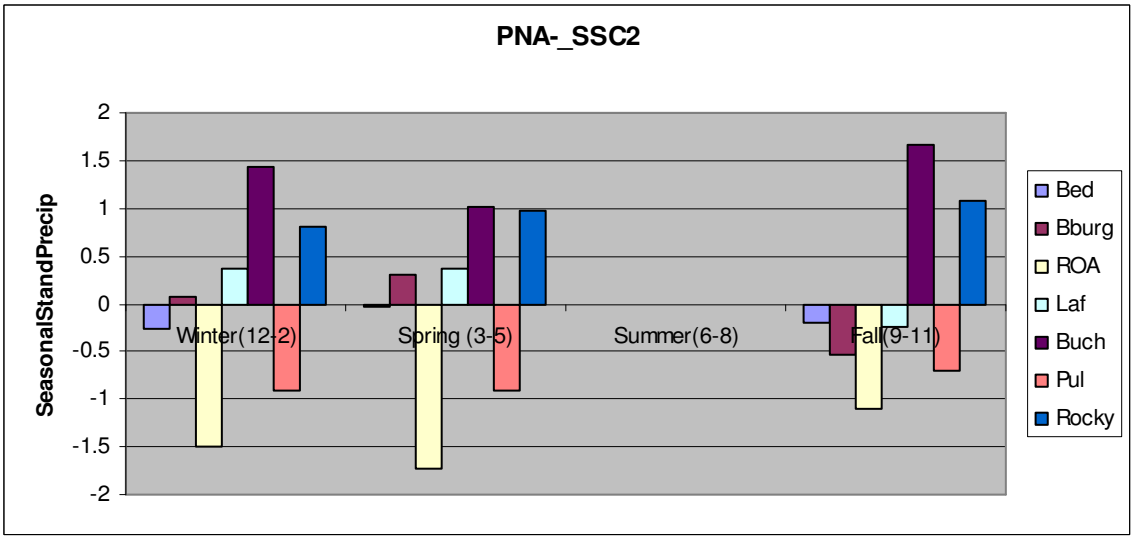
PNA-_SSC2
SeasonalStandPrecip
2
1.5
1
0.5
0
-0.5
-1
-1.5
-2
Winter(12-2)
Spring (3-5)
Summer(6-8)
Fall(9-11)
Bed
Bburg
ROA
Laf
Buch
Pul
Rocky

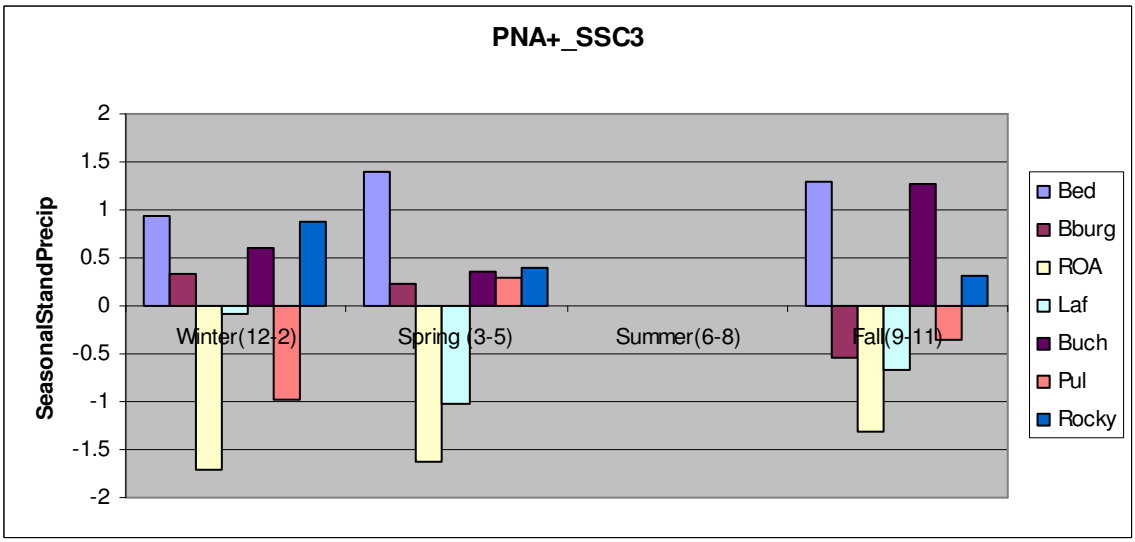
PNA+_SSC3
SeasonalStandPrecip
2
1.5
1
0.5
0
-0.5
-1
-1.5
-2
Winter(12-2)
Spring (3-5)
Summer(6-8)
Fall(9-11)
Bed
Bburg
ROA
Laf
Buch
Pul
Rocky

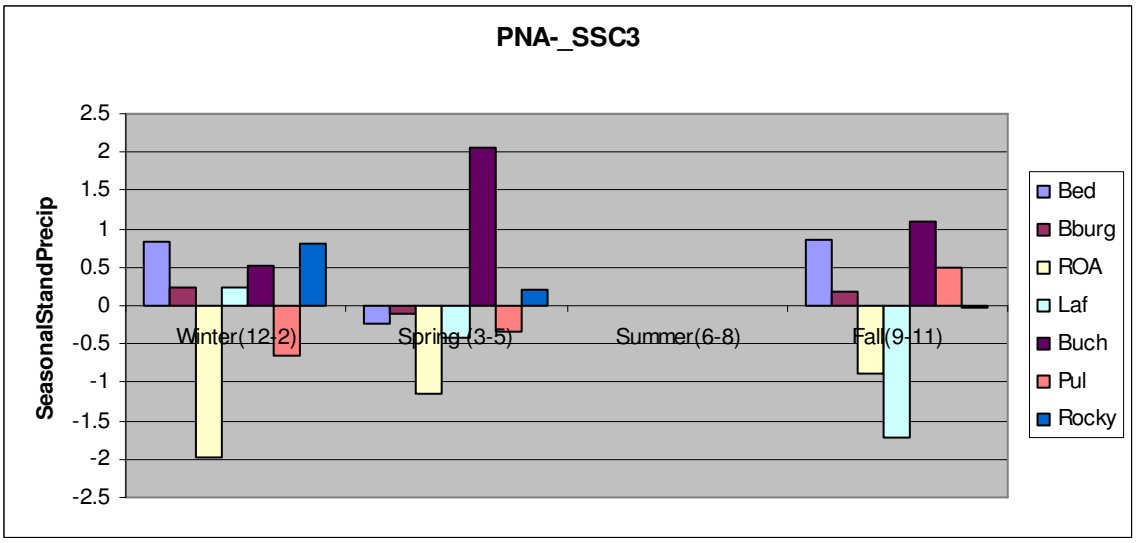
PNA-_SSC3
SeasonalStandPrecip
2.5
2
1.5
1
0.5
0
-0.5
-1
-1.5
-2
-2.5
Winter(12-2)
Spring (3-5)
Summer(6-8)
Fall(9-11)
Bed
Bburg
ROA
Laf
Buch
Pul
Rocky

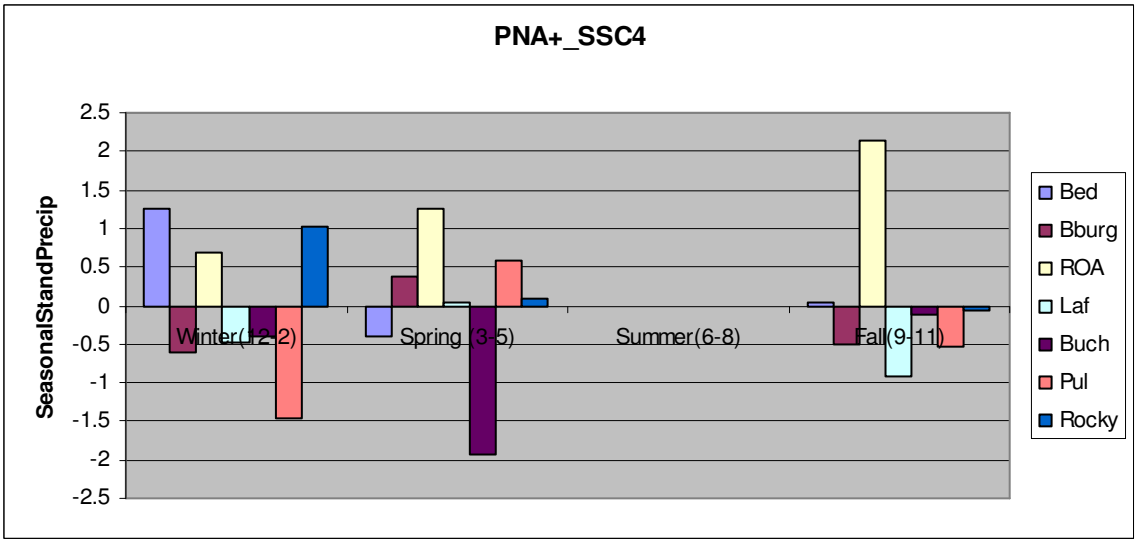
PNA+_SSC4
SeasonalStandPrecip
2.5
2
1.5
1
0.5
0
-0.5
-1
-1.5
-2
-2.5
Winter(12-2)
Spring (3-5)
Summer(6-8)
Fall(9-11)
Bed
Bburg
ROA
Laf
Buch
Pul
Rocky

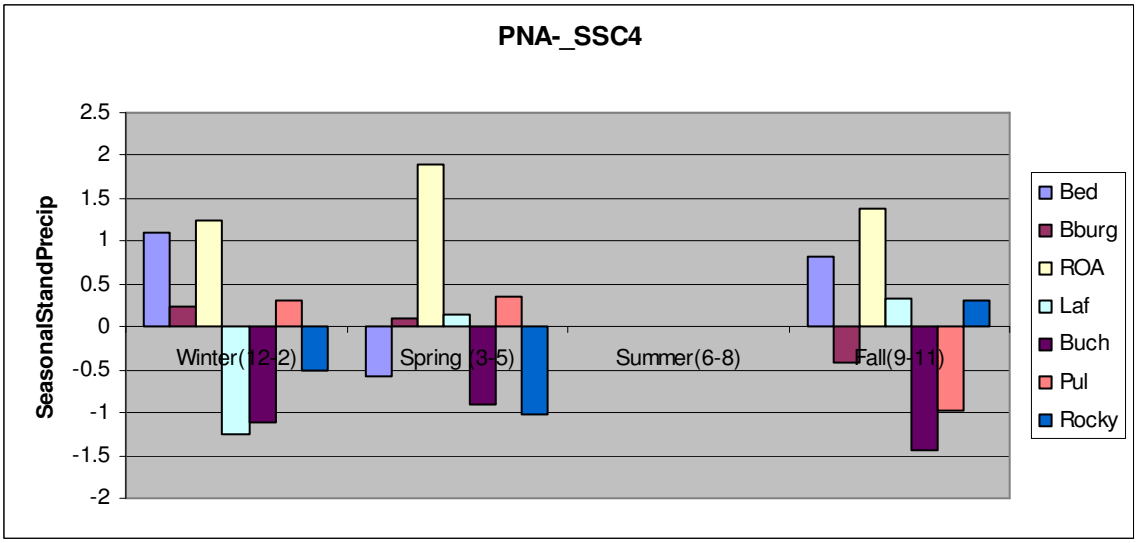
PNA-_SSC4
SeasonalStandPrecip
2.5
2
1.5
1
0.5
0
-0.5
-1
-1.5
-2
Winter(12-2)
Spring (3-5)
Summer(6-8)
Fall(9-11)
Bed
Bburg
ROA
Laf
Buch
Pul
Rocky

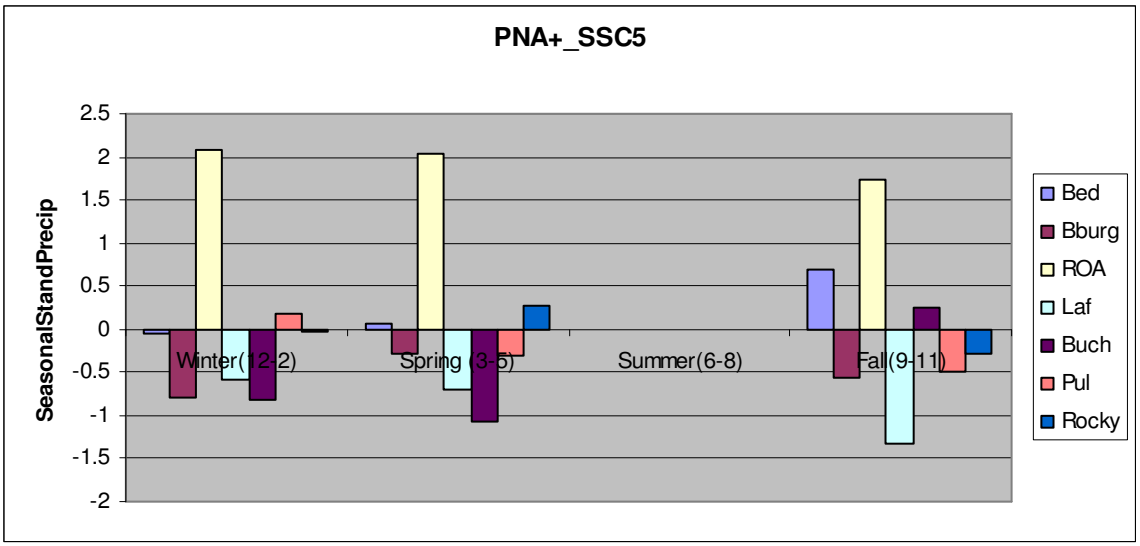
PNA+_SSC5
SeasonalStandPrecip
2.5
2
1.5
1
0.5
0
-0.5
-1
-1.5
-2
Winter(12-2)
Spring (3-5)
Summer(6-8)
Fall(9-11)
Bed
Bburg
ROA
Laf
Buch
Pul
Rocky

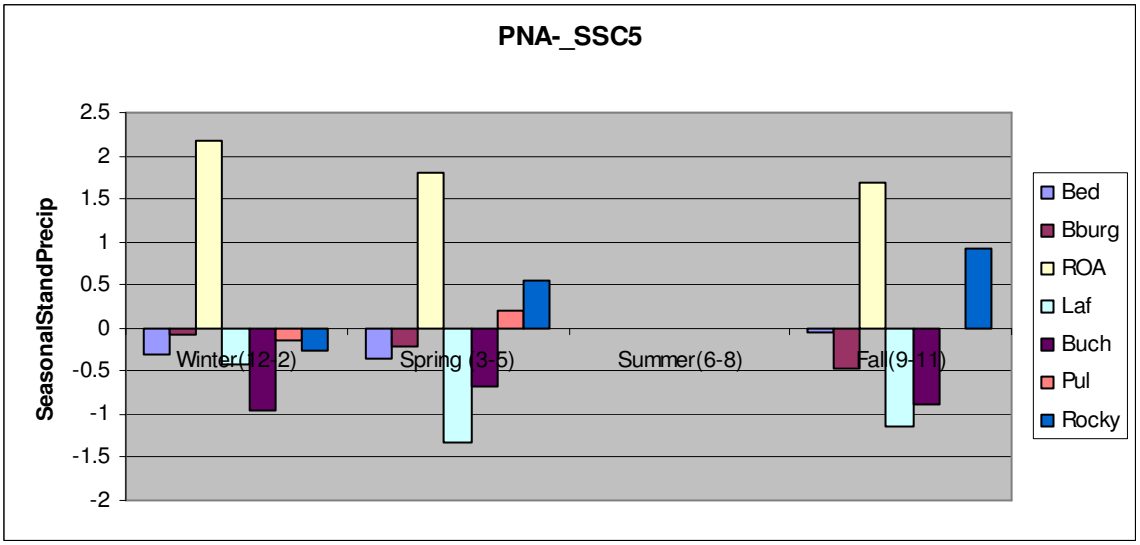
PNA-_SSC5
SeasonalStandPrecip
2.5
2
1.5
1
0.5
0
-0.5
-1
-1.5
-2
Winter(12-2)
Spring (3-5)
Summer(6-8)
Fall(9-11)
Bed
Bburg
ROA
Laf
Buch
Pul
Rocky

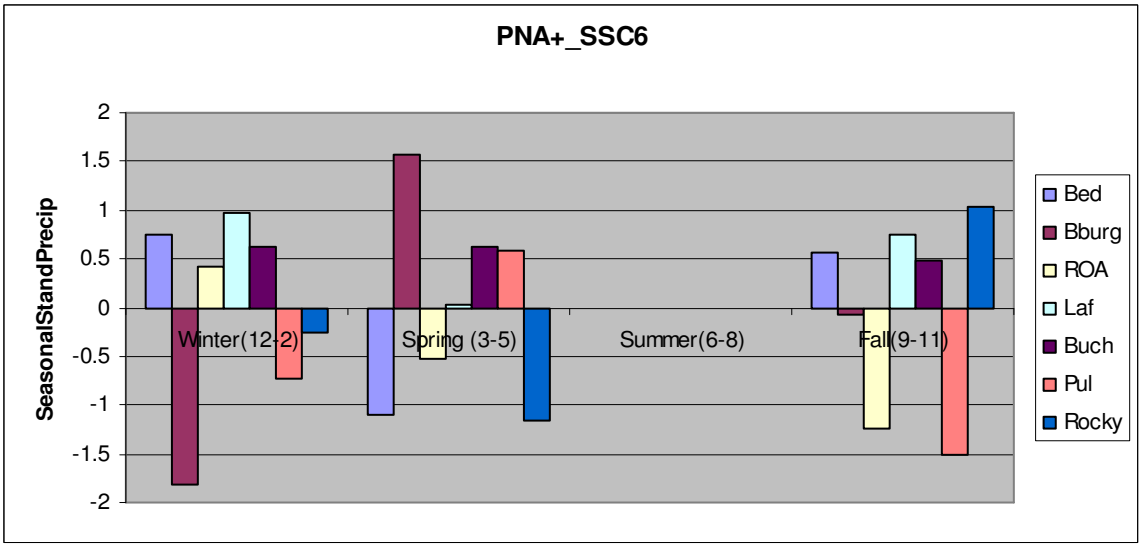
PNA+_SSC6
SeasonalStandPrecip
2
1.5
1
0.5
0
-0.5
-1
-1.5
-2
Winter(12-2)
Spring (3-5)
Summer(6-8)
Fall(9-11)
Bed
Bburg
ROA
Laf
Buch
Pul
Rocky

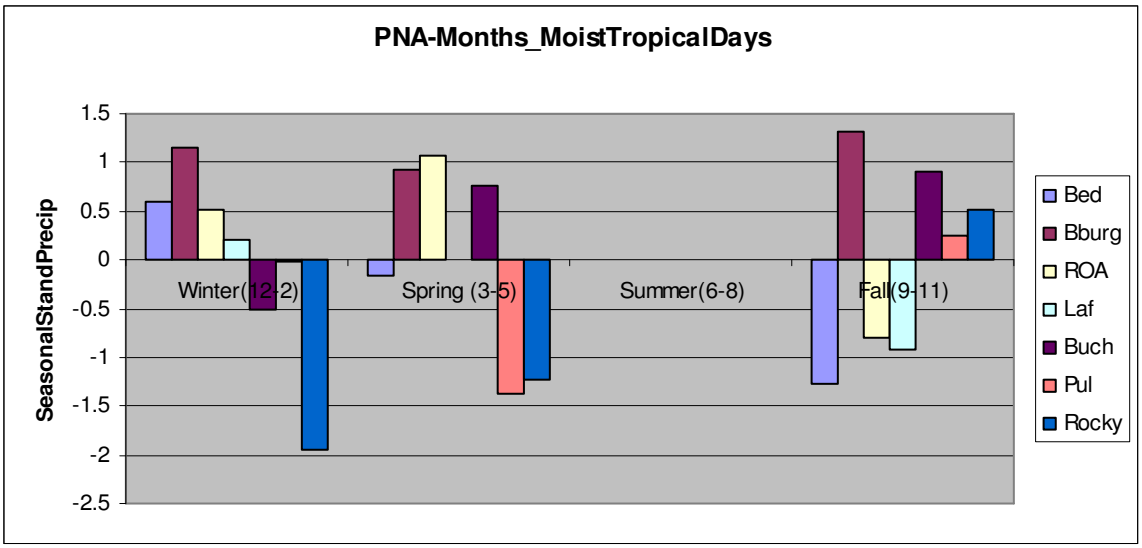

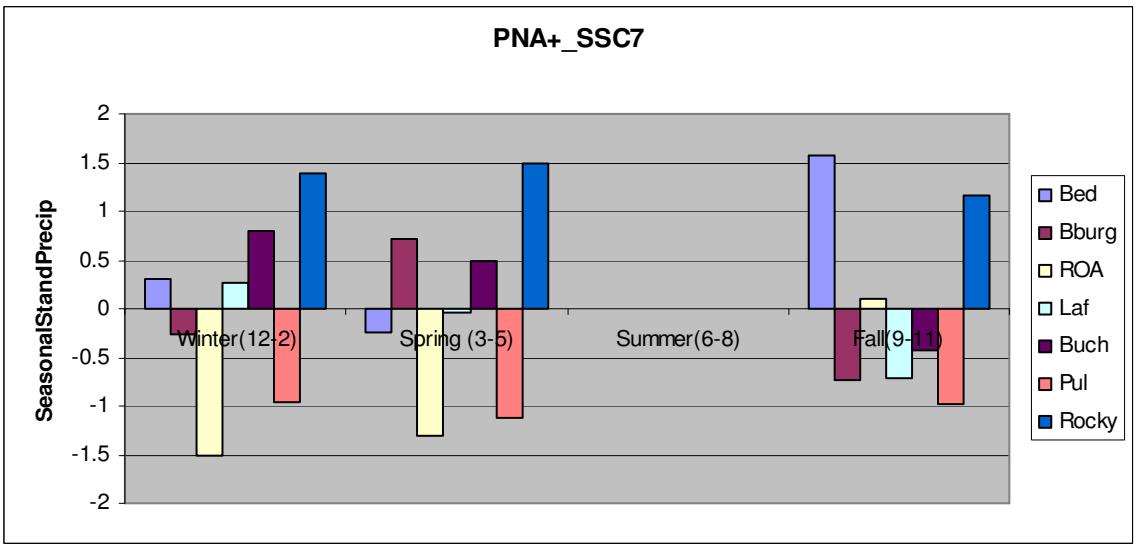

ENSO & AO+_SSC Conditioning

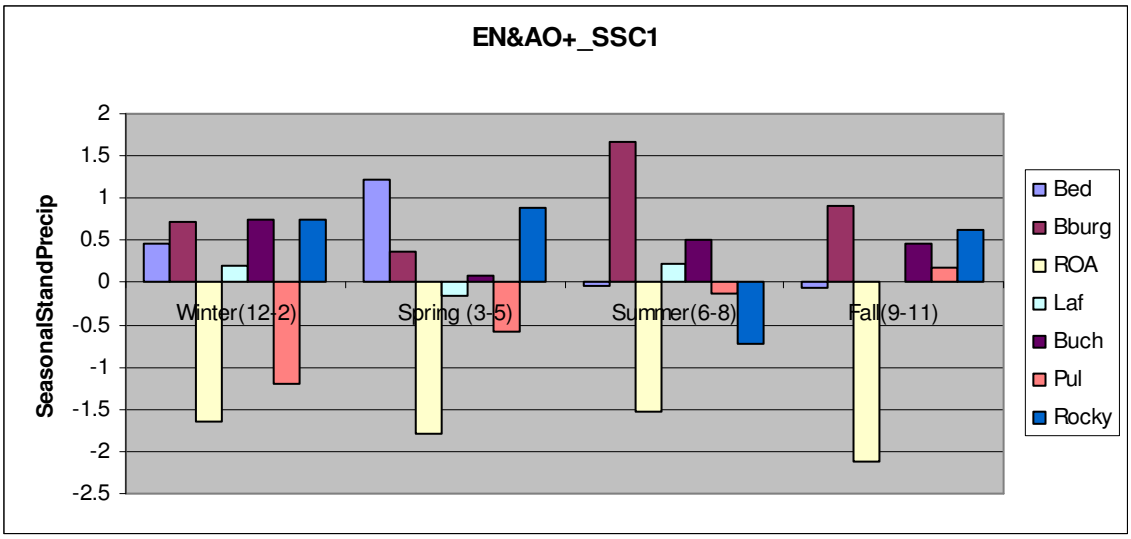
EN&AO+_SSC1
SeasonalStandPrecip
2
1.5
1
0.5
0
-0.5
-1
-1.5
-2
-2.5
Winter(12-2)
Spring (3-5)
Summer(6-8)
Fall(9-11)
Bed
Bburg
ROA
Laf
Buch
Pul
Rocky

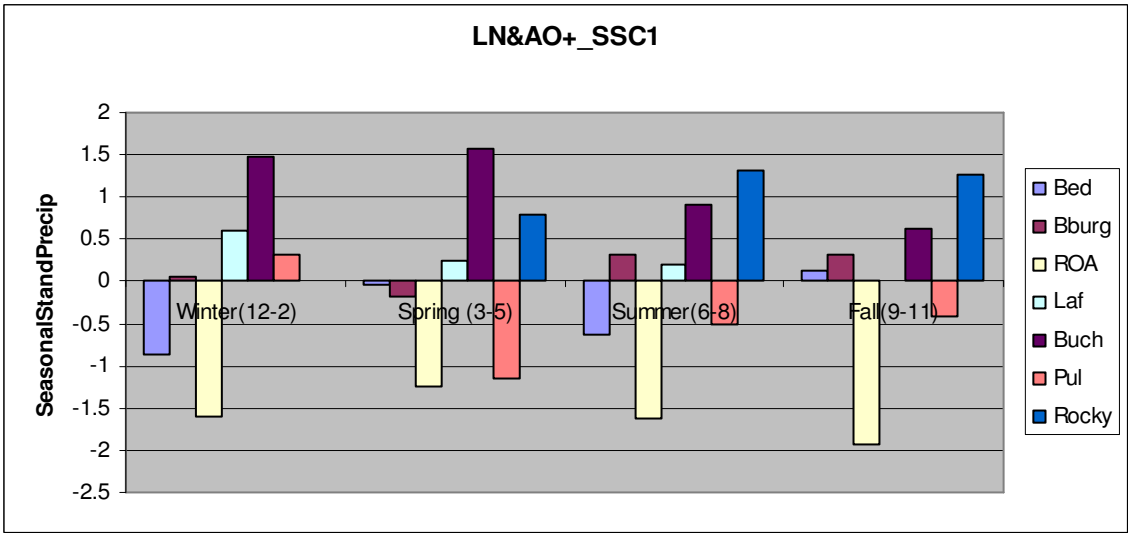
LN&AO+_SSC1
SeasonalStandPrecip
2
1.5
1
0.5
0
-0.5
-1
-1.5
-2
-2.5
Winter(12-2)
Spring (3-5)
Summer(6-8)
Fall(9-11)
Bed
Bburg
ROA
Laf
Buch
Pul
Rocky

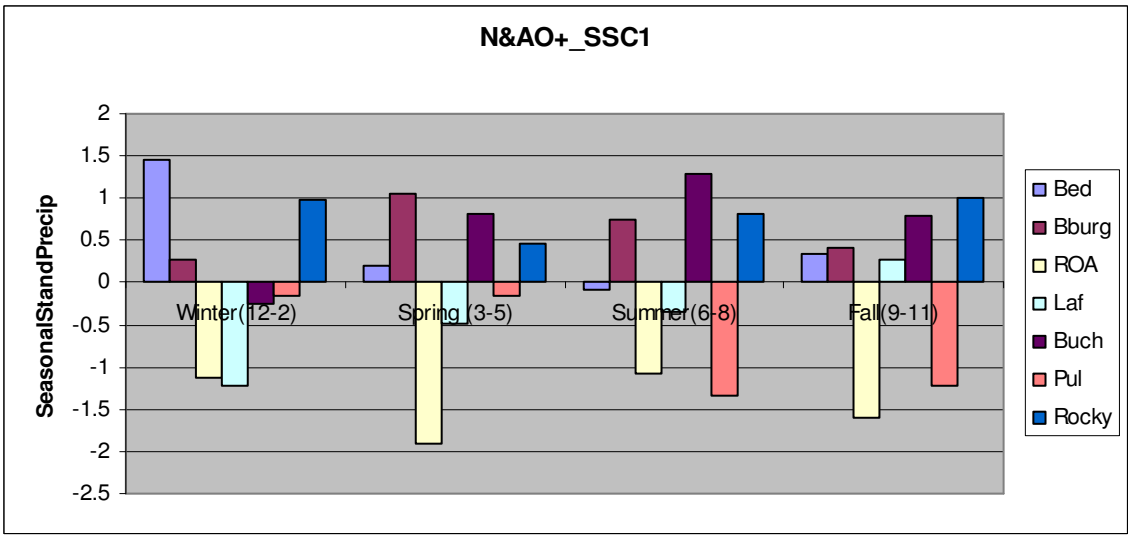
N&AO+_SSC1
SeasonalStandPrecip
2
1.5
1
0.5
0
-0.5
-1
-1.5
-2
-2.5
Winter(12-2)
Spring (3-5)
Summer(6-8)
Fall(9-11)
Bed
Bburg
ROA
Laf
Buch
Pul
Rocky

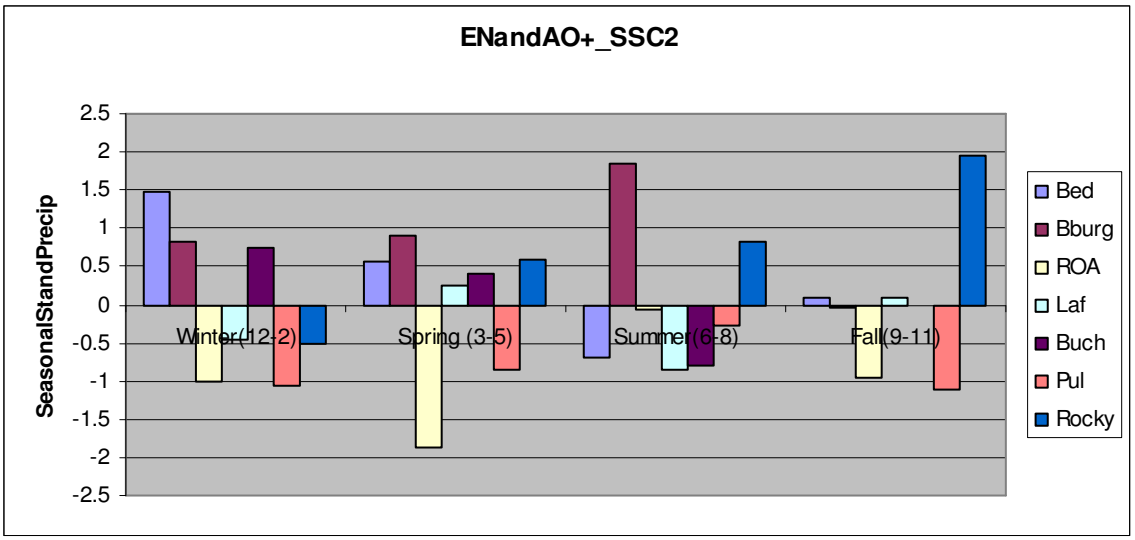
ENandAO+_SSC2
SeasonalStandPrecip
2.5
2
1.5
1
0.5
0
-0.5
-1
-1.5
-2
-2.5
Winter(12-2)
Spring (3-5)
Summer(6-8)
Fall(9-11)
Bed
Bburg
ROA
Laf
Buch
Pul
Rocky

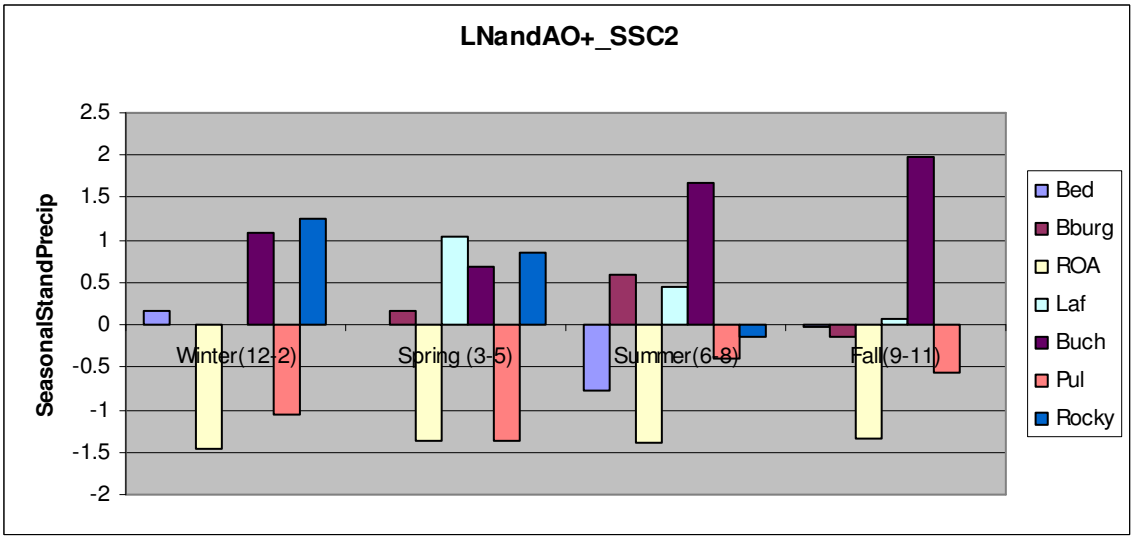
LNandAO+_SSC2
SeasonalStandPrecip
2.5
2
1.5
1
0.5
0
-0.5
-1
-1.5
-2
Winter(12-2)
Spring (3-5)
Summer(6-8)
Fall(9-11)
Bed
Bburg
ROA
Laf
Buch
Pul
Rocky

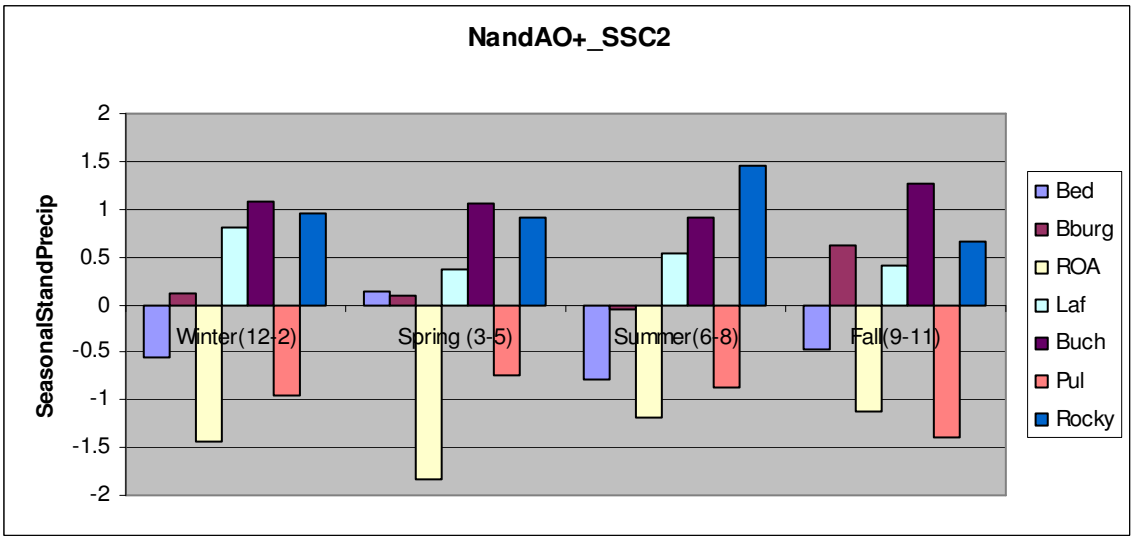
NandAO+_SSC2
SeasonalStandPrecip
2
1.5
1
0.5
0
-0.5
-1
-1.5
-2
Winter(12-2)
Spring (3-5)
Summer(6-8)
Fall(9-11)
Bed
Bburg
ROA
Laf
Buch
Pul
Rocky

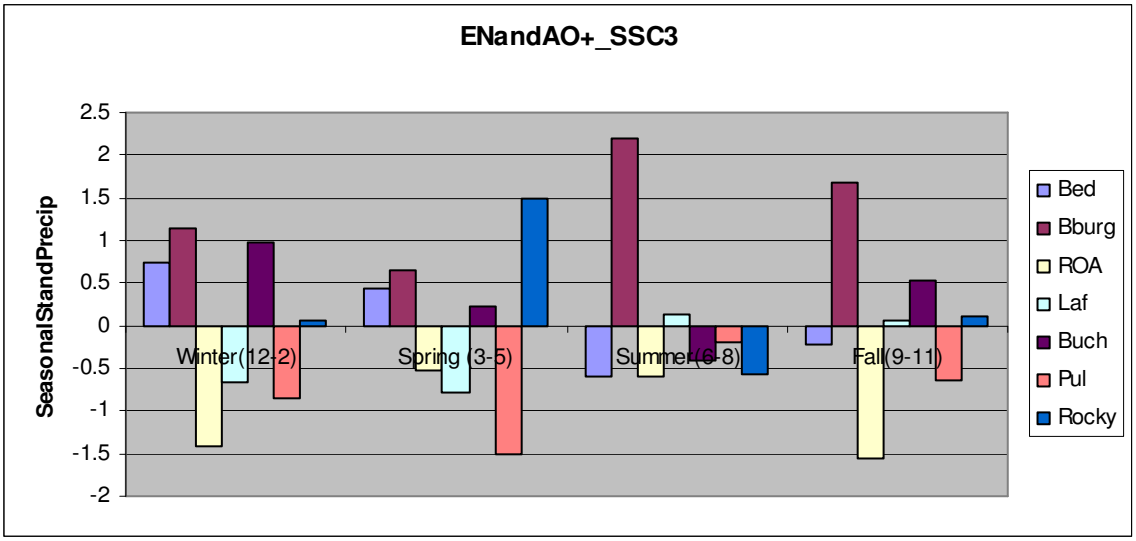
ENandAO+_SSC3
SeasonalStandPrecip
2.5
2
1.5
1
0.5
0
-0.5
-1
-1.5
-2
Winter(12-2)
Spring (3-5)
Summer(6-8)
Fall(9-11)
Bed
Bburg
ROA
Laf
Buch
Pul
Rocky

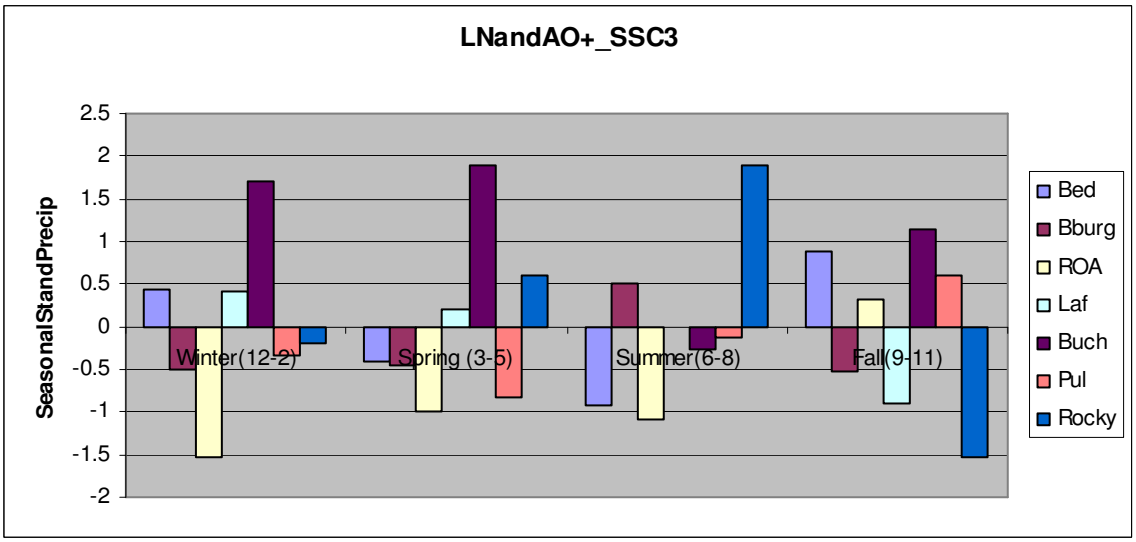
LNandAO+_SSC3
SeasonalStandPrecip
2.5
2
1.5
1
0.5
0
-0.5
-1
-1.5
-2
Winter(12-2)
Spring (3-5)
Summer(6-8)
Fall(9-11)
Bed
Bburg
ROA
Laf
Buch
Pul
Rocky

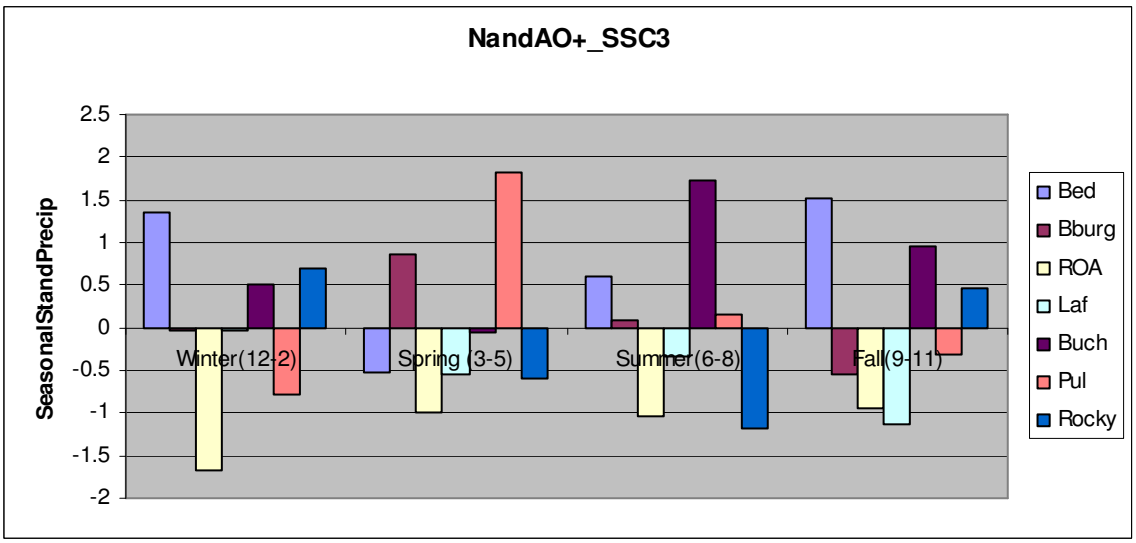
NandAO+_SSC3
SeasonalStandPrecip
2.5
2
1.5
1
0.5
0
-0.5
-1
-1.5
-2
Winter(12-2)
Spring (3-5)
Summer(6-8)
Fall(9-11)
Bed
Bburg
ROA
Laf
Buch
Pul
Rocky

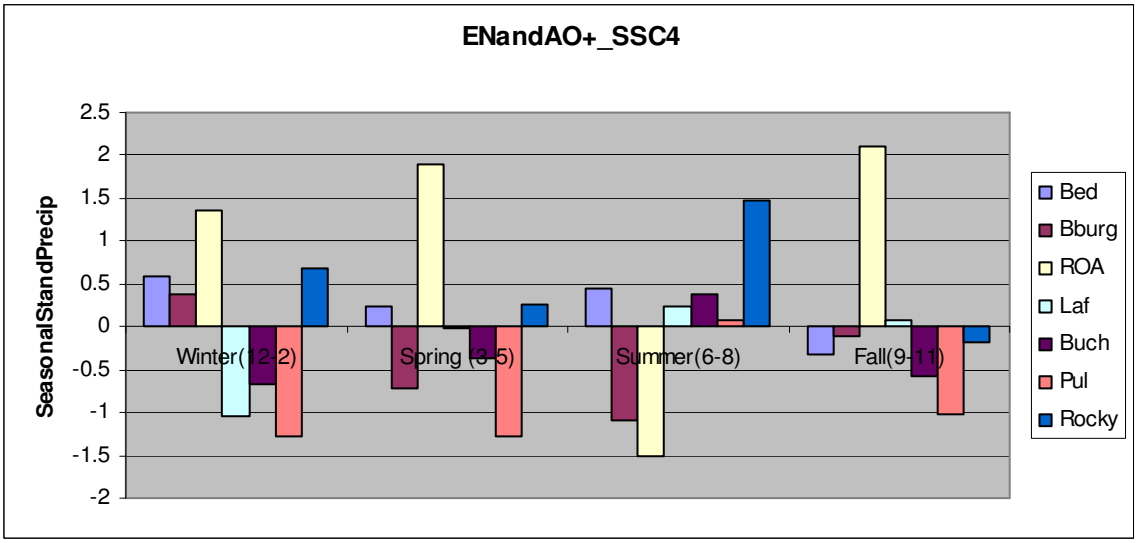
ENandAO+_SSC4
SeasonalStandPrecip
2.5
2
1.5
1
0.5
0
-0.5
-1
-1.5
-2
Winter(12-2)
Spring (3-5)
Summer(6-8)
Fall(9-11)
Bed
Bburg
ROA
Laf
Buch
Pul
Rocky

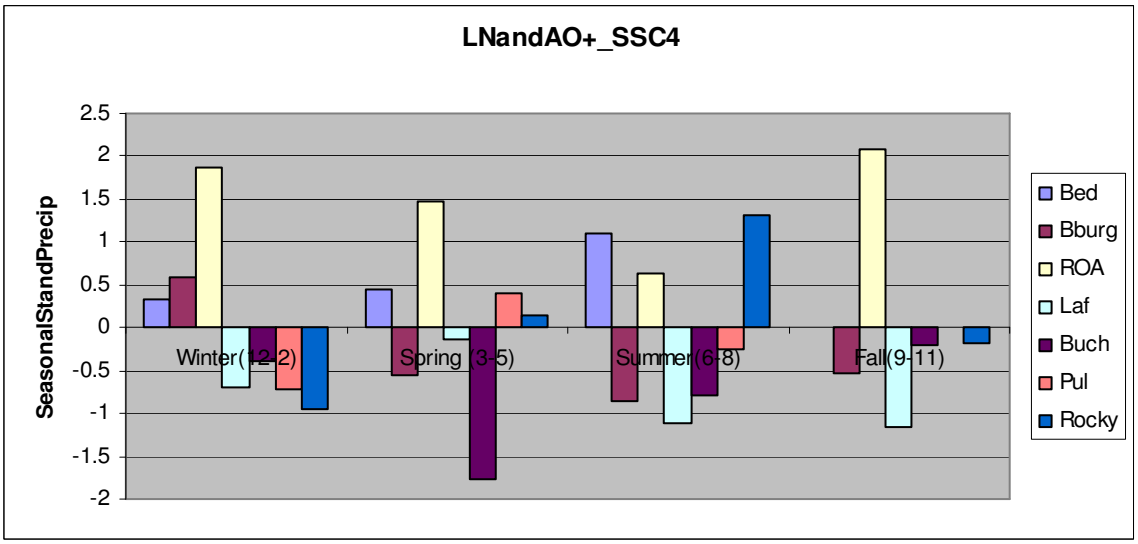
LNandAO+_SSC4
SeasonalStandPrecip
2.5
2
1.5
1
0.5
0
-0.5
-1
-1.5
-2
Winter(12-2)
Spring (3-5)
Summer(6-8)
Fall(9-11)
Bed
Bburg
ROA
Laf
Buch
Pul
Rocky

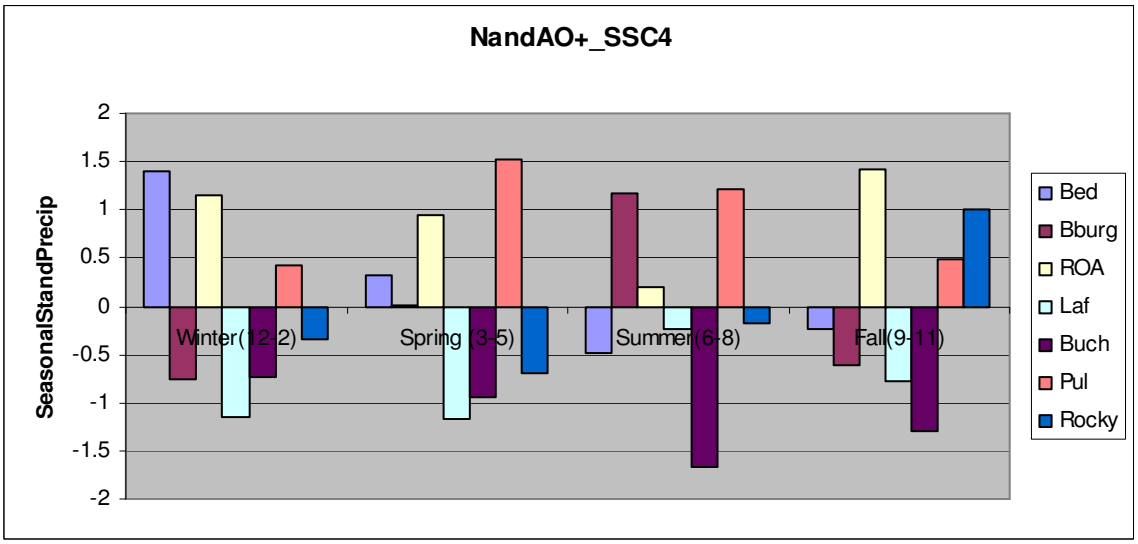
NandAO+_SSC4
SeasonalStandPrecip
2
1.5
1
0.5
0
-0.5
-1
-1.5
-2
Winter(12-2)
Spring (3-5)
Summer(6-8)
Fall(9-11)
Bed
Bburg
ROA
Laf
Buch
Pul
Rocky

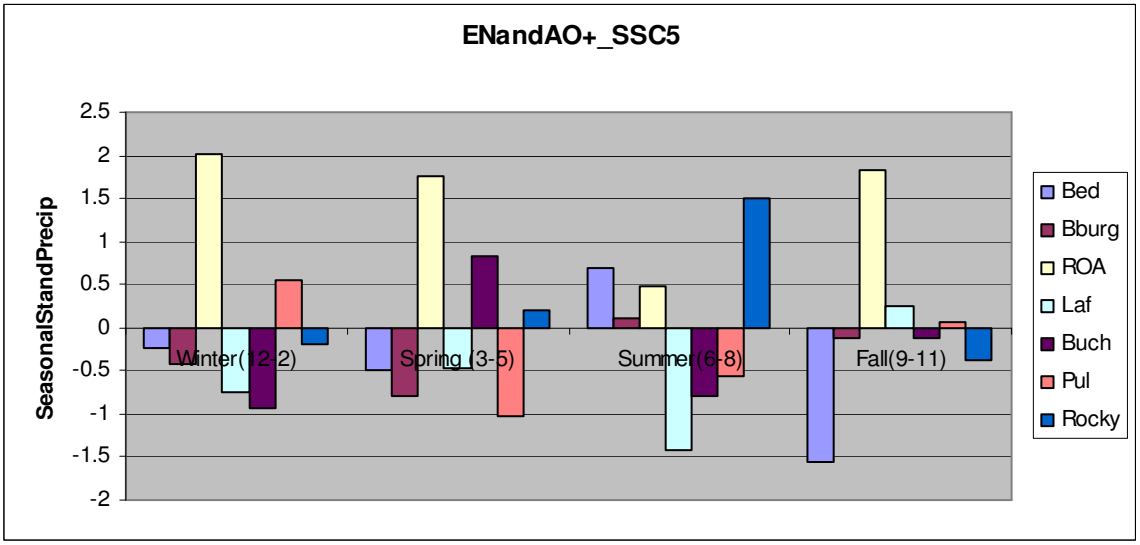
ENandAO+_SSC5
SeasonalStandPrecip
2.5
2
1.5
1
0.5
0
-0.5
-1
-1.5
-2
Winter(12-2)
Spring (3-5)
Summer(6-8)
Fall(9-11)
Bed
Bburg
ROA
Laf
Buch
Pul
Rocky

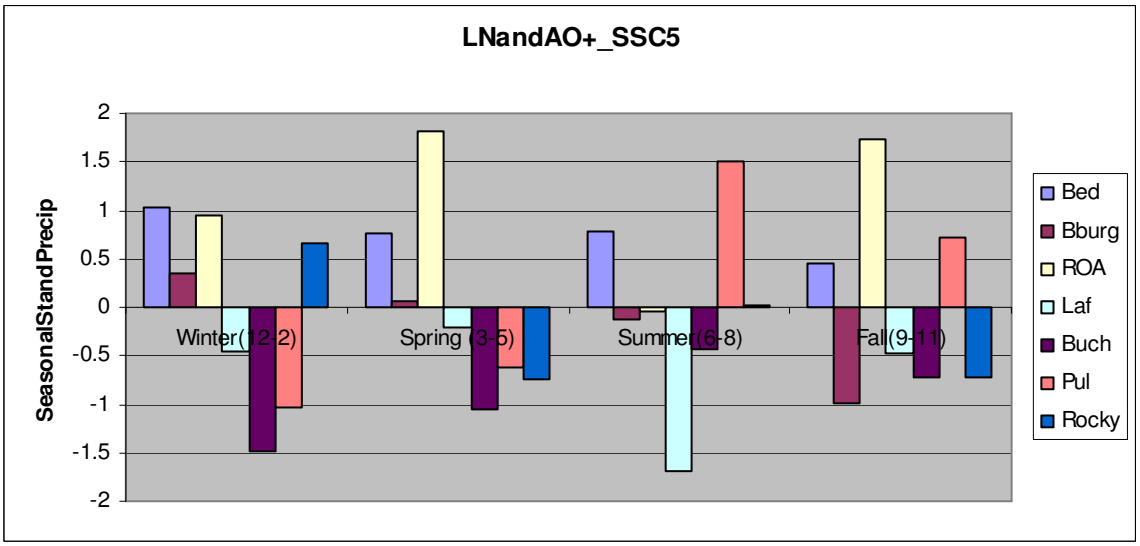
LNandAO+_SSC5
SeasonalStandPrecip
2
1.5
1
0.5
0
-0.5
-1
-1.5
-2
Winter(12-2)
Spring (3-5)
Summer(6-8)
Fall(9-11)
Bed
Bburg
ROA
Laf
Buch
Pul
Rocky

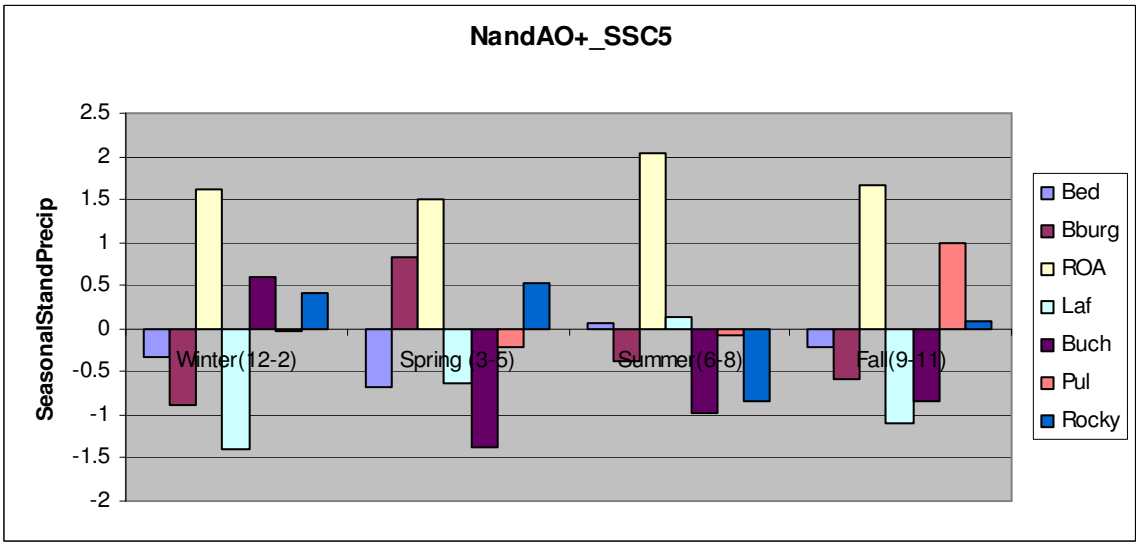
NandAO+_SSC5
SeasonalStandPrecip
2.5
2
1.5
1
0.5
0
-0.5
-1
-1.5
-2
Winter(12-2)
Spring (3-5)
Summer(6-8)
Fall(9-11)
Bed
Bburg
ROA
Laf
Buch
Pul
Rocky

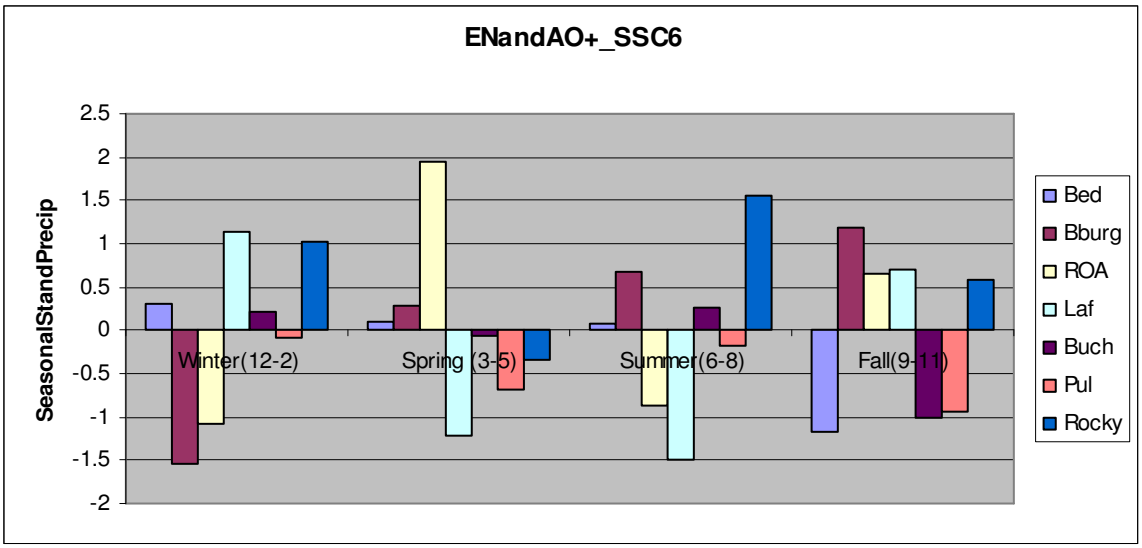
ENandAO+_SSC6
SeasonalStandPrecip
2.5
2
1.5
1
0.5
0
-0.5
-1
-1.5
-2
Winter(12-2)
Spring (3-5)
Summer(6-8)
Fall(9-11)
Bed
Bburg
ROA
Laf
Buch
Pul
Rocky

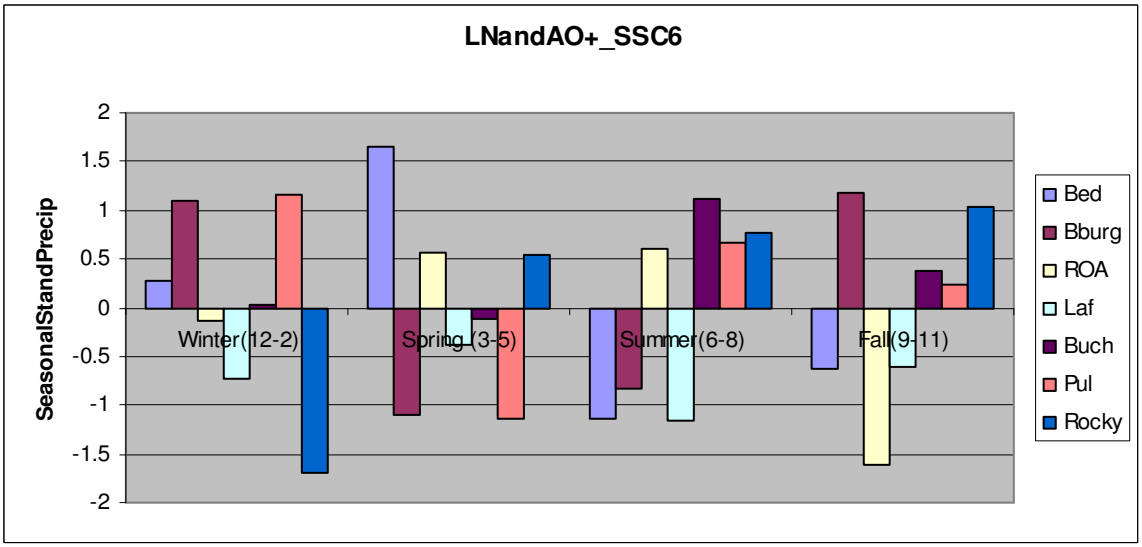
LNandAO+_SSC6
SeasonalStandPrecip
2
1.5
1
0.5
0
-0.5
-1
-1.5
-2
Winter(12-2)
Spring (3-5)
Summer(6-8)
Fall(9-11)
Bed
Bburg
ROA
Laf
Buch
Pul
Rocky

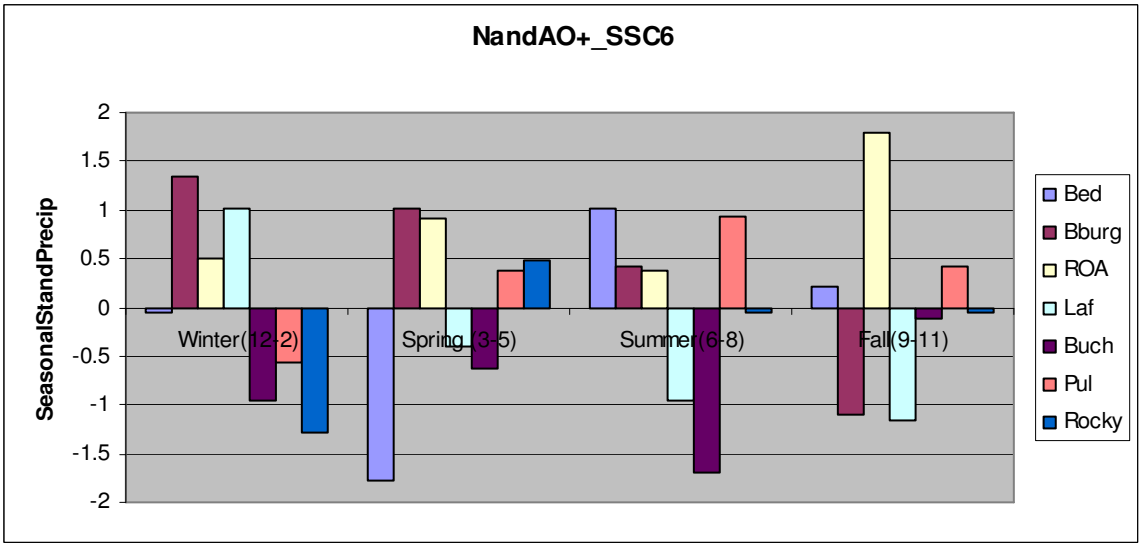
NandAO+_SSC6
SeasonalStandPrecip
2
1.5
1
0.5
0
-0.5
-1
-1.5
-2
Winter(12-2)
Spring (3-5)
Summer(6-8)
Fall(9-11)
Bed
Bburg
ROA
Laf
Buch
Pul
Rocky

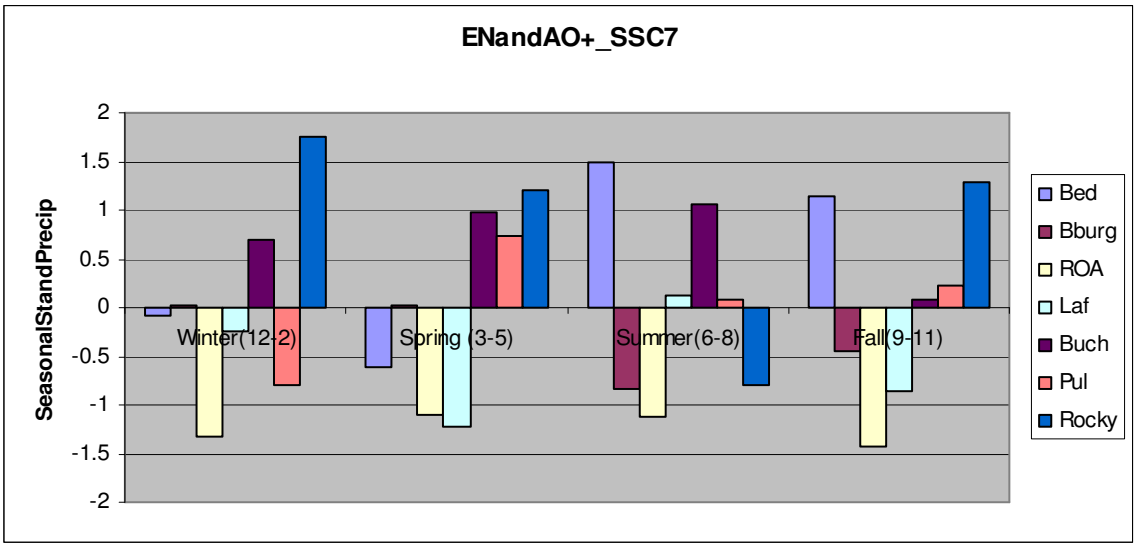
ENandAO+_SSC7
SeasonalStandPrecip
2
1.5
1
0.5
0
-0.5
-1
-1.5
-2
Winter(12-2)
Spring (3-5)
Summer(6-8)
Fall(9-11)
Bed
Bburg
ROA
Laf
Buch
Pul
Rocky

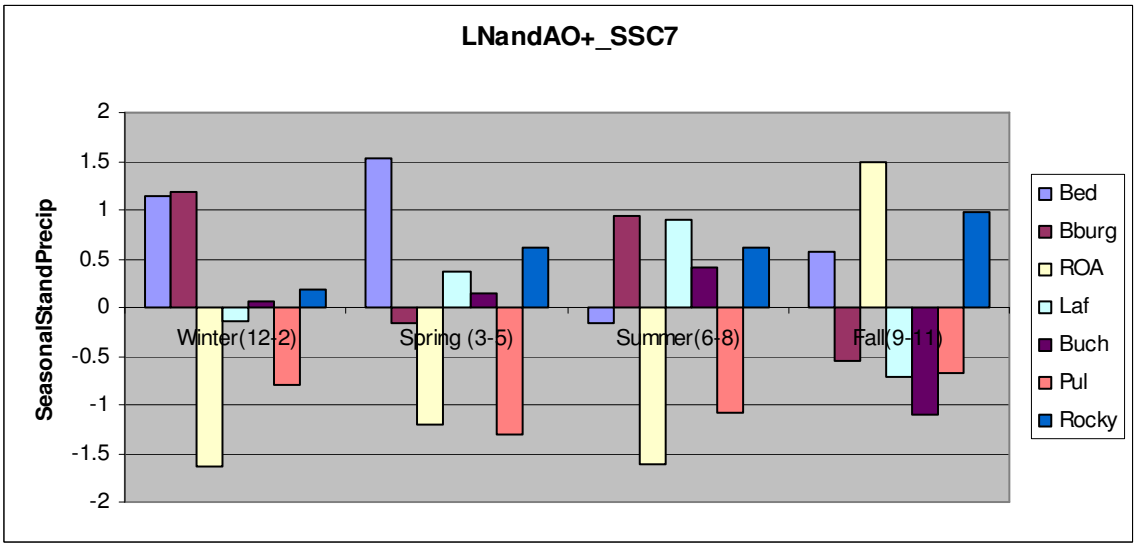
LNandAO+_SSC7
SeasonalStandPrecip
2
1.5
1
0.5
0
-0.5
-1
-1.5
-2
Winter(12-2)
Spring (3-5)
Summer(6-8)
Fall(9-11)
Bed
Bburg
ROA
Laf
Buch
Pul
Rocky

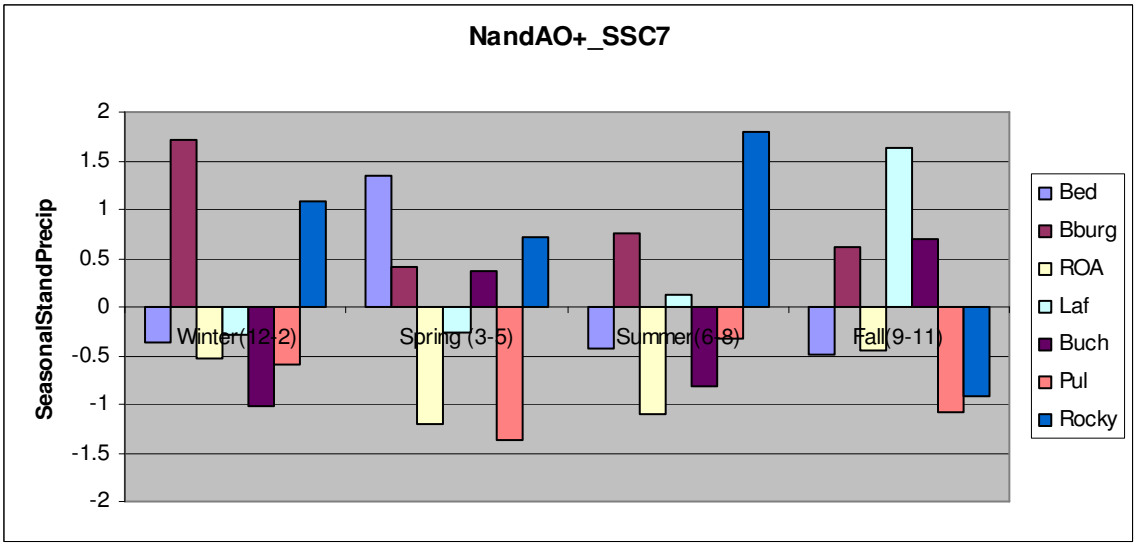
NandAO+_SSC7
SeasonalStandPrecip
2
1.5
1
0.5
0
-0.5
-1
-1.5
-2
Winter(12-2)
Spring (3-5)
Summer(6-8)
Fall(9-11)
Bed
Bburg
ROA
Laf
Buch
Pul
Rocky

ENSO & AO-_SSC Conditioning

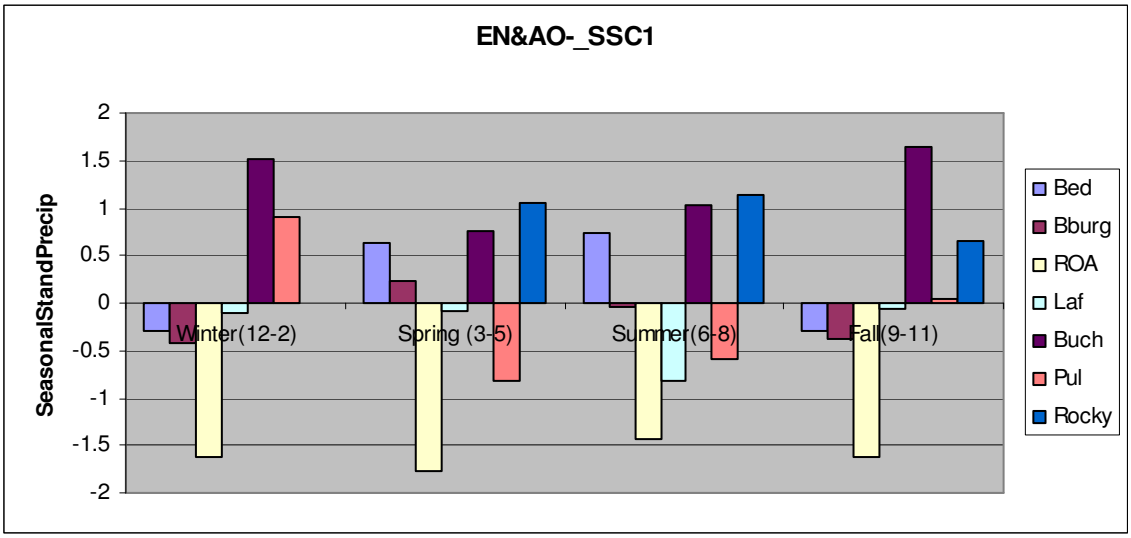

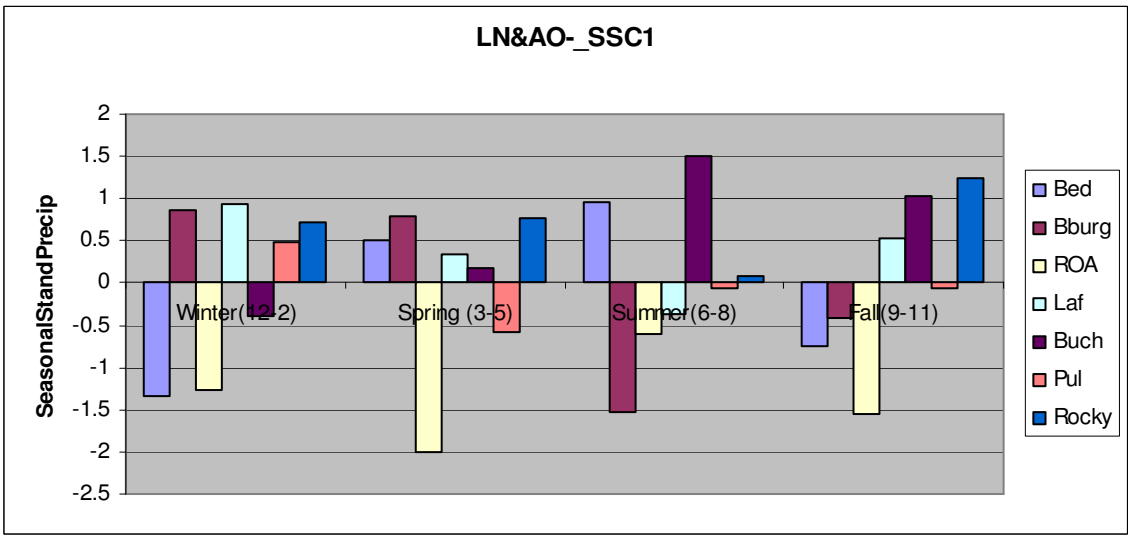

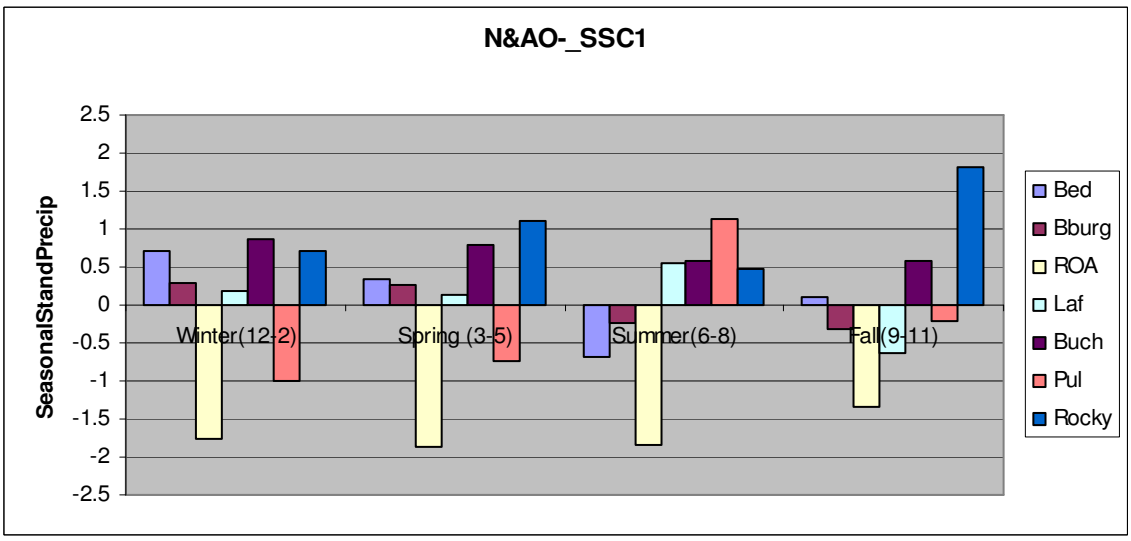

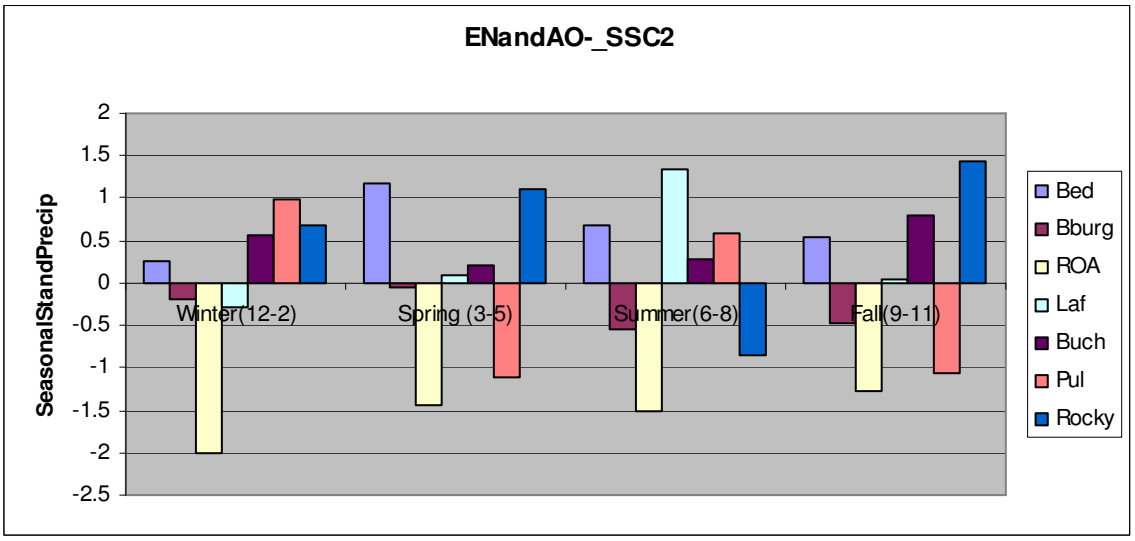
ENandAO-_SSC2
SeasonalStandPrecip
2
1.5
1
0.5
0
-0.5
-1
-1.5
-2
-2.5
Winter(12-2)
Spring (3-5)
Summer(6-8)
Fall(9-11)
Bed
Bburg
ROA
Laf
Buch
Pul
Rocky

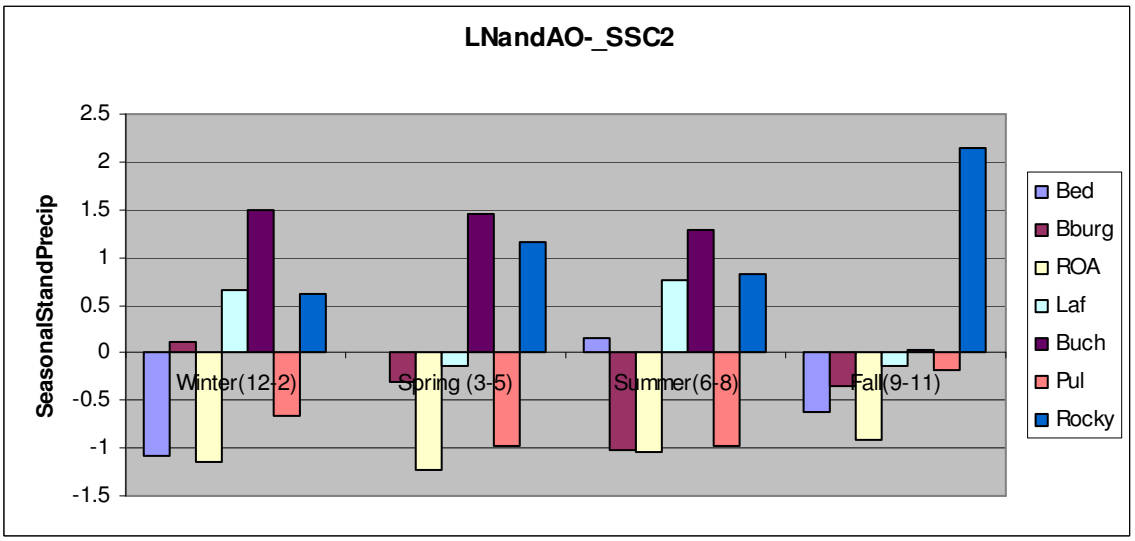
LNandAO-_SSC2
SeasonalStandPrecip
2.5
2
1.5
1
0.5
0
-0.5
-1
-1.5
Winter(12-2)
Spring (3-5)
Summer(6-8)
Fall(9-11)
Bed
Bburg
ROA
Laf
Buch
Pul
Rocky

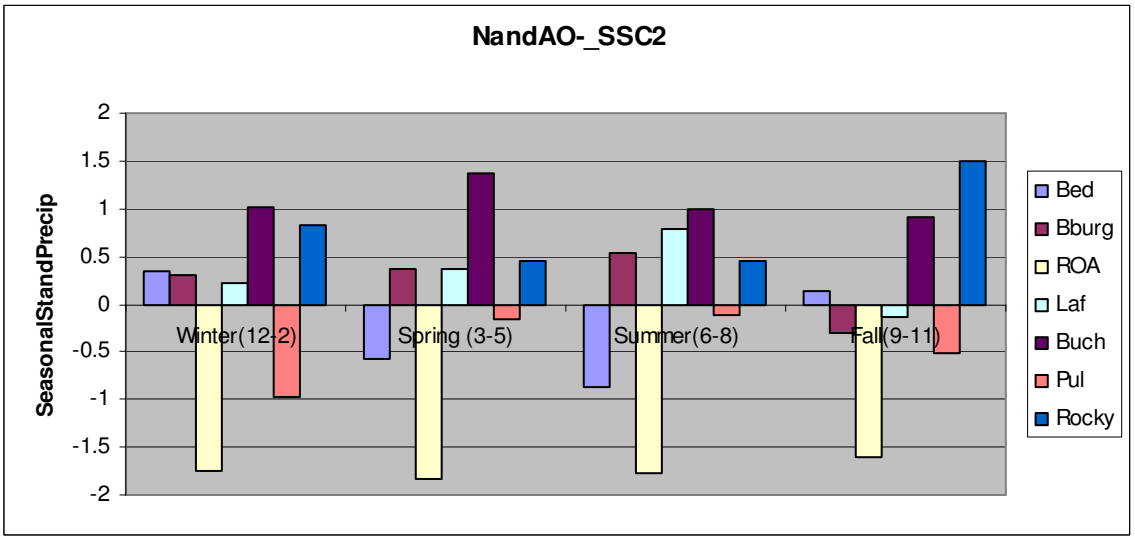
NandAO-_SSC2
SeasonalStandPrecip
2
1.5
1
0.5
0
-0.5
-1
-1.5
-2
Winter(12-2)
Spring (3-5)
Summer(6-8)
Fall(9-11)
Bed
Bburg
ROA
Laf
Buch
Pul
Rocky

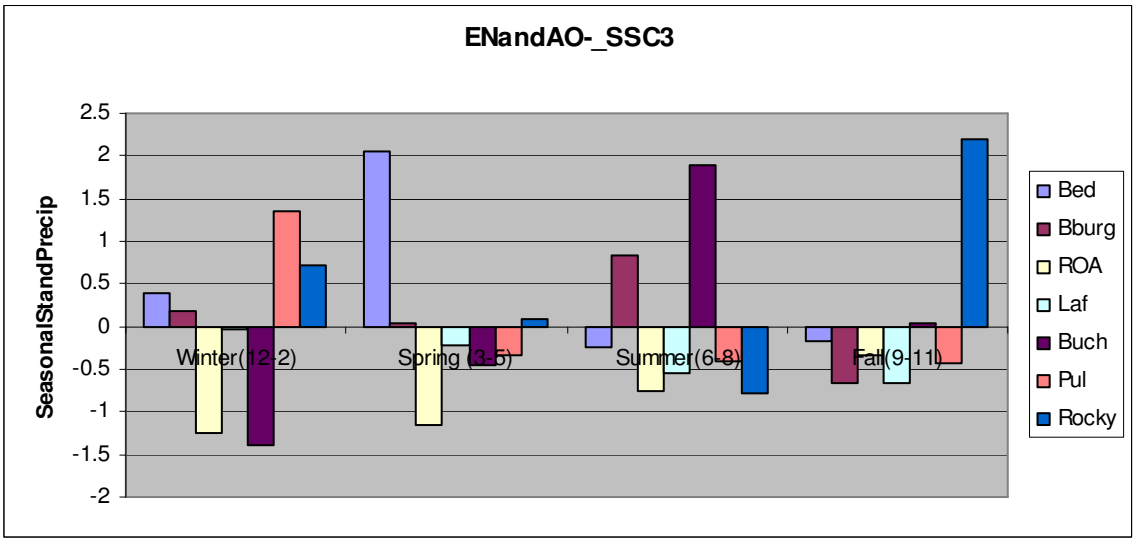
ENandAO-_SSC3
SeasonalStandPrecip
2.5
2
1.5
1
0.5
0
-0.5
-1
-1.5
-2
Winter(12-2)
Spring (3-5)
Summer(6-8)
Fall(9-11)
Bed
Bburg
ROA
Laf
Buch
Pul
Rocky

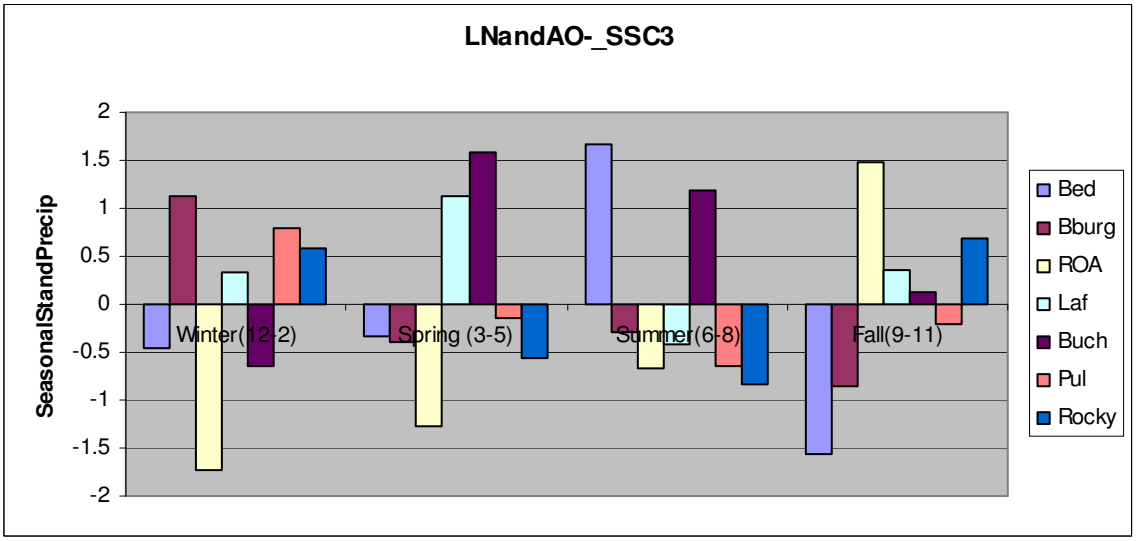
LNandAO-_SSC3
SeasonalStandPrecip
2
1.5
1
0.5
0
-0.5
-1
-1.5
-2
Winter(12-2)
Spring (3-5)
Summer(6-8)
Fall(9-11)
Bed
Bburg
ROA
Laf
Buch
Pul
Rocky

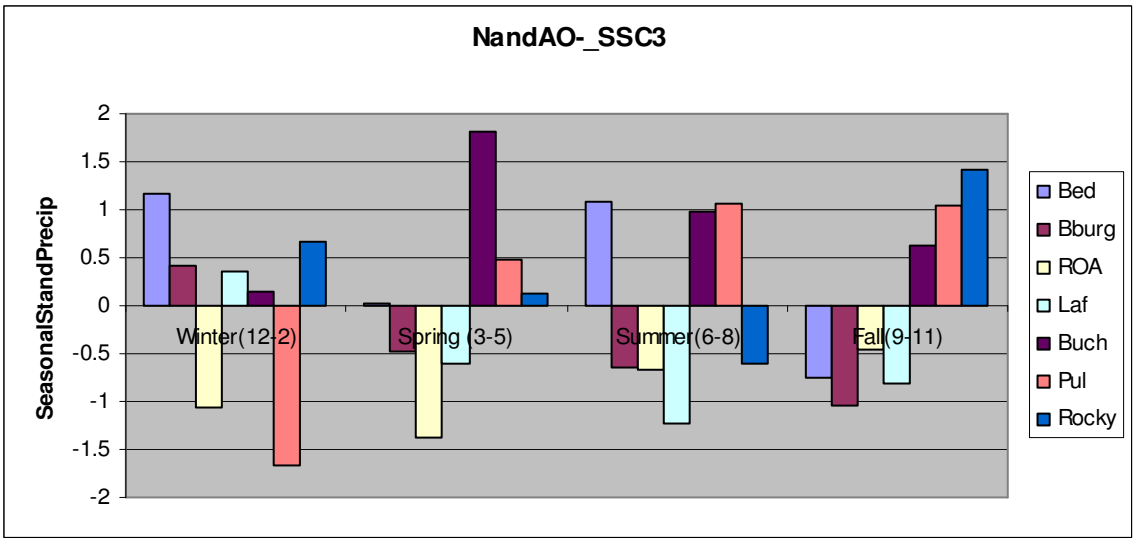
NandAO-_SSC3
SeasonalStandPrecip
2
1.5
1
0.5
0
-0.5
-1
-1.5
-2
Winter(12-2)
Spring (3-5)
Summer(6-8)
Fall(9-11)
Bed
Bburg
ROA
Laf
Buch
Pul
Rocky

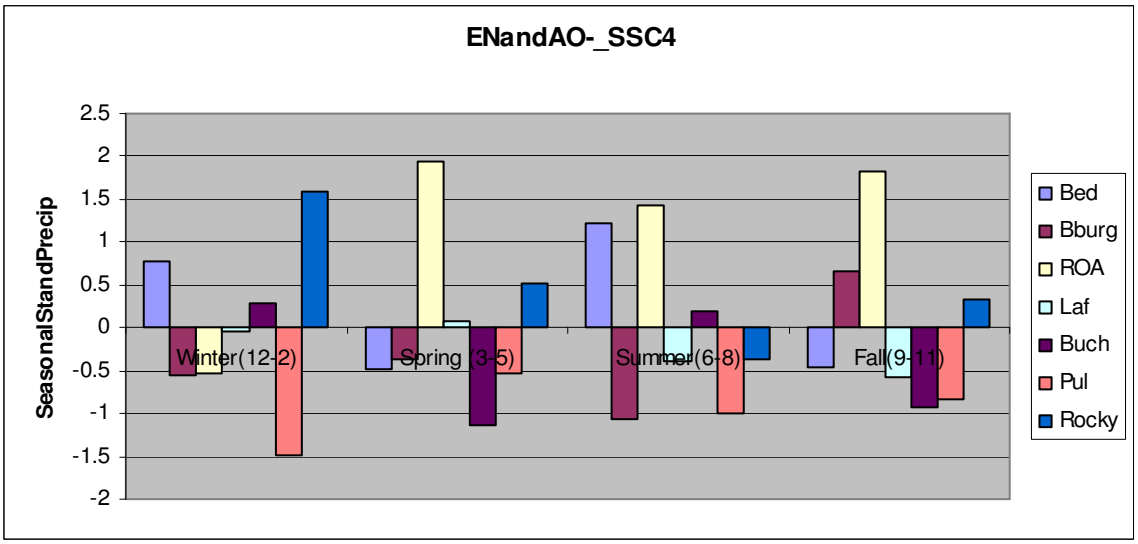
ENandAO-_SSC4
SeasonalStandPrecip
2.5
2
1.5
1
0.5
0
-0.5
-1
-1.5
-2
Winter(12-2)
Spring (3-5)
Summer(6-8)
Fall(9-11)
Bed
Bburg
ROA
Laf
Buch
Pul
Rocky

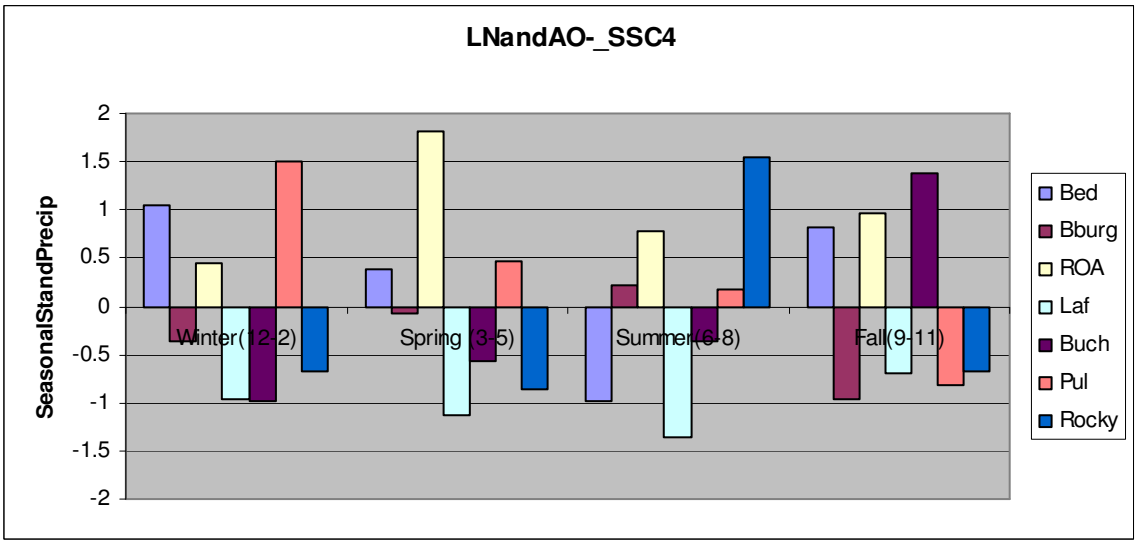
LNandAO-_SSC4
SeasonalStandPrecip
2
1.5
1
0.5
0
-0.5
-1
-1.5
-2
Winter(12-2)
Spring (3-5)
Summer(6-8)
Fall(9-11)
Bed
Bburg
ROA
Laf
Buch
Pul
Rocky

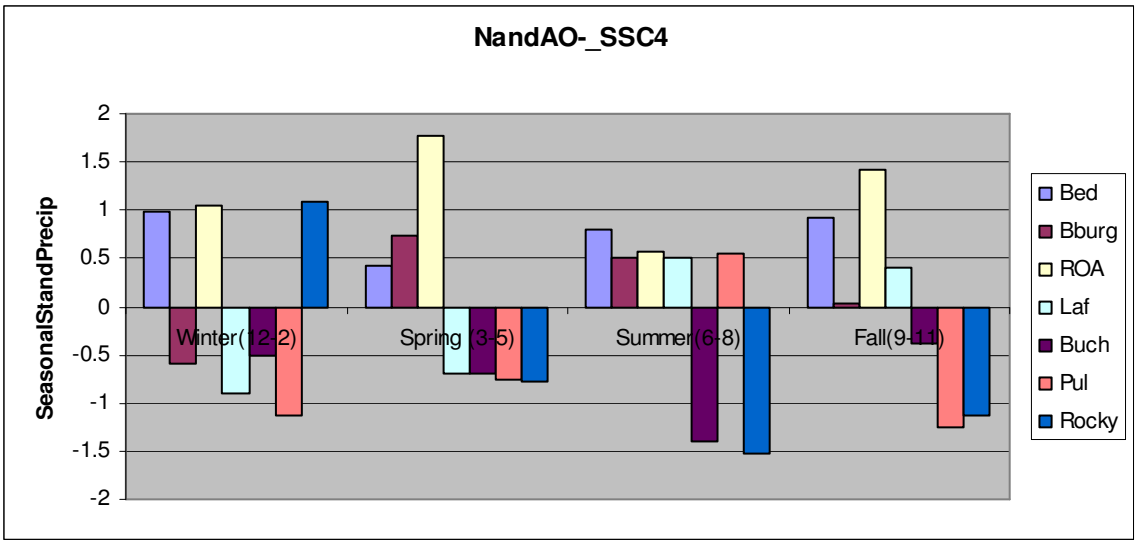
NandAO-_SSC4
SeasonalStandPrecip
2
1.5
1
0.5
0
-0.5
-1
-1.5
-2
Winter(12-2)
Spring (3-5)
Summer(6-8)
Fall(9-11)
Bed
Bburg
ROA
Laf
Buch
Pul
Rocky

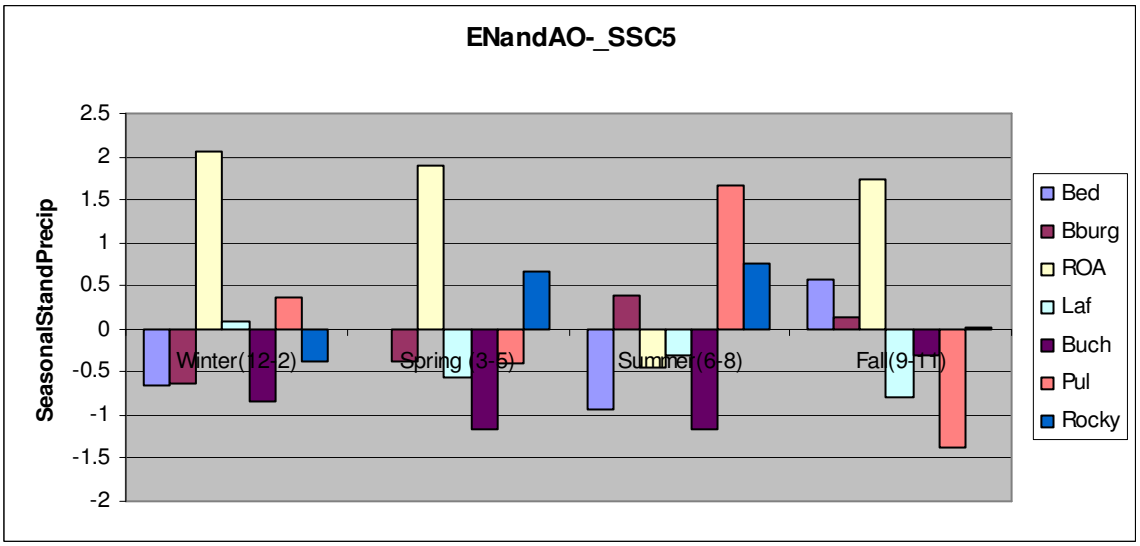
ENandAO-_SSC5
SeasonalStandPrecip
2.5
2
1.5
1
0.5
0
-0.5
-1
-1.5
-2
Winter(12-2)
Spring (3-5)
Summer(6-8)
Fall(9-11)
Bed
Bburg
ROA
Laf
Buch
Pul
Rocky

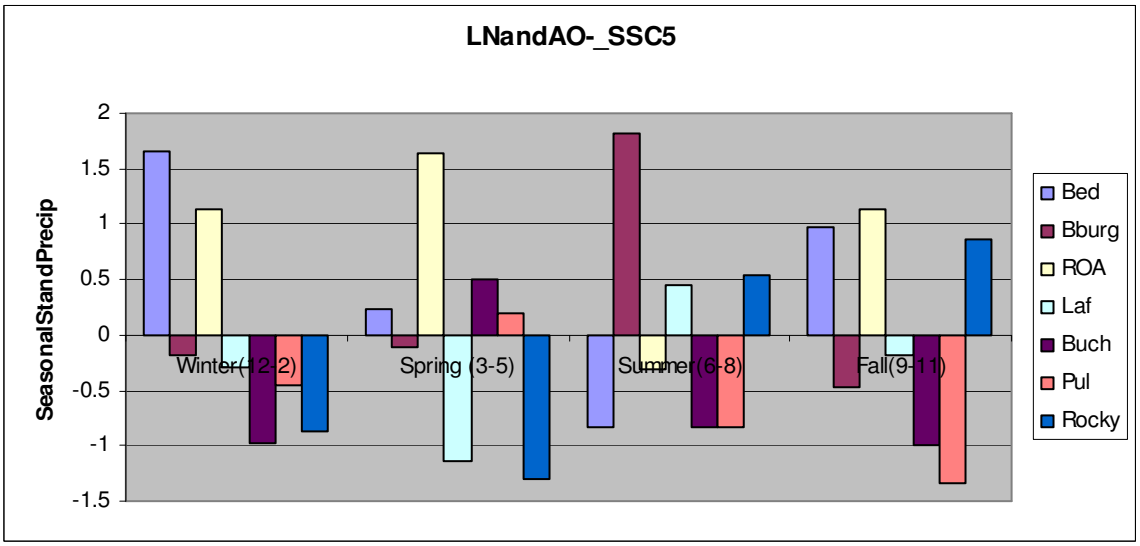
LNandAO-_SSC5
SeasonalStandPrecip
2
1.5
1
0.5
0
-0.5
-1
-1.5
Winter(12-2)
Spring (3-5)
Summer(6-8)
Fall(9-11)
Bed
Bburg
ROA
Laf
Buch
Pul
Rocky

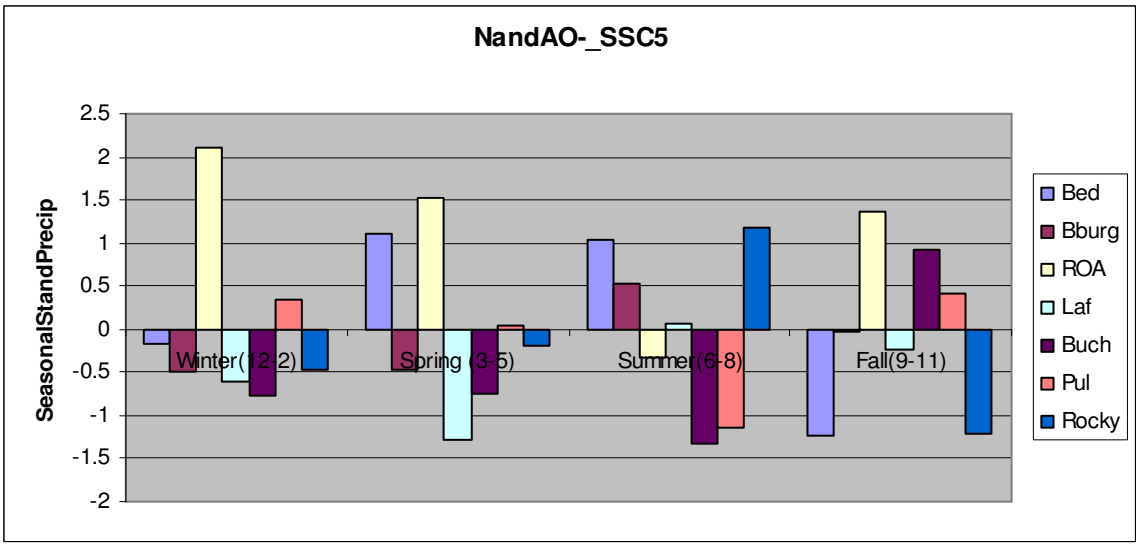
NandAO-_SSC5
SeasonalStandPrecip
2.5
2
1.5
1
0.5
0
-0.5
-1
-1.5
-2
Winter(12-2)
Spring (3-5)
Summer(6-8)
Fall(9-11)
Bed
Bburg
ROA
Laf
Buch
Pul
Rocky

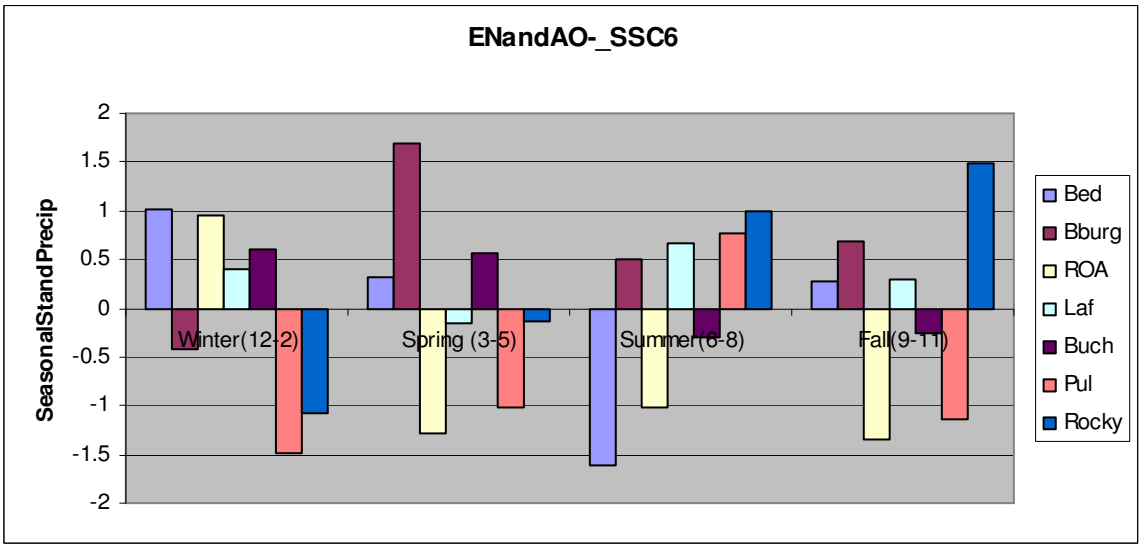
ENandAO-_SSC6
SeasonalStandPrecip
2
1.5
1
0.5
0
-0.5
-1
-1.5
-2
Winter(12-2)
Spring (3-5)
Summer(6-8)
Fall(9-11)
Bed
Bburg
ROA
Laf
Buch
Pul
Rocky

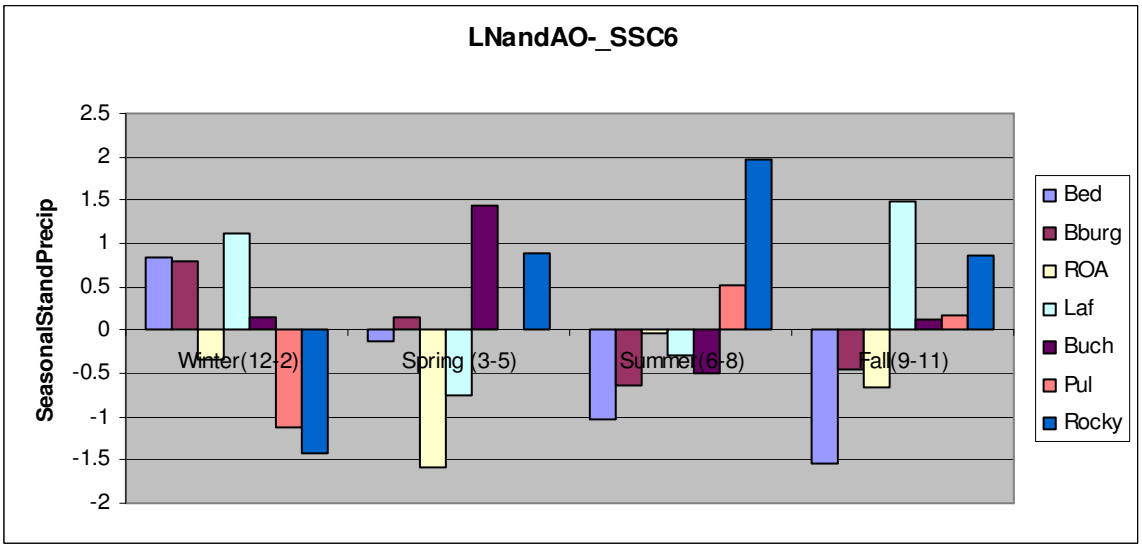
LNandAO-_SSC6
SeasonalStandPrecip
2.5
2
1.5
1
0.5
0
-0.5
-1
-1.5
-2
Winter(12-2)
Spring (3-5)
Summer(6-8)
Fall(9-11)
Bed
Bburg
ROA
Laf
Buch
Pul
Rocky

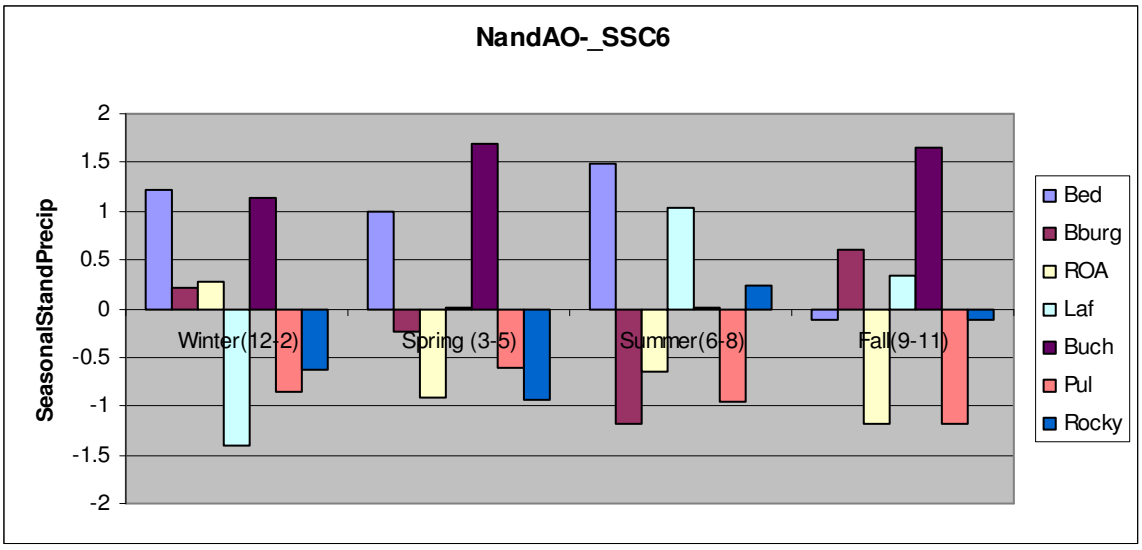
NandAO-_SSC6
SeasonalStandPrecip
2
1.5
1
0.5
0
-0.5
-1
-1.5
-2
Winter(12-2)
Spring (3-5)
Summer(6-8)
Fall(9-11)
Bed
Bburg
ROA
Laf
Buch
Pul
Rocky

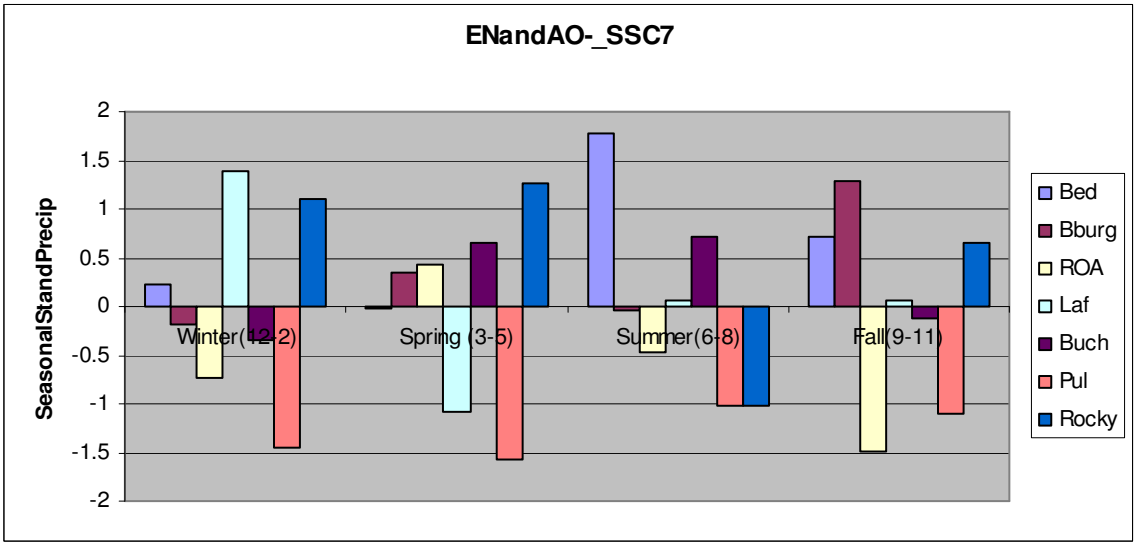
ENandAO-_SSC7
SeasonalStandPrecip
2
1.5
1
0.5
0
-0.5
-1
-1.5
-2
Winter(12-2)
Spring (3-5)
Summer(6-8)
Fall(9-11)
Bed
Bburg
ROA
Laf
Buch
Pul
Rocky

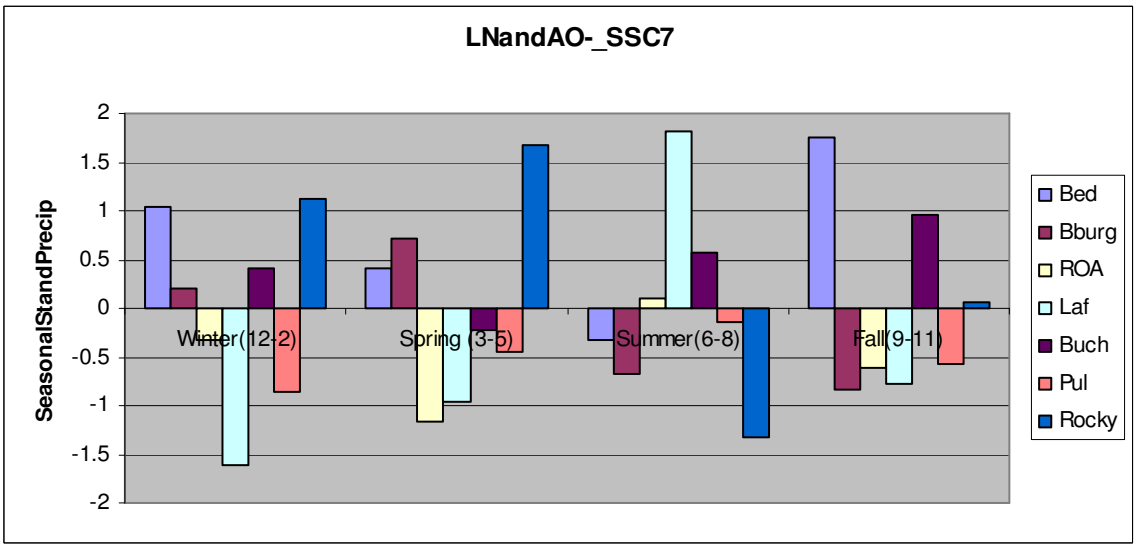
LNandAO-_SSC7
SeasonalStandPrecip
2
1.5
1
0.5
0
-0.5
-1
-1.5
-2
Winter(12-2)
Spring (3-5)
Summer(6-8)
Fall(9-11)
Bed
Bburg
ROA
Laf
Buch
Pul
Rocky

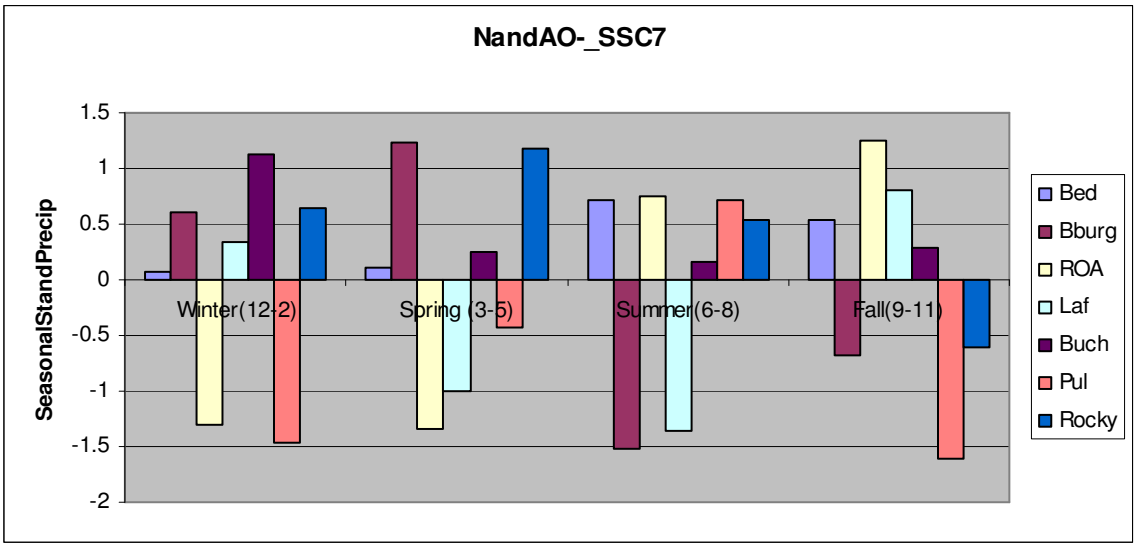

ENSO & NAO+_SSC Conditioning

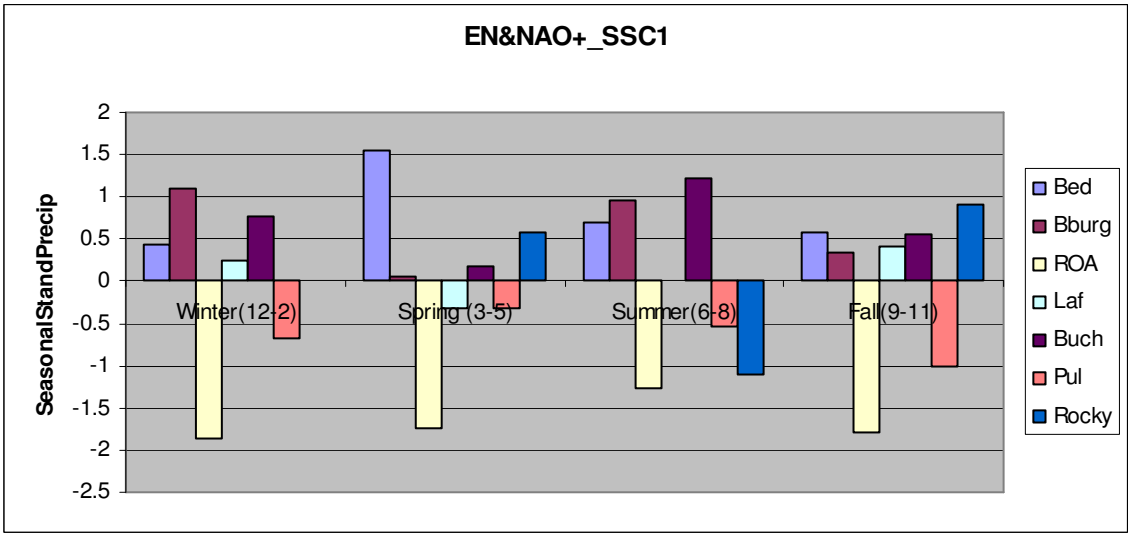

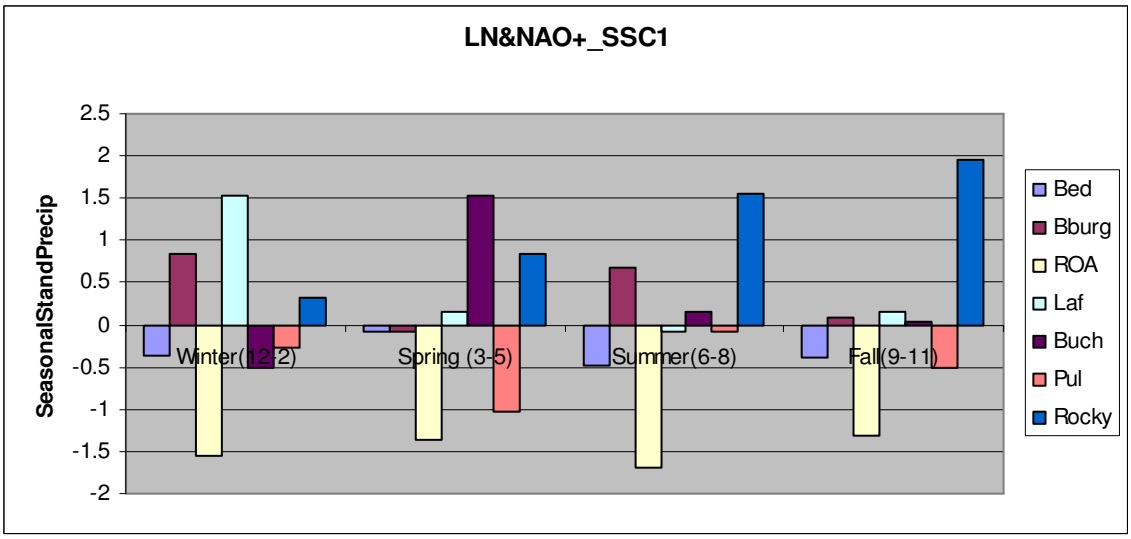
LN&NAO+_SSC1
SeasonalStandPrecip
2.5
2
1.5
1
0.5
0
-0.5
-1
-1.5
-2
Winter(12-2)
Spring (3-5)
Summer(6-8)
Fall(9-11)
Bed
Bburg
ROA
Laf
Buch
Pul
Rocky

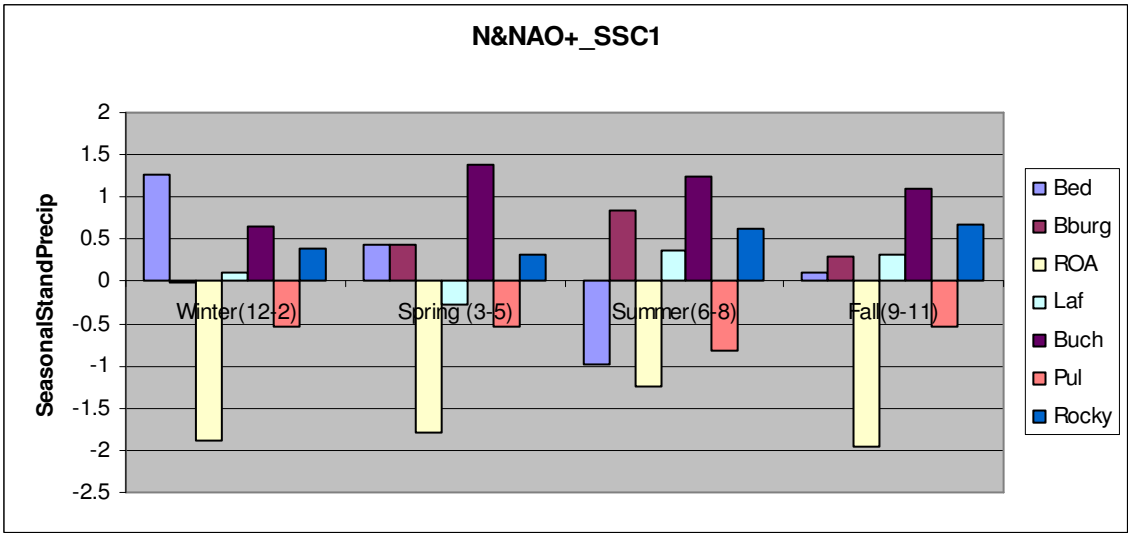
N&NAO+_SSC1
SeasonalStandPrecip
2
1.5
1
0.5
0
-0.5
-1
-1.5
-2
-2.5
Winter(12-2)
Spring (3-5)
Summer(6-8)
Fall(9-11)
Bed
Bburg
ROA
Laf
Buch
Pul
Rocky

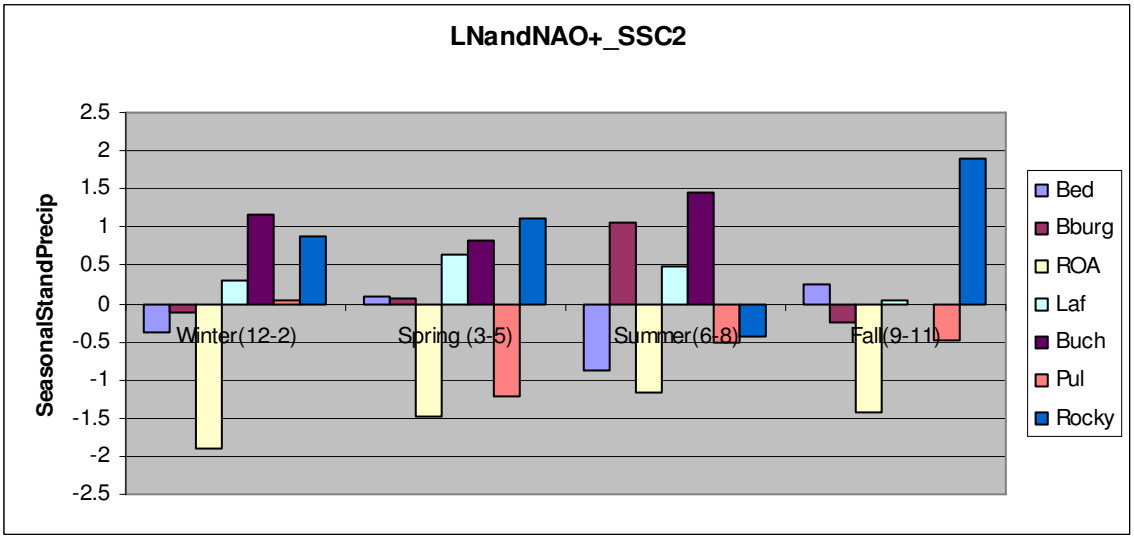
LNandNAO+_SSC2
SeasonalStandPrecip
2.5
2
1.5
1
0.5
0
-0.5
-1
-1.5
-2
-2.5
Winter(12-2)
Spring (3-5)
Summer(6-8)
Fall(9-11)
Bed
Bburg
ROA
Laf
Buch
Pul
Rocky

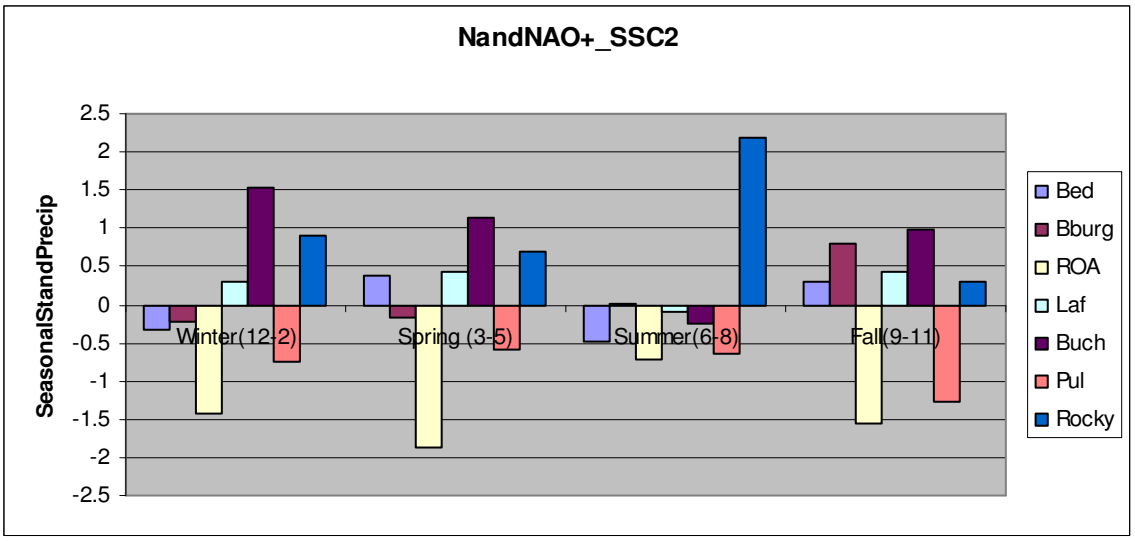
NandNAO+_SSC2
SeasonalStandPrecip
2.5
2
1.5
1
0.5
0
-0.5
-1
-1.5
-2
-2.5
Winter(12-2)
Spring (3-5)
Summer(6-8)
Fall(9-11)
Bed
Bburg
ROA
Laf
Buch
Pul
Rocky

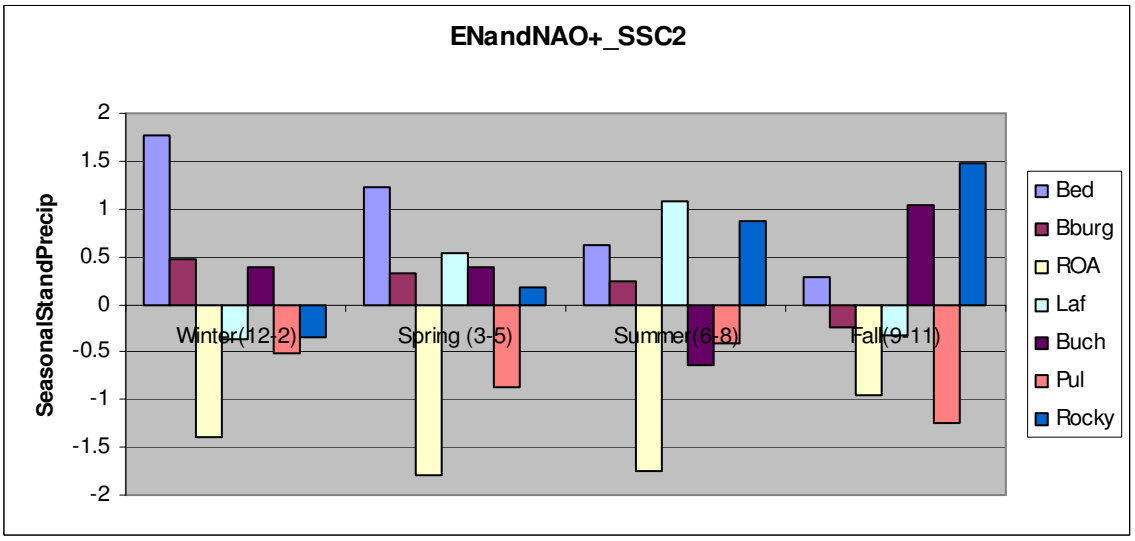
ENandNAO+_SSC2
SeasonalStandPrecip
2
1.5
1
0.5
0
-0.5
-1
-1.5
-2
Winter(12-2)
Spring (3-5)
Summer(6-8)
Fall(9-11)
Bed
Bburg
ROA
Laf
Buch
Pul
Rocky

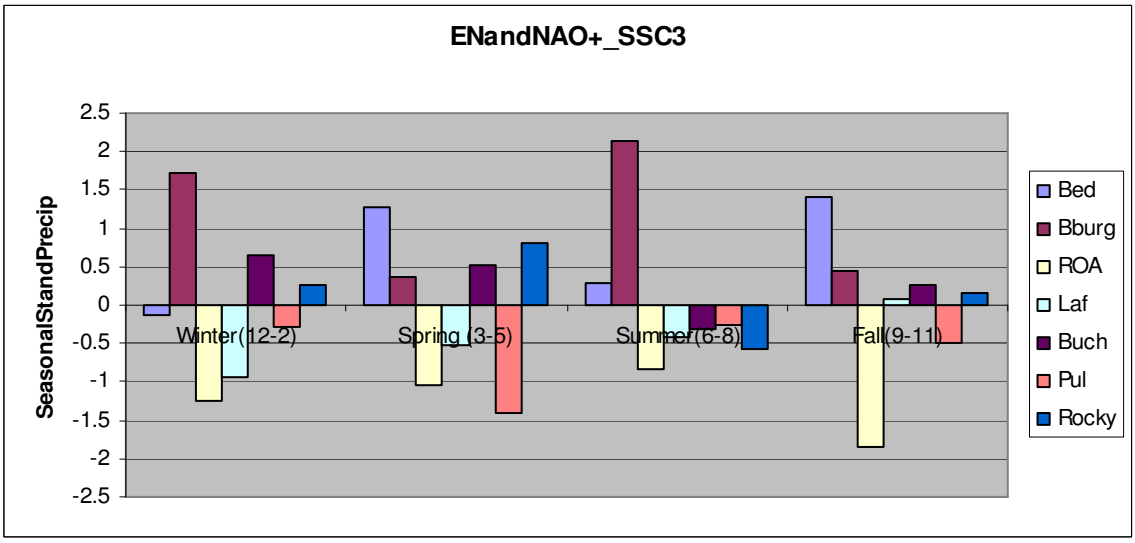
ENandNAO+_SSC3
SeasonalStandPrecip
2.5
2
1.5
1
0.5
0
-0.5
-1
-1.5
-2
-2.5
Winter(12-2)
Spring (3-5)
Summer(6-8)
Fall(9-11)
Bed
Bburg
ROA
Laf
Buch
Pul
Rocky

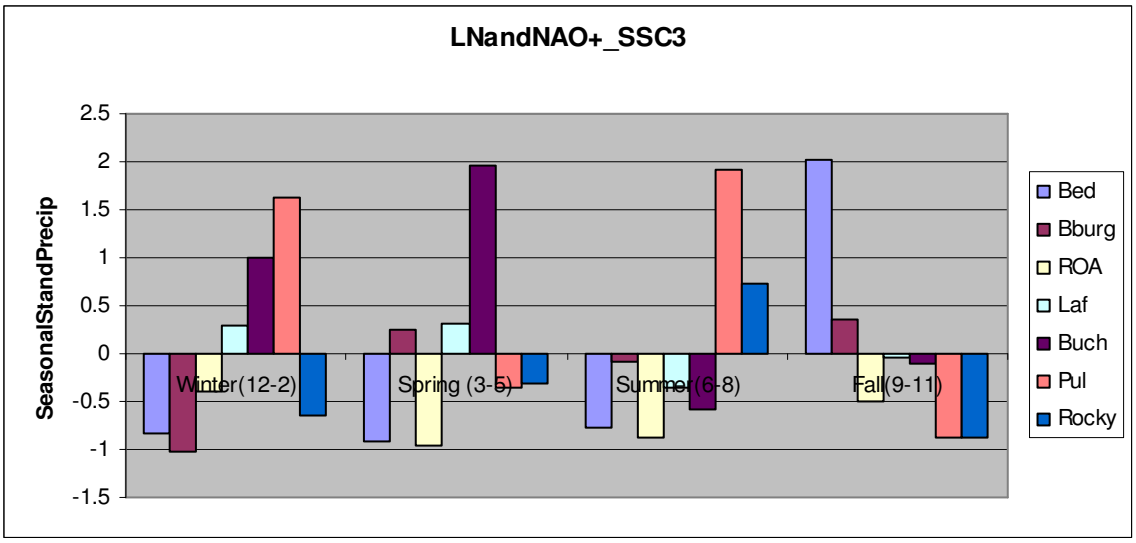
LNandNAO+_SSC3
SeasonalStandPrecip
2.5
2
1.5
1
0.5
0
-0.5
-1
-1.5
Winter(12-2)
Spring (3-5)
Summer(6-8)
Fall(9-11)
Bed
Bburg
ROA
Laf
Buch
Pul
Rocky

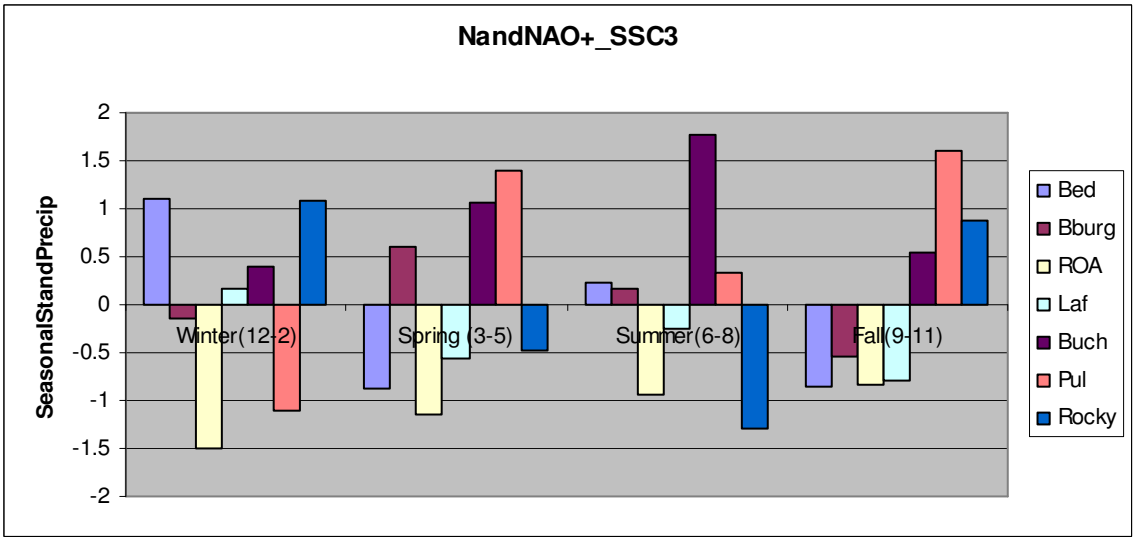
NandNAO+_SSC3
SeasonalStandPrecip
2
1.5
1
0.5
0
-0.5
-1
-1.5
-2
Winter(12-2)
Spring (3-5)
Summer(6-8)
Fall(9-11)
Bed
Bburg
ROA
Laf
Buch
Pul
Rocky

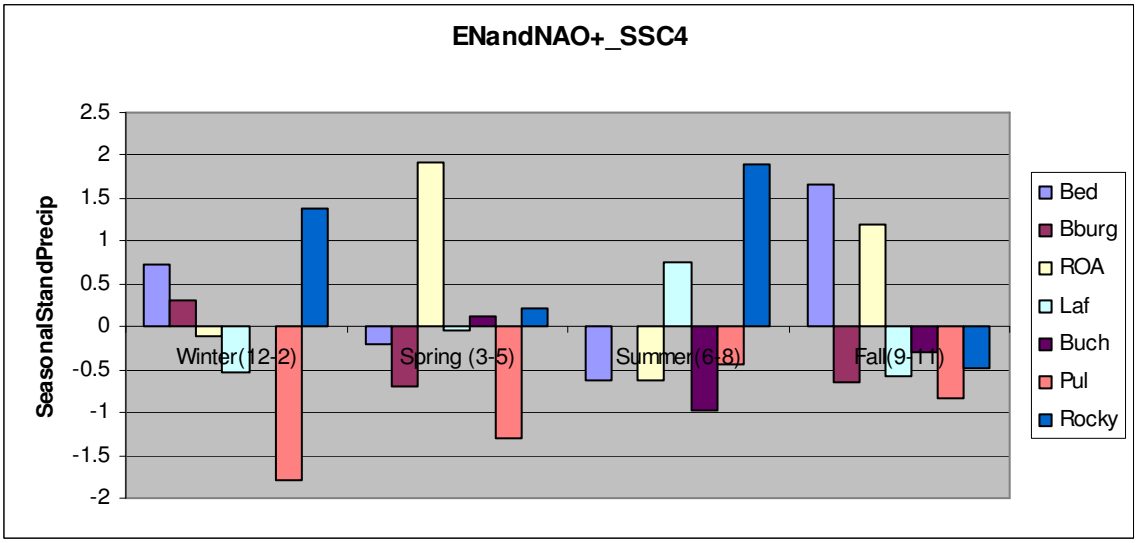
ENandNAO+_SSC4
SeasonalStandPrecip
2.5
2
1.5
1
0.5
0
-0.5
-1
-1.5
-2
Winter(12-2)
Spring (3-5)
Summer(6-8)
Fall(9-11)
Bed
Bburg
ROA
Laf
Buch
Pul
Rocky

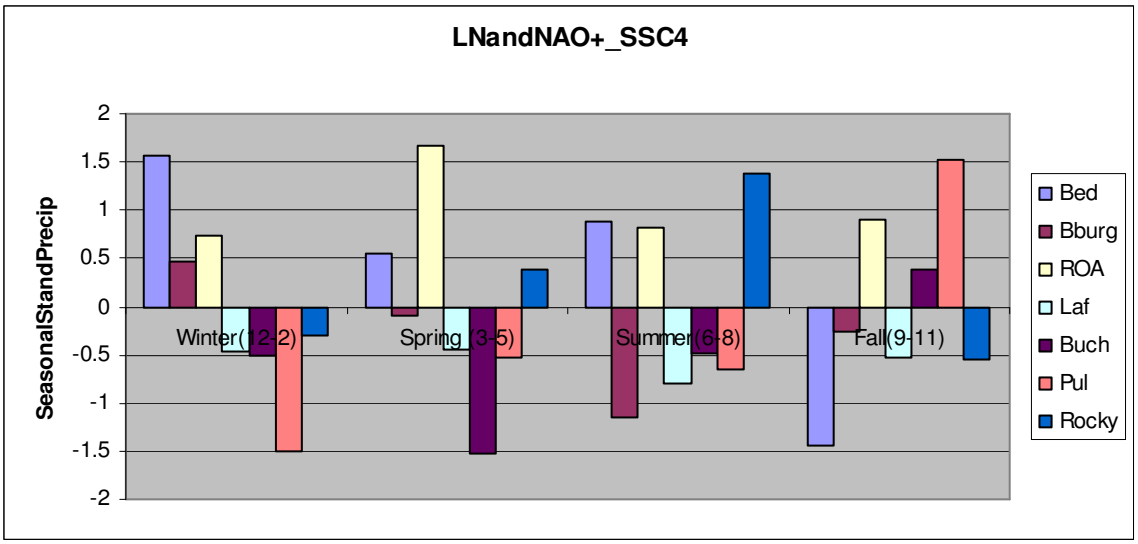
LNandNAO+_SSC4
SeasonalStandPrecip
2
1.5
1
0.5
0
-0.5
-1
-1.5
-2
Winter(12-2)
Spring (3-5)
Summer(6-8)
Fall(9-11)
Bed
Bburg
ROA
Laf
Buch
Pul
Rocky

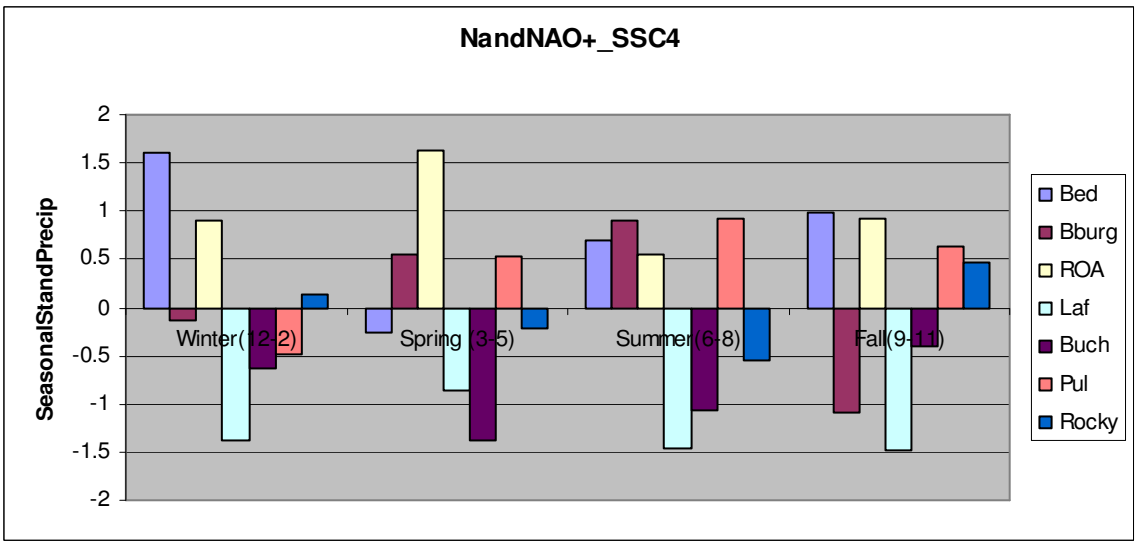
NandNAO+_SSC4
SeasonalStandPrecip
2
1.5
1
0.5
0
-0.5
-1
-1.5
-2
Winter(12-2)
Spring (3-5)
Summer(6-8)
Fall(9-11)
Bed
Bburg
ROA
Laf
Buch
Pul
Rocky

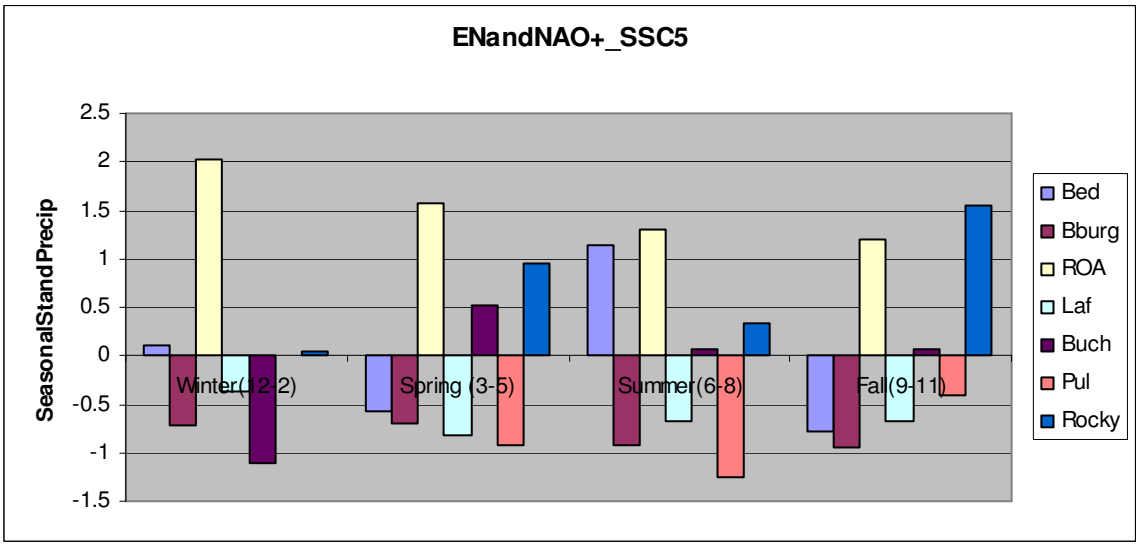
ENandNAO+_SSC5
SeasonalStandPrecip
2.5
2
1.5
1
0.5
0
-0.5
-1
-1.5
Winter(12-2)
Spring (3-5)
Summer(6-8)
Fall(9-11)
Bed
Bburg
ROA
Laf
Buch
Pul
Rocky

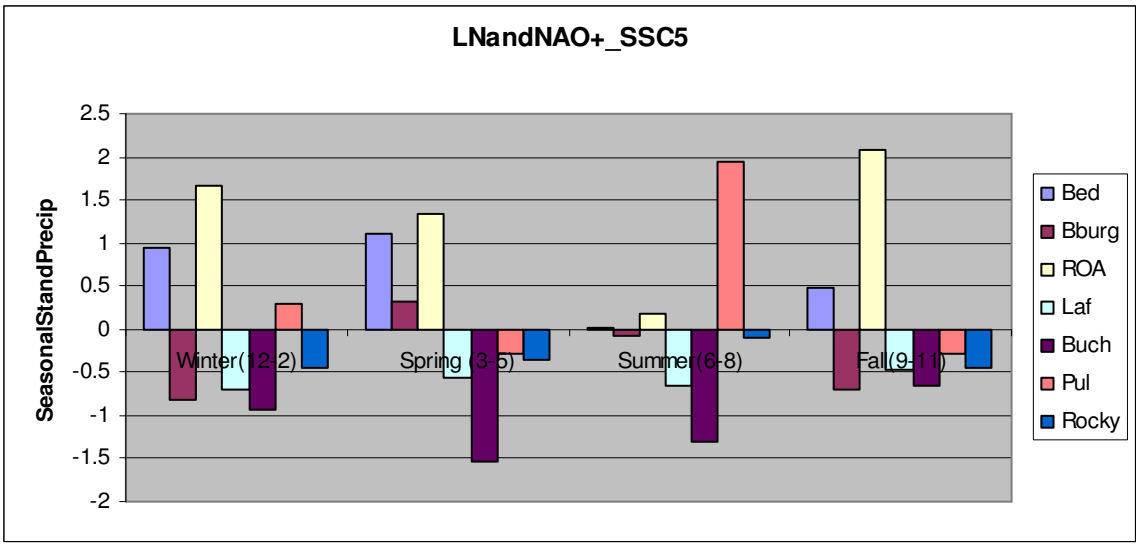
LNandNAO+_SSC5
SeasonalStandPrecip
2.5
2
1.5
1
0.5
0
-0.5
-1
-1.5
-2
Winter(12-2)
Spring (3-5)
Summer(6-8)
Fall(9-11)
Bed
Bburg
ROA
Laf
Buch
Pul
Rocky

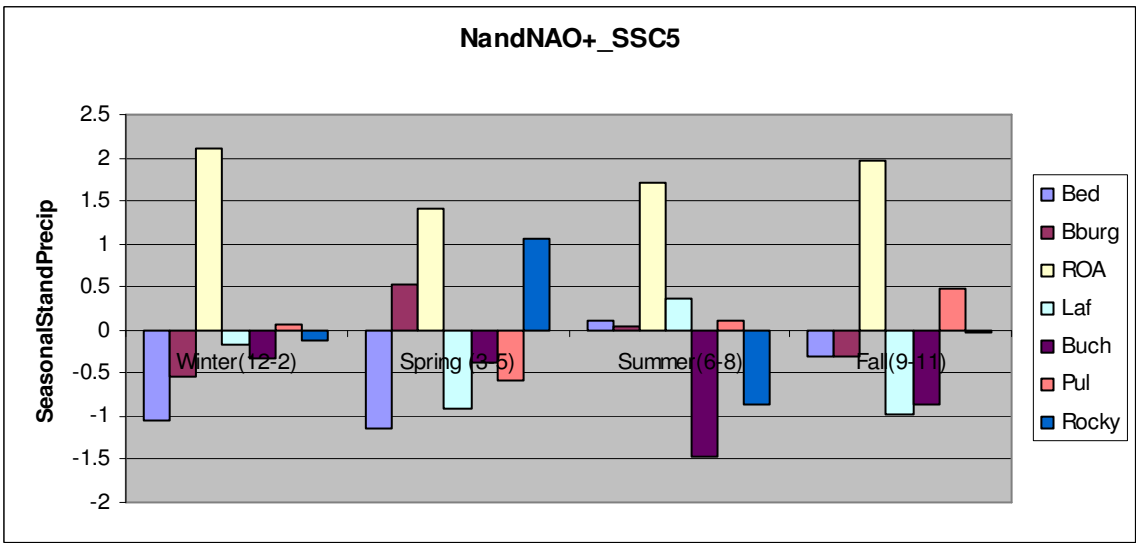
NandNAO+_SSC5
SeasonalStandPrecip
2.5
2
1.5
1
0.5
0
-0.5
-1
-1.5
-2
Winter(12-2)
Spring (3-5)
Summer(6-8)
Fall(9-11)
Bed
Bburg
ROA
Laf
Buch
Pul
Rocky

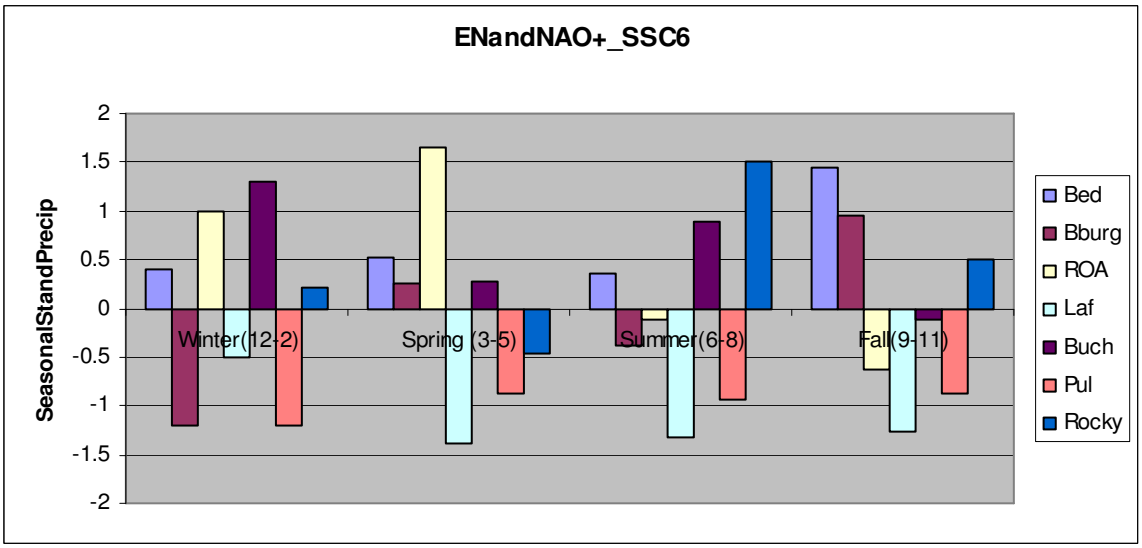
ENandNAO+_SSC6
SeasonalStandPrecip
2
1.5
1
0.5
0
-0.5
-1
-1.5
-2
Winter(12-2)
Spring (3-5)
Summer(6-8)
Fall(9-11)
Bed
Bburg
ROA
Laf
Buch
Pul
Rocky

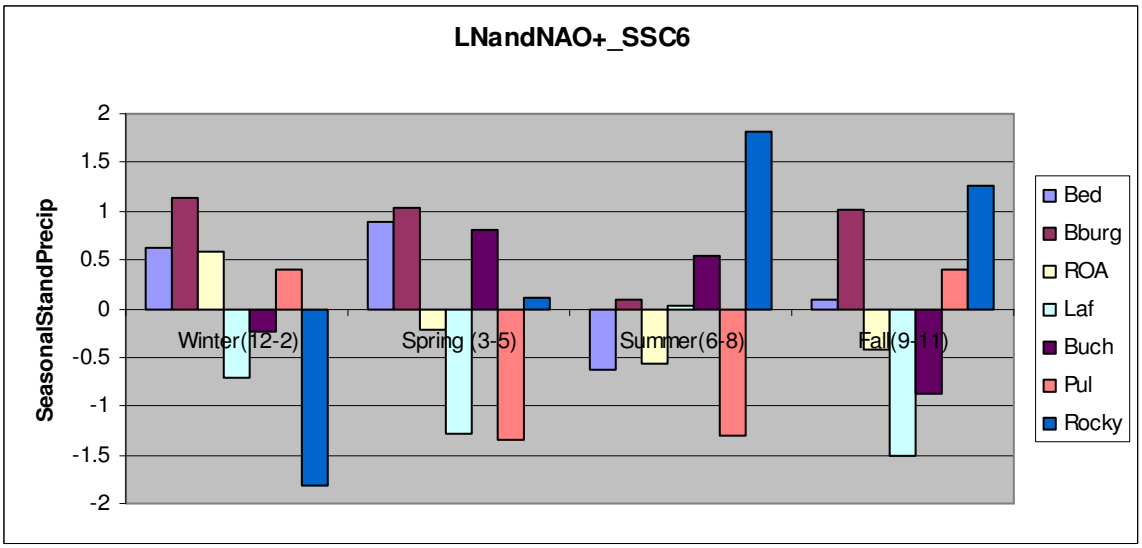
LNandNAO+_SSC6
SeasonalStandPrecip
2
1.5
1
0.5
0
-0.5
-1
-1.5
-2
Winter(12-2)
Spring (3-5)
Summer(6-8)
Fall(9-11)
Bed
Bburg
ROA
Laf
Buch
Pul
Rocky

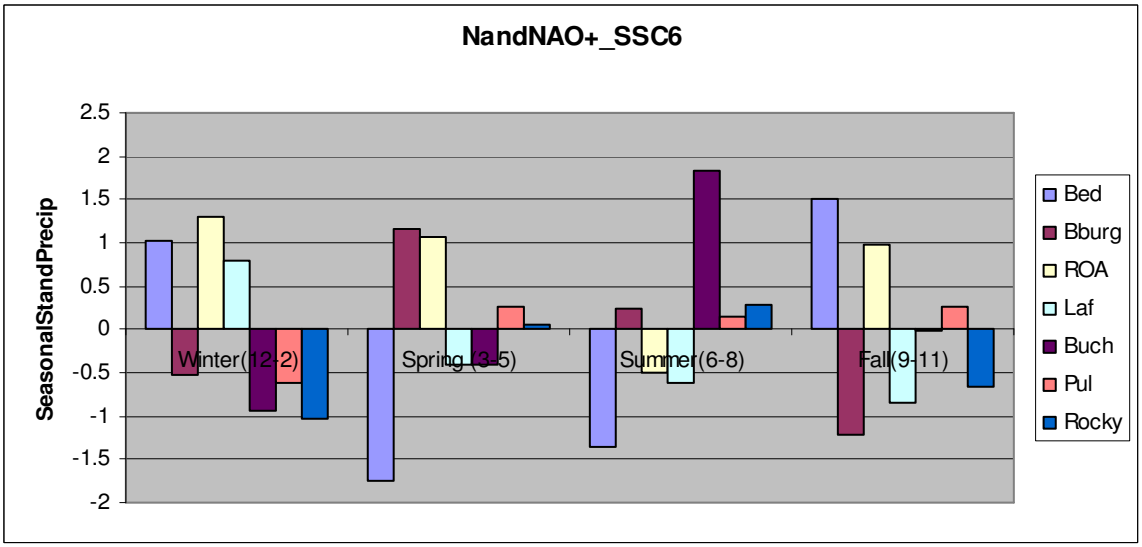
NandNAO+_SSC6
SeasonalStandPrecip
2.5
2
1.5
1
0.5
0
-0.5
-1
-1.5
-2
Winter(12-2)
Spring (3-5)
Summer(6-8)
Fall(9-11)
Bed
Bburg
ROA
Laf
Buch
Pul
Rocky

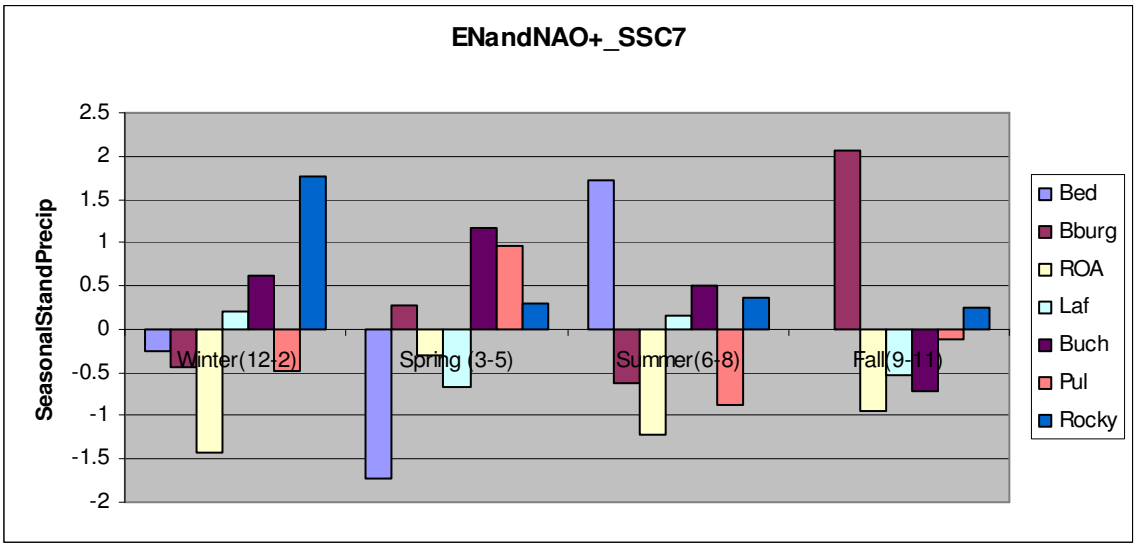
ENandNAO+_SSC7
SeasonalStandPrecip
2.5
2
1.5
1
0.5
0
-0.5
-1
-1.5
-2
Winter(12-2)
Spring (3-5)
Summer(6-8)
Fall(9-11)
Bed
Bburg
ROA
Laf
Buch
Pul
Rocky

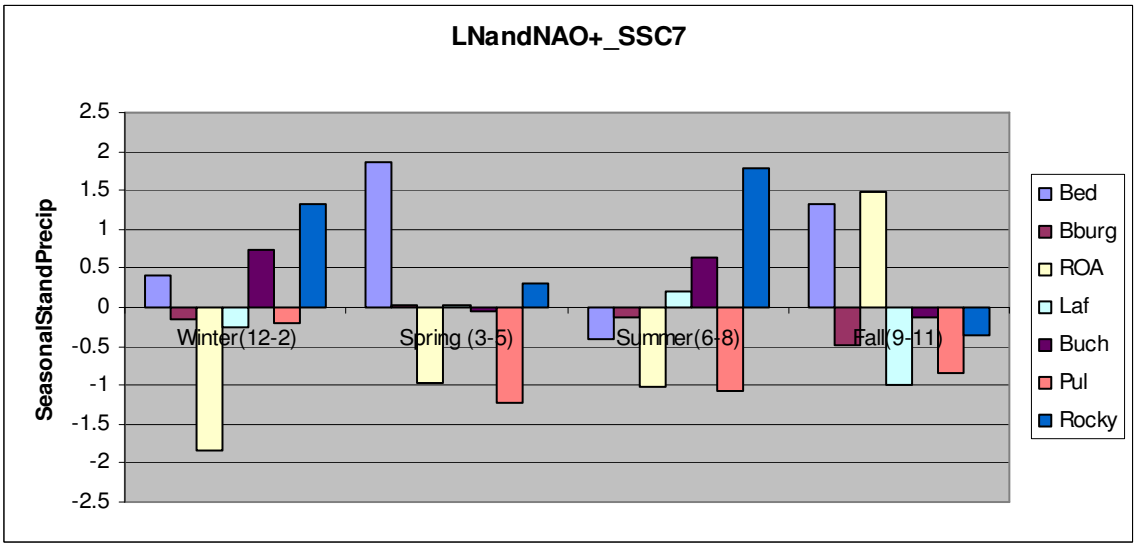
LNandNAO+_SSC7
SeasonalStandPrecip
2.5
2
1.5
1
0.5
0
-0.5
-1
-1.5
-2
-2.5
Winter(12-2)
Spring (3-5)
Summer(6-8)
Fall(9-11)
Bed
Bburg
ROA
Laf
Buch
Pul
Rocky

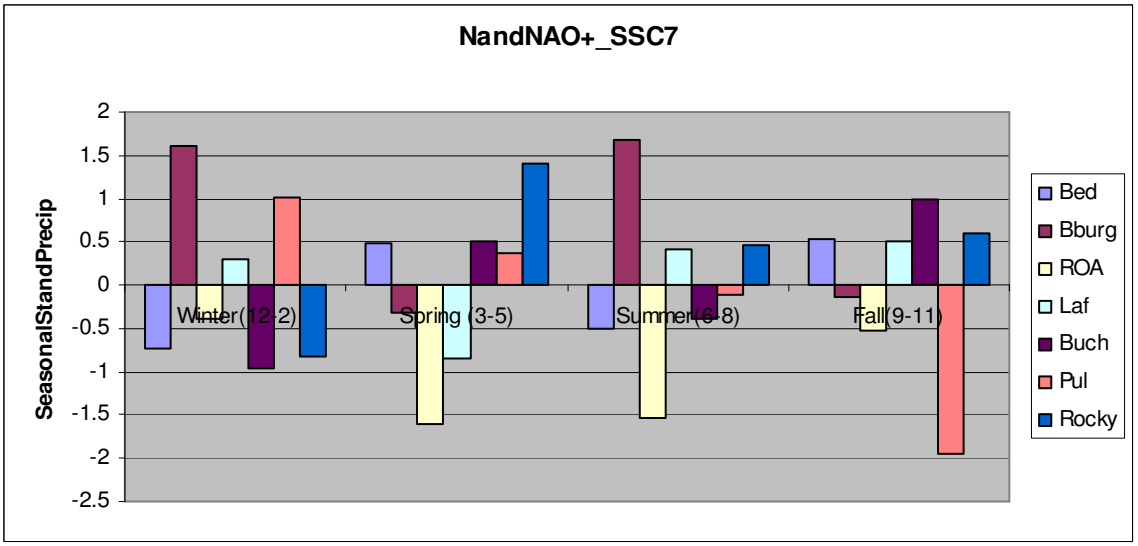
NandNAO+_SSC7
SeasonalStandPrecip
2
1.5
1
0.5
0
-0.5
-1
-1.5
-2
-2.5
Winter(12-2)
Spring (3-5)
Summer(6-8)
Fall(9-11)
Bed
Bburg
ROA
Laf
Buch
Pul
Rocky

Appendix D: Correlations

Table 36: Contemporaneous Correlations of Seasonally Aggregated Roanoke Precipitation and Teleconnective Indices

Winter Aggregated Results			Summer Aggregated Results	
Rain/SOI	-0.31735		Rain/SOI	0.199248266
Rain/SST	0.342091		Rain/SST	-0.232410087
Rain/NAO	-0.18336		Rain/NAO	0.298547808
Rain/AO	0.000695		Rain/AO	0.386041081
Rain/PNA	0.05337			
Spring Aggregated Results			Fall Aggregated Results	
Rain/SOI	-0.25547		Rain/SOI	0.044860754
Rain/SST	0.277866		Rain/SST	0.086146332
Rain/NAO	0.154546		Rain/NAO	0.002073424
Rain/AO	0.033794		Rain/AO	-0.015952884
Rain/PNA	0.314876		Rain/PNA	-0.137115965

(2) Lagged-correlations between monthly Roanoke precipitation (standaridized monthly) and the SOI and NAO (standardized monthly) during El Nino calendar years 1953, '57,'58, '63, '65, '66, '69, '72, '73, '76, '77, '82, '83, '86, '87, '91 thru '95, '97, '98, '02

Precipitation projected by k months (future)

$$C_{ZX}(k) = \sum_{t=1}^{N-k} (Z_t - \overline{Z})(X_{t+k} - \overline{X}) / N$$

$$(R_{ZX})_k = C_{ZX}(k) / (S_Z * S_X)$$

Where:

k = 0, 1, 2, 3, …,(N-1)

X_t : rainfall (future)

Z_t : index value (current)

N : Total number of data points – 53 years * 12 index values/yr → N = 636

S_Z : Standard Deviation of series "Z" – standardized series of indices

S_X : Standard Deviation of series "X" – monthly std. series of rainfall

$C_{ZX}(k)$: Covariance of lag "k"

$R_{ZX}(k)$: Correlation Coefficient

	Table 37: Cross Correlation Coefficent of Roanoke Monthly Total Standardized Precip. and Monthly Standardized SOI*, Rzx(k)																					
k	1953	1957	1958	1963	1965	1966	1972	1973	1976	1977	1982	1983	1986	1987	1991	1992	1993	1994	1995	1997	1998	2002
0	-0.05	-0.13	-0.09	-0.05	0.00	0.03	-0.15	-0.31	0.25	0.16	-0.19	-0.04	-0.19	-0.35	0.25	0.25	0.20	0.08	0.09	-0.19	-0.38	-0.31
1	-0.01	-0.16	-0.11	-0.08	0.16	0.20	-0.06	-0.27	0.12	-0.20	-0.15	-0.08	-0.13	-0.19	-0.04	0.13	0.26	0.05	-0.09	-0.27	-0.37	-0.09
2	0.41	-0.14	-0.28	0.04	0.22	0.31	-0.12	-0.36	0.03	-0.12	-0.23	-0.17	-0.06	-0.17	-0.07	-0.06	0.22	0.11	0.17	-0.07	-0.24	-0.21
3	0.06	-0.02	0.00	-0.19	0.02	-0.03	-0.07	-0.31	-0.01	-0.18	-0.12	-0.04	0.10	-0.18	-0.04	-0.12	0.02	0.15	0.20	-0.08	-0.23	-0.28
4	-0.13	-0.01	-0.12	-0.18	0.25	0.28	-0.06	-0.23	-0.06	-0.15	-0.01	0.05	-0.06	-0.17	-0.01	-0.03	0.08	0.07	0.09	-0.15	-0.23	-0.17
5	0.20	-0.02	0.20	-0.05	0.23	0.21	-0.14	-0.34	0.03	-0.27	0.11	0.13	-0.19	-0.16	0.18	-0.14	-0.15	-0.05	0.26	-0.05	-0.20	-0.36
6	0.09	0.00	-0.15	0.13	-0.03	0.07	-0.09	-0.31	0.02	-0.21	0.11	0.22	0.25	0.16	0.16	0.26	0.21	-0.16	0.05	-0.05	-0.16	-0.29
7	0.08	-0.11	-0.10	-0.07	-0.02	0.00	-0.10	-0.30	-0.03	0.02	0.07	0.11	0.09	0.02	0.00	0.04	0.18	0.12	0.18	-0.11	-0.21	-0.33
8	0.14	0.13	-0.01	-0.10	0.13	0.07	-0.05	-0.29	-0.01	-0.03	-0.08	-0.15	0.00	0.09	-0.15	-0.25	-0.12	-0.06	0.07	-0.08	-0.19	-0.22
9	0.13	0.07	0.06	0.01	0.06	0.06	0.00	-0.14	0.04	-0.09	-0.21	-0.13	0.08	0.11	0.08	-0.06	-0.15	-0.27	-0.14	-0.10	-0.16	-0.40
10	0.09	-0.10	0.07	0.17	-0.10	-0.03	-0.18	-0.38	0.06	-0.18	-0.20	-0.07	-0.07	0.15	0.06	0.13	-0.13	-0.11	0.09	-0.06	-0.10	-0.22
11	0.19	0.04	-0.11	0.03	0.04	0.18	-0.10	-0.22	0.00	0.00	-0.06	0.02	-0.08	0.12	0.00	-0.12	-0.22	0.06	0.13	0.04	0.08	-0.31
12	0.08	-0.05	0.14	-0.08	-0.18	-0.03	-0.14	-0.18	0.03	-0.10	0.05	-0.01	-0.05	0.04	-0.02	-0.19	-0.25	0.09	0.23	0.11	0.17	-0.22
13	-0.13	0.07	0.11	-0.04	-0.27	-0.15	0.11	0.00	-0.02	-0.10	0.04	-0.08	-0.03	0.09	-0.23	-0.09	0.07	0.06	0.03	0.16	0.27	-0.07
14	-0.27	-0.10	0.07	-0.08	-0.34	-0.11	0.20	0.04	-0.13	-0.06	-0.01	0.00	-0.20	-0.03	0.04	-0.27	-0.15	-0.06	-0.07	0.10	0.22	-0.17
15	-0.05	0.03	-0.10	-0.01	-0.17	-0.09	0.14	0.01	-0.10	-0.10	-0.02	-0.01	0.12	0.24	-0.04	0.06	0.02	-0.08	0.04	0.11	0.13	0.09
16	-0.07	0.02	0.01	-0.05	-0.09	0.01	0.07	0.12	-0.23	-0.21	-0.12	-0.26	0.01	0.03	0.00	0.40	0.27	0.16	0.06	0.08	0.09	-0.03
17	-0.30	0.09	0.00	-0.04	-0.15	-0.02	-0.08	0.01	-0.26	0.02	-0.12	-0.24	0.01	0.08	-0.11	0.14	0.17	0.11	0.06	0.10	0.00	-0.01
18	0.12	0.00	0.15	0.03	-0.08	0.13	0.02	0.09	-0.14	0.01	-0.10	-0.23	-0.04	0.11	-0.03	-0.12	0.10	0.08	0.02	0.13	0.05	0.03
19	0.06	0.12	-0.10	-0.09	-0.08	0.04	0.02	0.04	-0.17	-0.04	0.02	-0.07	-0.03	-0.03	0.03	0.21	0.34	-0.01	0.07	0.10	0.07	0.07
20	0.06	0.06	-0.06	0.13	-0.23	-0.03	0.07	0.16	-0.15	0.00	0.08	0.03	0.22	0.09	-0.02	0.04	0.02	-0.02	0.04	0.10	0.02	0.20
21	0.08	0.14	-0.06	-0.06	-0.14	-0.11	0.04	0.26	-0.20	0.11	0.23	0.10	0.04	-0.04	-0.02	0.00	-0.19	-0.05	-0.06	0.01	0.06	0.00
22	-0.18	0.00	0.03	0.00	0.08	-0.01	-0.02	0.23	-0.16	0.15	0.22	0.12	0.02	0.07	0.02	0.05	-0.01	0.02	0.02	0.06	0.04	0.10
23	-0.12	0.04	0.04	-0.10	0.05	-0.18	-0.02	0.20	-0.13	-0.01	0.09	0.15	0.05	-0.01	0.12	-0.10	-0.01	0.01	-0.07	0.02	0.03	0.00
24	-0.08	0.09	0.00	0.02	0.05	0.05	0.01	0.14	-0.09	0.07	-0.09	0.00	0.14	0.03	0.05	-0.07	-0.18	-0.03	-0.03	0.02	0.06	0.03
25	-0.05	0.01	0.01	0.12	0.10	-0.19	0.03	0.14	-0.02	0.12	-0.08	0.07	0.08	0.04	0.12	0.07	-0.20	0.05	-0.04	-0.01	-0.03	0.13
26	0.01	0.11	0.03	-0.04	0.06	-0.03	0.07	0.12	0.02	0.23	0.01	0.02	0.04	-0.04	-0.13	0.12	0.03	-0.04	-0.14	-0.02	0.00	0.22
27	0.04	-0.04	0.04	0.07	0.03	-0.01	0.03	0.11	0.01	0.12	0.09	0.08	-0.09	0.01	-0.12	-0.06	-0.11	0.05	-0.06	-0.09	-0.05	0.30
28	0.05	-0.01	-0.03	-0.05	0.07	-0.02	0.02	0.14	0.05	0.02	0.14	0.11	-0.06	-0.01	-0.05	-0.06	-0.09	0.04	-0.08	-0.06	-0.06	0.24
29	0.14	-0.02	-0.02	-0.03	0.12	-0.05	-0.06	0.14	0.02	0.03	0.15	0.07	0.03	0.00	0.03	-0.02	0.05	0.01	-0.10	-0.06	0.05	0.15
30	0.01	0.01	0.02	0.02	0.10	-0.05	-0.07	0.11	0.04	0.02	0.12	0.05	-0.01	-0.04	0.07	-0.08	-0.06	0.02	-0.01	-0.08	0.01	0.05
31	0.11	-0.01	0.03	0.01	0.00	0.01	-0.04	0.02	0.06	-0.03	0.01	0.07	0.07	0.01	0.02	-0.10	0.01	0.00	0.01	-0.02	0.06	0.02
32	-0.03	-0.04	0.01	-0.01	0.00	-0.06	0.04	-0.01	0.04	-0.07	0.00	-0.06	-0.03	0.00	0.00	-0.01	0.11	0.02	0.00	-0.05	0.01	0.02

Table 37 Continued: Cross Correlation Coefficent of Roanoke Monthly Total Standardized Precip. and Monthly Standardized SOI*, Rzx(k)																						
33	-0.05	-0.01	0.01	-0.01	0.01	0.04	0.04	-0.01	0.00	-0.03	0.00	-0.07	0.01	-0.02	-0.05	-0.03	0.06	0.00	0.01	-0.03	-0.01	0.02
34	-0.03	0.02	-0.02	0.02	0.00	0.03	0.05	0.00	-0.03	0.01	0.02	-0.03	-0.02	0.02	0.03	0.05	0.05	0.00	0.00	-0.02	-0.01	0.04
35	-0.04	0.03	-0.02	0.01	0.00	-0.01	-0.01	0.00	0.00	0.01	0.04	-0.04	0.00	-0.02	0.00	0.09	0.03	0.00	0.00	-0.01	0.00	0.01

*From NOAA

	Table 38: Cross Correlation Coefficent of Roanoke Monthly Total Standardized Precip. and Monthly Standardized NAO*, Rzx(k)																					
k	1953	1957	1958	1963	1965	1966	1972	1973	1976	1977	1982	1983	1986	1987	1991	1992	1993	1994	1995	1997	1998	2002
0	0.17	-0.17	-0.13	-0.33	-0.42	-0.34	0.21	0.06	0.30	0.18	-0.35	-0.23	-0.08	0.03	-0.07	0.27	0.47	0.29	0.10	0.18	0.12	-0.14
1	0.06	0.06	0.10	-0.02	0.16	0.26	-0.09	0.02	-0.07	-0.13	-0.21	-0.29	0.06	-0.09	0.05	0.20	0.35	0.21	-0.06	0.08	-0.05	0.09
2	-0.04	-0.13	-0.08	-0.03	-0.03	-0.02	-0.03	-0.03	0.27	0.28	0.08	0.11	0.07	0.10	0.02	0.13	0.05	-0.04	-0.20	-0.10	-0.18	-0.05
3	-0.01	0.10	0.21	0.04	0.05	0.03	-0.13	0.00	-0.19	-0.08	0.26	0.34	-0.30	-0.28	-0.08	0.03	0.08	0.14	0.03	-0.04	-0.14	-0.02
4	0.25	0.04	-0.17	0.12	0.30	0.29	-0.15	0.22	0.07	0.05	0.23	0.29	0.14	0.14	-0.14	-0.13	-0.01	0.02	-0.03	0.04	-0.06	-0.06
5	-0.36	0.19	0.22	0.12	0.00	0.12	0.13	0.27	-0.11	-0.05	0.15	-0.02	0.05	0.22	-0.28	-0.36	-0.46	-0.07	0.17	0.23	0.13	-0.14
6	-0.08	-0.31	-0.22	0.14	-0.07	0.01	0.12	0.04	0.01	0.08	-0.06	0.02	0.06	0.25	0.20	0.07	-0.07	0.00	0.10	0.06	0.08	-0.19
7	0.04	0.08	0.14	0.18	0.08	-0.09	-0.04	-0.02	-0.04	0.07	-0.03	0.08	-0.04	-0.08	0.12	-0.11	-0.18	-0.10	-0.02	0.06	0.12	-0.16
8	-0.06	-0.01	-0.04	-0.05	0.03	-0.02	-0.03	-0.14	0.02	-0.09	-0.23	-0.18	-0.07	-0.18	-0.13	0.05	-0.02	-0.31	-0.39	-0.11	-0.06	0.07
9	-0.12	0.18	0.06	0.03	0.02	0.08	0.28	0.03	-0.09	-0.17	-0.15	-0.21	0.04	0.12	0.13	0.11	-0.13	-0.20	-0.39	-0.22	-0.09	-0.18
10	0.05	-0.26	-0.12	0.06	0.05	-0.01	0.20	0.15	-0.06	-0.13	-0.16	-0.21	0.04	0.05	-0.01	0.24	0.12	0.06	0.15	-0.12	-0.21	0.16
11	0.36	0.07	0.02	0.06	-0.27	-0.16	0.04	0.08	-0.17	-0.11	0.13	0.15	0.31	0.28	0.03	-0.05	-0.05	0.07	0.11	0.12	0.21	0.10
12	0.12	-0.03	-0.01	-0.28	0.09	0.13	-0.08	0.19	-0.09	-0.17	0.19	0.18	-0.05	-0.05	0.14	0.01	-0.06	0.01	0.08	0.16	0.06	0.02
13	0.06	0.10	-0.09	0.06	-0.05	0.03	-0.06	-0.06	0.00	-0.07	0.17	0.23	0.15	0.22	-0.02	0.04	0.05	-0.10	-0.03	-0.03	0.03	0.17
14	0.22	-0.08	0.01	0.04	-0.16	0.06	0.15	-0.03	-0.06	-0.14	-0.14	-0.04	-0.07	-0.16	-0.07	-0.27	-0.21	0.08	-0.11	-0.04	0.03	0.03
15	-0.17	0.09	0.02	0.04	0.12	0.12	-0.14	-0.18	0.12	0.02	0.11	-0.02	0.10	0.05	0.09	-0.08	-0.05	0.00	-0.06	-0.04	-0.07	0.27
16	0.07	0.13	0.17	-0.03	0.06	-0.17	0.03	-0.04	-0.12	-0.11	-0.06	-0.30	0.04	0.03	0.14	0.06	0.13	-0.05	-0.24	-0.18	0.04	0.04
17	0.20	-0.06	-0.02	0.12	-0.30	0.04	-0.18	0.02	-0.03	0.16	-0.11	0.06	-0.17	-0.19	-0.10	-0.09	0.01	-0.01	-0.07	0.06	0.11	-0.06

Table 38 Continued: Cross Correlation Coefficent of Roanoke Monthly Total Standardized Precip. and Monthly Standardized NAO*, Rzx(k)																						
18	-0.11	0.11	0.11	-0.11	-0.10	-0.03	0.04	0.14	-0.20	-0.15	-0.25	-0.17	0.17	0.26	0.00	0.03	0.00	0.02	0.07	0.19	0.20	0.06
19	0.00	-0.05	-0.16	0.02	0.05	-0.14	0.21	0.05	-0.06	-0.03	-0.01	0.24	-0.19	-0.19	-0.17	0.24	0.21	0.12	0.07	0.15	-0.07	0.00
20	-0.04	0.11	0.01	-0.02	-0.15	0.02	-0.03	-0.22	-0.14	0.16	0.13	0.19	0.10	0.18	-0.06	-0.06	0.07	-0.13	-0.07	-0.04	-0.01	-0.22
21	0.03	-0.11	-0.06	0.08	0.04	-0.03	-0.04	-0.11	0.00	0.15	0.14	0.02	-0.05	-0.06	0.05	-0.02	0.01	0.01	0.02	-0.02	-0.13	0.02
22	-0.03	0.04	0.09	-0.06	0.13	-0.02	-0.12	-0.08	-0.10	0.06	0.08	-0.15	-0.13	0.05	-0.02	0.12	0.02	0.05	0.00	0.04	0.02	0.08
23	0.01	-0.08	0.08	-0.16	-0.09	0.00	-0.13	-0.08	-0.03	-0.02	0.03	-0.05	-0.04	-0.06	0.00	-0.07	0.08	-0.11	-0.11	0.02	0.06	-0.24
24	0.03	0.03	0.03	0.16	-0.11	0.05	0.00	-0.01	-0.02	0.11	-0.13	0.01	0.02	-0.13	-0.08	-0.12	-0.03	0.00	0.13	0.05	0.05	0.07
25	-0.01	-0.03	-0.07	-0.05	-0.02	-0.18	-0.15	-0.01	0.07	0.04	-0.20	-0.01	0.10	-0.01	0.02	0.11	-0.05	-0.08	-0.05	0.00	0.09	0.08
26	-0.06	0.18	-0.05	0.05	0.14	0.12	0.06	0.02	0.15	0.01	-0.07	-0.13	-0.04	-0.11	0.13	-0.05	0.08	0.05	0.12	0.04	-0.01	-0.15
27	-0.03	-0.01	0.01	0.03	0.15	-0.03	0.00	-0.06	0.17	-0.04	-0.08	-0.03	-0.14	0.06	0.09	-0.10	-0.02	0.10	0.09	-0.09	-0.15	0.06
28	-0.02	-0.03	0.01	-0.06	0.08	0.05	0.04	-0.09	0.10	-0.01	0.01	0.06	-0.02	0.00	-0.03	0.11	-0.02	0.01	-0.12	-0.06	-0.02	0.08
29	-0.11	-0.10	0.02	-0.03	0.13	-0.16	0.12	-0.05	0.04	0.01	0.03	0.07	0.05	0.01	-0.01	-0.02	-0.01	0.05	0.17	-0.07	0.01	0.01
30	0.11	-0.02	-0.01	0.02	0.00	0.04	-0.15	0.01	0.00	0.00	0.03	0.02	0.05	-0.02	-0.09	-0.09	-0.10	-0.02	-0.02	0.01	0.06	-0.01
31	-0.14	0.07	0.00	0.01	-0.10	-0.04	0.10	0.02	-0.06	-0.01	-0.07	-0.11	0.02	-0.03	-0.01	0.08	-0.04	-0.01	0.00	-0.02	0.07	0.06
32	-0.01	-0.03	0.03	-0.03	-0.04	0.08	0.02	0.03	-0.03	-0.01	0.07	0.02	-0.06	0.02	0.03	0.00	0.02	-0.01	0.08	-0.03	-0.05	-0.04
33	0.03	0.03	0.04	0.00	0.00	-0.02	-0.03	0.04	-0.05	0.00	-0.05	0.02	0.01	-0.07	-0.02	-0.04	0.01	-0.01	-0.04	-0.03	-0.01	0.00
34	0.00	-0.02	-0.03	0.01	-0.01	-0.07	0.03	0.01	0.02	0.00	0.07	0.02	-0.02	0.02	0.03	0.03	0.02	0.00	0.02	-0.01	0.00	0.02
35	0.05	0.01	-0.03	0.00	-0.01	0.00	-0.08	0.00	0.00	0.00	0.01	0.04	0.02	-0.04	-0.01	0.00	0.01	-0.01	-0.01	0.00	0.00	0.00

*From NOAA

Appendix E: Global Circulation Fundamentals

Considering a non-rotating Earth, there is a pressure gradient at every point in the atmosphere in the direction that is perpendicular to the isobar (lines of equal pressure) traveling through that point from higher to lower pressure. This pressure gradient force would be the only initiating mechanism of air parcel motion in the atmosphere if Earth was not rotating, as shown below in Figure 1 as vectors perpendicular to isobars. According to Newton's second law, air parcels travel in the direction of the net [pressure] force – thus winds are in the same direction as the net pressure force in a non-rotating Earth (Thompson 1996).

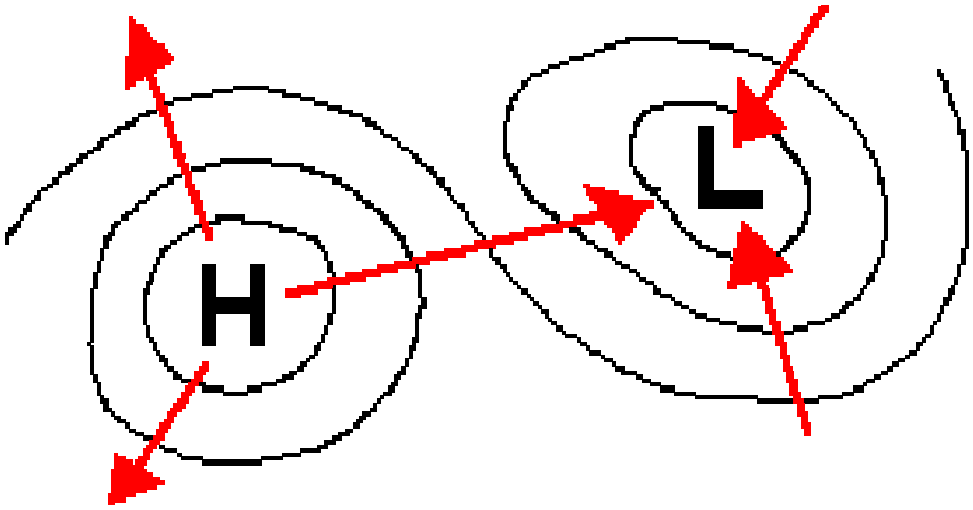

Figure 140. Pressure forces on a non-rotating Earth. (Reproduced from Thompson 1996)

Regarding a rotating Earth, the Coriolis effect deflects one-dimensional flow similarly to the arch-induced path one encounters when moving from the center to periphery on a rotating merry-go-round in the free atmosphere – away from ground surface frictional affects (Thompson 1996). (Wisener in Philander 1990) outlines the Coriolis effect by referring to a ring of air at the equator spinning about the polar axis at the same rate as the Earth's surface that is forced poleward, thus reducing its radius, and thus to conserve its momentum, must increase its angular velocity. From this interpretation, the Coriolis effect encourages westerly flow and is enhanced with increasing latitude.

As depicted in Figure 2, the Coriolis force, "CF", usually acts with roughly the same magnitude as the pressure gradient force, "PGF" to render balanced, geostrophic flow (Hasse and Dobson 1986). When the Coriolis and pressure gradient forces balance in the horizontal plane, the direction of geostrophic flow is rotated 90° off straight line

motion, parallel to isobars. Circulatory winds result from the deflection – forced change of direction – of air associated with a rotating frame of reference to the right in the Northern Hemisphere for geostrophic conditions. For this reason, regions of high pressure correspond to winds rotating in the clockwise direction while winds of low pressure circulations travel in a counter-clockwise direction. As a consequence, air masses are not explicitly propelled from centers of high pressure to low pressure centers, while the potential for eddy formation becomes apparent.

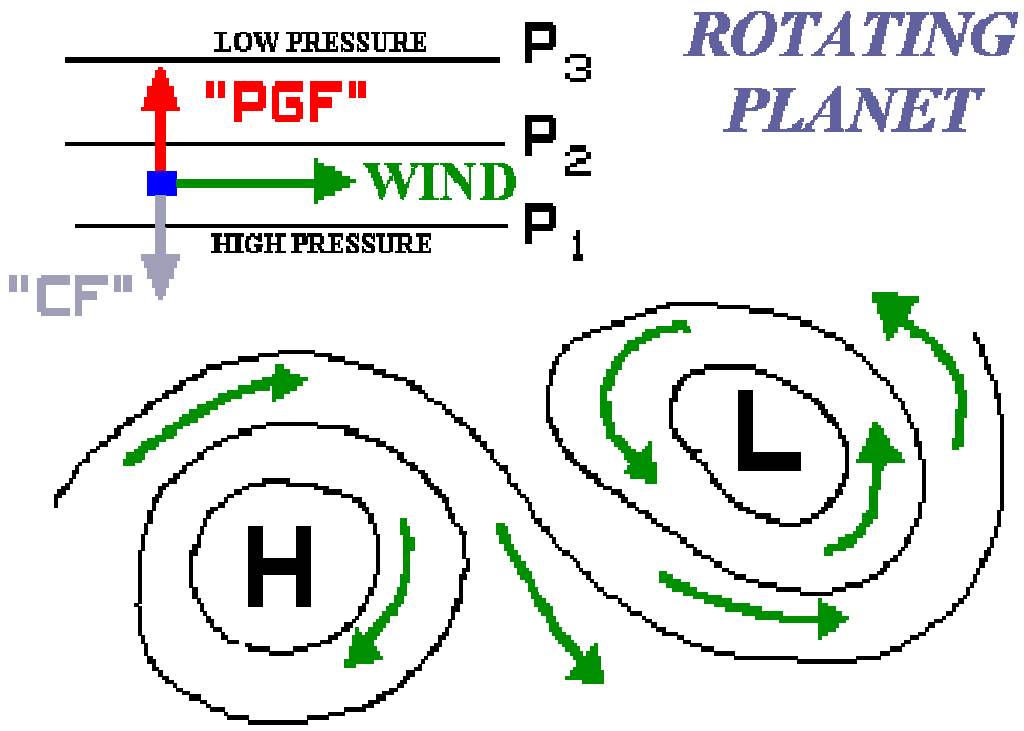

Figure 141. Horizonal view of geostrophic flow on a rotating Earth. (Reproduced from Thompson 1996)

Although Figure 2 aids understanding of high and low pressure circulations, flow perfectly parallel to the isobar lines is entirely hypothetical. (Hasse and Dobson 1986) report that friction between Earth's surface and the atmosphere imposes drag stresses which reduce near-surface wind speed. Decreased wind speed of near-surface air masses flowing around a center of high pressure permits the pressure gradient force to guide these air masses toward centers of low pressure and away from high pressure cores in a skewed, spiraling motion. Accordingly, flow around high pressure regions diverges out towards neighboring low pressure centers, while flow in low pressure areas is directed towards its center of circulation. To maintain continuity, convergent flow must ascend at the center of low pressure while diverging air masses in high pressure regions descend at their center of circulation (Hasse and Dobson 1986).

Depicted in Figure 3 is a vertical cross-section clarifying the ascending (descending) motion at the center of low (high) pressure; also worthy of note is the typically extensive cloud formation over a low pressure in a statically stable atmosphere (Thompson 1996). Water vapor within rising air that is condensing into liquid form, releases latent heat to the encompassing air causing the parcel's continued ascent because the parcel remains warmer and thus less dense than surrounding air.

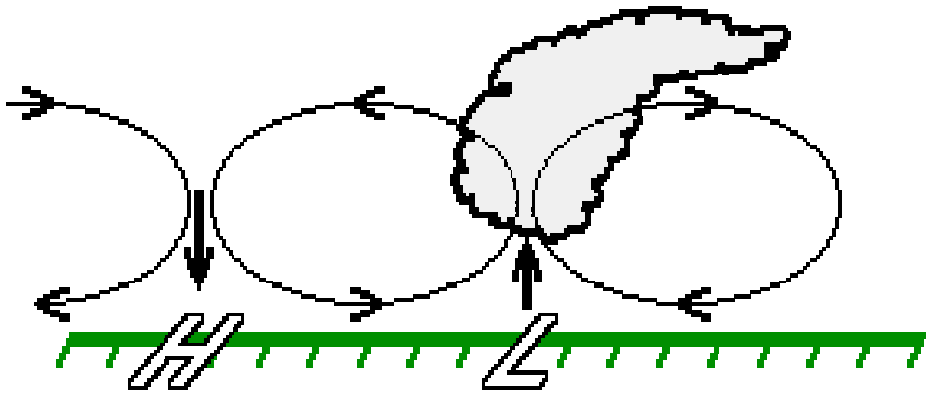

Figure 142. Meridonal circulation cells at regions of low and high surface pressures. (Reproduced from Thompson 1996).

Low pressure develops at the surface in regions of high convection – rising buoyant air currents – since this process transfers heat from warm, rising parcels to the atmosphere prior to reaching equilibrium given that the temperature of the parcel itself decreases with higher altitude. Consequent warming of the atmosphere reduces air density, and hence, induces low [surface] pressure (D'Aleo 2002). Raised temperatures over the high surface pressure develop in part due to compressional heating and simultaneously inhibit considerable cloud formation (Thompson 1996). A global circulation possessing a high surface pressure extent is the Hadley Cell, positioned at an approximate latitude of 30°N. This meridionally-oriented circulation is the effect of both compressional heating and formation of higher density air stemming from latitudinal cooling at the northern branch of the system.

Thermal Mechanisms for Global Circulation

Of the incoming radiation reaching the atmosphere's outer layer, about 30% is backscattered and reflected by the atmosphere as well as reflected by Earth's surface as short-wave, or solar radiation. Solar energy received by Earth's atmosphere and surface is eventually sent back to space as [outgoing] long-wave radiation. Outgoing long-wave radiation is a parameter used to define the global eastward propagating Madden Julian Oscillation because some atmospheric constituents, including water vapor and water droplets in clouds, carbon dioxide, and particulate matter, absorb this energy form; thus reduction in outgoing radiation is realized at the top of the atmosphere at locations

corresponding to increased cloud cover. The notion of "global warming" arises since these substances then emit long-wave radiation, initially absorbed, back to Earth's surface, by a process termed back-radiation. According to the first law of thermodynamics, the overall energy balance on the atmosphere must be closed. Since it emits more energy than it absorbs, the atmosphere is thermodynamically balanced by the sensible and latent (from evaporation) heat offered by Earth's surface. Gradients of this thermal balance across latitudinal and seasonal differences drive temperature differences throughout Earth's surface-atmosphere system, which in turn dictates synoptic atmospheric circulations. (Hasse and Dobson 1986)

Linking the energy balance of Earth's atmosphere-surface system and large-scale circulations, in part are the temperature gradients across altitudinal and latitudinal changes. When the change in temperature for changing altitude becomes sufficiently large, the atmosphere is in its statically unstable state and convection to higher altitudes – i.e. vertical motion – is readily apparent. Such conditions follow the presence of excessively warm ambient air near the surface and cooler than normal air aloft, which can partially be described by thermal conveyance and storage properties of Earth's liquid (oceans, fresh water bodies) and ground surfaces; enhanced vertical flow results from this unstable atmosphere. (Thompson 1996)

Given that the radiation received at the surface of Earth is inversely proportional to the thickness of the atmosphere overhead and recalling Earth's diagonal axis and annual revolution, the zonally-oriented line where the sun is the most directly overhead changes according to season. Circling the globe, this line at all points of longitude lies in the world's oceans and is termed the intertropical convergence zone (ITCZ). Uniting the intense evaporation in this region with mass continuity, adjacent surface air masses from the northern and southern hemispheres are drawn, or *converge* towards the ITCZ (Nielsen-Gammon 2003). Researching the likelihood of about 10 "cloudy" days per month, (Graham and Barnett in Philander 1990) studied three tropical oceans and confirmed this probability achieved its maximum value of 0.65 for sea surface temperature of 27.5°C.

Tropical Circulation

Meridionally oriented, the Hadley Cell is a tropical circulation driven by concentrated evaporation at the ITCZ. In general, since atmospheric pressure is the weight of a column of air from Earth's surface to the top of the atmosphere (tropopause) and the weight of cooler air encompasses more weight than an equal volume of warm air, surface high pressure regions tend to lie at the northern branch of the Hadley Cell (D'Aleo 2002). While positioning of its low pressure branch follows the ITCZ, the circulation's high pressure branch – defining the subtropical high near 30°N governed by latitudinal cooling – drives the surface trade winds at the equator (Hasse and Dobson 1986). Since the ITCZ attracts winds from the subtropical high pressure [belt] towards its low pressure and the Corilios force deflects flow to the right in the Northern Hemisphere, the surface trade winds blow from the northeast towards the equator before attaining a reliably westward direction – called the tropical easterlies (D'Aleo 2002).

As implied, the assembly of land and ocean surfaces along the tropics has a great deal of influence on the ITCZ global path. Describing the zonally-configured exchange

of tropical Pacific air masses, the Walker circulation results in part from the disruption of the ITCZ path caused by spacious western Pacific land surfaces (Nielsen-Gammon 2003). Three thermal properties differing between land and water surfaces impacting the Walker circulation are albedo, penetration of solar radiation, and thermal conduction. As Hasse and Dobson report, albedo is the percentage of incoming solar [longwave] radiation that is reflected and scattered from a surface (1986). Land surfaces exhibit a substantially increased albedo compared to water, thus the oceans surrounding western Pacific land absorb more heat from solar radiation. Secondly, Hasse and Dobson estimate solar radiation penetrates water a depth nearly five thousand times that of land surfaces (1986). Effectively distributing the absorbed heat throughout a larger depth, water's turbulent motions render elevated heat capacities, whereas poor molecular thermal conduction is a precursor for land's weaker storage characteristics. As a result from these contrasting properties, temperatures on off-equatorial land surfaces respond much more promptly to daily and seasonally-derived radiation changes than ocean temperatures. These contrary time scale reactions give rise to land-ocean exchanges of air masses in the tropical Pacific, which in turn help charge the large scale east-west Walker circulation as well as the El Nino-Southern Oscillation with intense convection/latent heat-born sea level pressures (Nielsen-Gammon 2003).

Mid-latitude Circulation

When the latitudinal thermal energy distribution extending poleward from the equator exceeds typical conditions, the atmosphere is baroclinically instable. This state, representing anomalous warm tropical conditions and below normal ambient temperatures at the polar regions, is important in describing synoptic-scale flow. Stout latitudinal temperature gradients run north-south in the temperate zones – between 30° and 60°N – with large changes occurring over relatively short distances, defining the so called "fronts" (Hasse and Dobson 1986). For geostrophic flow (i.e. when the pressure force equals the Corilois effect while neglecting surface friction, meaning no acceleration) the north-south temperature field corresponds to a purely meridional pressure gradient and thus entirely zonal flow paralleling isobars as in Figure 2; however when the temperate atmosphere is baroclinically instable, identifying an unsteady equilibrium between the pressure and Corilois force, portions of the potential energy at the equator is extracted to form transient eddies, or amplified disturbances/depressions, which induces a wavy pattern in zonal flow (Nielsen-Gammon 2003). Aligned with meandering westerly flow, as (Thompson 1996) reports, discrete pressure centers form in the temperate zones during baroclinic instability that allow the necessary thermal advection across latitudes.

The typical positive density gradient with ocean depth at higher latitudes aids the definition of the thermohaline circulation whereby ocean water at depth remains colder than surface water even for excessive sea surface temperatures; this opposes the action of heat diffusion in a fluid to attain thermal equilibrium (Sarachik in Nielsen-Gammon 2003). Describing the equator-poleward ocean current, the thermohaline circulation brings cold water at depth from a higher latitude towards the equator while warmer, near surface waters migrate north. A deemed "active" ocean-atmospheric interaction as referred to by (Sarachik 2003) is rendered when a warmed, higher latitude atmosphere

escalates underlying ocean temperatures, thereby obstructing the deeper ocean branch of the thermohaline circulation. Consequentially, densities of waters at higher latitudes lessen from both elevated temperatures and local rainfall, which cyclically impedes the north-south surface ocean circulation and prompts large-scale atmospheric response (Sarachik in Nielsen-Gammon 2003).

ENSO Fundamentals

An example of a so called active interaction is El Nino and La Nina – the positive and negative phases of the pronounced interannual atmospheric-ocean variability in the tropical Pacific: El Nino-Southern Oscillation (ENSO) (Sarachik in Nielsen-Gammon 2003). While the atmospheric constituent of the variability is the Southern Oscillation (SO), the ocean portion of the interaction is the El Nino or La Nina event. In addition to variant sea levels, regions of relatively warm and cold sea surface temperatures (SST) in the tropical Pacific basin are a principal result of changes in surface wind strength and direction (Trenberth 2003). Easterly trade winds at the equator, rationalized by the ITCZ-Hadley Cell relation, are deflected to the right in the Northern Hemisphere by the Corilios force; (D'Aleo 2002) asserts that the Hadley Cell is the most important element for ENSO. Given these surface winds operate the direction of the surface ocean currents, westerly warm water currents diverge away from the equator. Subsequently, there is upwelling of cooler water along the equator and under near-normal conditions, warmer waters advect towards to the western tropical Pacific. It follows that the thermocline, defining the transition from warmer surface waters to cooler abyssal waters, is much closer to the ocean surface in the central and eastern tropical Pacific verses the western portion of the basin during times of ENSO-neutral (Trenberth 2003). As the temporal sequence of SST distribution throughout the tropical Pacific basin is substantially tied to surface wind strength and direction, regions of enhanced convection and ensuing precipitation are therefore activated by atmospheric changes.

Congruent with the typically elevated thermocline in the eastern tropical Pacific, Bjerkness deciphered that the initially sinking dry air over this portion of the basin was furnished with progressively more moisture as it traverses the central tropical Pacific into its western portion according to the trade winds, thereby following the positive gradient of thermocline depth (Philander 1990). Warm, moist air develops over the highest temperature waters of the basin in the west, rises, and induces heavy precipitation over the western and central tropical Pacific. Westerly upper troposphere flow closes this zonal feedback loop termed the Walker Circulation (Philander 1990). Noteworthy is the action of dry air – vertically traveling parcels that possess limited water vapor become more dense than those containing elevated moisture since dry parcels are not offered latent heat stemming from condensation; thus rising moist parcels exist at higher temperatures and help propel drier parcels towards the surface.

During El Nino, easterly trade winds relax thereby lowering the thermocline in the eastern tropical Pacific while generating a warm ocean surface tongue east of the dateline; in a recursive framework the developing regions of enhanced convection in the central tropical Pacific aids the attenuation of the easterlies providing the Southern Oscillation signature and decreasing the typical Walker Circulation magnitude (D'Aleo

2002). Claimed by (Wyrtiki in Philander 1990), warm water migration with westerly winds in the tropical Pacific during El Nino events is realized through Kelvin waves.

During the onset of La Nina, subtropical pressures in the eastern and central Pacific build above average conditions and eventually stimulate increased easterly trade winds (D'Aleo 2002). Warm waters propagating with these intensified easterlies abnormally accrue in the western tropical Pacific (around Indonesia) leading to correspondingly [anomalous] low pressures here, while rendering eastern waters very cool from intense upwelling along the South American coast (D'Aleo 2002). Resiliently strong easterlies persist since high pressures east of the dateline are upheld by the cool (read: more dense) atmosphere and underlying ocean. Evolution of the latter stages of a La Nina event initiates migration of the anomalously warm western tropical Pacific waters eastward once the warm pool maximizes its spatial capacity.

ENSO and Teleconnections

Maturation of the El Nino phase prompts intensification of a subtropical atmospheric anticyclone above the central Pacific Ocean, where latent heat persists in the troposphere (Philander 1990). Associated with this subtropical high pressure center is amplification of the Hadley Cell, as perceived through a plot of the mean stream function provided in (Philander 1990). Depicted are anomalously high tropospheric winds, driven by elevated evaporation and resulting low pressure in the equatorial central Pacific, which diverge out from the subtropical high pressure center. The subtropical [westerly] jet stream north of the high pressure is strengthened during winter, influencing weather at this time in the mid-latitudes (Philander 1990). As a characteristic of El Nino winters, (Nielsen-Gammon 2003) cites that such escalation of the anticyclone in the Pacific fortifies the subtropical jet stream to be abnormally continuous around the globe. (Woolhiser 1992) report that winter precipitation in the southwest U.S. is related to large scale climatology disturbances verses highly convective events during the summer season, which complements the strong storm track across the southern U.S. that is the signature of El Nino.

References

D'Aleo, J.S. 2002. El Nino and La Nina. Oryx Press: Westport, CT. pp. 1-71

Hasse and Dobson 1986. Introductory Meteorology and Fluid Dynamics. D. Reidel Publishing. Boston: pp 1- 46.

Nielson-Gammon 2003. Handbook of Weather, Climate, and Water.. John Wiley and Sons, Inc. pp. 59-70.

Philander, S.G. 1990. El Nino, La Nina, and Southern Oscillation. Academic Press. pp.1-56.

Thompson 1996. Weather Fundamentals. http://www.atmos.umd.edu/~owen/POSTIX/index.html. Retrieved 2006.

Trenberth, K. 2003. Handbook of Weather, Climate, and Water: The El Nino-Southern Oscillation (ENSO) System. John Wiley and Sons, Inc. pp. 163-173.

Woolhiser, D.A. 1992. Modeling daily precipitation – progress and problems. Statistics in the Environmental and Earth Sciences. Edward Arnold: London. pp. 71-81.

Appendix F: Markov Result Tables

Table F1 – Non-Homogeneous SOI 7 Class Monthly Transition Matrices

Jan - Feb

SOI Class	1	2	3	4	5	6	7
1	1.0000	0.0000	0.0000	0.0000	0.0000	0.0000	0.0000
2	0.0000	0.5000	0.5000	0.0000	0.0000	0.0000	0.0000
3	0.0000	0.1500	0.6000	0.2500	0.0000	0.0000	0.0000
4	0.0000	0.0000	0.1034	0.7414	0.1379	0.0172	0.0000
5	0.0000	0.0000	0.0000	0.4706	0.4706	0.0588	0.0000
6	0.0000	0.0000	0.0000	0.0556	0.1111	0.8333	0.0000
7	0.0000	0.0000	0.0000	0.0000	0.0000	1.0000	0.0000

Feb – Mar

1	1.0000	0.0000	0.0000	0.0000	0.0000	0.0000	0.0000
2	0.1111	0.7778	0.0000	0.1111	0.0000	0.0000	0.0000
3	0.0000	0.2500	0.4583	0.2917	0.0000	0.0000	0.0000
4	0.0000	0.0000	0.0702	0.8421	0.0702	0.0175	0.0000
5	0.0000	0.0000	0.0000	0.2778	0.3889	0.3333	0.0000
6	0.0000	0.0000	0.0000	0.0000	0.3158	0.6842	0.0000
7	0.1429	0.1429	0.1429	0.1429	0.1429	0.1429	0.1429

Mar – Apr

1	1.0000	0.0000	0.0000	0.0000	0.0000	0.0000	0.0000
2	0.0769	0.7692	0.1538	0.0000	0.0000	0.0000	0.0000
3	0.0000	0.1333	0.4667	0.4000	0.0000	0.0000	0.0000
4	0.0000	0.0164	0.0820	0.7541	0.1148	0.0328	0.0000
5	0.0000	0.0000	0.0000	0.4118	0.4118	0.1765	0.0000
6	0.0000	0.0000	0.0000	0.0500	0.3000	0.6500	0.0000
7	0.1429	0.1429	0.1429	0.1429	0.1429	0.1429	0.1429

Apr – May

1	0.3333	0.6667	0.0000	0.0000	0.0000	0.0000	0.0000
2	0.0769	0.6154	0.2308	0.0769	0.0000	0.0000	0.0000
3	0.0000	0.1429	0.4286	0.4286	0.0000	0.0000	0.0000
4	0.0000	0.0667	0.0667	0.8167	0.0500	0.0000	0.0000
5	0.0000	0.0000	0.0000	0.3000	0.5500	0.1500	0.0000
6	0.0000	0.0000	0.0000	0.0000	0.5556	0.3889	0.0556
7	0.1429	0.1429	0.1429	0.1429	0.1429	0.1429	0.1429

May – June

1	1.0000	0.0000	0.0000	0.0000	0.0000	0.0000	0.0000
2	0.1250	0.6250	0.0625	0.1875	0.0000	0.0000	0.0000
3	0.0000	0.2308	0.6154	0.0769	0.0769	0.0000	0.0000

Table F1 Continued - Non-Homogeneous SOI 7 Class Monthly Transition Matrices

4	0.0000	0.0323	0.1452	0.6613	0.1290	0.0323	0.0000
5	0.0000	0.0000	0.0000	0.5417	0.3333	0.1250	0.0000
6	0.0000	0.0000	0.0000	0.0000	0.4000	0.6000	0.0000
7	0.0000	0.0000	0.0000	0.0000	0.0000	0.0000	1.0000

June – July

1	0.7500	0.2500	0.0000	0.0000	0.0000	0.0000	0.0000
2	0.0000	0.7333	0.2667	0.0000	0.0000	0.0000	0.0000
3	0.0000	0.1111	0.3333	0.5556	0.0000	0.0000	0.0000
4	0.0000	0.0000	0.0517	0.7586	0.1724	0.0172	0.0000
5	0.0000	0.0000	0.0000	0.3333	0.4286	0.2381	0.0000
6	0.0000	0.0000	0.0000	0.2727	0.0000	0.7273	0.0000
7	0.0000	0.0000	0.0000	0.0000	0.0000	0.0000	1.0000

July – Aug

1	0.6667	0.3333	0.0000	0.0000	0.0000	0.0000	0.0000
2	0.0714	0.7857	0.1429	0.0000	0.0000	0.0000	0.0000
3	0.0000	0.1538	0.5385	0.3077	0.0000	0.0000	0.0000
4	0.0000	0.0000	0.1563	0.7344	0.1094	0.0000	0.0000
5	0.0000	0.0000	0.0000	0.2632	0.5263	0.2105	0.0000
6	0.0000	0.0000	0.0000	0.0714	0.1429	0.6429	0.1429
7	0.0000	0.0000	0.0000	0.0000	0.0000	0.0000	1.0000

Aug – Sep

1	0.6667	0.3333	0.0000	0.0000	0.0000	0.0000	0.0000
2	0.0714	0.9286	0.0000	0.0000	0.0000	0.0000	0.0000
3	0.0000	0.3158	0.4211	0.2632	0.0000	0.0000	0.0000
4	0.0000	0.0000	0.1579	0.7544	0.0877	0.0000	0.0000
5	0.0000	0.0000	0.0000	0.2105	0.4211	0.3684	0.0000
6	0.0000	0.0000	0.0000	0.1538	0.3077	0.4615	0.0769
7	0.0000	0.0000	0.0000	0.0000	0.0000	0.3333	0.6667

Sep – Oct

1	0.6667	0.3333	0.0000	0.0000	0.0000	0.0000	0.0000
2	0.0000	0.9000	0.1000	0.0000	0.0000	0.0000	0.0000
3	0.0000	0.1765	0.5882	0.2353	0.0000	0.0000	0.0000
4	0.0000	0.0000	0.1296	0.7593	0.1111	0.0000	0.0000
5	0.0000	0.0000	0.0000	0.2353	0.7059	0.0588	0.0000
6	0.0000	0.0000	0.0000	0.0000	0.1429	0.8571	0.0000
7	0.0000	0.0000	0.0000	0.0000	0.0000	0.3333	0.6667

Oct – Nov

1	0.5000	0.5000	0.0000	0.0000	0.0000	0.0000	0.0000
2	0.0000	0.5909	0.3636	0.0455	0.0000	0.0000	0.0000
3	0.0000	0.2632	0.4737	0.2632	0.0000	0.0000	0.0000
4	0.0000	0.0000	0.0408	0.8163	0.1429	0.0000	0.0000

Table F1 Continued - Non-Homogeneous SOI 7 Class Monthly Transition Matrices

5	0.0000	0.0000	0.0000	0.3000	0.5500	0.1500	0.0000
6	0.0000	0.0000	0.0000	0.0000	0.2143	0.7857	0.0000
7	0.0000	0.0000	0.0000	0.0000	0.0000	0.5000	0.5000

Nov – Dec

1	1.0000	0.0000	0.0000	0.0000	0.0000	0.0000	0.0000
2	0.0000	0.5789	0.3684	0.0526	0.0000	0.0000	0.0000
3	0.0000	0.1579	0.4211	0.4211	0.0000	0.0000	0.0000
4	0.0000	0.0000	0.0192	0.8654	0.1154	0.0000	0.0000
5	0.0000	0.0000	0.0000	0.4286	0.4286	0.1429	0.0000
6	0.0000	0.0000	0.0000	0.0000	0.1333	0.8667	0.0000
7	0.0000	0.0000	0.0000	0.0000	0.0000	1.0000	0.0000

Dec – Jan

1	1.0000	0.0000	0.0000	0.0000	0.0000	0.0000	0.0000
2	0.0000	0.5000	0.4286	0.0714	0.0000	0.0000	0.0000
3	0.0000	0.2667	0.4667	0.2667	0.0000	0.0000	0.0000
4	0.0000	0.0159	0.0952	0.7937	0.0952	0.0000	0.0000
5	0.0000	0.0000	0.0000	0.1765	0.5882	0.2353	0.0000
6	0.0000	0.0000	0.0000	0.0000	0.0588	0.8235	0.1176
7	0.1429	0.1429	0.1429	0.1429	0.1429	0.1429	0.1429

Table F2 – Mean Monthly Transition Matrix of 3-Month Moving Mean SOI

SOI Class	1	2	3	4	5	6	7
1	0.7308	0.2692	0.0000	0.0000	0.0000	0.0000	0.0000
2	0.0387	0.6906	0.2265	0.0442	0.0000	0.0000	0.0000
3	0.0000	0.1990	0.4806	0.3155	0.0049	0.0000	0.0000
4	0.0000	0.0115	0.0950	0.7727	0.1108	0.0101	0.0000
5	0.0000	0.0000	0.0000	0.3348	0.4783	0.1870	0.0000
6	0.0000	0.0000	0.0000	0.0437	0.2295	0.6940	0.0328
7	0.0000	0.0000	0.0000	0.0000	0.0000	0.4286	0.5714

Table F3 – Steady State Results from Non-Homogeneous Chain of 3-Month Moving Mean SOI

	Class 1	Class 2	Class 3	Class 4	Class 5	Class 6	Class 7
	Jan						
Markov	0.0078	0.0958	0.1521	0.4552	0.1328	0.1407	0.0156
Empirical	0.0078	0.0938	0.1563	0.4531	0.1328	0.1406	0.0156
	Feb						
Markov	0.0078	0.0707	0.1862	0.4458	0.1409	0.1485	0.0000

Table F3 Continued – Steady State Results from Non-Homogeneous Chain of 3-Month Moving Mean SOI							
Empirical	0.0078	0.0703	0.1875	0.4453	0.1406	0.1484	0.0000
				Mar			
Markov	0.0157	0.1016	0.1166	0.4767	0.1330	0.1564	0.0000
Empirical	0.0156	0.1016	0.1172	0.4766	0.1328	0.1563	0.0000
				Apr			
Markov	0.0235	0.1015	0.1091	0.4687	0.1564	0.1408	0.0000
Empirical	0.0234	0.1016	0.1094	0.4688	0.1563	0.1406	0.0000
				May			
Markov	0.0156	0.1249	0.1014	0.4843	0.1877	0.0782	0.0078
Empirical	0.0156	0.1250	0.1016	0.4844	0.1875	0.0781	0.0078
				June			
Markov	0.0157	0.1251	0.1015	0.4843	0.1875	0.0781	0.0078
Empirical	0.0313	0.1172	0.1406	0.4531	0.1641	0.0859	0.0078
				July			
Markov	0.0156	0.1249	0.1014	0.4843	0.1877	0.0782	0.0078
Empirical	0.0234	0.1094	0.1016	0.5000	0.1484	0.1094	0.0078
				Aug			
Markov	0.0156	0.1249	0.1014	0.4843	0.1877	0.0782	0.0078
Empirical	0.0234	0.1094	0.1484	0.4453	0.1484	0.1016	0.0234
				Sep			
Markov	0.0157	0.1250	0.1015	0.4843	0.1876	0.0782	0.0078
Empirical	0.0234	0.1563	0.1328	0.4219	0.1328	0.1094	0.0234
				Oct			
Markov	0.0157	0.1251	0.1015	0.4843	0.1875	0.0781	0.0078
Empirical	0.0156	0.1719	0.1484	0.3828	0.1563	0.1094	0.0156
				Nov			
Markov	0.0156	0.1250	0.1015	0.4843	0.1876	0.0782	0.0078
Empirical	0.0078	0.1484	0.1484	0.4063	0.1641	0.1172	0.0078
				Dec			
Markov	0.0156	0.1249	0.1014	0.4843	0.1877	0.0782	0.0078
Empirical	0.0078	0.1094	0.1172	0.4922	0.1328	0.1328	0.0000

Table F4. SOI class monthly forecasts based on 4-month lagged prediction scheme from non-homogeneous Markov chain for 1982-'83, 2001-'02, and 2002-'03

Year of Observation	Month of Observation	SOI Class Observed	Yr. of Prediction	Month of Prediction	SOI Class Predicted by Markov	Actual SOI Class
1982	Jan	6	1982	May	3	3
1982	Feb	4	1982	June	4	2
1982	Mar	4	1982	July	4	1
1982	Apr	4	1982	August	4	1
1982	May	3	1982	Sept.	4	1
1982	Jun	2	1982	October	3	1
1982	Jul	1	1982	Nov.	4	1
1982	Aug	1	1982	Dec.	4	1
1982	Sep	1	1983	January	4	1
1982	Oct	1	1983	February	4	1
1982	Nov	1	1983	March	3	1
1982	Dec	1	1983	April	4	2
2001	Jan	6	2001	May	3	3
2001	Feb	6	2001	June	3	4
2001	Mar	5	2001	July	5	3
2001	Apr	4	2001	August	4	2
2001	May	3	2001	Sept.	4	4
2001	Jun	4	2001	October	4	3
2001	Jul	3	2001	Nov.	4	5
2001	Aug	2	2001	Dec.	4	2
2001	Sep	4	2002	January	4	5
2001	Oct	3	2002	February	4	6
2001	Nov	5	2002	March	3	3
2001	Dec	2	2002	April	4	3
2002	Jan	5	2002	May	3	2
2002	Feb	6	2002	June	3	3
2002	Mar	3	2002	July	4	3
2002	Apr	3	2002	August	4	3
2002	May	2	2002	Sept.	4	3
2002	Jun	3	2002	October	4	3
2002	Jul	3	2002	Nov.	4	3
2002	Aug	2	2002	Dec.	4	2
2002	Sep	3	2003	January	4	3
2002	Oct	3	2003	February	4	2
2002	Nov	3	2003	March	3	2
2002	Dec	2	2003	April	4	3

Appendix G: Instructions for Visual Basin Programs Used for this Thesis

Purpose: Provide instructions for most critical Visual Basic (VB) programs used to obtain results for chapters 1-3 for lay user to duplicate results found for these chapters.

Chapter 1 – Markov Modeling of the Troup SOI

1. From "TransProb Program.xls"

    a. Obtain non-homogeneous transition matrices:
        i. user enters number of classes in worksheet "Input" – restricted to 3, 5, or 7
        ii. user enters upper bounds for classes 1 and 2 (3 classes), 1-4 (5 classes), or 1-6 (7 classes) in worksheet "Input"
        iii. run VB program "TransProb"
        iv. if user enters 3 classes, worksheet "Output3" (cell rows 1-3) contains matrices, similarly for 5 classes (cell rows 1-5 in worksheet "Output5") and 7 classes (cell rows 1-7 in worksheet "Output7")

    b. Find steady state probability distributions for each month:
        i. done for 7 classes in Chapter 1
        ii. run VB program "SSclassProbs7" to attain constant stochastic matrices in worksheet "Output7"
        iii. cell rows 114-120 contain each month's constant stochastic matrix sequentially ([Jan] → [Dec]) from left to right
        iv. also outputted by "SSclassProbs7" are the empirical steady state probabilities for all 7 classes, and all months on worksheet "Empiricalprobs7"

    c. Find Mean Monthly matrix for homogeneous Markov chain
        i. run VB program "MeanMonthly"
        ii. the Mean Monthly matrix is outputted in worksheet ""HomoMarkov" in cells A20→G26
        iii. also in worksheet "HomoMarkov", mean recurrence times is solved using the Mean Monthly matrix via Excel's SOLVER linear programming

    d. Develop SOI monthly prediction scheme from non-homogeneous chain:
        i. upon attaining each of the 12 monthly transition matrices (cell rows 1-7 in worksheet "Output7")
            1. user enters starting month in cell E2 (e.g. "0" for January) and this start month's observed SOI class
            2. run VB program "Prediction"

3. cell A17 contains the SOI class prediction for the 4^{th} month in the future (e.g. SOI class observed for January predicts SOI class in May)

e. Obtain row vectors of stay-in probabilities for each class, for each monthly transition of the non-homogeneous Markov chain
   i. For 7 SOI classes, there exists 7 row vectors of stay-in probabilities
   ii. The stay-in probability for SOI class i for the January-February transition is $p_{i,i}^{(Jan,Feb)}$
   iii. Run VB program "MeanRes" to extract the 7 row vectors for 7 SOI classes from the 12 monthly transition matrices
      1. row vectors are outputted in worksheet "MeanRes_SOI" in rows 1-7 for classes 1 through 7

2. From "Residence using Geometric Mean approach.xls"

f. Attain expected mean residence for each class, conditioned on starting month:
   i. Copy 7 row vectors of stay-in probabilities from cells A1-L7 in worksheet "MeanRes_SOI" within "TransProb Program.xls" and paste into worksheet "Res7classes" within "Residence using Geometric Mean approach.xls" at cells A7-L13
   ii. For expectation calculation, user enters k_{max} in cell A46 and a factor in cell A49 of worksheet "Res7classes"
      1. Prompted to use $k_{max} = 48$ and factor = 12
   iii. Run VB program "MeanRes7Classes"
      1. expected residences for each of the 12 starting months, for each SOI class 1-7 outputted in worksheet "OutputExp" in cells A11 thru L17
         a. row 11-17 corresponds to class 1-7 and column A-L correspond to January-December

<u>Chapter 2 – Synoptic Scale Classification (SSC) and Application for Expected Seasonal Weather Distribution and Precipitation</u>

1. From "SSCWinterTransMatricies.xls" – winter precipitation analyzed in Chapter 2

a. Output each winter's SSC 90-member column array into appropriate sheet that is named for its SOI-AO category (e.g. worksheet "SSCTrans_ENAOP" designates all winter SSC arrays that came after a fall of El Nino-AO+)
   i. User enters number years of daily precipitation data (Roanoke used in Chapter 2) in worksheet "UserInfo" in cell A15

ii. User enters upper bound of SOI used as inclusive bound for El Nino (-5.0) in cell A16
iii. User enters lower bound of SOI used as inclusive bound for La Nina (5.0) in cell A17
iv. User enters upper bound of AO used as inclusive bound for AO- (-0.25) in cell A18
v. User enters lower bound of AO used as inclusive bound for AO+ (0.25) in cell A19
vi. Run VB program "WinterSSCTransMatrices" to output each winter's SSC array into the worksheet that is names for its corresponding fall average SOI-AO category

b. Compute number of transitions to and from each of the 7 SSC weather types for EACH winter SSC array previously outputted

i. This process done for EACH winter 90-member column array of SSC outputted to the sheet named for its preceding fall SOI-AO category, for each SOI-AO category:
1. For current SOI-AO category:
a. Copy first winter 90-member SSC column array from the worksheet named for this current SOI-AO category (e.g. "SSCTrans_LNAONeut" signifies those winter SSC arrays that occurred after the fall condition of La Nina-AO Neutral)
b. Paste this column array into homogeneous matrix computation worksheet also named for current SOI-AO category (e.g. paste into worksheet "LNAONeutHomoMats" for La Nina-AO Neutral)
c. Run VB program named for current SOI-AO category (e.g. for La Nina-AO Neutral, run VB program "ComputeHomoMat_LNAONeut") which outputs the number of days this 90-member column array of winter SSC values transitioned to and from each of the 7 SSC weather types (cells B1-H7) as well as the number of days existing in each SSC weather type (column I) in homogeneous matrix computation worksheet (e.g. "LNAONeutHomoMats")
d. Copy this matrix of transitions and number of occurrences of each SSC (cells B1-I7) into worksheet "SOLVER" within new workbook "SSCWinterHomoMats_Results.xls"
e. Repeat a-d for each winter existing for current SOI-AO fall category

c. Retrieve daily winter precipitation values at Roanoke for each winter day currently represented by the SSC weather type reported for that day

    i. This retrieving procedure done for all 9 SOI-AO categories, although 3 separate VB programs written to deal with the first 3 categories (El Nino & AO+, AO Neutral, AO-), second 3 categories (ENSO Neutral & AO+, AO Neutral, AO-) and last 3 categories (La Nina & AO+, AO Neutral, AO-)

    ii. For the first 3 SOI-AO categories:
        1. Run VB program "CollectPrecipData1thru3" to retrieve daily precipitation at Roanoke for ALL winters that belong to the first 3 SOI-AO categories
            a. This program initially prints all winter days including dry days (precip. = 0), arranges by the SSC weather type reported for its corresponding day, and outputs daily precipitation in worksheet named for current SOI-AO category (e.g. worksheet "ENAOPPrecip(1)" for El Nino-AO+)
                i. This winter daily precip. are days pooled from ALL winters belonging to the current SOI-AO category
            b. This program also segregates wet winter days from dry days and prints wet days, according to the SSC weather type reported for that specific day, in worksheet named for current SOI-AO category (e.g. "ENAOPPrecip(2)" for El Nino-AO+)
            c. In worksheet containing wet winter daily precip. arranged by the day's reported SSC weather type (e.g. ENAOPPrecip(2) for El Nino-AO+), the final entry in each SSC column vector is the fraction of dry days over the total number of days reported for that SSC weather type

    iii. For second 3 SOI-AO categories:
        1. Run VB program "CollectPrecipData4thru6" and repeat steps a-c listed immediately above

    iv. For last 3 SOI-AO categories:
        1. Run VB program "CollectPrecipData7thru9" and repeat steps a-c listed immediately above

Chapter 3 – Spatial Precipitation Analysis

1. From "All_Historical_Synoptic_Days.xls"

    a. Extract all days from historical (1950-2003) daily record to find all "frontal-precipitation days" – days on which all 7 stations received precipitation (Bedford, Blacksburg, Roanoke Airport, Lafayette, Buchanan, Pulaski, Rocky Mount)

        i. Run VB program "Historical_Frontal_Days"
            1. All frontal-precip. days outputted in the worksheet named according to the season within which each fell (e.g. all historical winter frontal-precip. days outputted in worksheet "WinterSynopticDays"
            2. All pooled winter days then entered into a MiniTab macro that ranks precipitation at each station, for all frontal-precip. days in winter

2. From "All_Historical_Synoptic_Days_Ranked.xls"

    a. For each station, for each winter in historical record (1950-2003), find the frequency/count of each rank 1-7 during frontal-precip. days

        i. Run VB program "Winter_Rank_Freq"
            1. Input data located in worksheet "WinterData"
            2. Output in worksheet "WinterFreqResults"
                a. Winter year in column A
                b. Bedford rank frequency/count columns B-H, corresponding to ranks 1-7, for each winter
                c. Blacksburg rank frequency/count columns J-P, corresponding to ranks 1-7, for each winter
                d. Roanoke rank frequency/count columns R-X, corresponding to ranks 1-7, for each winter
                e. Lafayette rank frequency/count columns Z-AF, corresponding to ranks 1-7, for each winter
                f. Buchanan rank frequency/count columns AH-AN, corresponding to ranks 1-7, for each winter
                g. Pulaski rank frequency/count columns AP-AV, corresponding to ranks 1-7, for each winter
                h. Rocky Mount rank frequency/count columns AX-BD, corresponding to ranks 1-7, for each winter

    b. For each winter (1950-2003), for each 2-station combination (21 total combinations): compute NORM(X) and NORM(Y)

        i. Run VB program "Winter_Rank_Spatial_Analysis"

1. Input data located in worksheet “WinterFreqResults”
2. Output in worksheet “WinterSpatialAnalysis”
    a. Number of frontal-precip. days for each winter in cells B2-BB2
    b. NORM(X) for each winter, for all 2-station combinations (21 total) in cells B3-BB23
    c. NORM(Y) for each winter, for all 2-station combinations (21 total) in cells B26-BB46